Acoustic and ecological investigations into predator-prey interactions between Antarctic krill (*Euphausia superba*) and seal and bird predators

by

Martin James Cox

A thesis submitted to
The University of St Andrews
for the degree of
Doctor of Philosophy

School of Biology and
School of Mathematics and Statistics
The University of St Andrews
April 2008

Thesis Declaration

I, Martin James Cox, hereby certify that this thesis, which is approximately 71,000 words in length, has been written by me, that it is the record of work carried out by me and that it has not been submitted in any previous application for a higher degree.

I was admitted as a research student in September 2004 and as a candidate for the degree of Doctor of Philosophy in September 2005; the higher study for which this is a record was carried out in the University of St Andrews between 2004 and 2008.

date ..... signature of candidate .....

I hereby certify that the candidate has fulfilled the conditions of the Resolution and Regulations appropriate for the degree of Doctor of Philosophy in the University of St Andrews and that the candidate is qualified to submit this thesis in application for that degree.

date ..... signature of supervisor .....

The following is an agreed request by candidate and supervisor regarding the electronic publication of this thesis:

Access to all or part of printed copy but embargo of all or part of electronic publication of thesis for a period of one year on the following grounds: publication would preclude future publication.

We request this embargo to allow us time to publish the research carried out in the analysis chapters of this thesis.

date ..... signature of candidate .....

date ..... signature of supervisor .....

Abstract

1. Antarctic krill (*Euphausia superba*) form aggregations known as swarms that vary greatly in size and density. Six acoustic surveys were conducted as part of multi-disciplinary studies at two study sites, the western and eastern core boxes (WCB and ECB), during the 1997, 1998 and 1999 austral summers, at South Georgia. A quantitative, automated, image processing algorithm was used to identify swarms, and calculate swarm descriptors, or metrics. In contrast to acoustic surveys of aggregations of other pelagic species, a strong correlation ($r = 0.88$, $p = 0.02$, 95% C.I.= 0.24 to 0.99) between the number of krill swarms and the mean areal krill density ($\hat{\rho}$) was found. Multivariate analysis was used to partition swarms into three types, based on contrasting morphological and internal krill density parameters. Swarm types were distributed differently between inter-surveys and between on- and off-shelf regions. This swarm type variation has implications for krill predators, by causing spatial heterogeneity in swarm detectability, suggesting that for optimal foraging to occur, predators must engage in some sort of adaptive foraging strategy.

2. Krill predator-prey interactions were found to occur at multiple spatial and temporal scales, in a nested, or hierarchical structure. At the largest inter-survey scale, an index of variability, I, was developed to compare variation in survey-scale predator sightings, sea temperature and $\hat{\rho}$. Using I and a two-way ANOVA, core box, rather than year, was found to be a more important factor in determining species distribution. The absence of Blue-petrels (*Halobaena caerulea*) and the elevated number of Antarctic fur seals (*Arctocephalus gazella*) suggest that 1998 was a characterised by colder than average water surrounding South Georgia, and a high $\hat{\rho}$ in the ECB. At the smaller, intra-survey scales (<80 km, <5 day), the characteristic scale (distances in which predator group size, or krill density were similar, L_s) were determined. For krill and predators L_s varied by survey and the L_s of krill also varied by depth within a survey. Overlap in L_s were stronger between predator species than between a predator species and krill, indicating predators were taking foraging cues from the activity of predators, rather than from the underlying krill distribution. No relationship was found between swarm characteristics and predator activity, suggesting either there is no relationship between krill swarms and predators, or that the predator and acoustic observation techniques may not be appropriate to detect such a relationship.

3. To overcome the 2-D sampling limitations of conventional echosounders, a multibeam echosounder (MBE) observed entire swarms in three-dimensions. Swarms found in the nearshore environment of Livingston Island situated in the South Shetland Islands, exhibited only a narrow range of surface area to volume ratios or roughnesses (R=3.3, CV=0.23), suggesting that krill adopt a consistent group behaviour to maintain swarm shape. Generalized additive models (GAM) suggested that the presence of air-breathing predators influenced the shape of a krill swarm (R decreased in the presence of predators: the swarm became more spherical). A 2D distance sampling framework was used to estimate the abundance, N, and associated variance of krill swarms. This technique took into account angular and range detectability (half-normal, $\hat{\sigma_r}$=365.00, CV=0.16) and determined the vertical

distribution of krill swarms to be best approximated by a beta-distribution ($\hat{\alpha}$=2.62, $\hat{CV}$=0.19; $\hat{\beta}$=2.41, $\hat{CV}$=0.15), giving the abundance of swarms in survey region as $\hat{N}$=5,062 ($\hat{CV}$=0.35). This research represents a substantial contribution to developing estimation of pelagic biomass using MBEs.

4. When using a single- or split-beam missing pings occur when the transmit or receive cycles are interrupted, often by aeration of the water column, under the echosounder transducer during rough weather. A thin-plate regression spline based approach was used to model the missing krill data, with knots chosen using a branch and bound algorithm. This method performs well for acoustic observations of krill swarms where data are tightly clustered and change rapidly. For these data the technique outperformed the standard MGCV GAM, and the technique is applicable for estimating acoustically derived biomass from line transect surveys.

Acknowledgements

- **Supervision**. I would like to thank all five of my supervisors for their help and support during my PhD. I have learnt a lot from all of them, and not just about science. I particularly want to thank Andrew Brierley, chief supervisor, for his continual enthusiasm and commitment to my PhD, particularly when I thought things had gone wrong. David Borchers, Centre for Research into Ecological and Environmental Modelling (CREEM), was very patient helping me with statistics, as was Monique Mackenzie (CREEM). I thank Keith Reid, British Antarctic Survey (BAS), for helping me understand predator-prey interactions and helped me put my research in context. Jon Watkins (BAS) for discussing krill swarms, and for organising my 2006 BAS fieldwork (cruise JR140).

- **Personal support**. My wife Joanne. My family, especially my Mum. My friends, particularly my best friend Nick Skipper, Carl Donovan, my office mates, Bruno Caneco, Rodrigo Wiff and latterly Eric Rexstad. Charles Paxton, Tom Brown, Gill Calder, Liliana Martins, Laura Marshall, Lindesay Scott-Hayward, Leslie New, Ewan Wakefield, Jarrod Santora, Andy and Alison Johnston, Danny Wake, Graeme McNeill, Steve Sessions, Darci Lombard, Jessica Lipsky, and Chris Haunton. Ali and Kelly MacLeod who took my into their home and saw me through my dog days. Michael Glaser, who many years ago started interest in science.

- **Financial support**. The Natural Environment Research Council (NERC) PhD studentship (NER/S/A/2004/12438) and BAS for CASE funding. Antarctic funding initiative for cruise JR140. The Royal Society for funding the nearshore multibeam investigation in 2006. The University of Washington and the Office of Naval Research for partially funding my participation in the 2005 Friday Harbour Marine Bioacoustics course. NERC for funding my participation in the 2005 Advances in Ecology short course at Silwood Park.

- **Logistical support** Officers and crew of *RRS James Clark Ross*, during cruises JR17, JR28, JR38 and JR140. Rennie Holt, Christian Reiss and Adam Jenkins for allowing me to participate in the 2006 and 2007 cruises in the US Antarctic Marine Living Resources Program (AMLR) The officers and crew of *R/V Yuzmorgeologiya* during the AMLR 2006 and 2007 South Shetland cruises. Personnel at the Cape Shirreff, Livingston Island for allowing the nearshore research team to stay in their home during the 2006 and 2007 AMLR surveys.

- **Statistical support**. Carl Donovan, Charles Paxton, Joanne Potts, Tiago Marques and Eric Rexstad (all CREEM).

- **Technical support**. David Demer, Steve Sessions, George Cutter (Fisheries Technology Division of the South West Fisheries Science Centre, La Jolla California), Joe Warren and Derek Needham for the design and fabrication of equipment to house the SM20 multibeam echosounder, on an inflatable boat. Steve Sessions, Marcel Van Den Berg and Adam Jenkins for skippering the inflatable boat, *R/V Roald*. Jeff Condiotty, from Simrad US, for loaning the SM20 multibeam echosounder. Matt Wilson for continual help with the Echoview acoustic processing software. Phil

Copland of Fisheries Research Services (FRS) Aberdeen for acoustics help with acoustics and providing a 120 kHz transducer for JR140. David Demer for acoustics help. Phil Copland, Eric Armstrong and Paul Fernandes (all FRS) loaned me a Echoview multibeam dongle that allowed me to processing the nearshore multibeam data. Peter Endeline (BAS), who organised the fishing and acoustics during JR140. Ewan Wakefield (BAS) for collecting predator observations during JR140.

Contents

Chapter 1

General Introduction

The aim of this PhD research was to examine the at-sea distribution and spatial interactions of Antarctic krill (*Euphausia superba*) and air-breathing predators, such as Antarctic fur seals (*Arctocephalus gazella*) and Black-browed albatross (*Thalassarche melanophris*). The purpose of this research was to gain insight into predator-prey dynamics to determine how predators find prey and how prey evade predators, and thereby enhance understanding of the functioning of a krill-centric ecosystem. Insight into predator-prey interactions is required for ecosystem management, particularly when an ecosystem approach to fisheries is used (Constable et al., 2000). During this research a scale based analysis approach was adopted.

The concept of scale has been used widely in ecology and broadly falls into two categories (Schneider, 2001). Firstly, allometric scaling, which uses a model to represent the relationship between two biological characteristics *e.g.* respiration to mass (Calder, 1983). In allometric scaling, the model parameters are statistically similar across species, but the ratio between the two measured biological quantities varies. Allometric scaling has been used to describe species spatial density where, for a given species of animal, the relationship between body mass and numerical density has been shown to follow an allometric scaling law: the larger the animal, the lower the numerical density. (*e.g.* Nee et al. 1991; Schmid et al. 2000). Habitats (Sole and Manrubia, 1995), food-webs (*e.g.* Garlaschelli et al. 2003), and marine predator foraging (Sims et al., 2008) have also been described by allometric scaling laws. The application of allometric scaling to acoustic observations of pelagic organisms, such as Antarctic krill, holds great promise, but is constrained by sampling and analysis techniques, so is not considered further in this research.

The second type of ecological scale is the measurement of spatial and temporal scales of a given ecosystem process *e.g.* diel vertical migration. Temporal and spatial scales have been used to describe the biological diversity of ecosystems (McCann, 2000; Beever et al., 2006), and to examine relationships between abiotic variables, such as temperature, and biotic variables, such as species abundance (Guisan and Zimmermann, 2000). Also,

the temporal and spatial scales in ecosystems have been used to elucidate ecosystem function (Levin, 1992) and to determine predator-prey interactions (*e.g* Scheider and Piatt 1986; Schneider 1989; Blaine and DeAngelis 1997). It is the spatial and temporal scales of predator-prey interactions, specifically krill predator-prey interactions, that will be considered in this research. In this investigation, characteristic scale is defined following Powell (1989) and Legendre and Legendre (1998) as the distance, or time, before the quantity of interest changes *e.g.* the distance over which a statistically similar number of animals are observed. This definition of characteristic scale is dependent on the sampling resolution (*e.g.*, $1m^2$ quadrat) and the process being studied, so is applicable from the micro (1 m) to macro (>100 km) (Legendre and Legendre, 1998). In this investigation the quantity of interest is the areal density of krill (gm^{-2} wet-mass) and frequency of air-breathing predator encounters.

Krill form swarms that range in size from 10s of metres to 10s of km (Hamner and Hamner, 2000; Watkins, 2000), and occupy most of the Southern Ocean (A= 20.3 million km^2). Predators may forage over huge areas of essentially empty water to find krill (*e.g.* Phillips et al. 2005). Understanding krill predator-prey interactions at various spatial and temporal scales is paramount for understanding ecosystem function (Murphy, 1995).

To further explain the motivation behind this PhD research, the remainder of this chapter briefly describes Antarctic krill and krill predators, particularly at Bird Island and South Georgia (54^oS 35^oW, Figure 1.1). Previous studies into krill air-breathing predator interactions around South Georgia are reviewed. Finally, throughout these reviews, research areas of krill predator-prey interactions that this PhD contributes to, or extends, are given.

1.1 Predator-prey interaction scales

The spatial and temporal scales at which predators and prey occur are used to characterise predator-prey interactions (Legendre and Legendre, 1998) and can be used to determine the spatial and temporal overlap between predators and prey (Blaine and DeAngelis, 1997). The spatial and temporal scales of predators and prey and their interaction, or overlap, are important for gaining insight into ecosystem processes and the behaviour of predators and prey that inhabit them (Fauchald, 1999). The measurements of the scale of predator-prey interactions are also of interest because these interactions contribute to the successful functioning of ecosystem food webs: if predators cannot find prey, or if prey cannot at least occasionally find a predator-free refuge, then species extinction may occur.

If a scale-dependent approach to predator-prey analyses is adopted, and additional

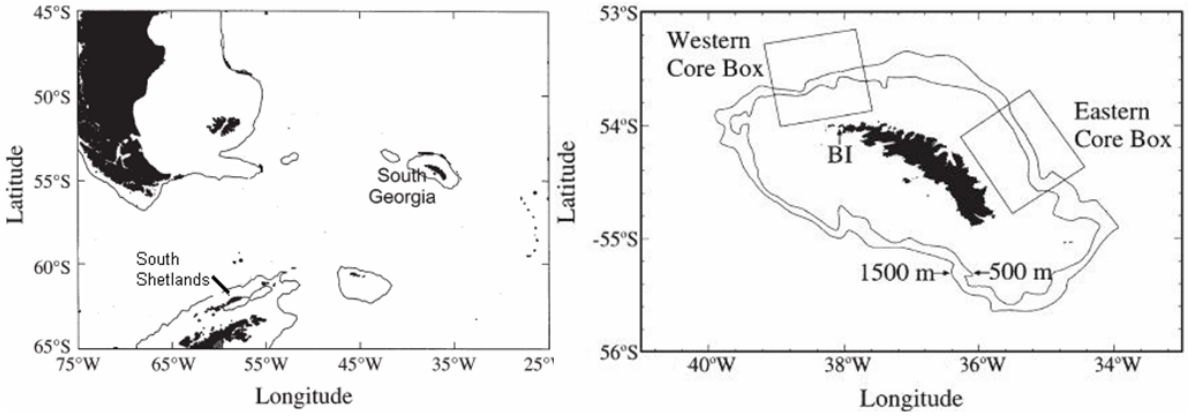

(a) Atlantic sector of Southern Ocean (b) Island of South Georgia

Figure 1.1: Panel (a) shows the general location of South Georgia and South Shetland Islands. Dashed line is the 500 m isobath. Panel (b) shows the location of Bird Island (BI), and the two British Antarctic Survey study sites, the Western and the Eastern core boxes, where the krill and predator data were collected. Figure modified from Atkinson et al. (2001).

ecosystem environmental data are collected, *e.g.* temperature, it is possible for researchers to explore the possible environmental mechanisms driving predator-prey interactions (Rose and Leggett, 1990). Also, simply examining an ecosystem at large scales may mask small scale processes, such as anti-predation behaviour (*e.g.* group anti-predation behaviour, Hamilton 1971). Equally, only examining predator-prey interactions at small scales may mask the influence of large-scale events, such as El Niño on an ecosystem (Knowlton, 1992). Because of the potential to induce analysis-scale limitations, the research conducted in this PhD was carried out at multiple temporal (from seconds to year) and spatial scales (and 10s m to 300 km).

Since the observation and interpretation of predator-prey interactions can occur at multiple spatial scales, these interactions can be described as existing in a nested, or hierarchical structure (Wu and Louckes 1995, Figure 1.2). Within a hierarchical system predators are concerned with assessing the density of prey in a given patch and tracking patches of prey as they forage through the prey field. Fauchald (1999) described two factors which determined how predators collected information on a patchily distributed prey. Firstly, the encounter rates between predators and prey were important because a high number of encounters will increase the information available to a predator. Secondly, a large number of encounters with different density patches will enable a predator to discriminate between patch profitability. Figure 1.2 is an example of predator-prey interactions within a study area (A_1), and occur in a hierarchical structure consisting of three spatial scales:

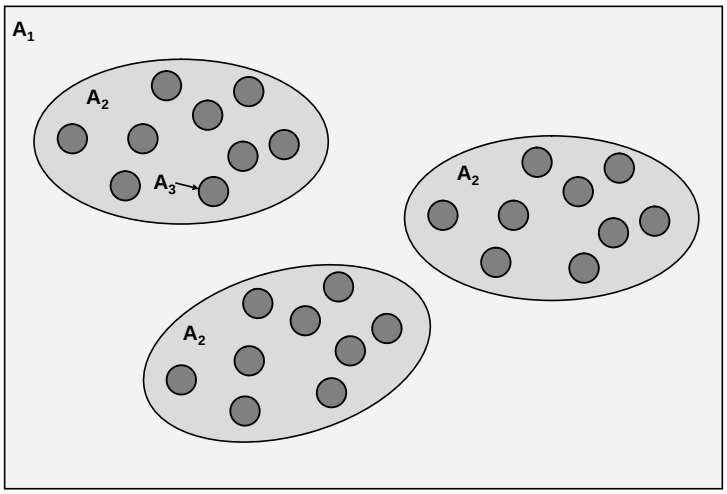

Figure 1.2: An example of the conceptual scale-dependent hierarchical patch structure used to define marine predator-prey interactions. The entire study area is contained in area A_1 (light grey), which provides the largest analysis scale possible. Nested within this area are patches of predators and prey that are of higher density and shorter temporal persistence ($A_{2...3}$). Some have described this as a fractal landscape (*e.g* Russell et al. 1992)

$\mathbf{A}_1$: The largest scale, the entire study site. Example analyses: (1) At this large scale the environment is likely to be heterogeneous so to successfully forage many predators must adjust their movement in response to the environment (*e.g.* temperature). Movements will cause predator and prey population dynamics to vary in response to a changing environment (Lima and Zollner, 1996). Linking environment to predator and prey densities may help determine the underlying processes driving species at the population level, if links exist (Pinaud and Weimerskirch, 2007); and (2) The breeding success of predators at population scales, often inter-annual, can be used to determine predator reproductive strategy. For example, during times of low prey abundance predators may choose adult survival, rather than provisioning offspring, which would result in breeding failure (Croll et al., 2006).

$\mathbf{A}_2$: The scale of these patches is determined by the search strategy of predators and the sensory perception of the predator. Example analyses: (1) These patches could be used to determine the sensory range of predators (*e.g.* Nevitt et al. (1995); Sims and Quayle (1998)); and (2) If the behaviour of predators and prey is not entirely driven by foraging, the scale of predator activity could be used to determine the scale of social interaction (Schreiber and Vejdani, 2006).

$\mathbf{A}_3$: At the smallest scale, once a predator has located prey, the escape response of the prey and the feeding technique of the predator will dictate the spatial and temporal overlap (Weissburg and Browman, 2005). At the smallest scale, negative

predator-prey associations may be observed that are either caused by the consumption of prey by predators or the prey anti-predation behaviour (Rose and Leggett, 1990).

Note: The scales of areas A_2 and A_3 are representations of a continuous process and are species and analysis dependent. Both predators and scientists observe the environment through a scale dependent process (Levin, 1992; MacNally and Quinn, 1998). Neither one can sample an entire ecosystem instantaneously, and this influences the "picture", or information about the ecosystem that is available for analysis. Also, processes at one scale in the hierarchical model may influence those at other scales. For example, anti-predation behaviour of prey in area A_3 will ultimately influence the distribution of the predator population in area A_1.

Observing predator-prey interactions at sea is often difficult as these interactions frequently occur within a system of highly dynamic processes (Hunt et al., 1992a). Furthermore, compared to terrestrial herbivore-plant predator-prey interactions, marine interactions frequently take place where both the predators and prey maybe highly mobile, making observation, analysis and interpretation difficult. Thus it is vital to select the appropriate sampling method (Croll et al., 1998). Example marine predator-prey interactions that take place in hierarchical structures are described in the next section.

1.2 Marine predator-prey interactions

The distribution of predators and prey in the marine environment can be described as a hierarchical patch structure (Fauchald, 1999; Pinaud and Weimerskirch, 2007). The distribution of predators and prey in A_1 (Figure 1.2) may be caused by oceanographic events (Atkinson et al., 2001). Note, hierarchical patch structures are not restricted to three levels, as in Figure 1.2, but can be nested in multiple levels (Fauchald, 1999).

Multiple scale responses of a marine predator, the least auklet (*Aethia pusilla*), to changes in zooplankton prey distribution in the Chirikov Basin, northern Berring Sea, were observed by Russell et al. (1992). Using geostatistics, auklet-zooplankton spatial associations were detected at the 10 km scale, which was found to be driven by the underlying physical predator-prey overlap and observation scale. Within the 10 km scale zooplankton were found in patches of similar densities that occurred at a scale of 0.5 km, which is evidence of a nested structure.

The spatial autocorrelation between predator or prey observations has been used to determine the characteristic scale at which predators and prey function (Fauchald et al., 2000), which has been used to define the spatial extent of patches of predators and prey. This characteristic scale can in turn can be used to determine the spatial overlap between

predators and prey (Fauchald, 1999; Fauchald et al., 2000), and may provide guidance for determining if predator or prey observations should be aggregated for further analysis.

Fauchald et al. (2000) used spatial autocorrelation to determine the characteristic scale predator-prey interactions between murres (*Uria* sp.) and capelin (*Mallotus villosus*) in the Barents Sea. Three scales of patchiness were found. Overlap between murres and capelin were found at the largest scale >300 km. At the intermediate scale, ∼50 km, overlap between murres and capelin was found at the ∼3 km scale. At the smallest analysis scale <5 km, a decreasing, but significant association was found between the murres and capelin. This reduction in spatial-association may have been caused by capelin anti-predation behaviour. The spatial autocorrelation approach was adopted in this research to study predator-prey interactions.

1.3 Antarctic krill

Antarctic krill (hereafter referred to as krill) reside in the pelagic environment which is highly dynamic, spatially and temporarily patchy, and influenced by physical drivers that occur at many temporal and spatial scales (Haury et al., 1985). As a species, krill is of vital importance in the Southern Ocean food web (Constable et al., 2000) which, at its most simple, comprises a three-link chain: phytoplankton, krill, whale (Reid et al., 1999a). Krill is the most abundant of the Southern Ocean euphausiid species, both numerically and by biomass (Atkinson et al., 2001, 2004), and is of vital importance to many land breeding seal and bird predators (Croxall et al., 1988b; Gonzalez et al., 2000; Reid and Croxall, 2001), as well as fish (Kock et al., 1994; Everson et al., 1999).

Monitoring the krill population is not only important for investigating predator-prey interactions, but also for fisheries management (Constable et al., 2000). Long-term monitoring is also important for detecting population variability that may arise as a consequence of climate change (Fraser and Hoffman, 2003; Clarke et al., 2007). This is particularly relevant around the Antarctic Peninsula (Reid and Croxall, 2001; Parkinson, 2002), an area that is one of the fastest warming locations on Earth.

1.3.1 Krill behaviour

There are two aspects of krill behaviour that are particularly relevant to this research: swarming and diel vertical migration. Both of these influence the spatial and temporal distribution of krill at scales that are relevant to air-breathing predators, and can be examined with the data that were available or collected in the course of this investigation.

Krill swarms have been described as a fundamental unit of krill ecology (Mangel and Nicol, 2000). Swarms of krill occur at densities from <1 to 10,000 individuals/m^3 (Hamner

and Hamner, 2000) and have lengths ranging from 10 m to tens of km (Watkins and Murray, 1998; Watkins, 2000). Potential advantages conferred to krill by forming swarms are: (1) a reduced chance of predation by increased surveillance capacity (O'Brien, 1987; Hamner and Hamner, 2000); (2) cohesive movement in response to predation attack (Hamner et al., 1983; O'Brien, 1989; Romey, 1995; Hofmann et al., 2004); (3) enhanced foraging (Hamner and Hamner, 2000); and (4) reduced energy expenditure (Ritz, 2000). An understanding of krill swarms is important for understanding predator foraging behaviour. Veit et al. (1993) suggested that foraging birds and seals may bypass smaller krill aggregations in anticipation of finding areas of higher density. Alternatively small krill swarms may be ignored by predators because they are unprofitable (Cresswell et al., 2007), or remain undetected. Consequently the influence of krill swarms on predators may be density dependent i.e. influenced by a few large swarms of krill, making characterising the variation in krill swarms important.

Vertical movement of krill, that typically occurs as diel-vertical migration (DVM) is thought to be an anti-predation mechanism (Demer and Hewitt, 1995). DVM is also thought to facilitate feeding (Ritz, 1994) and may enable krill to travel by advection (Tarling et al., 1998) by adjusting their depth in response to ocean currents. So through vertical migration krill can at least partially control their dispersion, by moving vertically through a water column, amongst stratified currents. Krill DVM is of profound importance for air-breathing predators, particularly flying birds. At night krill are frequently found in shallow water (<10 m, Demer and Hewitt 1995). However, during daylight hours krill descend to deeper depths (>25 m, Taki et al. 2005), that are beyond the diving ranges of most species of flying bird krill predators (see Croxall and Prince 1980a, 1997; Croxall et al. 1999).

1.3.2 Sampling krill

Krill are typically sampled using nets and and active acoustics (Hewitt and Demer, 2000). Net sampling is time consuming and consequently has limited spatial resolution. Further, depending on the gear used, nets may reduce the spatial resolution (Watkins et al., 1992). Acoustic surveys are used to sample krill in a manner not possible with nets (Hewitt and Demer, 2000). Acoustic surveys are generally conducted from research vessels using hull-mounted vertically-downward looking single- or split-beam echosounders (SBE), following line transect survey designs (Brierley et al., 1997b). Echosounders typically have a 7^o beam width, so only sample a narrow region under the research vessel. Volume backscatter (S_v) observations from a calibrated echosounder insonifying a given volume of water are scaled by target strength (TS) models (*e.g.* Greene et al. 1991) and length-wetmass models (*e.g.* Morris et al. 1988) to estimate krill density ($\hat{\rho}$). Both the TS and length-wetmass models

require krill length as an argument, so net sampling is required to scale the acoustic observations to obtain $\hat{\rho}$ (see Demer and Hewitt 1995 for the calculation of $\hat{\rho}$).

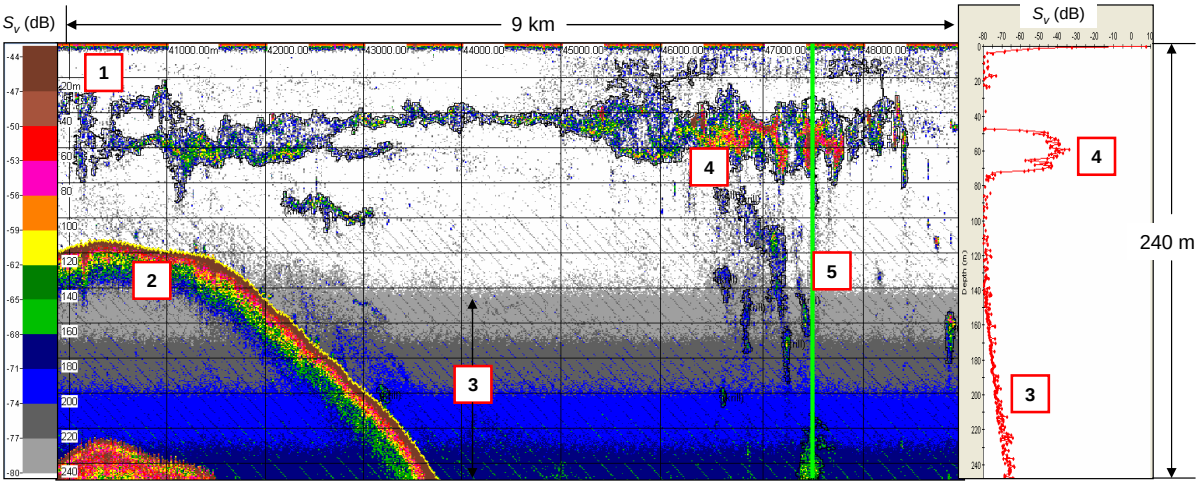

Figure 1.3: A 120 kHz echogram of volume backscatter (centre panel, S_v, logarithmic domain), with a -80 dB threshold, from a line transect survey at South Georgia. This is a cross-section view of the water column, a 9 km a long transect length to a range of 240 m. The grid is 1 km along by 20 m deep. [1] At short ranges (<10 m) the transmission mark (very high S_v) and transducer nearfield in which no meaningful acoustic data can be collected; [2] The seabed with the yellow line is the sounder detected seabed; [3] Time varied gain noise, which can be removed (see Watkins and Brierley 1996); [4] A high density krill swarm; [5] S_v samples within a single ping, shown in the farthest right panel.

Acoustic observations are often combined in an echogram, which is a two-dimensional (2-D) matrix of the one-dimensional (1-D) acoustic samples (range or time). Krill are acoustically identified and $\hat{\rho}$ calculated in a processing grid imposed on the echogram (*e.g.* the grid shown in Figure 1.3 has dimensions 1 km horizontally and 20 m vertically). Image processing techniques applied to this echogram can identify krill swarms as observed by the SBE without the use of a superimposed grid (see Reid and Simmonds 1993; Barange 1994). At small spatial scales (<10 km) acoustically identified krill swarms, rather than gridded acoustically derived krill densities may yield an improved representation of the krill available to predators (see Chapter 2).

There are two limitations in acoustic observations that are relevant to the study of krill predator-prey interactions. Firstly, SBE with vertical beams, are typically hull-mounted and cannot observe krill distribution in the upper 10 m of the water column, which is where the majority of flying-bird krill predators forage. Secondly, with post-processing, SBE effectively only sample krill swarms in a 2-D vertical strip, which is unlikely to represent the complex krill sample boundaries (Figure 1.3), nor does it represent the smallest horizontal scale at which predators might forage: that of a krill swarm. In the course of this investigation a multibeam echosounder (MBE) was used to acoustically

sample entire krill swarms, a first for a Antarctic krill, to overcome the SBE 2-D sampling limitations, and improve understanding of predator-prey interactions.

1.3.3 Krill biomass estimation

Krill may become the next important global fishery (Nicol and Foster, 2003). The fundamental role of krill in the Southern Ocean ecosystem, and the need to monitor krill stocks, was recognised in the Convention on the Conservation of Antarctic Marine Living Resources (CCAMLR), which is part of the Antarctic Treaty System. As part of the CCAMLR ecosystem approach to fisheries management, krill was chosen as one of the target species for monitoring (Kock, 2000; Constable et al., 2000). In addition to assessing the direct effect of commercial fisheries on the krill stock, the CCAMLR ecosystem approach to fisheries also considers the effect of krill fishery on krill predators (Anonymous, 2002; Garcia and Cochranem, 2005). Clearly, determining unbiased $\hat{\rho}$ and the associated variance estimate (Var$[\hat{\rho}]$) is important for successful ecosystem monitoring and this research contributes to this by: (i) quantifying krill swarm sizes and densities (Chapter 2); (ii) investigating the relationship between swarm abundance and $\hat{\rho}$ (Chapter 2); and (iii) determine if swarms avoid research vessels (Chapter 5).

The variability in swarming behaviour of krill makes the design of high-precision stock assessment surveys difficult (Watkins, 2000). This is partly because of the extremely high density of some swarms. For example, during a BAS survey at South Georgia in 1998, a particularly high krill density year, a single swarm contained 12% of the estimated total area krill biomass (Brierley et al., 1999b). Also, krill swarms are typically much smaller than the inter-transect line spacing. These large, high density, single swarms appear to be rare events, and a typical line-transect survey may miss such a high density swarm. This will negatively bias areal krill density estimates (Hewitt and Demer, 2000).

Establishing a relationship between the number of swarms (n_s) and $\hat{\rho}$ (Chapter 2) is important because n_s will influence the encounter rate of krill swarms by predators and krill catchability. The $n_s \simeq \hat{\rho}$ relationship is dependent upon how krill behave. For example, as $\hat{\rho}$ varies krill could maintain swarms of a similar internal size and density, which would reduce n_s in low $\hat{\rho}$ (Petitgas et al., 2001). If krill attempt to maintain similar n_s during lower $\hat{\rho}$ then individual swarm characteristics will change the net-sampling of krill during systematic net sampling surveys and because the krill-length frequency distribution is required to scale the acoustic observations this may bias biomass estimates.

Because MBE sample a large volume of water, following Gerlotto et al. (2004) it is possible to examine the horizontal distribution of krill swarms with respect to the research vessel (Chapter 5). When using an MBE, avoidance behaviour is observed as a non-random distribution of horizontal distances from the survey vessel. If acoustic surveys

are conducted using a vertically-downward looking SBE then avoidance behaviour would decrease the precision of biomass estimates.

1.4 Krill predators

For successful foraging to occur krill predators must be able to track the distribution of krill. This can be difficult in dynamic environments, where incomplete information must be used by predators to make foraging decisions (Stephens and Krebs, 1986). There are two characteristics of krill that determine the information available to a krill predator: availability and detectability.

The availability of krill to a predator is determined by the of krill abundance (Chapter 2), and the horizontal and vertical distribution of krill swarms(Chapters 2 and 6), and also horizontal and vertical distributions of the predator. For example, krill swarms to a depth of 50 m are available to be detected by Antarctic fur seals that routinely dive to 50 m (Boyd et al., 1997), but not to a non-diving bird species that can only sample krill near the surface *e.g* cape petrels (*Daption capense*). The detectability of krill varies by the size and internal density of swarms, with larger, high density swarms being detected (O'Brien, 1987, 1989), and the sensory acuity of the predator (Nevitt et al., 2004).

Chapters 2, 3 and 4 make use of data collected by British Antarctic Survey (BAS) in the region around South Georgia (Figure 1.1). This region is characterised by a high biomass of krill (Atkinson et al., 2001), and the tendency of krill to form aggregations have enabled colonies of seals and seabirds to successfully breed on the island (Reid and Croxall, 2001). The average demand for krill by Macaroni penguins (*Eudyptes chrysolophus*) and Antarctic fur seals during the January breeding period is estimated to be 32,000 tonnes per day (Boyd and Croxall, 1996). The dependence of seals and birds on krill means that when the January predator breeding season coincides with years of low krill density, predators suffer widespread breeding failure (Brierley et al., 1999b; Croxall et al., 1999; Reid et al., 1999a).

It was suggested by (Tarling et al., 2007) that the krill population at the South Georgia region is not self sustaining and relies on a flux of krill into the region, with no krill recruitment occurring locally. In Chapter 3, the affect of different water masses transporting krill to the South Georgia region was investigated by exploring the relationship between mean water temperature (used as a proxy for different water masses, see Meredith et al. 2005), $\hat{\rho}$ and predator sightings. Hunt et al. (1992b) demonstrated that at-sea sightings of resident South Georgia bird species, such as Black-browed albatrosses and (Antarctic) prions (*Pachyptila* sp. *desolata*) did not vary as a function of changes in sea-surface temperature (SST), but variation in Blue-petrels (*Pterodroma mollis*) petrels were

correlated with SST and left South Georgia after breeding. However, research conducted by Hunt et al. (1992b) was somewhat limited by survey design: two different line transect patterns were used, in different areas, and the analysis ignored zero counts. To overcome the limitations of the Hunt et al. (1992b) surveys, data from a common inter-annual line-transect survey design were used in Chapter 3 and in Chapter 4 all data were retained in the analysis i.e. zero-count predator observations were retained.

Hunt et al. (1992a) determined the spatial overlap between krill and Macaroni penguins and Antarctic fur seals was 70 and 100 km, and 10 and 100 km respectively. Within this study, krill-predator correlations reduced with decreasing analysis scale. Decreasing correlation between analysis scale and whale sightings was also reported by Reid et al. (2000b), which may have been either caused by a density-dependent predator foraging i.e. there are more krill than whales, so there will be a mismatch in spatial association. Alternatively, at smaller scales, splitting krill into along transect lengths may mask correlations by splitting larger swarms, or combining smaller swarms. In Chapter 4 the relationship between predator abundance and krill swarm characteristics was investigated, as was the relationship between krill density and predator distributions aggregated at systematic along transect length intervals.

The non-random distribution of the spatial at-sea distribution of krill predators around South Georgia and strong cross-correlations between krill and predators was found by Veit et al. (1993) when analysing predator-prey interactions at 1 n.mi. intervals. At smaller scales, the lack of correlation between krill and predators found by Hunt et al. (1992a) and Reid et al. (2000b) may not have been caused by analysis techniques. The formation of a krill swarm takes time and it is unlikely that swarms will be immediately detected by predators. Also, once attacked krill are likely to engage in anti-predation behaviour, which may cause the swarm to disperse (O'Brien, 1987; Hamner and Hamner, 2000). Consequently at smaller spatial scales (<1 n.mi) only weak predator-prey correlations may exist, and the predator-prey relationships operate in both directions: because anti-predation behaviour will influence prey abundance, as well as the prey distribution driving predator distribution (Veit et al., 1993).

In addition to a relationship between predators and krill Grënbaum and Veit (2003) showed that local enhancement, which is indirect detection of krill by predators, occurred. Predators cue on other predators that are already exploiting a patch of prey, and generally is a highly effective foraging strategy for Black-browed albatrossses at South Georgia. Multi-species feeding aggregations around South Georgia were observed by Harrison et al. (1991), within which Antarctic fur seals, Black-browed albatross, Macaroni penguins and prions, were the most abundant species. Within these flocks Black-browed albatrosses appear to dominate among the flying bird species. Harrison et al. (1991) suggested that the

foraging activity of diving predators was forcing krill to the surface, making it accessible to non-diving flying bird species.

An important limitation of the studies conducted by Harrison et al. (1991), Hunt et al. (1992a) and Veit et al. (1993) was that, within a given along-transect observation interval, krill density from the minimum observation depth to 250 m was used to investigate krill predator-prey interactions, which does not represent the krill available to predators. In Chapter 4, correlations between predator sightings and krill density were assessed for krill located between different depth horizons allocated by the diving depths of different predator species.

In Chapter 4 analysis scale was used to focus the investigation on a subset of krill predator species and interaction scales from an overwhelming number of combinations of predator-prey interactions. The very small scale (<200 m) interactions between krill and air-breathing predators were investigated in Chapter 5 using a MBE deployed during a line transect survey (120 m inter-transect spacing). In Chapter 5 the anti-predation behaviour of krill was also examined by quantifying changes in 3D swarm morphology in the presence of predators.

1.5 Multi-scale techniques

The remaining two analysis Chapters (6 and 7) of this PhD develop and apply statistical techniques that can be used at a range of spatial scales. In Chapter 6 a 2D distance sampling framework was used to estimate swarm abundance and associated variance from MBE observations. This technique is applicable to estimating abundances for MBE observations of both aggregative and solitary pelagic organisms.

Finally, Chapter 7 develops a surface fitting technique that could be applied to most ecological surface fitting problems at any spatial scale. In Chapter 7 the surface fitting technique was used to address an acoustic problem that effects both calculations of $\hat{\rho}$ and determining individual krill swarm boundaries, that of missing pings. When acoustic surveys are conducted from research vessels the acoustic data quality is, at least in part, dependent on sea state. As weather conditions worsen so does data quality. Generally missing pings are ignored when analysing acoustic data, and this will negatively bias density estimates, with the magnitude of the bias being related to the proportion of missing to successfully observed pings. For krill surveys conducted around South Georgia, missing pings are a problem, and in this research a new surface fitting technique is used to predict missing ping values.

1.6 Summary and investigation aims

The at-sea distributions of marine predators and prey is influenced by multiple biotic and abiotic events and are often found in a hierarchical patch structure, that occur at multiple spatial and temporal scales, making observing and interpreting marine predator-prey systems complex. In the case of krill and air-breathing predators, interactions describing at-sea distribution will allow the foraging techniques used by predators to be elucidated, determine the spatial and temporal scales at which predator-prey interactions occur, and have application in ecosystem modelling, to aid ecosystem management.

When examining krill predator-prey interactions there are four main survey design and analysis considerations : (1) predator distribution is not just driven by krill distribution; (2) predator and krill distribution is likely to be influenced by events that occurred outside of the survey region; (3) krill distribution influences predator distribution and vice versa; and (4) observing predators and prey may influence their behaviour *e.g.* vessel avoidance by krill predators.

To characterise krill predator-prey interactions, this PhD research considered the following areas of krill acoustics and krill predator-prey interactions:

1. The objective identification of krill swarms observed acoustically, using an SBE, at South Georgia. The results of this identification were used to examine the potential relationship between the n_s and $\hat{\rho}$. A variety of morphological and acoustic energy characteristics were extracted from the identified swarms and used to split the swarms into type. The spatial and temporal distribution of swarm types was assessed and its effect on predators considered (Chapter 2).

2. The large-scale inter-survey variation in the number of encountered krill predators in relation to the mean study site water temperature and $\hat{\rho}$ was assessed. Fifteen South Georgia predator species were split into three predefined predator functional groups: small flying birds, large flying birds and divers, and the inter-survey variability in each group was characterised (Chapter 3).

3. Small spatial scale (<10 km) interactions between the top five numerically dominant krill predator species at South Georgia were assessed. A scale-based approach was adopted to determine the spatial scale of krill-predator and inter-predator species cross-correlations (Chapter 4).

4. A multibeam echosounder (MBE), deployed from a small boat, was used to acoustically observe krill swarms in 3D. The 3D swarm descriptors were used to determine, krill abundance, the variation in krill swarm morphology in the presence of air-

breathing predators and will assess the potential for MBEs to be used to conduct krill biomass surveys (Chapter 5).

5. Recent developments in 2D distance sampling theory were used to estimate the depth probability density function of krill swarms and the swarm range detection function based on multibeam observations. These two distributions were used estimate the abundance of swarms and associated variance of swarms in the survey area (Chapter 6).

6. A newly developed multi-dimensional generalized additive modelling (GAM) framework was used to predict volume backscatter observations in missing pings, and compared to a "standard" GAM for surface fitting (Chapter 7).

Chapter 2

Characteristics of Antarctic krill swarms around South Georgia

2.1 Introduction

Spatial patchiness in hydrographic conditions is a common characteristic of the pelagic environment (Barange, 1994). Antarctic krill (*Euphausia superba*), exhibit amongst the most extreme patchiness (*cf* Herring, Beare et al. 2002), making spatial patchiness important in many aspects of krill ecology, such as feeding (Hamner and Hamner, 2000), reproduction (Watkins et al., 1992) and anti-predation responses (O'Brien, 1987). The aggregative behaviour of krill must balance the requirements of feeding whilst also minimising predation risk (Hardy and Gunther, 1935).

Krill aggregations are often referred to as swarms (Marr, 1962) that vary greatly in size and packing density (Mauchline, 1980; Miller and Hampton, 1989), and have been described as a fundamental unit of krill ecology (Hamner and Hamner, 2000; Mangel and Nicol, 2000). In this investigation krill swarms encompasses aggregations where individuals have a random, or polarised distributions.

Antarctic krill (herein referred to as krill) forms a fundamental component in the classical short Southern Ocean food web that connects primary producers to high trophic level predators such as whales and seabirds (Murphy, 1995; Hamner and Hamner, 2000; Reid et al., 2000b). Indeed it is the tendency of Antarctic krill to form swarms that makes them an important prey item for many marine vertebrate predators (Hewitt and Demer, 2000) and, as such, variation in krill swarm abundance and characteristics may have an impact on predator-prey interactions (Hunt, 1991). Variation in krill swarm structure, that has been described as hierarchical in nature (Murphy et al., 1988), makes krill swarms available to different species of predators that have a variety of foraging strategies (Croxall and Prince, 1997; Croxall et al., 1999). Spatially, hierarchical swarm structure can be thought of as the relationship suggested by (Watkins and Murray, 1998),

where high density swarms exist in low density layers. See Chapter 1 Figure 1.2 for an example of a hierarchical spatial structure.

Understanding the mechanisms of swarm formation is also important to allow informed ecosystem management decisions to be made (Hewitt and Demer, 2000). This is particularly important during the breeding season of land based krill predators when their foraging ranges are constrained, making them very sensitive to local flucations in krill density (Trathan et al., 2006).

Determining the relationship between the number of aggregations and biomass is important. If an aggregation to biomass density-dependent relationship exists then krill predator foraging efficiency may decrease, due to increasing search time. Also, fisheries management strategies need to consider the potential for krill to decrease their spatial range to maintain a consistent number of swarms and density within swarms. This phenomenon is known as the "basin effect", and occurs when the spatial-range and, but not the abundance of a pelagic species collapses (MacCall, 1990). If the basin effect occurred in krill this could be observed through the analysis of krill swarm metrics (*cf* Petitgas et al. 2001).

Should commercial fisheries operate in the same area as krill predators there is the potential for competition between both (Murphy et al., 1997; Reid et al., 2004). Furthermore, descriptors of swarm characteristics could be used in an ecosystem-based approach to fisheries management (see Garcia and Cochranem 2005). Specifically, variation in krill swarm metrics could be used in a model determining the changes in the krill stock to due to exploitation by commercial fisheries, or environmental drivers (Hewitt and Demer, 2000).

2.1.1 Acoustic observations of krill swarms

Acoustic techniques are often used to observe krill (Woodd-Walker et al., 2003). Ship-based active acoustic techniques allow rapid observation of water column targets over a large area. Compared to net samples, acoustic surveys have enabled estimation of mean areal krill density ($\hat{\rho}$), hence biomass, and rapidly, compared to net sampling, provide an indication of the spatial variability of krill distribution (Ricketts et al., 1992). Net samples, however, are still required to validate the criteria for acoustic identification of krill, and to provide the krill length frequency data required to scale the acoustic observations to density (Demer and Hewitt, 1995; Simmonds and MacLennan, 2005). Net samples have also been used to examine the sex and stage-classes of large krill swarms (*cf* Watkins et al. 1992; Watkins and Murray 1998).

Image processing techniques enable the extraction and analysis of a variety of aggregation characteristics of pelagic marine organisms from acoustic data (Reid and Simmonds,

1993). From these techniques quantitative metrics (or continuous variables) of individual fish schools and krill swarms can be extracted, using standardised methods (see Reid et al. 2000a). Metrics of pelagic aggregations have been used to: (1) identify species, for anchovy *Engraulis capensis*), sardine (*Engraulis capensis*) and round herring (*Etrumeus whiteheadi*) see Lawson et al. 2001; (2) characterise aggregations (sardine schools *e.g.* Coetzee 2000) and; (3) determine interactions between pelagic aggregations and the environment *e.g.* Atlantic herring (*Clupea harengus*) see Maravelias et al. 2000). There are also techniques available to correct for acoustic observation bias over varying depth, caused by acoustic beam shape and echosounder ping rate (see Diner 2001).

In addition to estimating krill biomass for fisheries management purposes, acoustic surveys have been conducted in the vicinity of colonies of land-breeding krill predators to access the impact of the variability in krill biomass on predator performance (Hunt et al., 1992a; Veit et al., 1993; Brierley et al., 1997b). Availability of krill has been linked to the reduced breeding success of central placed foraging predators based at Bird Island, South Georgia (54^{o}S 35^{o}W) (Reid and Arnould, 1996; Reid et al., 1997b), with krill scarcity being correlated with a reduction in predator breeding success (Brierley et al., 1997b, 1999b; Reid et al., 2005).

For the last 20 years British Antarctic Survey (BAS) has conducted acoustic surveys at South Georgia, in the vicinity of Bird Island. Bird Island is home to colonies of land-breeding seals and penguins, many of which are dependent on krill as their principle prey item (Brierley et al., 1999b; Croxall et al., 1999). The BAS acoustic surveys have shown a high inter-annual variation in mean krill biomass (Brierley et al., 1997b,a) and spatial distribution (Brierley et al., 2003b). Variability in Antarctic krill biomass poses a significant challenge to predators, by either increasing competition between species (Barlow et al., 2002), forcing adaption of foraging strategy or switching from krill to other prey items (Croxall and Prince, 1997; Croxall et al., 1999). In this investigation swarm metrics were calculated from six acoustic surveys that took place at South Georgia in the 1997, 1998 and 1999 austral summers.

Along transect areal density estimates ($\hat{\rho}$) from 1 to 10 km are typically used in predator-prey interaction studies (*e.g* Harrison et al. 1991; Hunt et al. 1992a). In this investigation, rather than use an arbitrary along transect interval, the krill swarm is the sampling unit, and this approach may provide new insight into krill and krill predator interactions.

2.1.2 Objectives

Hewitt and Demer (2000) stated that there were four main potential deliverables from quantitative krill swarm research: (1) improvement in the reliability of survey designs, to

enable unbiased abundance estimates (McClatchie et al., 1994); (2) defining the prey field in predator-prey studies (*e.g.* Reid et al. 2000b); (3) description of the dominant scale of aggregations, thereby enabling comparisons with potential biotic and abiotic drivers of krill distribution (see Trathan et al. 2003; Genin 2004); and (4) quantitative description of krill swarm metrics to examine variation in patterns within region and with different regions with time (*e.g.* Lascara et al. 1999). The results of this investigation can be used in conjunction with all these research areas, but this Chapter will concentrate on defining the swarm-based prey field and explore inter-survey variation in krill swarm metrics that might have $\hat{\rho}$ or a geographical basis.

2.2 Materials and Methods

The data used in this investigation were collected during multi-disciplinary cruises on-board the *RRS James Clark Ross*, during the 1997, 1998 and 1999 Austral summers (Table 2.1). Net and acoustic data were collected in two study sites, the eastern and western core boxes (ECB and WCB), with ten 80 km long transects in each box (Table 2.1). The transects were orientated perpendicularly to the continental shelf break with a pseudo-random transect separation distance (see Brierley et al. 1997b, Figure 2.1). Two acoustic transects were run each day, during daylight hours, to avoid bias in krill biomass estimates caused by diurnal vertical migration (Demer and Hewitt 1995; Brierley et al. 1999b) and were run moving upstream of the prevailing current to attempt to avoid re-observing persistent krill swarms.

	Western core box				Eastern core box			
Cruise	Start date	End date	length	duration	Start date	End date	length	duration
JR17	29/12/1996	02/01/1997	527.25	26:45	23/12/1996	27/12/1996	556.59	28:17
JR28	24/01/1998	28/02/1998	682.88	37:56	30/01/1998	03/02/1998	664.00	36:37
JR38	02/01/1999	06/01/1999	701.18	38:40	27/12/1998	31/01/1998	678.97	38:45

Table 2.1: Cruise dates, total transect length (km) and survey duration (hh:mm)

2.2.1 Acoustic sampling

Data were collected using a Simrad EK500 scientific echosounder operating 38 and 120 kHz hull mounted (draft = 6m), split-beam transducers. To enable enumeration of krill density, both EK500 frequencies were calibrated, at least once per cruise, in sheltered water sites around South Georgia, using standard sphere techniques (see Foote et al. 1987). The echosounder was configured so that both frequencies pinged simultaneously, once every 2.5 s. Acoustic data were collected to a range of 250 m.

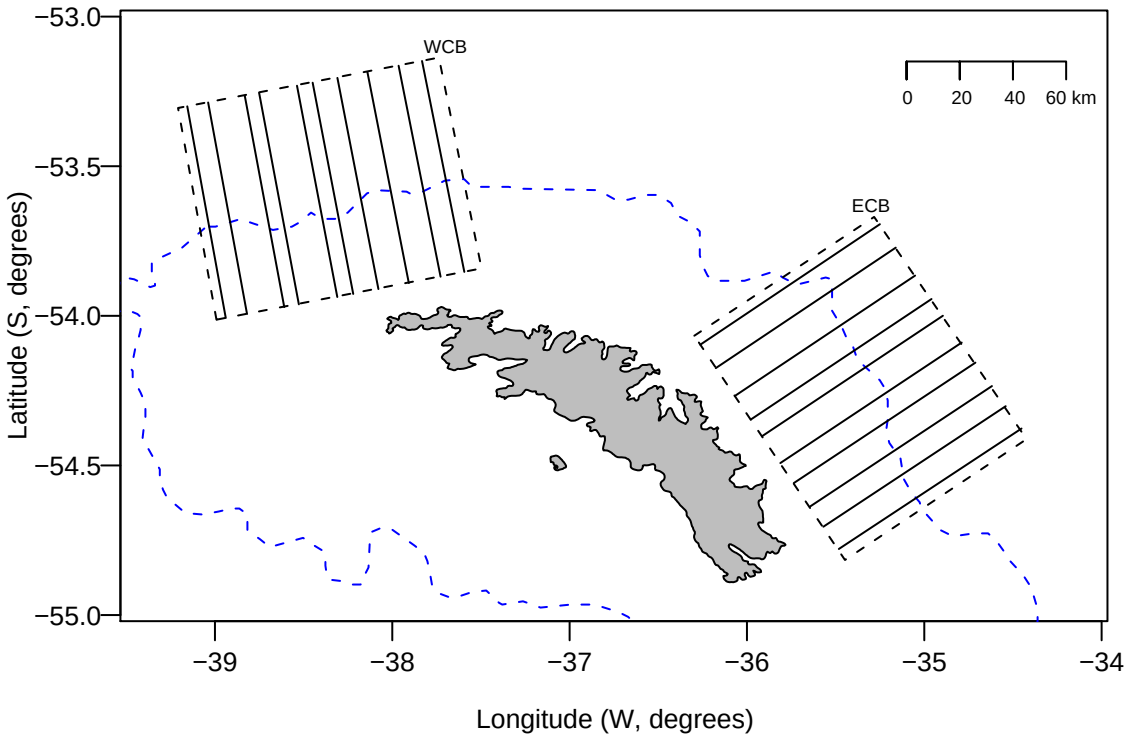

Figure 2.1: The Island of South Georgia, location of British Antarctic Survey multidisciplinary research cruises from the 1996 austral summer. Location of the two study sites (black dotted line). Both sites are 100 km x 80 km , span the continental shelf (500 m isobath, black dashed line), and contain 10 x 80 km line transects (solid black lines), with a pseudo-random spacing (Brierley et al., 1999b).

2.2.2 Net sampling and analysis

Fishing took place at night using a multiple opening and closing, rectangular mid-water trawl 8m^2 (RMT8, see Roe and Shale 1979), with a 4.5 mm mesh. The RMT8 was equipped with three nets, but during double-oblique trawls only two were used. Net samples were sorted immediately onboard with 100 individual krill being sub-sampled from each net. Sub-sampled individuals were measured from the tip of the telson to the front of the eye, giving the length measurement required as an argument for the Morris et al. (1988) length to wet mass relationship.

RMT fishing followed two protocols. Firstly, double-oblique trawls, at fixed stations were carried out. Secondly, target fishing of krill swarms seen on the echograms. The net trajectory was determined relative to the echosounder transducers by using net depth and length of cable out sensors, monitored in real time, and these observations used to calculate the distance of the net behind the echosounder transducers. When combined with ship speed, the distance of net behind transducers was used to determine the time-lag between the net and echosounder transducers, which in turn was used with net depth

to obtain the net position on the echogram during target fishing.

2.2.3 Acoustic processing

Post-processing of acoustic data was carried out using Echoview v3.5 (SonarData, Hobart). The acoustic data were calibrated, then edited to remove returns from the seabed and the transducer nearfield (see Simmonds and MacLennan 2005), surface noise and false-bottom returns. TVG-amplified noise was removed using the technique described by Watkins and Brierley (1996). No statistically significant differences were observed between on and off continental shelf TVG-amplified noise. Samples from both frequencies (38 and 120 kHz) were convolved using a uniform three-by-three moving kernel filter (see Reid and Simmonds 1993). Convolving the data reduced the sampling volume mismatch, increased the signal to noise ratio and reduced the effect of missing pings on krill swarm boundaries.

To reduce sampling volume overlap between adjacent pings, swarms detected at depths greater than 150 m (*cf* Woodd-Walker et al. 2003) were ignored. In addition to making the krill swarms identified here comparable to other studies, a cut off depth of 150 m was also selected because of beam geometry and vessel speed. At 150 m the diameter of the sampling volume was approximately 16.8 m for 38 kHz and 9.5 m for 120 kHz, and was considered a compromise between the average 12.5 inter-ping distance and sampling overlap between adjacent acoustic samples at 150 m. The 150 m cut off depth removed 16% of krill swarms (n=2,959 remained), but only 5% of swarm biomass. Swarms with a relative school length image compared to the beam width (Nb) of less than 1.5 were also excluded from the analysis (see Diner 2001), which resulted in 2 swarms being removed.

Krill swarm detection took place in three steps. Firstly, the acoustic data were prepared for the school detection algorithm. Secondly, sensitivity analysis carried out of krill swarm algorithm detection parameters. Thirdly, selected detection parameters were used to extract krill swarm data for all available transects.

Automated aggregation detection

The "Schools" module of Echoview v3.5 software package was used to detect pelagic aggregations in convolved 120 kHz echograms. This module is based on the Shoal Analysis and Patch Estimation System (SHAPES, see Barange 1994). The SHAPES algorithm assesses acoustic data as a matrix of S_v observations. The user selects a processing threshold, and elements in the array above this are assessed by the algorithm in a three stage process. Firstly, candidate swarms are identified, these are elements in the S_v matrix that exceed the processing threshold, are adjacent and the length and height of the group exceed

minimum values of minimum candidate length and minimum candidate height SHAPES algorithm parameters. Spatial discontinuities within a school, which potentially give the appearance of multiple schools, where only one exists, are compensated using the vertical and horizontal linking distances. The SHAPES parameters, maximum horizontal linking distance and maximum vertical linking distance define a search area, which is a search ellipse that is moved around the boundary of each candidate school in turn. Where another candidate school falls within the search ellipse the current candidate school boundary is extended to encompass both candidate schools i.e. it is assumed that both candidate schools are a single school. Finally the total minimum height and length SHAPES algorithms are used to select only candidate schools, or linked candidate schools with dimensions that exceed these parameters. For further details of SHAPES (see Barange 1994; Coetzee 2000).

Prior to running the SHAPES algorithm on the full three years of data a sensitivity analysis of the number of detected krill swarms for a range of SHAPES algorithm parameters for the selected transects was undertaken. The purpose of this was two fold. Firstly, to determine the variation in swarm position, morphological and energetic parameters with respect to the swarm detection parameters. Secondly to define, for the purposes of this research, a krill swarm.

Not all acoustically detected aggregations were necessarily krill. The acoustic data were partitioned using the dB difference technique, under which krill aggregations were identified as aggregations falling in the 2 to 12 dB range for S_v 120-$S - v$ 38 kHz (see Madureira et al. 1993; Brierley et al. 1997b). The dB difference was evaluated for all S_v data within the krill swarm boundaries identified from the 120 kHz convoluted acoustic data, with these boundaries being applied to the 38 kHz convoluted acoustic data, giving two acoustic samples for the dB difference technique.

Swarm descriptors

Once swarms of krill had been identified, krill swarm metrics (Table 2.2) were obtained, again using the Echoview "Schools" module. Corrections to swarm geometry as derived by Diner (2001) were applied to swarm morphology. Krill swarm mean S_v values ($S_v = 10log_{10}(s_v)$) were converted to volumetric krill density (ρ_v) using a TS scale factor calculated from the frequency-distribution of krill caught in the RMT8 ($\hat{\pi}_l$) the Demer and Conti (2005) individual krill theoretical target strength model (σ_{bs}, in the linear domain) and the Morris et al. (1988) length to wetmass relationship (w), giving:

$$k = \frac{w(\hat{\pi}_l)}{\sigma_{bs}(\hat{\pi}_l)} \tag{2.1}$$

and

$$p_v = s_v k \tag{2.2}$$

To enable comparison between swarms, the p_v was standardised by corrected swarm length (L_c) divided by 1000 m. This gave a metric describing the contribution made by an individual krill swarm to the overall survey area biomass.

$$p_{vc} = p_v \times \frac{L_c}{1000} \tag{2.3}$$

2.2.4 Statistical analysis

Initially the frequency distribution of all krill swarm metric variables was determined, and it became apparent that all krill swarm metrics considered had a unimodal distribution, the majority being right-skewed. Three statistical approaches for the analysis of krill swarms were adopted. Firstly, the differences in swarm metrics between core boxes and years were determined: the frequency distributions of krill swarm metrics were non-normal, Kruskal-Wallis tests were used with Bonferroni correction (Legendre and Legendre, 1998). Secondly, the empirical cumulative frequency distribution (ECFD) of krill swarm p_vs were determined for each year and core box. Differences in between-survey ECFDs were identified using the KolmogorovSmirnov test, again corrected for multiple testing. This was carried out to determine if krill maintain consistent krill swarm characteristics irrespective of changes in the overall krill biomass that were observed between year and box. It was also carried out because of the high variability in mean areal krill density that occurs between surveys in both core boxes at South Georgia (Brierley et al., 1999b).

Finally, evidence for the existence of discrete swarm types (as opposed to a continuum of swarms) was tested. Krill swarm types were determined using partition analysis that was carried out on the results of the principle component analysis (Johnson, 1998). Three swarm types were selected for the partition analysis. These were based on the Miller and Hampton (1989); Hamner and Hamner (2000) three-swarm classification: (1) dense swarm type containing 1,000 to 100,000 krill/m^3; (2) intermediate density swarm type from 1 to 100 krill/m^3 and; (3) low 0.1 to 1 krill/m^3 swarm type.

Type	Name	Symbol	units	
E	Mean volume backscatter	S_v	dB re 1 m^2/m^3	-
E	Nautical area backscattering coefficient	NASC	m^2/n.mi^2	-
E	Minimum volume backscatter	S_v	dB re 1 m^2/m^3	-
E	Maximum volume backscatter	S_v	dB re 1 m^2/m^3	-
M	Mean height	H	m	-
P	Mean swarm depth	z_s	m	-
P	Latitude and Longitude	(φ, λ)	^{o}	
M	Corrected length	L_c	m	see Diner 2001
M	Corrected perimeter	P_c	m	see Diner 2001
M	Corrected area	A_c	m^2	see Diner 2001
M	Image compactness	IC	-	$IC = P_c^2/(4\pi A_c)$
E	Horizontal roughness coefficient	R_H	-	$R_H = \frac{1}{\bar{s}_v(n_h-1)} \sum_i^{n_h-1}(s_{vj} - s_{vj+1})$
E	Vertical roughness coefficient	R_V	-	$R_V = \frac{1}{\bar{s}_v(n_v-1)} \sum_i^{n_v-1}(s_{vj} - s_{vj+1})$
P	Distance to shore	d_s	km	Distance to closest point of land at South Georgia
P	Distance to 500 m isobath	d_{iso}	km	Distance to continental shelf break (500 m isobath)
P	Time of day	t	-	standardised time of day
M	Fractal dimension	F_d	-	see Nero and Magnuson (1989)
M	Unevenness	U	-	see Weill et al. (1993)
M	Rectangularity	R_t	-	see Scalabrin and Mass (1993)
E	Volumetric density	ρ_v	-	see Section 2.2.3
M	Length/Height ratio	l/h -	-	
P	Horizontal NND	NND_h	km	nearest neighbour distance
P	Vertical NND	NND_v	m	-
P	Seabed depth	z	m	-
E	dB difference	dBdiff	dB re m^2/m^3	120-38 kHz

Table 2.2: Krill swarm descriptive metrics. E = energetic; M = Morphological; P = Position. Linear mean volume backscatter $\bar{S}_v = mean[10log_{10}(s_v)]$; number of samples in a given swarm is n_x, in either the horizontal h, or vertical v dimensions.

2.3 Results

Prior to undertaking the krill swarm analysis, it was necessary to determine the most appropriate parameters used in the SHAPES algorithm. These parameters are important because they allow a quantitative definition of a krill swarm to adopt within this research, and perhaps beyond. This approach enabled objective, consistent, identification of krill swarms, between surveys. Initially the affect of processing-threshold was assessed (Figure 2.3). Sensitivity analysis showed that the number of detected swarms (N_d) with variation in processing threshold (S_vt) exhibited a sigmoidal relationship. N_d was consistent between S_vt= -65 to -75 dB and -95 to -100 dB, with the lower threshold being at the limit of the EK500 acoustic sensitivity. It is unclear from Figure 2.3 which processing threshold should be selected, consequently -80 dB was selected to allow comparison with the Woodd-Walker et al. (2003) krill swarm study.

A unit change in SHAPES parameter distance does not elicit the same change in the number of detected swarms for all SHAPES parameters (Figure 2.3). The horizontal linking distance shows a minimum N_d at 80 m, so this was selected and equates to a six ping inter-candidate swarm spacing. The N_d swarms had low variation with maximum vertical linking distance, consequently 10 m was selected. The smallest potential krill swarm was selected as 30 m horizontally, two or three pings, since there is a linear decrease in N_d after a distance of 35 m. The minimum candidate height of 10 m was selected since the decrease in N_d tended towards linearity after 10 m. The total minimum height of 10 m was chosen to enable all individual swarms with minimum height of 10 m to be retained by the SHAPES algorithm. This height is consistent with the recommendations for acoustic krill identification given in Watkins and Brierley (2002) of a 10 m deep integration interval. A 40 m minimum horizontal linking distance was selected since the number of detected swarms decreased at distances greater than 40 m. These SHAPES distances are summerised in Table 2.3.

Schools detection parameter	value
Minimum total school length	30 m
Minimum total school height	10 m
Minimum candidate length	30 m
Minimum candidate height	10 m
Maximum vertical linking distance	10 m
Maximum horizontal linking distance	40 m
Data threshold setting	-80 dB

Table 2.3: Selected Shoal Analysis and Patch Estimation System (SHAPES, see Barange 1994) detection parameters and threshold value for krill swarm detection.

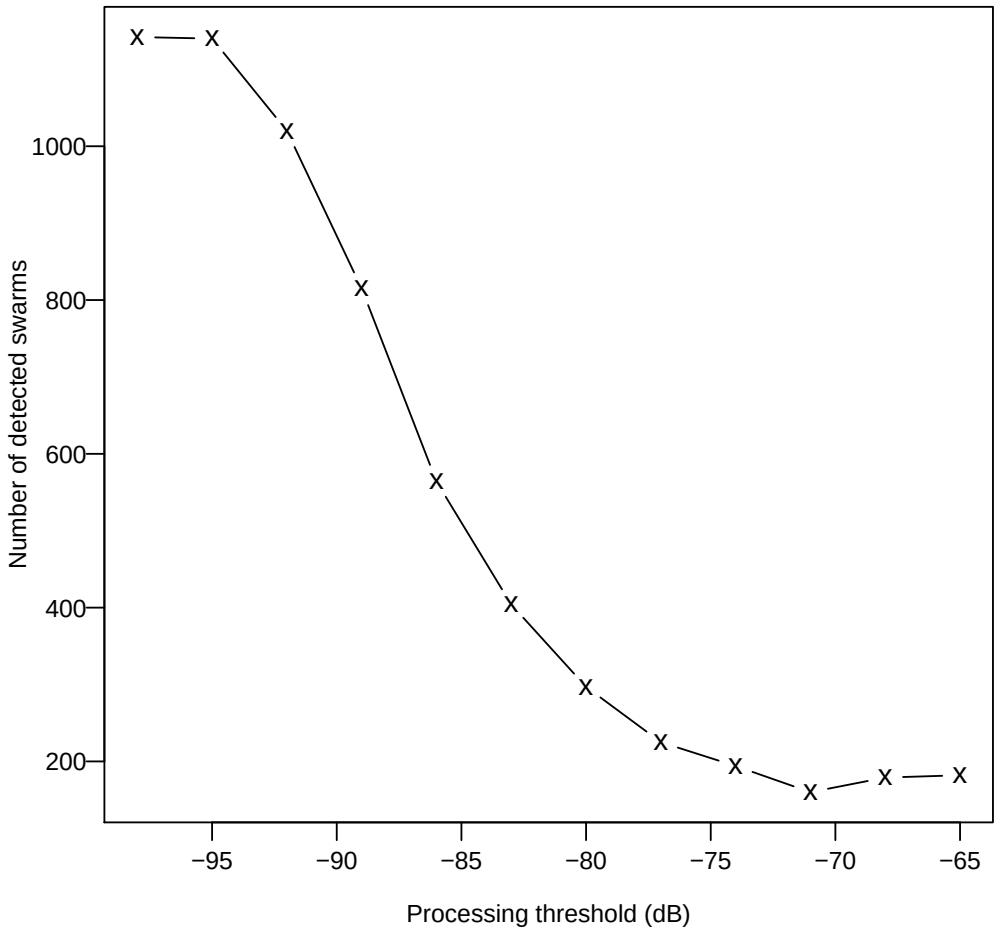

Figure 2.2: Variation in the total number of detected krill swarms (identified using the procedure in Section 2.2.3) across 12 randomly selected transects caused by changes in the threshold sensitivity (S_{vt}). Included swarms are limited to those with mean ranges less than 150 m, with a mean length greater than 10 m and height greater than 3 m.

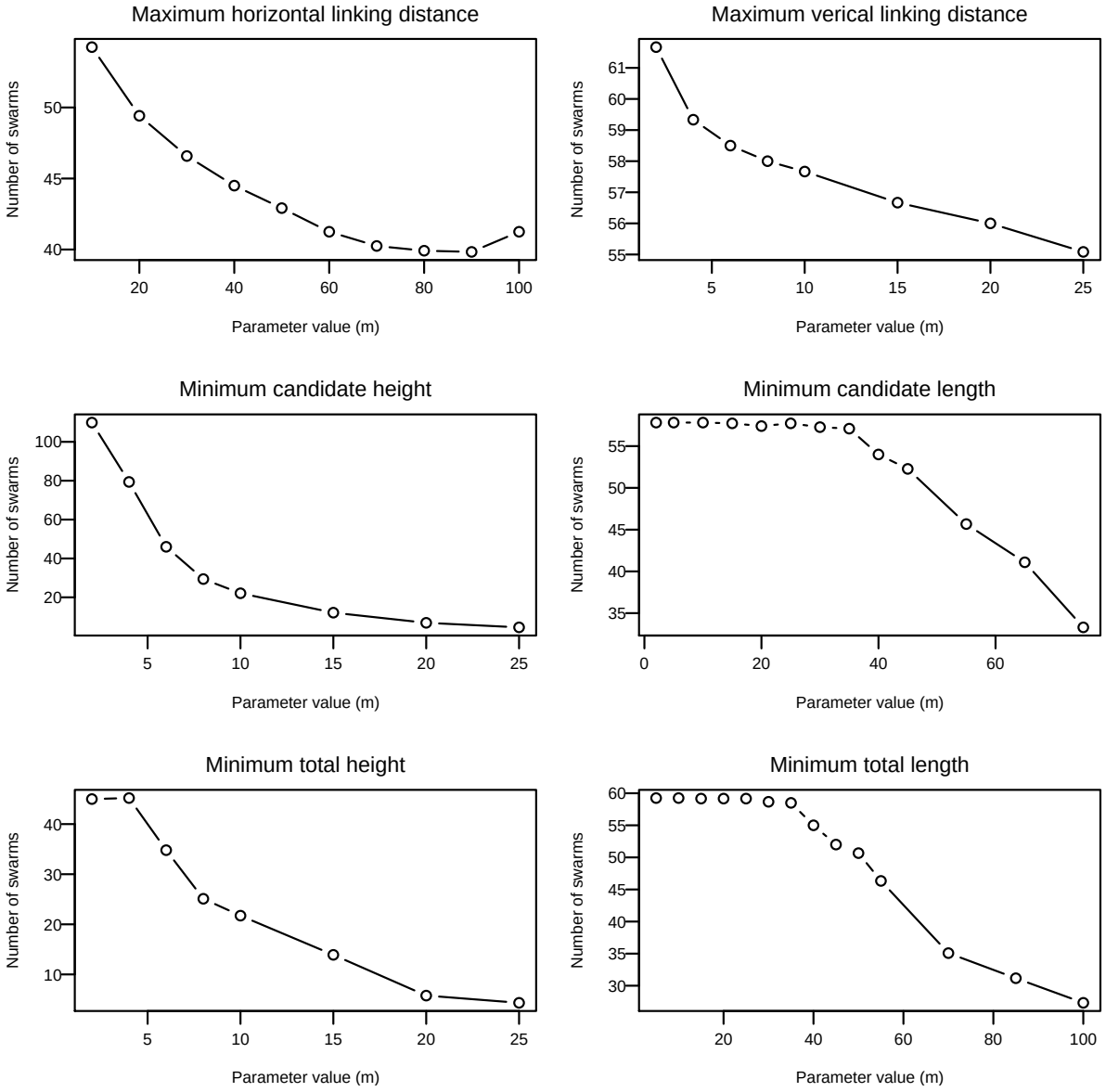

Figure 2.3: Changes in the number of detected krill swarms with variation in the SHAPES detection parameters. Note the different y-axis scales.

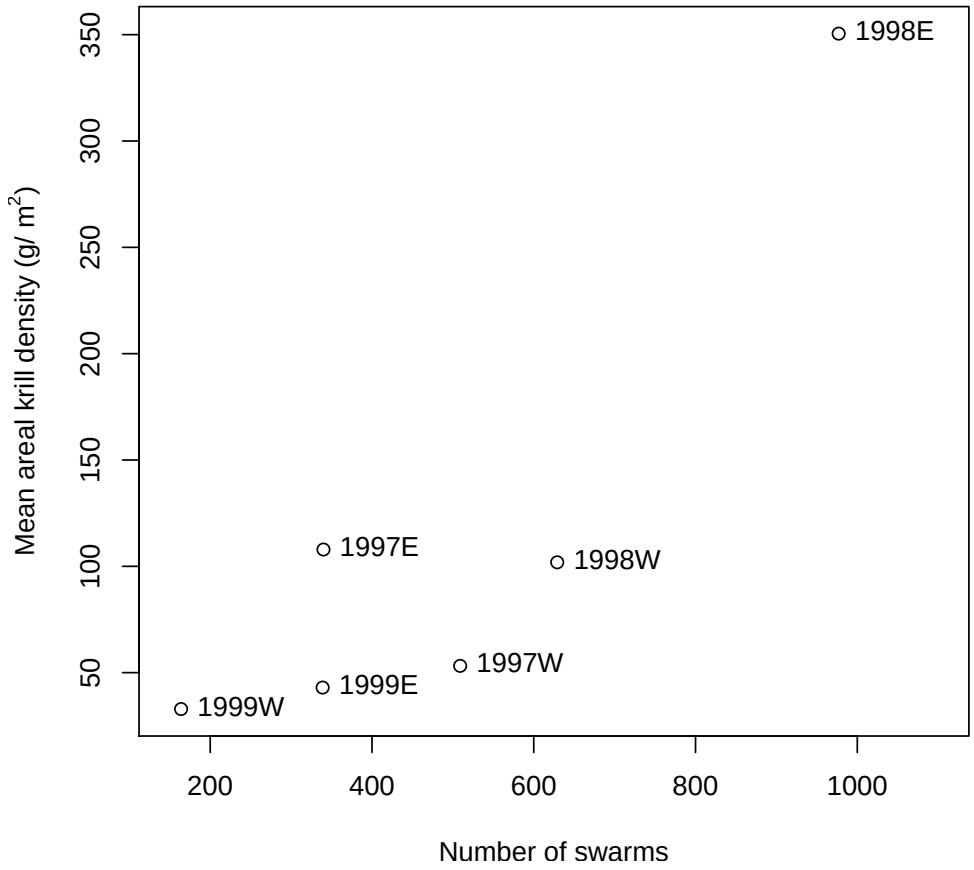

Figure 2.4: The relationship between number of detected krill swarms and mean areal krill density ($\hat{\rho}$) calculated using the Demer and Conti (2005) krill TS model and Jolly and Hampton (1990) $\hat{\rho}$ technique.

2.3.1 Krill swarm summary

Across the six surveys 2958 krill swarms were detected. Krill swarms had a higher density in the ECB, with krill swarms in the 1998 austral summer being on average an order of magnitude higher in the ECB (Table 2.6). The krill swarms were of a similar height between surveys, but because krill swarm lengths were longer in the WCB, they also had a larger length/height ratio. Krill swarms had a larger inter-swarm nearest neighbour distance (NND) in the WCB (Table 2.6), which is not simply a function of the number of krill swarms because the number of swarms was comparable between boxes within year. Also, there is strong correlation between mean areal krill density and the number of krill swarms in a core box ($r = 0.88$, $p = 0.02$, 95% C.I.= 0.24 to 0.99, Figure 2.4).

Metric	Western core box 1997	Western core box 1998	Western core box 1999	Eastern core box 1997	Eastern core box 1998	Eastern core box 1999	χ^2
Number of swarms	509	629	164	340	977	339	
Encounter rate (n/l)	0.64	0.30	0.20	0.44	1.20	0.43	
Survey area areal density (g/m^2, $\hat{\rho}$)	53.2(0.20)	101.9(0.12)	32.9(0.22)	107.9(0.12)	350.5(0.15)	43.0(0.37)	
Mean Sv (dB re 1 m^2/m^3)	-72.23(0.1)	-72.5(0.09)	-74.59(0.05)	-56.89(0.17)	-63.8(0.16)	-74.35(0.08)	914.02
NASC (m^2/nmi^2)	501.46(4.35)	221.98(4.21)	79.21(5.39)	4,800.68(1.64)	1,776.75(2.33)	289.16(8.46)	814.56
Maximum Sv (dB re 1 m^2/m^3)	-65.93(0.13)	-65.35(0.13)	-65.61(0.14)	-49.36(0.22)	-54.82(0.23)	-67.27(0.13)	749.03
Minimum Sv (dB re 1 m^2/m^3)	-82.58(0.04)	-83.32(0.06)	-85.53(0.05)	-80.61(0.04)	-82.67(0.05)	-84.49(0.05)	407.82
Mean height (m)	10.22(0.75)	9.92(0.64)	12.87(1.11)	11.77(0.45)	11.32(0.61)	10.13(0.71)	119.18
Mean depth (m)	67.8(0.67)	59.0(0.68)	63.7(0.59)	67.9(0.72)	67.9(0.64)	73.1(0.65)	38.90
Latitude (dd.dd)	-51.5(0.9)	-48.69(1.49)	-53.6(0)	-54.28(0)	-51.02(1.14)	-54.32(0)	2,054.80
Longitude (dd.dd)	-36.35(1.26)	-33.51(2.13)	-38.33(0.01)	-35.32(0.01)	-32.23(1.77)	-35.36(0.01)	2,190.63
Corrected length (m)	513.17(1.86)	622.39(2.08)	2733.91(2.39)	203.73(2.52)	475.72(2.66)	920.05(2)	353.76
Corrected perimeter (m)	2,138.47(2.38)	2,651.39(2.58)	16,573.09(2.65)	584.32(2.43)	1,851.75(2.73)	5,856.54(2.91)	452.41
Corrected area (m^2)	7,270.29(3.33)	10,234.49(3.94)	92,985.06(3.07)	2,492.6(3.54)	8,407.3(5.2)	16,314.99(4.06)	162.49
Image compactness	67.15(1.76)	69.26(1.73)	349.13(1.87)	15.75(2.36)	48.27(1.9)	204.42(1.87)	669.35
Distance to shore (km)	60.71(2.36)	59.08(3.76)	47.56(0.45)	51.10(0.48)	58.32(3.06)	45.71(0.43)	74.92
Distance to 500 m isobath (km)	18.78(0.63)	17.76(0.62)	18.08(0.73)	19.90(0.58)	18.02(0.6)	16.60(0.73)	112.84
Fractal dimension	1.4(0.1)	1.4(0.09)	1.53(0.06)	1.23(0.11)	1.35(0.1)	1.52(0.08)	835.67
Unevenness	1.64(0.39)	1.63(0.38)	2.28(0.5)	1.22(0.27)	1.58(0.39)	2.37(0.41)	576.54
Rectangularity	2.25(0.42)	2.48(0.43)	2.83(0.3)	1.73(0.45)	2.26(0.42)	2.68(0.35)	335.34
Volumetric density (g/m^3)	8.64(4.25)	3.32(4.41)	1.17(7.1)	104(1.67)	34.02(2.15)	4.39(5.64)	814.68
Length/Height ratio	21.34(1.01)	20.86(1.03)	46.08(1.22)	9.75(1.34)	14.94(1.1)	28.28(1.03)	409.78
Horizontal NND (km)	7.11(20.86)	16.31(14.08)	1.06(1.33)	0.8(1.74)	10.46(17.49)	0.61(0.97)	193.37
Vertical NND (m)	1.43(1.76)	1.11(1.37)	1.83(1.15)	2.27(1.87)	0.75(1.47)	1.49(1.9)	137.75
Seabed depth (m)	365.92(0.40)	290.00(0.46)	340.21(0.46)	355.77(0.56)	341.06(0.61)	336.97(0.59)	86.31
dB difference 120-38 kHz (dB re 1 m^2/m^3)	7.15(0.38)	8.87(0.26)	7.16(0.41)	7.93(0.28)	7.77(0.34)	7.28(0.4)	154.84

Table 2.4: Mean and coefficient of variation (0.10 = 10%) for krill swarms detected between 1997 to 1999 in the western and eastern core boxes. Mean area areal density ($\hat{\rho}$) and variance estimates were calculated using the Jolly and Hampton (1990) technique, see Brierley et al. 1999b. Note χ^2 values are from Kruskal-Wallis test, the results of which show all parameters are significantly different between surveys at $p < 0.05$ with Bonferroni correction.

The spatial distribution of krill swarms in terms of number per km (encounter rate) shows considerable inter-survey and inter-annual variation (Figure 2.5). From visual inspection of these plots, and formal spatial autocorrelation tests (lagged by per km transect interval), there is no evidence of swarm spatial clumping occurring in any of the surveys. Nor are there any regions that swarms are absent within a particular survey, which is important for predator foraging. Also, these data do not suggest an increase in the number of swarms in the vicinity of the continental shelf break, the 500 m isobath (blue dashed line, Figure 2.5), but there does appear to be an increase in krill swarm encounter rate at the transect ends closest to land.

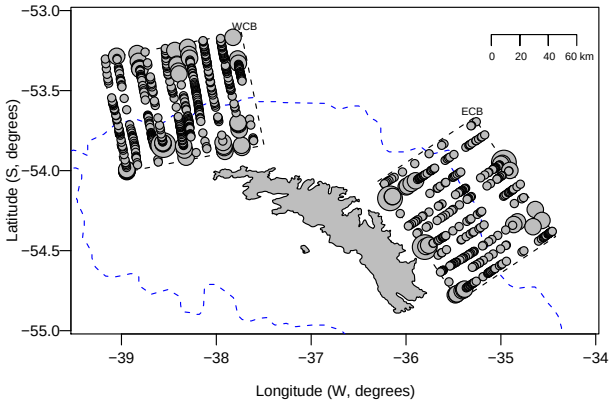

(a) 1997 (JR-17)

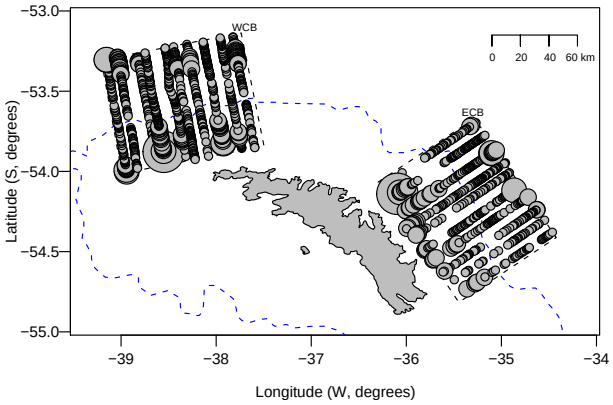

(b) 1998 (JR-28)

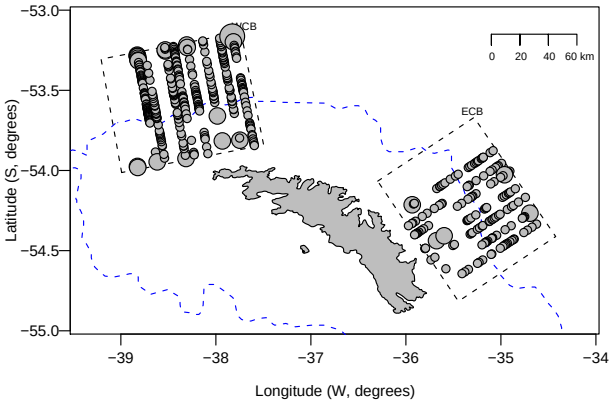

(c) 1999 (JR-38)

Figure 2.5: The spatial distribution of krill swarm abundance at South Georgia for the three years of surveying. The area of each circle is proportional to the abundance of krill swarms in 1 km along transect intervals. The 500 m isobath is shown as a grey dashed line and the core box boundaries as black dotted lines. Note more than 50% of the pings in transects one and two were missing, due to bad weather, so were dropped from the analysis.

	JR17E	JR28W	JR28E	JR38W	JR38E
JR17W	**D = 0.59** ***p*< 2.2e^{-16}**	D = 0.10 p = 0.01	**D = 0.37** ***p*< 2.2e^{-16}**	D = 0.13 p = 0.04	D = 0.06 p= 0.42
JR17E	- -	**D = 0.59** ***p*< 2.2e^{-16}**	**D = 0.25** ***p*=3.0e^{-14}**	D =**0.50** ***p*< 2.2e^{-16}**	**D = 0.6**1 ***p*< 2.2e^{-16}**
JR28W	- -	- -	**D= 0.37** ***p*< 2.2e^{-16}**	**D = 0.18** ***p*=3.8^{e-4}**	D = 0.13 p= 1.2^{e-3}
JR28E	- -	- -	- -	**D = 0.27** ***p*< 2.48e^{-9}**	**D= 0.37** ***p*=2.2e^{-16}**
JR38W	- -	- -	- -	- -	D = 0.12 p = 0.11

Table 2.5: Between survey Kolmogorov-Smirnov tests for differences in the ECDF of scaled volumetric krill density (ρ_{vs}). Bonferroni correction applied to the 5% significance level (p=0.05) corrected for 15 tests, giving p <3.33e^{-3}, that are shown in bold.

2.3.2 Variation in krill swarm density

The scaled krill swarm volumetric density (ρ_{vs},Equation 2.3) showed significant between survey variation (Table 2.5). Of particular interest are surveys JR17E in 1997 and JR28E in 1998 that were both significantly different to other surveys and each other, had the second and first highest $\hat{\rho}$ (Table 2.6), suggesting that the biomass of swarms ρ_{vs} is distributed differently in these years. In 1999, a low $\hat{\rho}$ year the EDCF of ρ_{vs} in JR38E was similar to WCB surveys. These results and the strong correlation (Figure 2.4) between the number of swarms and $\hat{\rho}$ suggest that there is inter-survey variation between krill swarms and some dependence between krill swarm structure and $\hat{\rho}$.

2.3.3 Krill swarm type classification

The first three principle components (PC) explained 22.8%, 18.3% and 9.5% of the variability in the krill swarm metrics. Using Mardia's criterion (Johnson, 1998), metrics that contribute to the highest variability in PC1 were energetic measurements, such as S_v, the roughness coefficients, and volumetric density, that all have the same direction and similar magnitudes (Table 5.4). Krill swarm morphological metrics (Table 2.2) also contributed to PC1: again all morphological metrics are in the same direction, opposite to the energetic metrics, and of similar magnitudes. The pattern in eigen values in PC2 is less clear, all significant eigen values are positive, and are a mix of energetic and morphological metrics, but excludes all position metrics. PC3 is dominated by the environmental metrics: seabed depth and distances to 500 m isobath and South Georgia. Interestingly, no positional metrics were significant in the first three PCs. To summarise each PC and variance explained:

- PC1: energetic and morphological metrics, operating in different directions (23%).
- PC2: energetic and morphological metrics, operating in the same direction (18%).
- PC3: Environmental metrics, seabed depth and distances to continental shelf and South Georgia (10%).

The results suggest that energetic and morphological metrics dominate the variability in krill swarms, and compared to this variability, position metrics, including nearest neighbour distance, contribute little to the overall krill swarm variability. Following Mauchline (1980); Hamner and Hamner (2000) the PC results were used to split the krill swarms into three partition groups, and further inspection was conducted to examine the split in krill swarm type by survey (Table 2.7).

Variable	PC1	PC2	PC3
% variation explained	22.8	18.3	9.5
cumulative % variation	22.8	41.2	50.7
Mardia's criterion	0.21	0.22	0.39
Mean Sv (dB re 1 m^{-1})	**-0.3**	**0.25**	
NASC (m^2/nmi^2)	**-0.24**	**0.23**	
Maximum Sv (dB re 1 m^{-1})	**-0.23**	**0.31**	
Minimum Sv (dB re 1 m^{-1})	-0.2	-0.13	
Mean height (m)		**0.29**	-0.1
Mean depth (m)			
Latitude (dd.dd)	0.15	-0.14	-0.25
Longitude (dd.dd)	-0.14	0.11	
Corrected length (m)	**0.26**	**0.31**	
Corrected perimeter (m)	**0.26**	**0.32**	
Corrected area (m^2)	**0.23**	**0.31**	
Image compactness	**0.28**	**0.29**	
Horizontal roughness coefficient	**-0.23**	**0.27**	
Vertical roughness coefficient	**-0.22**	**0.26**	
Distance to shore (km)			**-0.56**
Distance to 500 m isobath (km)			**0.55**
Time of day			
Fractal dimension (Nero and Magnuson, 1989)	**0.29**		0.13
Unevenness (Weill et al., 1993)	**0.24**	0.13	
Rectangularity (Scalabrin and Mass, 1993)	0.21		0.13
Volumetric density (kg/m^3)	**-0.26**	**0.22**	
Length/Height ratio	**0.26**	0.18	
Horizontal NND (km)			
Vertical NND (m)			
Seabed depth (m)		-0.08	**-0.44**
dB difference 120-38 kHz (dB re 1 m^{-1})			0.12

Table 2.6: The first three principal components of krill swarm metrics. Principal component analysis was performed on the normalised correlation matrix of continuous krill swarm metrics (Table). Swarm metrics with a significant influence on an individual principal component (j) are highlighted. Significant influence determined by eigenvector elements (u_{ij}) that have a value greater than Mardia's criterion ($u_{ij} > 0.7max(|u_j|)$). Eigenvector elements <0.1 are not shown.

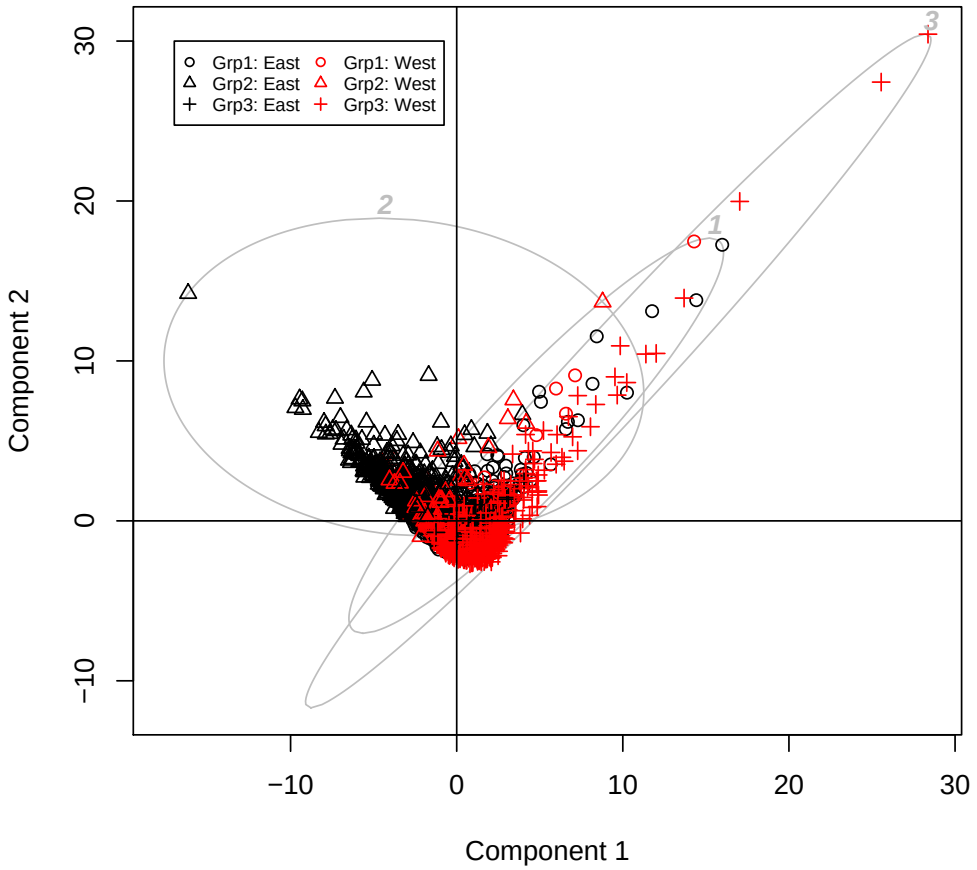

Figure 2.6: The three krill swarm class partition analysis displayed in reduced space: x-axis principle component 1, y-axis principle component 2. Partition group size shown as grey ellipses, numbered by group membership. Each krill swarm observation is colour coded by core box and symbol is by group membership.

Krill swarm type

Krill swarm type was determined by partition analysis. On the PC1 and PC2 component planes there was overlap between krill swarm type group one and three, but swarm type two showed distinct separation (Figure 2.6). Also in the PC1 and PC2 plane there appears to be considerable separation between swarms in the WCB and those in the ECB, although the source of these differences are unclear from Figure 2.6. This core box difference is marked for type two swarms in the ECB.

Examination of PC planes 1 to 3 and 2 to 3 show some separation between swarm types, but overlap remains (Figure 2.7). It is apparent that type three swarms in the WCB have the highest variability. Membership of the three krill swarm type groups was uneven. Groups one and three contained a similar number of swarms 1,117 and 1,173 respectively, whilst group two contained 669 swarms (Table 2.7). Differences between swarm type energetic measurements showed that type two swarms were 50 times more dense than the other swarm types, and the large coefficient of variation (CV) showed

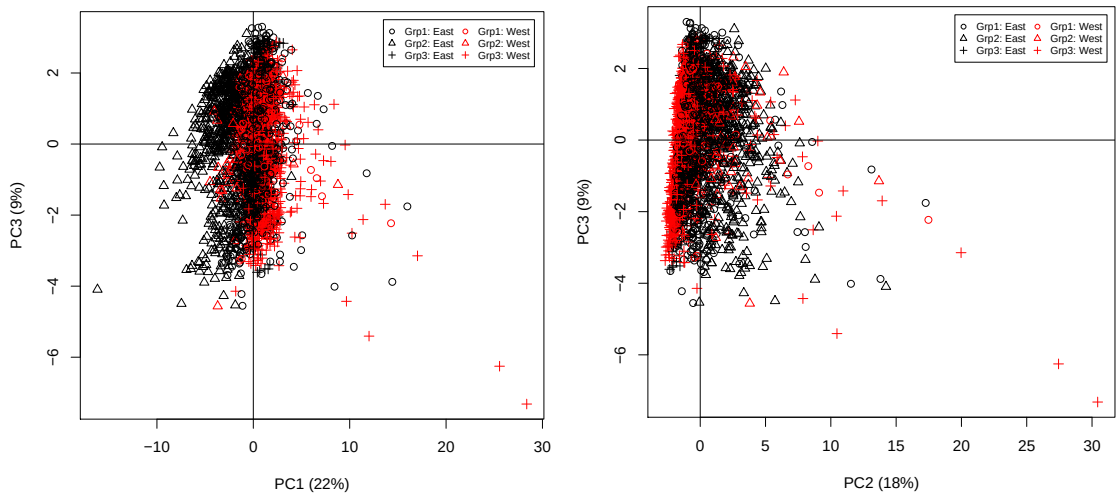

(a) PC1 and PC3 plane

(b) PC2 and PC3 plane

Figure 2.7: Krill swarm type determined by partition analysis. Results are displayed on the reduced factorial planes between paries of principle components. Each swarm observation is colour coded by box and group membership.

that krill density varied widely within swarm type group. Swarm morphology also varied between groups, with type two swarms being taller, and shorter that the other groups. This gave type two swarms a larger length/height ratio and a smaller corrected area. Finally, type two swarms were on average found at shallower depths, in shallower seabed areas, that were closer to the shore. To summerise the three swarm types:

- Type one swarms: low density, intermediate size, found in deeper water, furthest from the shore.
- Type two swarms: denser, smaller swarms, found in shallower water and closer to the shore.
- Type three swarms: lowest density, largest size.

The proportion of swarm types found in each survey showed that the WCB had a consistent proportion of krill swarm types (Table 2.8, Figure 2.8). The picture was different in the ECB, with the 1997 and 1998 surveys having consistent proportion of krill swarm types. In 1999 the ECB krill swarm type proportions changed, with the small, dense type two swarms making up on 3% of the swarm types, while the proportions of type one swarms increased to 84%. During 1997 and 1998 in the ECB the type two swarms were predominantly found on shelf, whilst the other types were roughly evenly distributed between on and off shelf waters. This approximately even split is the same for type one and three swarms in the WCB (Table 2.8, Figure 2.8).

The spatial distribution of krill swarm types for each survey (Figure 2.8) shows that there is large variation between surveys. The generally lower $\hat{\rho}$ in the WCB is shown by

Swarm metric	Group 1	Group 2	Group 3
Number of swarms	1,117	669	1,172
Mean S_v (dB re $1m^{-1}$)	-71.94 (0.09)	-53.11(0.09)	-74.17(0.05)
Mean height (m)	10.85 (0.48)	12.75(0.48)	9.21(0.71)
Mean depth (m)	103.28 (0.62)	62.97(0.62)	87.26(0.67)
Corrected length (m)	672.13 (2.2)	311.55(2.2)	832.71(3.16)
Corrected area (m^2)	13,708.59 (3.35)	5,041.14(3.35)	16,947.62(6.18)
Distance to shore (km)	54,074.23 (0.53)	38,621.72(0.53)	47,363.81(0.44)
Fractal dimension (Nero and Magnuson, 1989)	1.43 (0.1)	1.25(0.1)	1.43(0.09)
Volumetric density (g/m^3)	2.14 (1.3)	92.95(1.3)	0.62(2.33)
length/Height ratio	20.04 (1.11)	10.45(1.11)	26.09(1.14)
Seabed depth (m)	382.14 (0.55)	282.65(0.55)	316.56(0.44)

Table 2.7: Mean of krill swarm metrics for each of the three-partition krill swarm types. Coefficient of variation (CV) is given in brackets 10%=0.1. These results were obtained using the entire krill swarm data set.

	Western core box			Eastern core box		
Swarm type	1	2	3	1	2	3
1997	7 (2.4, 4.6)	6 (5.5, 0.5)	87 (32.9, 54.1)	44 (20.3, 23.7)	55 (40.2, 14.8)	1 (1, 0)
1998	8 (6.7, 1.3)	6 (5.4, 0.6)	86 (53, 33)	52 (32.3, 19.8)	41 (34, 7)	7 (2.7, 4.3)
1999	12 (8.3, 3.7)	1 (0.5,0.5)	87 (37.5, 49.5)	84 (37.5, 46.5)	3 (2.1, 0.9)	13 (11.4, 1.6)

Table 2.8: Percentage of krill swarm type found within a survey. The brackets give the percentage, again within a survey, of a swarm type that occur (on shelf, off shelf).

Swarm type	On-shelf	Off-shelf
1	46.9	53.1
2	80.9	19.1
3	51.2	48.8

Table 2.9: Percentage of krill swarm types split by on and off shelf continental shelf.

the reduced number of swarms with larger ρ_{vs}. There are few type two swarms in the WCB (Table 2.8), but these swarms contribute a disproportionately high ρ_{vs} to the WCB $\hat{\rho}$. Also, the higher density swarms in the WCB are generally located on the continental shelf. In 1999, a year with low $\hat{\rho}$, there is a reduced number of swarms in the WCB, with much of the ρ_{vs} coming from type one and two swarms.

In the ECB during 1997 and 1998 swarm biomass was dominated by high density, type two swarms (Tables 2.7 and 2.8). There were few low density, type three swarms in the ECB (Table 2.8) during 1997 and 1998. Also, high density swarms were more evenly distributed throughout the ECB compared to the WCB. During 1999 in the ECB, also a low $\hat{\rho}$, there were few type two swarms, but these contributed considerably to the overall biomass.

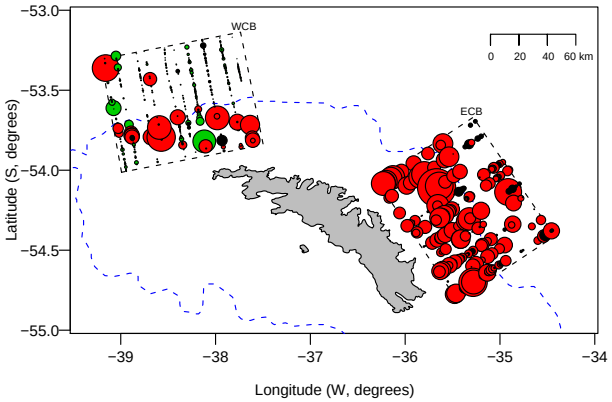

(a) 1997 (JR-17)

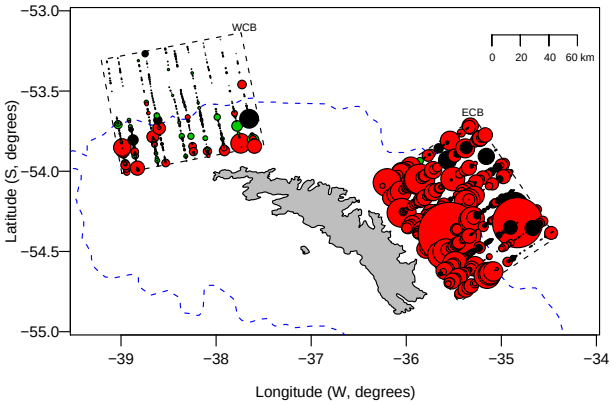

(b) 1998 (JR-28)

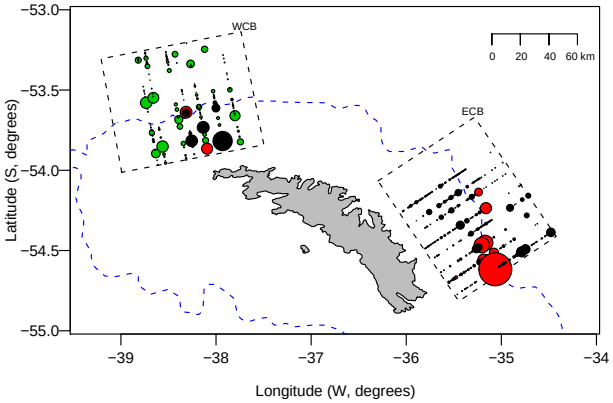

(c) 1999 (JR-38)

Figure 2.8: Locations of the three swarm types determined by partition analysis (type 1 black; type 2 red; type 3 green). Area of circle is proportional to scaled swarm density (ρ_{vs}) with a constant scale across surveys.

2.4 Discussion

Using the SHAPES algorithm enabled the objective identification of krill swarms across six surveys. The results of this identification have shown that there was considerable variation in both the number of krill swarms and swarm characteristics between surveys (Table 2.6). Further, there was strong correlation between the number of detected krill swarms (n_s) and mean areal krill density ($\hat{\rho}$). Also, evidence of spatial segregation of krill swarm type by site and on-off shelf was apparent (Figure 2.8).

2.4.1 Defining a krill swarm

It was not an objective of this research to define what a generic krill swarm is. Rather, this investigation used objective krill swarm identification that enabled inter-annual and inter-site comparisons to be made, by using consistent criteria to identify krill swarms. Since this investigation did not seek to define what a krill swarm is, the choice of SHAPES parameters is not of fundamental importance to this study. However, the SHAPES parameters did have to be biologically plausible. In the case of the height parameters a minimum height of 10 m was selected because this was the minimum integration cell height recommended by Watkins and Brierley (2002) to identify krill. The choice of horizontal distances was less clear, but certainly in the case of the minimum candidate distance and minimum total length distances of greater than 40 m reduced the number of detected krill swarms (Figure 2.3). This result suggests that the minimum swarm length, during the three years of surveying, was approximately 40 m. The horizontal linking distance sensitivity analysis suggests that either around 25% of swarms are found within 50 m of adjacent swarms, or that these swarms that are linked together are actually separated by missing pings, instead of biology. So the linking distance SHAPES model parameters are overcoming an observation artefact, rather than linking biologically adjacent swarms.

Of the seven parameters used in the SHAPES algorithm, threshold sensitivity ($S_v t$) enabled examination of the energetic distribution of krill swarms. In the sensitivity analysis training set approximately 15% of krill swarms were high density, defined by $\bar{S}_v$ >-70 dB (lower asymptote, Figure 2.2), so an increased processing threshold did not reduce the number of swarms, but did increase $\bar{S}_v$, and decrease swarm size metrics such as swarm perimeter and swarm area.

An important finding of decreasing $S_v t$ was that the number of krill swarms did not decrease. This would be expected if dense swarms were located within diffuse layers. In this case lowering the $S_v t$ to less than $\bar{S}_v$ of the diffuse layer would mean that the higher density swarms would be included in the layer boundary, so n_s would decrease. This is strong evidence that at the time of these surveys at South Georgia, swarms were single

units, rather than high density regions located in longer, more diffuse layers. This is in contrast to the findings of Watkins and Murray (1998) who observed, in a survey around the Antarctic Peninsula, higher density krill regions located within longer, more diffuse, layers.

The school detection parameters selected during sensitivity analysis were partly determined by biological criteria, predominantly the krill packing density, and partly by observation characteristics, for example survey speed and echo sounder ping rate. This makes it difficult to apply the school detection parameters to other regions, or surveys from other research vessels with different echosounder settings. The selection of consistent SHAPES parameters, do however, allow comparison between surveys, assuming there is no significant change in the processes driving krill swarm formation. Even if variation of drivers of krill swarm formation did occur between surveys then the selected SHAPES parameters will be a mean of the influence of these drivers on krill swarms, so will allow inter-survey comparison.

2.4.2 Survey areal density and swarm abundance

This research has demonstrated a link between krill stock, represented by $\hat{\rho}$, and the number of krill swarms seen (n_s). This is in contrast to Petitgas et al. (2001) who analysed the results of six acoustic surveys, conducted around Europe, with target species: Herring, Sprat, Anchovy or Sardine. The Petitgas et al. (2001) investigation found no discernable pattern between stock abundance $\hat{\rho} \sim n_s$. This lack of relationship may have been caused by the target species being observed at relatively high abundances, so insufficient data were available to search for $\hat{\rho} \sim n_s$ density dependence.

Potentially the range of $\hat{\rho}$ observed during the krill surveys may have enabled the $\hat{\rho} \sim n_s$ to be observed, since these surveys included years of exceptionally high and low $\hat{\rho}$, as defined by Brierley et al. (1999b). There were, however, too few data points (n=6) to model potential density dependence (Figure 2.4). Nevertheless a strong correlation existed between these two variables. It would be unwise to extrapolate this finding, either spatially or temporally, so it is not recommended that this result is generalised outside of this region.

The $\hat{\rho} \sim n_s$ relationship is also demonstrated by the differences in the distributions of ρ_{vs} between surveys (Table 2.5) this is not surprising given the between survey differences in ρ_{vs}. However, it is not simply an increase in n_s that causes an increase in $\hat{\rho}$. Examining the the mean energetic measurements of krill swarms by survey (Table 2.6) shows differences between surveys; those surveys of high $\hat{\rho}$, such as JR28E, also have high energetic measures. Also, the KolmogorovSmirnov test (Table 2.5), examines the height differences between two ECDF curves (see Paramo et al. 2003), so a simple proportional

Swarm type	Swarm density statistics krill/m^3			Mauchline (1980) and Hamner and Hamner (2000) swarm classification (krill/m^3)
	2.5%C.I.	97.5%C.I.	mean	
1	0.4	87.5	9.9	1 to 100
2	11.5	1,059.3	267.3	1,000 to 100,000
3	0.4	15.5	2.7	0.1 to 1

Table 2.10: Comparison of numerical swarm classification numerical density (krill/m^3) between types suggested by Mauchline (1980) and Hamner and Hamner (2000) and the three-swarm type partition analysis used here (Section 2.2.4). To calculate krill/m^3 the Demer and Conti (2005) individual krill TS model with a mean krill length of 43.5 mm was used.

increase in krill swarms, across all possible swarm densities, would not have caused these between survey differences. Consequently, the structure of ρ_v of swarms is changing between surveys, particularly during JR17E and JR28E, that are markedly different to the other surveys.

2.4.3 Krill swarm morphology

There are marked differences between krill swarms observed during different surveys (Tables 2.6 and 5.4), which illustrates the high variability of krill around South Georgia (Brierley et al., 1997b; Atkinson et al., 2001). The primary sources of swarm variability are energetic and morphological (Table 5.4). Position metrics explained little of the krill swarm variability which suggests that there are no discernable gradients in swarm type throughout the surveys.

Following Mauchline (1980); Hamner and Hamner (2000) three swarm types were selected for the partition analysis, and there are considerable differences between the krill swarm types (Table 2.7). The types determined here, using partition analysis, do indeed show some overlap with the Mauchline (1980) krill aggregation criteria (Table 2.10). However, there are differences between the two classification schemes. The higher (type 2 in this investigation) and lower (type 3) swarms density do not coincide with the Mauchline (1980); Hamner and Hamner (2000) swarm classifications, because the numerical density of the swarm types derived in this study were truncated. In the case of the higher density swarms (type 2) this is likely to have been caused simply by no swarms of this density being encountered. For the low density swarms (type 3) this mismatch i.e. the type 3 swarms being of a higher density than swarms in the Mauchline (1980) and Hamner and Hamner (2000) schemes, may have been caused by the SHAPES algorithm parameters. The choice of $S_v t$=-80 dB will have excluded low density swarms, as would the length and height SHAPES parameters if low density swarms are typically smaller than 30 m in length and 10 m high.

The classification of krill swarms allowed the spatial distribution of swarm type to be assessed. The type two, high density swarms, that are common in the ECB predominantly occurred on shelf during 1997 and 1998 (Table 2.8). This ECB pattern of the on/off shelf distribution of krill swarms is consistent with observations made by Murphy et al. (1991) and Trathan et al. (2003). However, the lower density krill swarms dominating the WCB is not consistent with swarms observed in the ECB and may have resulted from the mismatch in predation pressure between the core boxes (see, Reid et al. 1999b, 2000b, and the next Chapter) or overlap between classes in the partition analysis (Figure 2.6). The drivers of this on/off shelf variation in krill swarm characteristics are unclear. Trathan et al. (2003) showed that along transect krill density was related to sea temperature, and there are significant differences in on and off shelf temperature in both coreboxes (Brandon et al., 1999; Meredith et al., 2005).

In the waters surrounding the Antarctic Peninsula Lascara et al. (1999) showed that large seasonal variation in $\hat{\rho}$ occurred along with changes in krill swarm metrics. Krill swarms of similar types to those found here were observed: smaller, denser, shallower swarms (type 2, in this study) and larger, more diffuse, deeper swarms (types 1 and 3). Furthermore, Lascara et al. (1999) found persistent, high density swarms,in on-shelf areas around the Antarctic Peninsula, which may be akin to the type 2 on-shelf swarms observed in the ECB in 1997 and 1998. The stochastic dynamic programming model of Cresswell et al. (2007) also showed that higher density swarms were found onshelf.

Overall, the mechanisms generating different swarm types remain unclear. Both Siegel (1988) and Lascara et al. (1999) postulated that swarm differences may be caused by size and maturity separation, which was based on acoustic and net samples. Watkins and Murray (1998) found significant segregation of the sex, size and maturity in krill swarms separated by only a few hundred metres in a survey conducted off the Antarctic Peninsula. The findings of these studies follow the conceptual seasonal model of krill stage class separation in relation to on/off shelf activity described by Siegel (2005). Although in the case of krill around South Georgia it appears that on/off shelf krill separation may be driven by mechanisms operating at smaller temporal scales smaller than seasonal, since surveys were performed at similar times of year (Table 2.1). It also appears that not all swarm types are affected by the on/off shelf swarm partitioning mechanisms (Table 2.9) and there is considerable inter-annual variation between on/off shelf swarm activity, particularly in the ECB.

2.4.4 Implications for krill predators

Several temporal and spatial scales of krill behaviour have been shown in this study, many of which may influence the foraging behaviour of air-breathing krill predators, of-

ten through changes in the detectability of a krill swarm, by a predator. Krill swarm detectability is driven by the number of swarms in the foraging area and the characteristics of those swarms. The high inter-survey variability of the number of swarms and swarm characteristics, available to land-based air-breathing predators at South Georgia (Table 2.6) suggests that, for optimal foraging to occur, predators must employ some sort of adaptive foraging strategy (Stephens and Krebs, 1986).

The number of swarms in a foraging area influences detectability by encounter rate; the greater the number of swarms the higher the probability of a predator encountering one. The variation in characteristics between swarms types influences detectability. For example, type 2 swarms are on average found in shallower water, making them more detectable than the other types. Conversely, type 2 swarms are smaller than type 1 and 3 which may lower their detectability. Furthermore swarm detectability exhibits scale dependent variability, increasing from: (i) krill swarm nearest-neighbour distance (0.6 to 16 km, Table 2.6); (ii) on/off shelf scales of 40 to 50 km; (iii) core box scales of 80 to 100 km and; (iv) inter-core box scales of up to 200 km. Additionally, there is temporal variability that acts from a few minutes to inter-annually. The complex nature of the drivers of krill, hence krill themselves, illustrate the necessity for predators to employ an adaptive foraging strategy.

Significant inter-annual variation in Antarctic fur seal diving behaviour was shown by Mori and Boyd (2004) using data collected from time-depth recording (TDR) animal tags, demonstrating that fur seals are capable of adaptive foraging behaviour. In this study the krill prey field was derived form fur seal dive behaviour to obtain an index of patch quality (IPQ), that was strongly correlated with $\hat{\rho}$. Interestingly using the IPQ Mori and Boyd (2004) reported that 1998 in the WCB was a year of poor krill patch quality, with fur seals used relatively low quality patches, at a greater depth. The results here are in agreement with this finding, with a low volumetric swarm density being found in the WCB in 1998 (Table 2.6). Also, in 1998 the WCB was dominated by low density, type 3 swarms (Tables 2.7 and 2.8). Unfortunately, only in 1998 did the work by Mori and Boyd (2004) and this investigation overlap, so it is not possible to examine fur seal diving behaviour in a year of extremely low $\hat{\rho}$. The $n_s \sim \hat{\rho}$ correlation (Figure 2.4), alluded to a possible density dependent relationship validates the IPQ. If $n_s \sim \hat{\rho}$ is a density dependent relationship then IPQ will decrease with decreasing patch quality represented by decreasing $\hat{\rho}$.

2.4.5 Further work

- Given that krill swarms probably arise from biological and environmental forcing interactions (Miller and Hampton, 1989; Barange et al., 1993) the relationship between krill swarm characteristics and oceanographic variables should be investigated.

Should a strong degree of physical forcing between krill swarms and a single physical driving mechanism be found, krill distribution could be used to explore the driving mechanism. However, it is unlikely that a single mechanism is responsible for the krill distribution, as layers of krill have been observed comprising of higher density patches within low density layers, suggested that the underlying process or processes may be scale-dependent.

- Future studies could examine the internal structure of krill swarms. Previous investigations have shown that Antarctic krill is not optimally packed within a krill swarm (*e.g.* Barange et al. 1993). It has been suggested that this is caused by behaviour and not physical driving forces (O'Brien, 1989; Barange et al., 1993). Assessing swarm internal structure could also be used to examine the potential masking effect of a high $S_v t$ on swarm boundaries i.e. krill swarm boundaries may be eroded at high $S_v t$.

- The apparent link between $n_s \sim \hat{\rho}$ requires further investigation. Initially, krill swarms could be identified and metrics extracted for digital acoustic data held by BAS for the South Georgia region. This would increase the sample size and would allow a potential density dependence relationship to be investigated.

- Simultaneous target fishing of krill swarms and acoustics should be undertaken to further examine the size, stage and lengths of individual krill swarms (*cf* Watkins and Murray 1998) and used in a multi-variate analysis framework (*e.g.* Woodd-Walker et al. 2003) to provide further information for krill swarm type classification, and potentially allow an activity to be assigned to a krill swarm.

- Attempting to discern the differences in krill swarm metrics between surveys has explored a limitation of these acoustic line transect observations of krill: these surveys are a snap shot of the krill distribution around South Georgia. Consequently krill swarm data do not contain information on the evolution of an individual krill swarm, so it is not possible to determine the state in which the krill swarm is observed. This means that the mean krill swarm state over a survey is observed rather than that of an individual krill swarm. It cannot be determined if Antarctic krill are leaving, or joining a swarm, or whether swarms are merging or separating Barange et al. (1993). Therefore, investigation of the evolution of a krill swarm may require individual krill swarms to be observed from a research vessel (see Hewitt and Demer 1996). The acoustic wave guide equipment used by Makris et al. (2006) that rapidly observes large areas, may allow changing krill swarm structure to be observed. Combining the large spatial coverage of line transect surveys, and the

temporal coverage of moored instruments such as those used by Brierley et al. (2006) is likely to improve understanding of the South Georgia ecosystem.

- Combining the results of swarm classification to spatially explicit models (e.g. Marin and Delgado 2001) may allow improvements to be made to estimates of krill, krill-predators and fisheries models such as those used by Reid et al. (2004).

2.4.6 Summary

This investigation has shown that during the five day surveys conducted at two sites around South Georgia there was high variability in both the number and characteristics of krill swarms. Strong correlation was observed between the number of krill swarms and mean areal krill density. The three-types of krill swarm used in the multi-variate partition analysis showed overlap with krill swarm types previously defined by Mauchline (1980) and Hamner and Hamner (2000). The three swarm types exhibited broadly agreed with swarm types seen by Lascara et al. (1999) on the Antarctic peninsula, as did the on/off shelf locations of the swarm types: high density swarms were found to persist in certain on shelf areas. It should be remembered however, that swarm metrics showed overlap (Figure 2.6), so the classification of swarm type, may not represent the underlying aggregative behaviour of krill.

The question still remains as to what the driving mechanisms are for the generally lower $\hat{\rho}$ in the WCB compared to the ECB. Potentially this is caused by predation (Brierley et al., 1997b), but it may also be caused by different water masses advecting krill into the South Georgia area (Trathan and Murphy, 2003; Meredith et al., 2005). Are predators causing the $\hat{\rho}$ difference between boxes, or is the different predator distribution between boxes a consequence of the $\hat{\rho}$ difference? In the next chapter the large scale, core box, relationships between predator encounters and $\hat{\rho}$ are investigated.

Chapter 3

Variability in the at-sea distribution of air breathing krill predators off South Georgia during three summer surveys, 1997 to 1999

3.1 Introduction

This chapter examines spatial and temporal variation in the at-sea distribution of air-breathing krill predators around the island of South Georgia (54^oS 35^oW). Sixteen predator species, classified into three functional groups, were recorded over two study sites, one to the northwest, the other northeast of South Georgia, on three summer cruises (1997 to 1999). Mean sea surface temperature and krill density, at the spatial-scale of the study site (80 x 100 km), were considered as potential drivers of variation in predator distribution. Variance in predator encounters was also assessed using a newly created summary metric, the 'index of variability'.

3.1.1 Marine predator-prey interactions

Marine predators forage in a heterogeneous environment and are generally dependent on spatially- and temporarily-varying aggregations of food resources (Horne and Schneider, 1995; Boyd, 1996; Sims et al., 2006, 2008). Characterising the variation in the foraging areas of marine predators, in response to changes in environmental conditions and prey availability is important in determining their ecological role (Barlow and Croxall, 2002; Reid et al., 2005) and in determining potential conflicts between predators and fisheries (Murphy et al., 1997; Reid et al., 2004).

At large scales (60 to 120 km) there is often a position correlation between prey and predators (Reid et al., 2004). The repeated aggregation of prey may be caused

by areas that have either environmentally favourable properties (Fauchald et al., 2000), or because of physical forcing mechanisms, such as upwelling (*e.g.* Genin 2004). At smaller scales predator-prey interactions, which must take place for consumption to occur, are frequently difficult to observe and interpret. Prey may adopt various types of anti-predation behaviour in response to predators, making the spatial relationship between predators and prey at small scales less predictable or measureable. For example, when prey are diluted or dispersed (Hamilton, 1971) in response to predators, there will be a progressive development of a negative spatial association with predators. Further, at small spatial scales (0.1 to 10 km), the state in which the predator-prey interactions are observed in is unknown. Generally when prey are observed to be diluted or dispersed, the mechanism causing this behaviour cannot be determined: a low-density of prey may have been caused by predator grazing, with the predators no longer being co-located with the prey at the time of observation. Alternatively, if the prey have formed dense aggregations, or are in an environmental refuge (Horne and Schneider, 1994), there may be a positive association with predators (Murphy et al., 1988). Therefore, while at larger spatial scales (50 to 200 km), time is less influential, at small scales (0.1 to 10 km) both spatial and temporal factors interact to obscure the spatial relationship between predators and prey (Haury et al., 1985).

Antarctic krill are known to aggregate at a variety of spatial scales. At the small spatial-scale krill have been observed to use both dilation and aggregation as an anti-predation behaviour (O'Brien, 1987; Hamner and Hamner, 2000). At large spatial-scales it has been suggested that krill aggregate over rapid changes in bathymetry (Mackas et al., 1985; Watkins, 2000).

The response of prey to the presence of predators varies with spatial scale. At larger scales prey may not engage in anti-predation behaviour since predators may be tracking a physical process as a proxy of prey distribution, rather than actively foraging. At smaller scales prey may exhibit anti-predation behaviour, in response to predator attack or localised predator searching behaviour. Fauchald et al. (2000) describe the varying spatial scale of prey (capelin) as a hierarchical patch structure, within which the small-scale aggregative behaviour of predators and prey is capable of masking the signal of predator-prey interactions at larger-scales. This is particularly problematic when predators and prey aggregate at different scales. Variation in the spatial scale of schooling small pelagic fish was observed by Petitgas et al. (2001) with the number of schools in a groups of schools, or clusters, being related to cluster density. Observing predator-prey interactions, particularly in the marine environment, is not a trivial task. Ultimately, the goal of predator-prey studies is to observe the spatial and temporal structure of the prey and predators, thereby allowing the foraging strategy of the predators, including searching

for prey and feeding, to be elucidated (Croll et al., 1998). These predator-prey interactions maybe complex because of spatial and temporal variation, and are made especially complex when these interactions are comprised of multi-predator species interactions (e.g. Croxall and Prince 1997 and Silverman and Veit 2001), under which predator species may be locating prey by reference to the foraging activities of other predators (*e.g.* Harrison et al. 1991), rather than the prey itself.

3.1.2 Predator-prey interactions at South Georgia

Observation from research vessels of the at-sea distribution of marine birds and mammals can be problematic: it can be difficult to detect and identify predators, and very time consuming to track individuals *in-situ*. Early predator-prey investigations in the South Georgia area were carried out from RRS *John Biscoe* (Hunt et al., 1992a). These investigations focused on the at-sea spatial distributions of Antarctic krill, observed using active underwater acoustics, and visual observations of Antarctic fur seals (*Arctocephalus gazella*) and Macaroni penguins (*Eudyptes chrysolophus*) in the vicinity of breeding colonies, in the area around Willis and Bird Islands (54^{o}00'S, 38^{o}011'W). Given the large population sizes of air-breathing krill predators at South Georgia there is an expectation that there will be a high density of predators in the surrounding sea (Trathan et al., 1998) Hunt et al. (1992a) discovered that Antarctic fur seals and Macaroni penguins not only made use of nearshore concentrations of Antarctic krill, but also moved further offshore, possibly to avoid competition (Veit et al., 1993). This pattern was also observed by Barlow et al. (2002), who concluded that there is considerable spatial overlap and competition between fur seals and Macaroni penguins.

An assessment of predator-prey interactions between Antarctic krill (*Euphausia superba*) and air-breathing predators is difficult, since the predator search strategy/behaviour is largely unknown. Further, foraging strategies vary between krill predator species in respect to both in horizontal and vertical (diving) foraging horizons. For example, during the breeding season at South Georgia, Macaroni penguins are constrained to forage within a relatively short distance of land due to the restricted time they can spend away from their nest because of chick provisioning requirements, and their swim speed. Trathan et al. (1998), estimated that 70% of individuals were found within 40 km from land. Consequently, the foraging strategy of Macaroni penguins is completely different to that of Black-browed albatross (*Thalassarche melanophris*) for example, which have been shown to have an activity range of 640,000 km^2 in the vicinity of South Georgia.

Marine predator-prey observations are generally collected using line transect surveys conducted from a research vessel, and this sampling strategy is not normally adaptive with respect to either predator or prey density so does not reflect the behaviour of sen-

tient marine predators foraging for prey. Conventional line-transect surveys are adopted because predator surveys are typically opportunistic conducted during voyages that have been designed to study krill (*e.g.* CCAMLR 2000 survey Reid et al. 2004). Even if an adaptive survey design was adopted, it is unlikely that the design could replicate the horizontal foraging movements of the many air-breathing marine predators involved.

3.1.3 Investigation aims

Given: (1) the high apparent inter-annual variability of krill areal density ($\hat{\rho}$)= 1.87 to 150.99 g/m^2 at South Georgia (Brierley et al., 1997a,b); (2) the proportional relationship between air-breathing predator breeding success and krill biomass (Reid et al., 2005); and (3) the variability in the predator at-sea positions derived from biologging studies (Trathan and Croxall, 2004), it is likely that the at-sea distribution of predators will reflect changes in prey distribution. The aim of this investigation is to use contemporaneous observations of air-breathing krill predators and acoustic observations of krill, collected during one month, over three years, in two study areas at South Georgia, to consider variability in the large-scale spatial distribution of predators, using three assessments: (1) descriptions of the predator species assemblages observed; (2) the relative effect of spatial and temporal variability on that species assemblage; (3) the relationship between any such spatial and temporal variability and krill density and with water temperature. Meredith et al. (2005) showed temperature varied between water masses at South Georgia and frontal zones have been shown to act as environmental refuges for pelagic organisms (Rose and Leggett, 1990; Genin, 2004), so it is appropriate to include water temperature here.

3.2 Materials and methods

3.2.1 Sampling techniques

Visual predator observation and active acoustic survey data were collected along line transects at two study sites (core boxes), to the north west, the western core box or WCB and north east, the eastern core box ECB of South Georgia (see Figure 2.1, Chapter 1). Each box was 80 km by 100 km rectangle and was surveyed via ten 80 km line transects, that had a pseudo-random spacing of between 7 and 16 km (Brierley et al., 1997a). Each transect crossed the continental shelf break and was orientated perpendicularly to it. Two transects were run each day, during daylight hours, by the RRS *James Clark Ross* travelling with a nominal speed of 10 knots. Data were collected in summer, during month long cruises, over three years from 1997 to 1999. Predator observations were made from

the bridge (height = 14 m), and acoustic measurements from downward, hull mounted transducers. Acoustic data gathered continuously, but effort varied for visual predator observations because of effort and observer fatigue (see Table 2.1, Chapter 2).

The species, group size, activity (e.g. foraging or transiting), and time of encounter for all seabird and marine mammal encounters were recorded continuously along each transect. A team of two researchers, one observer and one scribe, counted all species of seabirds and mammals encountered in a box with 100 m side lengths, 100 m in front of the bow, which is effectively a strip-transect as described by Tasker et al. (1984). The total number of predators observed was standardised for survey effort (time) for each transect.

It was not always possible to identify predators to species level at sea. Common and South Georgia diving petrels were recorded as Diving petrel sp., but these candidate species are ecologically similar (Reid et al., 2004), so is unlikely to bias analysis. In the case of unidentified prions, encounters would almost entirely have been with Antarctic prions (*Pachytila desolata*) given the very large population (>2x10^7 pairs) that nest on South Georgia (Prince and Croxall, 1983; Hunt et al., 1992b). Similarly, in the case of Northern and Southern Giant petrels, specific identification was often not possible. Whilst, in the case of fur seals, it is recognised that specific identification of *Arctocephalis sp.* at-sea is not 100% certain, the high probability of all seals observed being *Arctocephalus gazella* meant that for practicality these sightings were recorded as *Arctocephalus sp. (gazella).*

3.2.2 Index of variability

An index of variability (I) was devised as a metric to describe the between-cruise variability of each species in each core box. The metric I assesses the deviation in the proportion (p) of the total number of predators (N_y) of a species sighted in the given year (y) from a theoretical uniform proportion (p_u) of predator sightings across years ($p_u = 1/y$). In the case of data considered in this study $p_u = 1/3$, since there were three surveys. I is calculated from:

$$I = \sum_{y=1}^{Y} |p_y - p_u| \qquad 0 \geq I < 1 \tag{3.1}$$

where, y is the number of years of surveying, $p_y = n_y / \sum_{y=1}^{Y} n_y$, n_y is the number of predators of a given species in a study region in year y. An index of variability of 0 shows a no change in the number of predators per year, between years, and $\simeq$1 denotes maximum change in the proportion of predators, i.e. the largest inter-annual variability.

3.2.3 Covariate data

Two potential driving factors, one biological and one physical, influencing the temporal- and spatial-variation in the at-sea distribution of krill predators were considered: estimates of the mean area density of Antarctic krill (wet mass g/m^2, $\hat{\rho}$) and the mean potential water column temperature (^{o}C, $\bar{\theta}$). Estimates of $\hat{\rho}$ were obtained using the Jolly and Hampton (1990) technique, but were an update of previously published values (Brierley et al., 1999b), where the Demer and Conti (2005) individual krill acoustic target strength model was used to scale echo intensity to krill density, rather than the Greene et al. (1991) model used previously: this will serve to increase density since individual krill target strength is reduced. The potential temperature ($\bar{\theta}$) data were obtained from Trathan et al. (2003).

3.3 Results

The results presented here are divided into three sections: firstly, an initial examination of the species assemblage present; secondly, an assessment of the spatial and temporal-variability between the WCB and the ECB from 1997 to 1999; and finally, an examination of the particular nature of this variation and its relationship between $\hat{\rho}$ and $\bar{\theta}$.

Thirty four species of air-breathing predators were recorded during the three surveys at South Georgia, contributing to a total predator count of n=50,823. Of these, there were 16 species for which the total number of individuals recorded exceeded 30 (Table 3.1); only these species were included in subsequent analyses. These selected predator species represent 99% of the total number of predators sighted, and assuming independence in predator encounters, 30 individuals will be representative of a given predator species operating in a core box, i.e. 30 observations are sufficient to elucidate predator behaviour in a core box. The most numerous species were Antarctic prion (*Pachyptila sp. (desolata)*) N=30,311, Antarctic fur seal (*Arctocephalus sp. (gazella)*) N=7,029 and Wilson's storm petrel (*Oceanites oceanicus*) N=3,447. On the basis of an examination of the relative proportion of each species recorded in the WCB and ECB (Figure 3.1), and shared biological characteristics, principally body size and foraging strategy, the 16 species were assigned to three functional groups: i) large flying birds; ii) small flying birds; and iii) divers. Predator diet varied between groups and species (Table 3.1).

The first functional group, large flying birds, was made up of five species: the Black-browed albatross (*Thalassarche melanophris*); Grey-headed albatross (*T. chrysostoma*); Light-mantled sooty albatross (*Phoebetria palpebrata*); Wandering albatross (*Diomedea exulans*) and Giant petrel (unid.) (*Macronectes sp.*). The White-chinned petrel (*Procellaria aequinoctialis*), also had greater numbers in the WCB in each year, fell between the

large and small flying bird functional groups. Based on a study of seabird niche separation conducted by Croxall and Prince (1980a) the White-chinned petrel was included in the large flying bird group. All species in the large flying bird group (with the exception of the Light-mantled sooty albatross) had a higher proportion of sightings in the WCB in each year (Figure 3.1).

Seven species made up the small flying bird functional group: Blue petrel (*Halobaena caerulea*); Antarctic prion (*Pachyptila sp. (desolata)*); Cape petrel (*Daption capense*); Soft-plumaged petrel (*Pterodroma mollis*); Black-bellied storm petrel (*Fregetta tropica*); Wilson's storm petrel (*Oceanites oceanicus*) and Diving petrel (*Pelecanoides sp.*). This functional group showed greater variability in the relative proportion of sightings between the core boxes (Figure 3.1), with only Antarctic Prions having a greater proportion of sightings in the WCB.

The remaining species make up the third functional group, the divers, which contained Antarctic fur seal (*Arctocephalus sp. (gazella)*); Gentoo penguin (*Pygoscelis papua*); King penguin (*Aptenodytes patagonicus*) and Macaroni penguin (*Eudyptes chrysolophus*). The diver functional group, with the the exception of fur seals, generally occurred in greater proportions in the ECB.

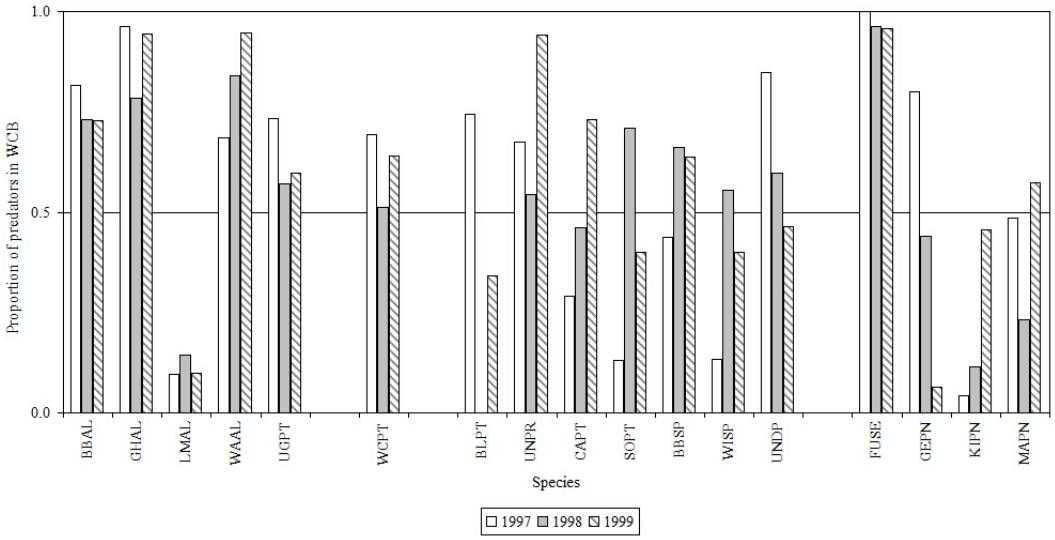

Figure 3.1: The proportion (p) of predator encounters, occurring in the western core box (WCB), for each species, by year (if p=1, all predators occur in the WCB for a given year). Across all species and years $\bar{p}$=0.56 showing that more predator species choose to forage in the WCB. See Table 3.1 for species abbreviations.

Species	code	n	n_{gs}	Primary prey items
Antarctic Fulmar (*Fulmarus glacialoides*)	ANFU	1	1	Antarctic silverfish & krill (Arnould and Whitehead, 1991)
Antarctic tern (*Sterna vittata*)	ANTE	23	2	Fish & crustaceans (Jazdzewski and A., 1999)
Black-browed albatross (*Thalassarche melanophris*)	BBAL	1271	2	Cephalopod, krill & fish (Croxall and Prince, 1997)
Black-bellied storm petrel (*Fregetta tropica*)	BBSP	548	1	Fish & crustacean (Hahn, 1998)
Blue-eyed shag (*Phalacrocorax atriceps bransfieldensis*)	BESH	4	1	Fish & cephalopod (Casaux and Barrera-Oro, 1993)
Blue petrel (*Halobaena caerulea*)	BLPT	482	1	Krill (Prince, 1980)
Brown skua (*Catharacta lonnbergi*)	BRSK	17	1	Carrion (Ainley et al., 1993a)
Cape petrel (*Daption capense*)	CAPT	225	1	Antarctic silverfish & krill (Arnould and Whitehead, 1991)
Chinstrap penguin (*Pygoscelis antarctica*)	CHPN	5	2	Krill (Croxall and Furse, 1980)
Southern elephant seal (*Mirounga leonina*)	ELSE	3	1	Fish & krill (Brown et al., 1999)
Antarctic fur seal (*Arctocephalus sp. (gazella)*)	FUSE	7029	5	Krill (Boyd, 1996)
Grey backed storm petrel (*Garrodia nereis*)	GBSP	11	1	(Rainbow, 1989)
Gentoo penguin (*Pygoscelis papua*)	GEPN	789	7	Krill (Croxall and Prince, 1997)
Grey-headed albatross (*Thalassarche chrysostoma*)	GHAL	289	1	Cephalopod and fish (Croxall and Prince, 1997)
Grey Petrel (*Procellaria cinerea*)	GRPT	1	1	Cephalopods (Ridoux, 1994)
Great shearwater (*Puffinus gravis*)	GRSW	13	1	Cephalopods (Croxall and Prince, 1996)
Humpback whale (*Megaptera novaeangliae*)	HUWH	1	1	Krill (Hardy and Gunther, 1935)
Kerguelen Petrel (*Pterodroma brevirostris*)	KEPT	2	1	Fish & crustaceans (Ainley et al., 1993b)
King Penguin (*Aptenodytes patagonicus*)	KIPN	160	2	Fish (Olsson and W., 1997)
Light-mantled sooty albatross (*Phoebetria palpebrata*)	LMAL	45	1	Squid and krill (Thomas, 1982)
Macaroni penguin (*Eudyptes chrysolophus*)	MAPN	566	3	Krill (Croxall and Prince, 1997)
Minke Whale (*Balaenoptera acutorostrata*)	MINK	5	2	Krill (Armstrong and Siegfried, 1991)
Royal albatross (*Diomedea epomophora*)	ROAL	4	1	Cephalopods and fish (Imber, 1999)
Snow Petrel (*Pagodroma nivea*)	SNPT	12	2	Fish (Ridoux and Offredo, 1988)
Soft-plumaged petrel (*Pterodroma mollis*)	SOPT	179	1	
Sooty shearwater (*Puffinus griseus*)	SOSW	3	1	Fish (Jackson, 1988)
Southern Right whale (*Eubalaena australis*)	SOWH	2	2	Krill (Hardy and Gunther, 1935)
Giant petrel(unid) (*Macronectes sp.*)	UGPT	267	1	Krill and carrion (see Croxall and Prince 1980a)
Diving petrel(unid) (*Pelecanoides sp.*)	UNDP	2158	2	Krill and copepods (Reid et al., 1997b)
Penguin(unid) (*Pygoscelis/Eudyptes sp.*)	UNPN	12	1	-
Prion(unid) (*Pachyptila sp. (desolata)*)	UNPR	30311	8	Krill (Reid et al., 1997a)
Wandering albatross (*Diomedea exulans*)	WAAL	171	1	Squid (Weimerskirch et al., 2005)
White-chinned petrel (*Procellaria aequinoctialis*)	WCPT	2263	2	Krill and fish (see Croxall and Prince 1980a)
Wilson's storm petrel (*Oceanites oceanicus*)	WISP	3447	1	Krill (Beck and Brown, 1972)

Table 3.1: The total number of individuals sighted for 34 predator species during three years of surveying, effort corrected, is shown (n). The mean group size $\hat{n_{gs}}$ across years is also given. The predator codes as used in Figures 3.1 and 3.2.

A statistical assessment of the variability in predator distribution was performed using a two-way ANOVA with fixed-effects "core box" and "year", and an interaction term "core box" x "year". The sampling unit was number of individuals (n), standardised for effort (time), of each predator species encountered on each transect. There were significant differences between core boxes (Table 5.7), but not for year, for the large flying bird group. The results from the small group were more equivocal, with two species, Soft-plumaged petrel and Wilson's storm petrel, showing a difference between year, while only prions showed a significant between core box effect. For Antarctic fur seals there was a significant difference between core box, and year and there was a significant interaction term. In the case of King penguins there were differences between core box and year.

Based on the overall results of the ANOVA (Table 5.7) it would appear that core box was a more important factor than year in the differences in species occurrence, particularly for the large bird group (8 species are significantly different). Furthermore, the lack of consistent interaction terms between core box and year (4 species significantly different) suggests that these inter-core box differences were the predominant factor influencing these differences in predator distribution i.e. geography rather than time is the main source of variability.

Species name	Western core box						Eastern core box						Two-way ANOVA		
	JR-17		JR-28		JR-38		JR-17		JR-28		JR-38		core box	year	core X year
	n	CV	n	CV	n	CV	n	CV	n	CV	n	CV			
Black-browed albatross	313	0.17	273	0.20	374	0.08	71	0.08	100	0.10	140	0.05	14.15(**0**)	0.61(0.44)	0(0.99)
Grey-headed albatross	80	0.08	47	0.06	138	0.04	3	0.17	13	0.09	8	0.11	140.03(**0**)	0.93(0.34)	0.08(0.78)
Light-mantled sooty albatross	2	-	2	-	1	-	19	0.13	12	0.07	9	0.11	18.22(**0**)	3.26(0.08)	0.27(0.6)
Wandering albatross	24	0.11	68	0.12	52	0.13	11	0.10	13	0.11	3	0.32	26.68(**0**)	0.91(0.34)	3.25(0.08)
White-chinned petrel	575	0.11	303	0.07	601	0.10	255	0.08	290	0.05	339	0.13	7.55(**0.01**)	1.86(0.18)	0.06(0.8)
Black-bellied storm petrel	35	0.13	237	0.06	70	0.07	45	0.09	121	0.06	40	0.09	3.2(0.08)	0.43(0.52)	0.13(0.72)
Blue petrel	234	0.18	0	-	57	0.08	81	0.24	0	-	110	0.06	0.54(0.47)	0.48(0.49)	3.07(0.09)
Cape petrel	27	0.20	18	0.19	68	0.10	66	0.11	21	0.12	25	0.09	0.03(0.86)	0.55(0.46)	9.54(**0**)
Soft-plumaged petrel	14	0.16	44	0.15	4	0.17	93	0.20	18	0.24	6	0.16	0(0.99)	6.42(**0.01**)	0.12(0.73)
Diving petrel (unid)	1312	0.14	98	0.11	208	0.04	233	0.10	66	0.19	241	0.11	3.59(0.06)	3.04(0.09)	0.73(0.4)
Prion (unid)	3084	0.13	5746	0.10	14293	0.22	1489	0.07	4824	0.09	875	0.06	8.07(**0.01**)	1.84(0.18)	0.99(0.32)
Wilson's storm petrel	137	0.10	1054	0.05	206	0.07	896	0.12	846	0.05	308	0.08	3.55(0.07)	4.68(**0.04**)	1.35(0.25)
Antarctic fur seal	827	0.09	4531	0.14	1427	0.05	1	-	178	0.09	65	0.10	121.01(**0**)	5.99(**0.02**)	7.12(**0.01**)
Gentoo penguin	24	0.20	91	0.19	36	0.23	6	0.23	116	0.14	516	0.18	0.71(0.4)	1.89(0.18)	3.28(0.08)
King Penguin	1	-	9	0.21	26	0.11	23	0.16	70	0.10	31	0.10	10.64(**0**)	4.01(**0.05**)	1.15(0.29)
Macaroni penguin	72	0.19	49	0.10	118	0.08	76	0.08	163	0.12	88	0.14	0.01(0.92)	0.61(0.44)	3.46(0.07)

Table 3.2: Number of predators (n) in each study site, split by year. Coefficient of variation (CV) calculated between the number of predators sighted on a transect ($n_i, i = 1..10$) within a study site. Two way ANOVA, total number of predators of each species per transect as the sampling unit, and core box and year as effects, with a core box x year interaction term. Effects with p <0.05 are highlighted.

Site	JR-17 $\hat{\rho}$ (g/m^2)	JR-17 $\hat{p}_1$	JR-17 $\bar{\theta}$(^{o}C)	JR-28 $\hat{\rho}$(g/m^2)	JR-28 $\hat{p}_2$	JR-28 $\bar{\theta}$(^{o}C)	JR-38 $\hat{\rho}$(g/m^2)	JR-38 $\hat{p}_3$	JR-38 $\bar{\theta}$(^{o}C)	I ($\hat{p}$)
West	53.16	0.353	0.319	54.39	0.361	-0.290	43.00	0.289	0.570	0.088
East	101.91	0.210	0.660	350.51	0.723	-0.250	32.58	0.067	0.665	0.779

Table 3.3: Summary of estimates of Antarctic krill mean area density ($\hat{\rho}$), mean water column potential temperature ($\bar{\theta}$), yearly proportion ($\hat{p}_{1..3}$) and index of variability (I).

3.3.1 Variation in predator distribution between study regions

A comparison of the total number of individuals sighted in the WCB and the ECB across years showed that 11 of the 16 predator species had the greatest proportion of sightings in the WCB (Table 5.7 and Figure 3.1). Across all years and predator species a higher number of predators occurred 56% of the time in the WCB. Within the large flying bird group all members, except the Light-mantled sooty albatross (which had the fewest sightings), had a higher proportion of sightings in the WCB. In the small flying bird group only prions were present in consistently greater numbers in the WCB in each year. There was no such pattern in the proportion of sightings in other predator species within this group. Similarly, in the divers group only one predator, the Antarctic fur seal, was present in greater numbers in the WCB, whereas the King penguin had significantly more sightings in the ECB (the only species for which this was the case). The index of variability (I) for Antarctic fur seals was high ($I > 0.7$), but similar in both the ECB and WCB (Figure 3.2), whereas King penguin I was greater in the WCB than ECB.

3.3.2 Potential drivers of inter-annual variability

In the ECB $\hat{\rho}$ was highly variable ($I = 0.8$) and had an inverse relationship with $\bar{\theta}$, whereas $\hat{\rho}$ in the WCB showed relatively little variation ($I = 0.1$) and did not appear to show any relationship with $\bar{\theta}$ (Table 3.3). Variability in $\bar{\theta}$, measured using I, was the same for both the WCB and ECB, suggesting that variation in $\bar{\theta}$ occurs at scales greater than the study sites and their separation (180 km).

In Figures 3.3 to 3.5 the horizontal dashed line at $p = 1/3$ represents a constant proportion, or number, of predators observed during each survey. The large flying bird group showed relatively little variation between years, and there was a consistent pattern in the WCB and ECB. Overall the inter-annual variability of the small flying bird group showed consistent, structured variability with respect to $\hat{\rho}$ and $\bar{\theta}$ in the WCB, but not in the ECB (Figure 3.3). In the WCB small birds could be clustered in two subdivided types: Black bellied storm petrels, Soft plumaged petrels and Wilson's storm petrels that followed a pattern concordant with changes in $\hat{\rho}$ and inversely related to $\bar{\theta}$, whereas Blue

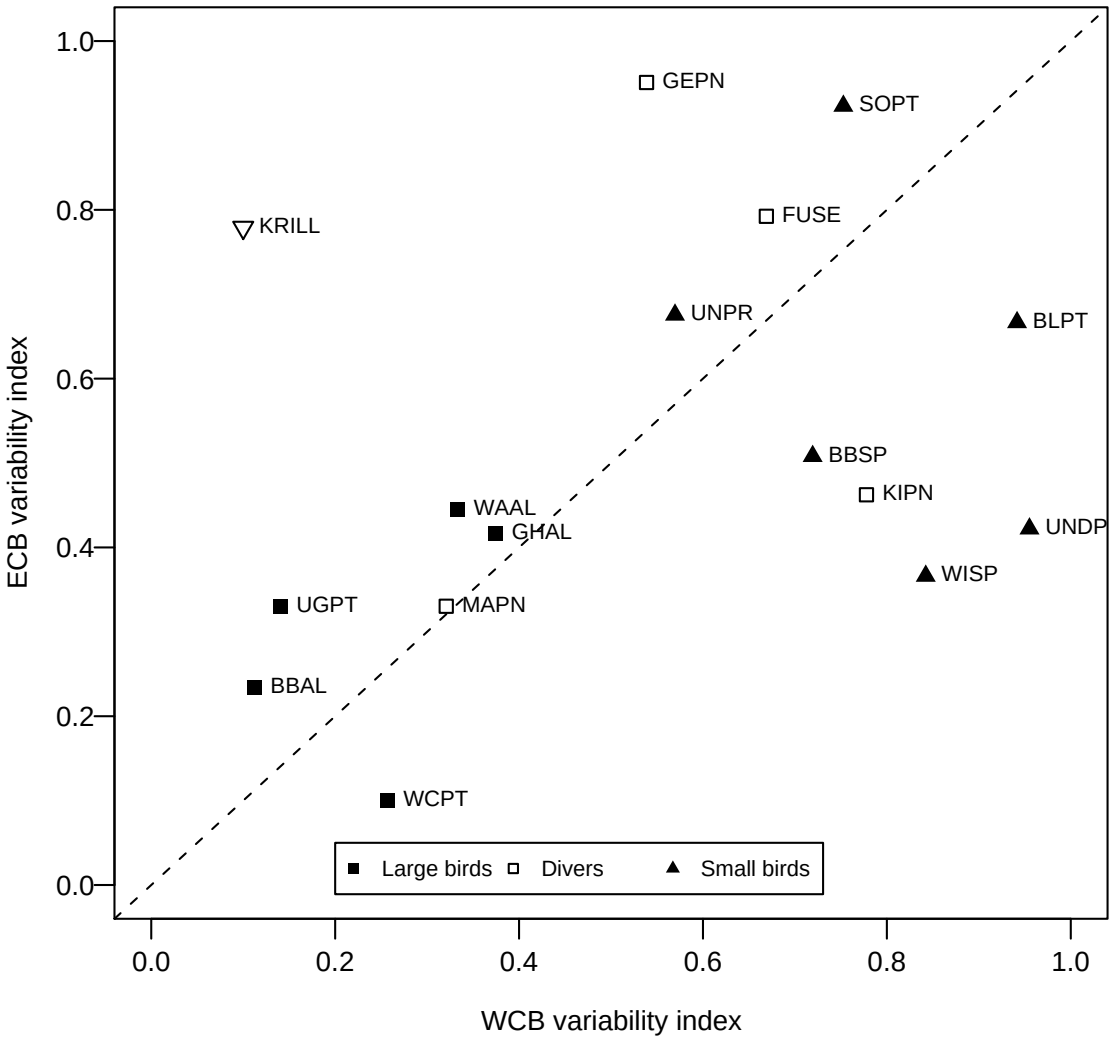

Figure 3.2: Index of variability as described in Section 3.2.2 for the west and east core boxes. Predator species symbols are coded by functional group. This figure can be interpreted as follows. Should a predator species have an identical pattern of variability at both study sites, then that species will fall on the diagonal dashed line. Predator species showing low variability across study sites will fall on the line, near the origin. Whereas predator species showing large variability at both study sites will fall near the maximum of the dashed line. The null hypothesis of a uniform distribution of predators would yield points at the origin.

petrels and unidentified diving petrels showed the opposite variation with respect to both covariates. The most striking result of inter-annual variability of the small bird group was the absence of Blue petrels from either box in 1998 (Table 5.7), but this would seem not not to be driven by either $\hat{\rho}$ or $\bar{\theta}$. The diving predator group exhibited high inter-annual variability in both boxes (Figure 3.5). Antarctic fur seals were the only predators in the

diving predator group to show a consistent pattern of inter-annual variation in both boxes. In the ECB this pattern of inter-annual variability in Antarctic fur seal encounters closely tracks the inter-annual variation in krill density and in both the WCB and ECB has an inverse relationship with $\bar{\theta}$.

The intra-site pattern of variation in the Macaroni penguin encounters had an inverse relationship (Figure 3.5). The greatest proportion of Macaroni penguins were observed in the ECB in 1998 ($p_{1998,ECB} = 0.5$), whilst in the WCB during 1998 the lowest proportion ($p_{1998,WCB} = 0.2$) was observed. This inverse relationship of Macaroni penguin encounters explains why I is similar in both sites (Figures 3.1 and 3.2).

Overall, all members of the large flying bird group, when compared with other functional groups, had a low I (Figure 3.4). Small flying birds, with the exception of the Soft-plumaged petrel, had higher I especially in the WCB. The diver group showed no consistent pattern, although the Macaroni penguin showed a consistently low I that was similar in both boxes, arising from apparently concordant changes in the number of sightings.

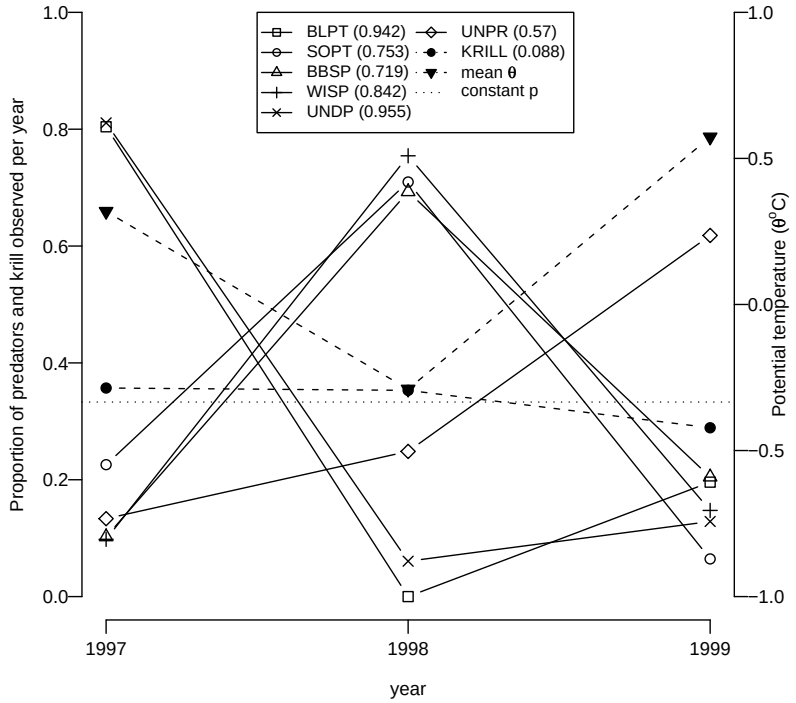

(a) Western core box

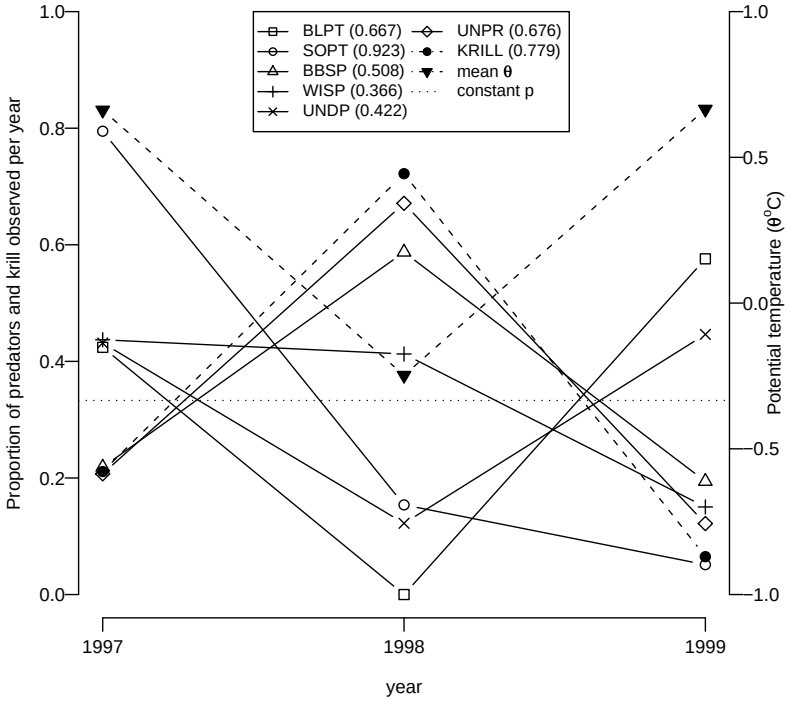

(b) Eastern core box

Figure 3.3: Proportion of the small flying bird functional predator group and krill observed per year. Absolute values of mean potential temperature $\bar{\theta}$ are inverted solid triangles. Predators are split by study site. The indices of variability (I) for each predator species and krill are given in the legend.

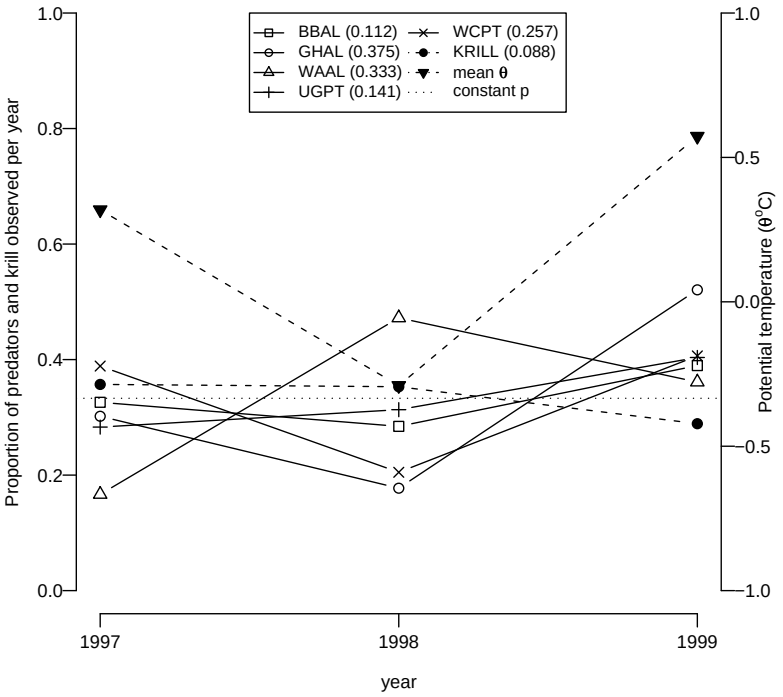

(a) Western core box

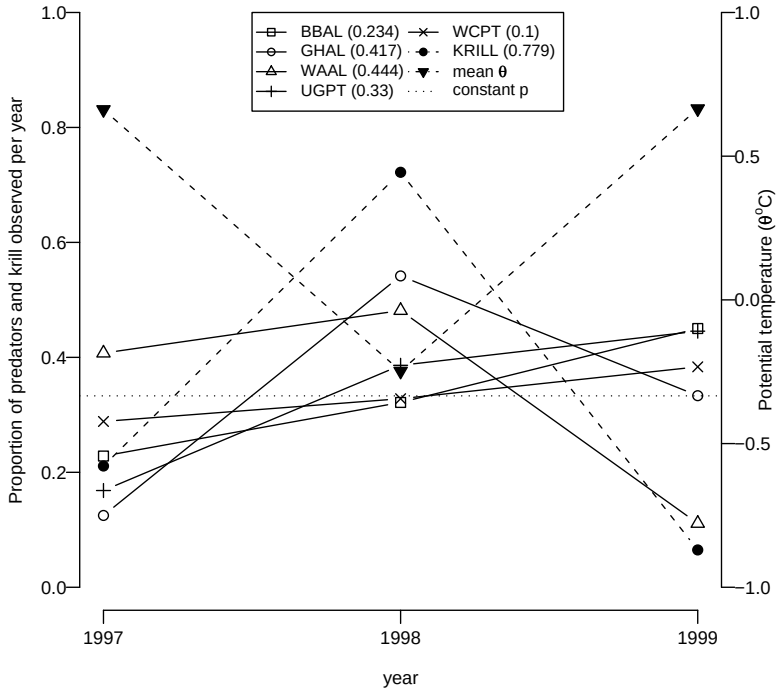

(b) Eastern core box

Figure 3.4: Proportion of the large flying bird functional predator group and krill observed per year. Absolute values of mean potential temperature $\bar{\theta}$ are inverted solid triangles. Predators are split by study site. The indices of variability (I) for each predator species and krill are given in the legend.

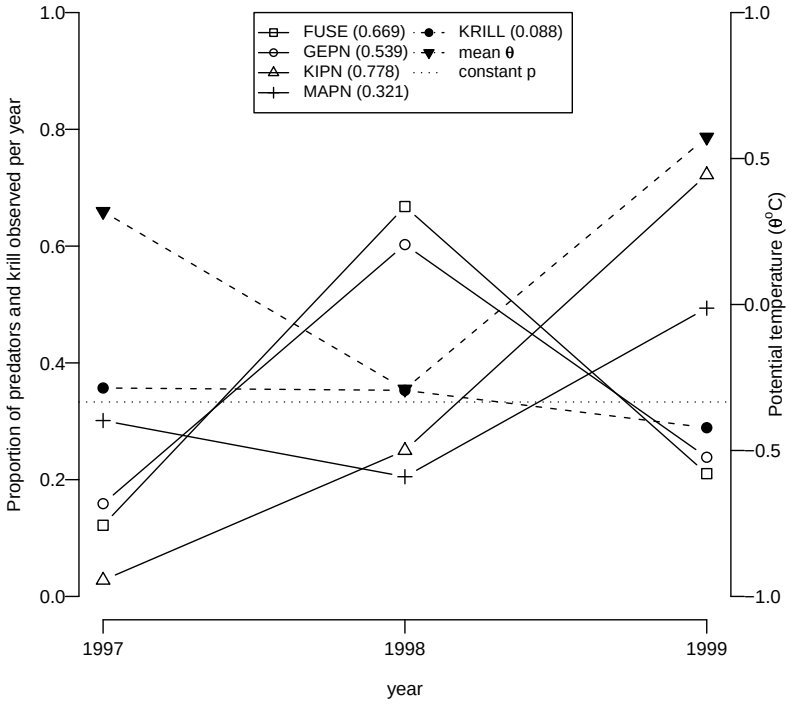

(a) Western core box

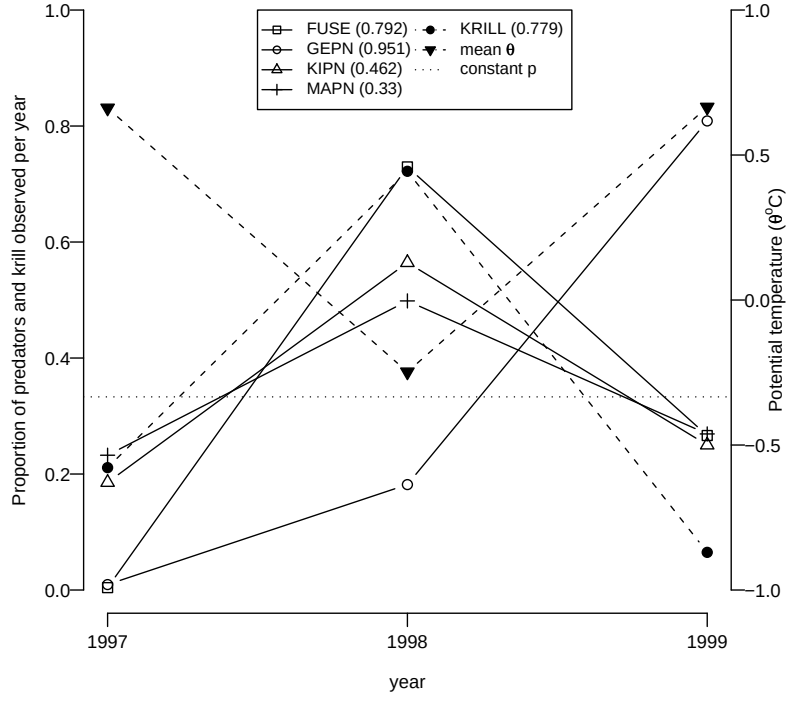

(b) Eastern core box

Figure 3.5: Proportion of the diver functional predator group and krill observed per year. Absolute values of mean potential temperature $\bar{\theta}$ are inverted solid triangles. Predators are split by study site. The indices of variability (I) for each predator species and krill are given in the legend.

3.4 Discussion

3.4.1 Summary of findings

There were quite distinct differences in numbers between core boxes and years that are broadly consistent between the predator species groups, notwithstanding some species-specific variation (Figure 3.2). Overall, species abundances in 1997 and 1999 were quite similar, but 1998 appears to be quite different, exemplified by the absence of Blue petrels in both boxes and an order of magnitude increase in Antarctic fur seals in the ECB (Table 5.7), which coincided with anomalously low temperatures occurring in the ECB (Meredith et al., 2005), and an unusually high density of krill ($\hat{\rho}$)= 350.51 g/m^2 in the ECB (Brierley et al. 1999b, Table 3.3). The key findings of this investigation are that core box is a major determinant of species abundance than year and that despite the consistently higher krill density in the ECB krill predator abundances are higher in the WCB.

3.4.2 Selection of functional groups

Generally the species functional groups showed consistent patterns in inter-site (Figure 3.2) and inter-survey variability i.e. there was a qualitative clustering of the predator functional groups. In the large bird group, low numbers of light-mantled sooted albatross, had a lower relative proportion of sightings occurring in the WCB, which is consistent with breeding and spatial distributions derived from satellite tracking data (Phillips et al., 2005). These lower Light-mantled sooty albatross numbers may have been caused by competition due to dietary overlap with Grey-headed albatross, Black-browed albatross and White-chinned petrel forcing the Light-mantled sooty albatross to adopt larger foraging ranges.

In the divers functional group, Antarctic fur seals and Macaroni penguins, the two main consumers of krill at South Georgia, showed a similar scale of spatial variability in both boxes (I, falling on the dotted line, Figure 3.2), with Antarctic fur seals having a higher inter-annual variability. Over the past 25 years the Macaroni penguin population at South Georgia has declined by *c.* 50% (Trathan et al., 1998). The cause of this decline is unknown (Trathan et al., 2006), but it has been suggested that a contributing factor maybe the competitive exclusion of Macaroni penguins by Antarctic fur seals (Barlow et al., 2002). Given that both species dive to similar depths (10 to 60 m Croxall and Prince 1980b; Boyd and Croxall 1992; Reid and Arnould 1996), feed on similar sizes of krill (Reid et al., 1999a,b) and have similar breeding seasons, so are constrained in their foraging trip duration at a similar time of year (Williams and Croxall, 1991), the potential for competition between the two species clearly exists (Barlow et al., 2002). Compared to

Macaroni penguins, Antarctic fur seals may be better able to respond to changes in krill availability, for example by expanding their breeding range (Boyd, 1993) and by foraging further from shore (Barlow et al., 2002), which would give Antarctic fur seals a competitive advantage over Macaroni penguins. The differences in the pattern of I between Macaroni penguins and Antarctic fur seals (Figures 3.2 to 3.5) suggests competitive exclusion exists, particularly in the WCB.

All species in the small flying bird group had a higher index of variability (I) than species in the large flying bird group in both boxes (Figure 3.2). This may be due to the greater foraging ranges of the large flying bird group that would serve to dampen local variability in the more wide ranging species (Croxall and Prince, 1980a). With the exception of Soft-plumaged petrel and Antarctic prions, members of the small bird functional group have a higher variability in the WCB. Soft-plumaged petrels do not breed at South Georgia, therefore changes in their foraging distribution may arise from different factors (Croxall and Prince, 1980a), such as environmental changes at their breeding site.

3.4.3 Inter core-box variation

The results of this study suggest that spatial differences between the two core boxes are more important than temporal ones in determining the number of predator species occupying a core box and their abundances. Variation in the proportions of predator sightings between the study sites provides evidence against the null hypothesis of equal abundances of predators being present in both study sites (Figure 3.1). This inter-core box variation may be driven by changes in oceanographic conditions, which might influence krill biomass entering the South Georgia region (Trathan and Murphy, 2003; Meredith et al., 2005) i.e. changes in core-box oceanographic conditions may be caused by different water masses entering the core boxes, which change the rate of local krill flux (Trathan and Murphy, 2003). Trathan et al. (1998) showed that the South Georgia breeding population of Macaroni penguins was more than order of magnitude larger than the other breeding populations.

In the ECB there were concordant changes in $\hat{\rho}$ and the abundance of predator species ($\hat{N}$, Figures 3.3 to 3.5). Broadly, there was also an inverse relationship between $\hat{\rho}$ and $\bar{\theta}$. However, in the WCB there was no such relationship between $\hat{\rho}$ and $\hat{N}$ and, compared to the ECB, a weaker inverse relationship with $\bar{\theta}$. The historical view of elevated krill abundance, hence more whales, in colder years (Atkinson et al., 2001), does not hold in the ECB.

Species in both the small and large flying groups are highly mobile compared to the divers group, so variation in species abundances (Table 5.7) suggest that both the flying groups are using this mobility to enhance foraging potential, with the large flying bird

functional group showing a preference for the WCB, whilst the small bird functional group preferred the ECB. Harrison et al. (1991) showed empirical evidence of Black-browed albatross dominating multi-species flocks around South Georgia: therefore, the small flying bird group may be avoiding competition with, and indeed the potential for becoming prey of, the larger flying birds during foraging, which is an alternative explanation for the separation of the two flying-bird functional groups (Figure 3.2).

The inter-core box variation also gives an indication of the extent to which a species foraging niche is influenced by small-scale drivers. The analysis here is insufficient to determine the actual foraging niche drivers, only a measurement of the effect of all variables influencing foraging. The lower I of the large flying bird group compared to the small flying bird group suggests that the large flying bird group is not so susceptible to variation in foraging niche at the core box scale because this group forages at spatial scales larger than the core boxes. Alternatively, the large flying bird group is less able to respond to small spatial scale niche changes, so members of this group use a consistent, wide ranging, foraging strategy, that may serve to smooth regional prey variation.

3.4.4 Variation in predator distribution: oceanographic drivers

Across the three years there were differences in $\bar{\theta}$ between the core boxes, with 1998 being the coldest (Table 3.3). Meredith et al. (2005) suggested that inter-site differences between boxes were driven by the northward deflection of the SACCF away from South Georgia by the Northwest Georgia Rise. The WCB and ECB differences were magnified because as the ECB is sheltered from prevailing westerly winds that reduce wind-induced mixing of cold meltwater from the island in that box.

In 1998 the water surrounding South Georgia had anomalous characteristics and these were evident in both core boxes. Water temperature was much colder than other years (Meredith et al., 2005), suggesting oceanographic variability between boxes in 1998 was coupled. Trathan and Murphy (2003) and Meredith et al. (2005) suggested that this cooler water originated, during 1997, in the ocean upstream of South Georgia, its effect potentially strengthened as a result of an El Niño event. Since it is believed that substantial krill recruitment does not occur locally (Tarling et al., 2007), the 1998 cooler water masses around South Georgia may have advected elevated densities of krill to the region and account for the inverse relationship between $\hat{p}$ and $\bar{\theta}$ in the ECB, which has been postulated since the Discovery era. There are too few observations in this study to generalise a relationship between $\hat{p}$ and $\bar{\theta}$, so it is not possible to quantitatively determine if predators predict larger-scale krill availability by tracking changes in $\bar{\theta}$ at large scales whilst being central placed foragers. However, it would appear that the elevated number of Antarctic fur seals and absence of Blue-petrels are caused by both species responding

Year	Cruise	Signy Island Fur seal count	South Georgia SST (^{o}C) WCB mean	WCB range	ECB mean	ECB range
1997	JR17	15,192	2.7	0.1 to 4.8	2.0	-0.2 to 3.9
1998	JR28	9,415	2.1	0.3 to 3.1	1.6	-0.3 to 2.6
1999	JR38	16,126	2.3	0.6 to 4.3	1.9	0.2 to 3.8

Table 3.4: Antarctic fur seal counts at Signy research station, South Shetlands (BAS, unpublished data) and sea-surface temperature (SST, obtained from SeaWiFS) in the western (WCB) and eastern core boxes (ECB) at South Georgia. The reduced number of fur seals in 1998 is consistent with fur seals not moving south from South Georgia, to Signy in the summer, during a season of cold water.

to anomalous low-temperature water (Table 3.3).

A biologging study of post-breeding adult Antarctic fur seals, from Bird Island, conducted by Boyd et al. (1998) showed foraging preferences varied between males and females. Female Antarctic fur seals, constrained by the requirement to support young, foraged in the vicinity of the South Georgia continental shelf break to the north-west of Bird Island (Boyd et al., 2002). Tracked male Antarctic fur seals travelled from South-west South Georgia towards the South Orkney Islands and foraged at Signy Island, South Orkney Islands (60^{o}43'S, 45^{o}36'W, distance = 986 km). The Signy Island Antarctic fur seal count showed an inverse relationship with the total number of at-sea Antarctic fur seals encountered at South Georgia (Table 3.4, BAS unpublished data). In the ECB in 1998, most of the Antarctic fur seals observed were male (Reid, *pers. obs.*), suggesting fewer male Antarctic fur seals travelled south to forage at the South Orkney Islands. Indeed the reduced numbers of Antarctic fur seals at Signy Island in 1998 coincided with lower sea-surface temperature in the WCB and ECB, which suggests that Antarctic fur seals were responding to changes in temperature, not krill density and illustrates the large-scale nature of the oceanographic/temperature effect.

There are two potential mechanisms for the difference in male fur seals numbers at South Georgia and the South Shetlands. Firstly, in 1998 an extremely high $\hat{p}$ was observed in the ECB. This elevated $\hat{p}$ may have also occurred in the WCB but, perhaps because of predation pressure, was not detected at the core box scale by the acoustic survey. This depends on the standing stock of krill and krill flux into the South Georgia region (*cf* Murphy 1995). Secondly, if an increased biomass of krill was transported to the South Georgia area in 1998, it may have been unnecessary for male fur seals to travel south to avoid competition with females. Both male and female fur seals would have been able to forage on higher density krill patches (Boyd et al., 1998).

Potentially, the absence of Blue petrels in 1998 (Table 5.7) may have been a function

of the JR28 survey starting one month later (Chapter 2.1 Table 2.1), since Blue petrels are believed to be numerically more abundant in winter (Prince, 1980). However, there are no data on the foraging distribution of Blue petrels or how distribution might change during the breeding season, therefore we are not in a position to speculate on the exact causes of this absence in 1998. It does, however, remain a very interesting observation.

If the time of survey had contributed to the absence of Blue-petrels, then it is reasonable to consider that a similar effect might have influenced the numbers of Antarctic fur seals, since the 1998 survey was conducted later in their breeding season (Chapter 2 Table 2.1 and Figure 3.7): the Antarctic fur seal population might already have begun to disperse by February. A time series of monthly-average sea surface temperature (SST, Figure 3.7) in both core boxes shows that the reduced temperature is not a function of simply a later-survey, and that SST one month either side of the 1998 (JR28) survey was also colder than the surveys 1997 and 1999: even if the survey had been conducted at a time consistent with the other two surveys (December) the same effect of the cold $\bar{\theta}$ would have been observed.

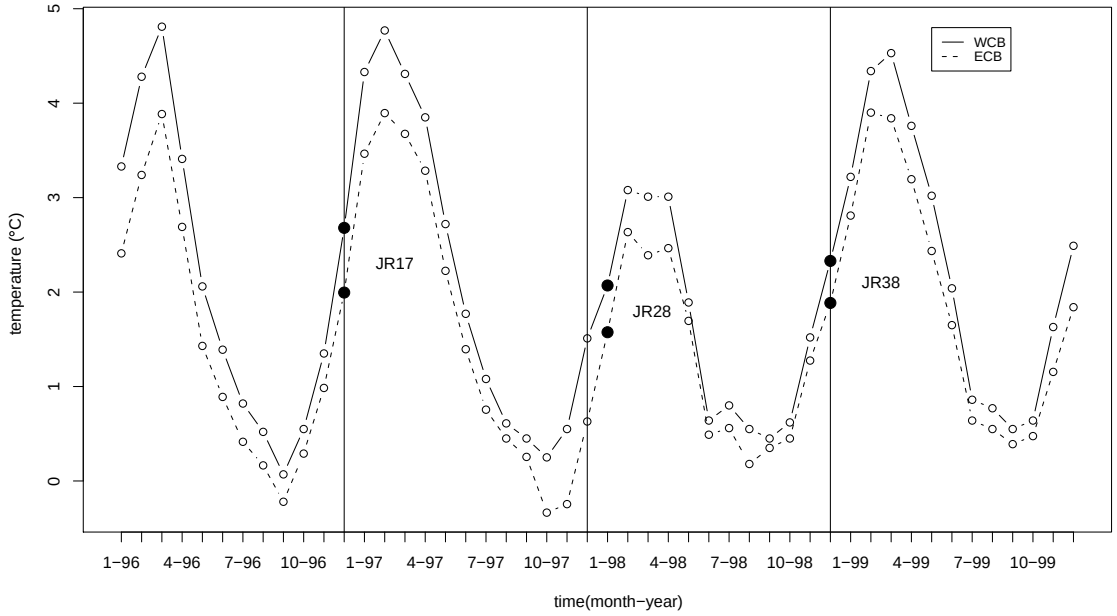

Figure 3.6: Sea surface temperature (SST, source: SeaWiFS) in the western (WCB) and eastern (ECB) core boxes with the cruise dates shown as large solid black circles on both WCB and ECB SST lines. SST was lower during cruise JR28 despite the cruise taking place in January instead of December. December of each survey year is shown as a vertical line.

3.4.5 Inter-annual variation

Although the numbers of predators ($\hat{N}$) was higher in the WCB, the absolute values and inter-annual variation in $\hat{p}$, was low in the WCB when compared to the ECB (Table 5.7 and Figures 3.3 and 3.4). This suggests that the inter-annual variation in WCB $\hat{N}$ are not driven by changes in $\hat{p}$; at least by those reflected in the snapshot measurements made in these surveys. From the three years of data, only $\hat{\rho}$ during the 1999 survey was higher in the WCB than the ECB. A pattern of higher $\hat{p}$ in the WCB was observed by Brierley et al. (1999b) for only one year (1994) out of five (1990, 1994, 1996, 1997 and 1998). As with 1999, the low $\hat{p}$ in 1994 occurred during an overall low krill density year (low krill density classified as $\hat{p} = 33.4$ g/m^2, as defined by Brierley et al. (1999b) rescaled using the Demer and Conti (2005) target strength model).

Using the sinusoidal model (Figure) for within year temporal krill density variation created by Saunders et al. (2007) the minimum and maximum line transect survey $\hat{p}$ measurements can be estimated. Whilst this model ignores inter-annual variation in drivers of krill density, the Saunders et al. (2007) model is instructive for showing that the line transect surveys used to calculate $\hat{p}$ in JR28 (late January 1998) in this investigation take place near the predicted time of maximum $\hat{p}$, 5 weeks after 1st January (Table 3.5). Surveys JR17 and JR38 were conducted in late December and early January during which the Saunders et al. (2007) model predicts $\hat{p}$ is at 65% of its maximum (Table). Consequently, the high $\hat{p}$ observed during the later JR28 cruise, may have partially been caused by the time of year that the cruise was conducted. However, the time of year corrected $\hat{p}$ (Table 3.5) show that 1998 was still a year of exceptionally high $\hat{p}$. Also, it should be remembered that for the purposes of studying krill predator-prey interactions it would be inappropriate to use the time of year scaled $\hat{p}$ because this would introduce a temporal mismatch between the krill and air-breathing predator observations.

		Western core box			Eastern core box		
Year	Cruise	$\hat{p}$	scale factor	scaled $\hat{p}$	$\hat{p}$	scale factor	scaled $\hat{p}$
1997	JR17	53.16	1.52	80.80	101.91	1.52	154.90
1998	JR28	54.39	1.07	58.20	350.51	1.07	374.50
1999	JR38	43.00	1.52	65.36	32.58	1.52	49.52

Table 3.5: Seasonal peak mean krill density estimates ($\hat{p}$, g/m^2) using the Saunders et al. (2007) model and the line-transect $\hat{p}$ point estimates and time of survey. The scale factor was estimated using the Saunders et al. (2007) sinusoidal model for $\hat{p}$ temporal variation. Note: using the Saunders et al. (2007) scaling 1999 in the ECB is no longer considered a year of low krill density.

Both core boxes were influenced by large-scale physical drivers in all years, however

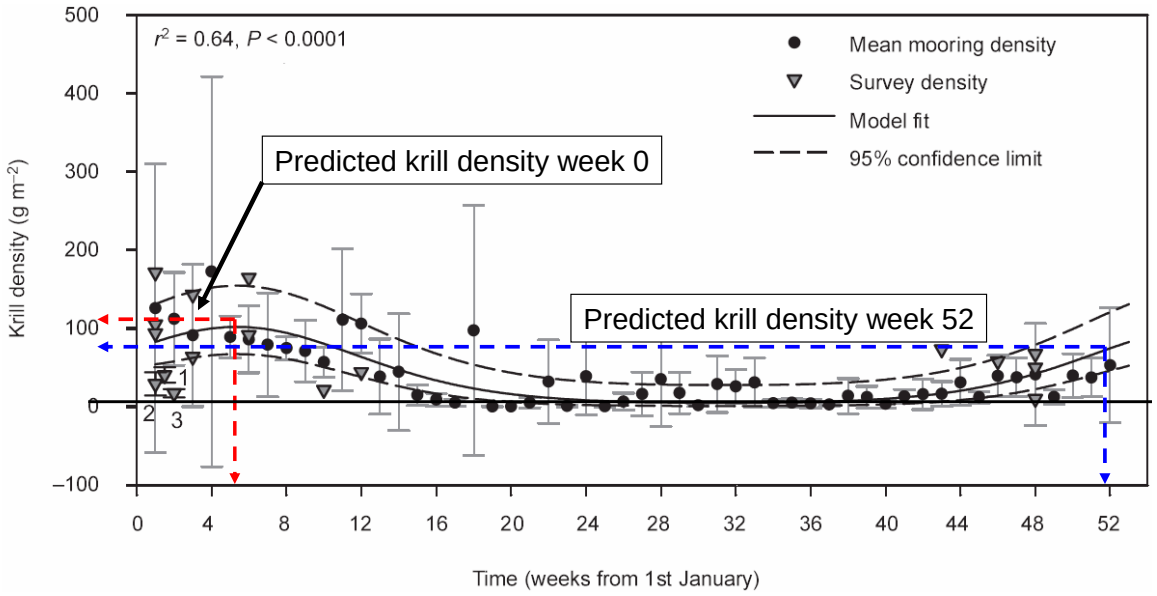

Figure 3.7: The sinusoidal model developed by Saunders et al. (2007). This model was used to rescale the one month later JR28 mean areal krill density estimates ($\hat{\rho}$). Using this model the difference between $\hat{\rho}$ at week 52 (blue line) and $\hat{\rho}$ at week 0 (red line) of 35% was used to calculate the scale factor in Table 3.5.

local (small-scale) predator sightings (n) and $\hat{p}$ may result from local physical processes or could be biologically driven as suggested by Meredith et al. (2005). Finer-scale models of the local-scale physical processes around the South Georgia shelf should help determine the role of biological forcing in $\hat{p}$ dynamics. For example, the higher number of predators in the WCB may have been caused by a lower inter-annual variation in $\hat{p}$, while this might appear to make foraging potentially less energetically profitable than the ECB, this might be balanced by making the distribution of prey more predictable. This lower variation in $\hat{p}$ may be caused by consistent advection of krill into the WCB or, in contrast to the ECB, a higher level of predation which dampens variation in $\hat{p}$, so a high density of krill never accumulates in the WCB.

The lower density of krill in the WCB compared to the ECB (Table 3.3; Brierley et al. 1999b) is sufficient to sustain predators that forage in the WCB (*e.g.* Hunt et al. 1992a; Reid et al. 2000b), suggesting there are other reasons why predators chose to forage in this lower region of $\hat{p}$. For example, krill may have a lower detectability in the ECB by predators. This may be caused by krill forming smaller swarms, or multiple krill swarms clustering differently in the ECB (Trathan et al., 2003). Alternatively, krill may be distributed at deeper depths, making swarms harder to locate, preventing surface feeders from foraging and requiring greater energy expenditure by divers (Mori and Boyd, 2004). Finally, the spatial location of krill may be more predictable to predators in the WCB, making a simple foraging strategy effective (*e.g.* Trathan et al. 2006) enabling

individual animals to optimize foraging, using experience from previous trips (Staniland et al., 2004). The swarm characteristics reported in Chapter 2 go some way to supporting this, particularly swarms in the WCB. Swarm types in the WCB show a consistent split inter-annually and between the proportion of a swarm type that is found on and off shelf (Table 2.8).

3.4.6 Summary

The results of this investigation have shown that core box is more important than year for determining the number of air-breathing predator species present and their abundances. Further, despite the higher density of krill in the ECB, more predators were found in the WCB: the reasons for this remain unclear. The absence of Blue petrels and the elevated abundance of Antarctic fur seals suggest that 1998 was an anomalous year, characterised by colder than average water surrounding South Georgia, and a high density of krill in the ECB.

It is apparent that simply examining snap shot krill density on the scale of a core box cannot explain why more predators appear to be foraging in the WCB, a region of lower instantaneous $\hat{p}$. Consequently, it may be necessary to examine the distribution of krill at a finer spatial scale the rate of krill flux in the boxes, to consider in more detail areas that may have high $\hat{p}$, such as the continental shelf break (Trathan et al., 2003). Using moored instruments Brierley et al. (2006) showed three step changes in krill abundance in a 28 day time series in the WCB. That study demonstrates that it is important to reconcile differences in temporal variation between predators and prey in the South Georgia ecosystem. This also showed the limitations of the acoustic estimate of $\hat{p}$, used in this investigation, which assumed that an instantaneous snap shot of krill over a typical 5-day core box survey was representative of a seasonal krill $\hat{p}$, and could not examine temporal variation in krill density or predator encounters during a survey.

Given the openess of the South Georgia ecosystem to local and remote environmental variability this investigation has been useful for detecting the influence of ocean-wide events. Within the limitations of the data available, the qualitative influence of these events has been shown, but small scale observations and analysis is required to examine predator-prey interactions and further assess interactions between krill and air-breathing predator species. These issues will be addressed in the following chapter.

Chapter 4

Small-scale spatial and temporal interactions between Antarctic krill and air-breathing predators at South Georgia, 1997 to 1999

4.1 Introduction

In the previous two chapters it has been shown that there was significant variation in the mean areal krill density ($\hat{\rho}$) between the two South Georgia study sites. The eastern core box (ECB) had consistently higher $\hat{\rho}$ than the WCB. In chapter 2, it was shown that the number of krill swarms (n_s) and $\hat{\rho}$ were strongly correlated. Also, krill swarm types were shown to be different between core boxes and on and off continental shelf regions. This chapter examines the small-scale (<10 km) spatial overlap between krill and air-breathing predators.

The research in this chapter has been conducted to determine the characteristic spatial scale (L_s) of krill thereby allowing indirect assessment of the prey-field available to predators. The assessment of krill distribution has been split into depth horizons, thereby enabling the availability of krill to predators to be determined.

The characteristic scale of krill predator species can be used to determine if predators forage in similar sized groups, which gives an indication of foraging search efficiency. The cross-correlation between characteristic scales of krill and predators determine the foraging overlap, and may also determine the cues a predator use. For example, facultative feeding, where predators do not use the prey distribution to as a foraging cue, rather another foraging predator may be used as a cue, which would be shown by high inter-species characteristic scale (Grënbaum and Veit, 2003). Finally, a negative cross-correlation between predators is suggestive of competition avoidance (Veit et al., 1993).

4.1.1 Marine predator-prey interactions

Observing scale dependent predator-prey interactions in the marine environment can be difficult. Often studies are based on acoustic and visual observations made from research ships conducting line transect surveys (*e.g.* Hunt et al. 1992a; Croll et al. 1998; Fauchald and Erikstad 2002). Marine surveys are time consuming, with the nominal research vessel survey speed being only 10 knots (equivalent to c 440 km of line transect observations per day). Ship based observers only sample a narrow strip transect along the sea surface (Figure 4.3), and vertically-downward looking conventional echosounders, with a narrow beam width, typically being 7^o, only sample a small volume of water (Gerlotto et al., 1999). Analyses are often conducted assuming that the spatial coverage of surveys is achieved instantaneously, thereby providing a snapshot of a predator-prey system, which ignores rapid biotic and abiotic changes that can occur in the marine environment. Further, the relationship between predators and prey is likely to be complex, may be density dependent and occur at multiple spatial scales (*e.g.* Sims et al. 2008). Also, because the marine predator is likely to use a different search strategy to a research ship, there will be a sampling mismatch: there is no requirement for a predator to search for prey until the maximum available prey is encountered, predators simply need to find patches that where quality is above some minimum threshold. Therefore, simply expecting a positive relationship between predator and prey abundances is generally naive.

When considering predator-prey interactions as presence-absence it is possible to observe a predator-prey system in four states (Table 4.1). Incorporating predator behaviour may help determine the state in which a predator-prey system is observed, but given the many potential behaviours of predators interpreting predator-prey interactions can be difficult. Even if predators and prey are co-located this does not mean that foraging is taking place. For example, predators could be resting between foraging bouts, be transiting to or from an alternative foraging site, or be satiated. This makes the observation of predator behaviour vital for interpreting predator-prey interactions (Table 4.1).

4.1.2 Krill predator-prey interactions

The availability of krill to predators influences the foraging success of predators in two ways. Firstly, krill in deeper water are less likely to be detected by the krill predator species considered in this research (Tables 4.2 and 4.3). Secondly, many of the flying bird species are only capable of surface feeding or making brief dives in the top few metres of the water column, so krill deeper than this, even if detected, remain inaccessible. The mechanism for the detection of krill by land-based diving predators is unclear, but given the diving capabilities of species in this group, krill deeper than 80 m will typically remain

Predator	Prey	Explanation
Absent	Absent	Simply, neither predators or prey are present. Predators have eaten prey to below a detectable threshold and departed. Unsuitable environment for prey
Absent	Present	Prey not detected by predators. Predators have eaten some prey and departed. Predators foraging and diving so remain undetected from the surface (availability bias).
Present	Absent	Predators in transit. Predators searching for prey. Predators engaged in social (non-foraging) activity. Prey eaten or dispersed.
Present	Present	Predators feeding. Predators satiated. Predators avoiding inter-specific competition. Chance overlap.

Table 4.1: Potential states of presence/absence in a marine predator-prey system, incorporating air-breathing predators.

undetected. Consequently, examining the acoustically derived density of krill ($\hat{p}$) through the entire vertical observation range (z=250 m), as has been carried out in previous research (*e.g.* Hunt et al. 1992a and Reid et al. 2000b), may weaken the apparent spatial association between krill and predators.

In a 1998 survey, at the core box scale, Reid et al. (2000b) found a positive relationship between mean area krill density and the abundances of ten species of whale. This positive relationship weakened at smaller spatial scales, a result which was believed to be caused by a mismatch in the abundances of krill swarms and whales: there were more krill swarms than whales, so at smaller spatial scales fewer swarms were co-located with whales, thus weakening the overall spatial relationship between krill and whales.

4.1.3 Objectives

The objectives of this chapter are to use the contemporaneous krill density and air-breathing predator sightings collected during three multi-disciplinary research cruises between 1997 and 1999 to: (1) determine the spatial scale of operation of krill and krill-predators at South Georgia across study sites and years, using a variety of techniques; (2) examine the implications of the differences in vertical distribution of krill for predator distributions; and (3) suggest how sampling on multi-disciplinary research cruises can be

improved to better examine the spatial relationships between predators and prey.

4.2 Materials and Methods

4.2.1 Sampling techniques

Line transect surveys comprising concurrent, continuous, hydroacoustic krill and visual air-breathing predator observations were conducted from the RRS *James Clark Ross* (JCR) in summers 1997, 1998 and 1999 in the vicinity of South Georgia, at two study sites, the WCB and the ECB (Figure 2.1, Chapter 1).

Predator observations

Times of encounter for all marine seabird and mammal sightings, along with predator species, group size and activity (e.g. feeding or transiting) were recorded continuously along each transect. A team of two researchers, one observer and one scribe, counted all species of seabirds and mammals encountered in a square with side length = 100 m, located 100 m in front of the JCR's bow, which is effectively a strip-transect design, as described by Tasker et al. (1984) (Figure 4.1). For species in the divers and large flying bird groups (Table 4.2) only encounters where predators were observed to be foraging were used. All observations from the small flying bird group were included because it is difficult to identify foraging behaviour in these species.

During post-processing, the time of predator observation was used to assign the JCR's GPS position (latitude: φ_S, longitude: λ_S) to each predator encounter. In this investigation interactions between krill and air-breathing predators were assessed in post-processing over along transect aggregation intervals of 0.5 to 10 km. Within an aggregation interval the abundance of predators (n), or groups of predators, and the density of Antarctic krill (g/m^2 wet mass) was calculated. To avoid potential bias caused by the offset-JCR position being assigned to a predator encounter it was necessary to relocate the ship's geographic position, as observed from the GPS antenna to calculate geographical position at the centre of the predator observation box (φ_P, λ_P, Figure 4.1). To adjust for the position difference caused by the along transect distance between the JCR's GPS antenna and the centre of the predator observation box, the JCR's GPS position assigned to a predator sighting was relocated by 175 m forward of the GPS antenna position, to the centre of the observation box using the geodetic inverse calculation. This calculation uses the observer geographic position, in this case the JCR GPS antenna (φ_S, λ_S), and the range (r=175 m) and bearing (θ_S, JCR heading) to determine the predator geographic position (φ_P, λ_P). The translation was performed using GeoCalc, v3.09 (Blue Marble Geographics).

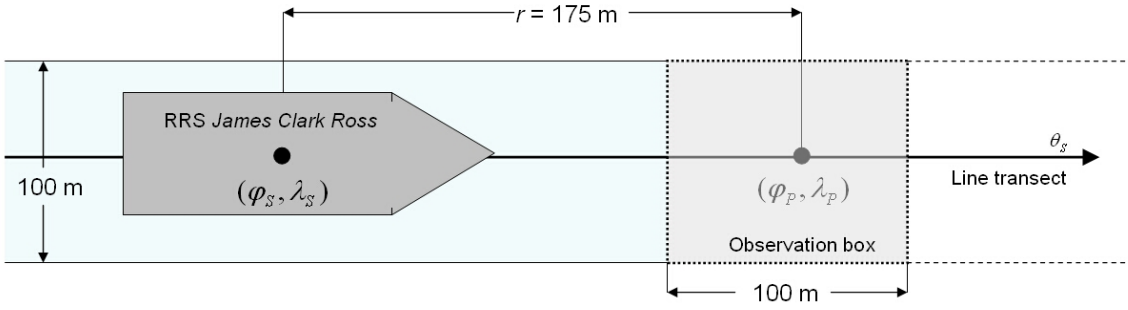

Figure 4.1: Plan view of the predator observation square. The centre of the observation square (side length = 100 m) is located 100 m in from the bow of the RRS *James Clark Ross*, creating a strip transect with a width of 100 m. The ship position (φ_S, λ_S), determined by the time of predator sighting was relocated 175 m along the current transect θ_S, using the geodetic inverse calculation, giving the geographic coordinates at the centre of the predator observation box (φ_P, λ_P) i.e. the predator's true position at time of observation.

Krill observations

The spatial distribution and density of Antarctic krill was determined using active acoustic observations from a vertically downward looking, calibrated, EK500 scientific echosounder (Simrad, Norway) operating at 38 and 120 kHz frequencies with a ping repetition rate of 1 ping per 2.5 s, which at a nominal ship speed of 10 knots gave a ping spacing of 12.5 m. Acoustic data were post-processed enabling krill density to be described using two methods:

1. **Grid method**: krill density was calculated in discrete, equal along track intervals and depths. A matrix of krill densities, with the spatial dimension of each element being 250 m along transect and 10 m deep, was created and the mean-variance relationship, correlation, spatial auto-correlation of krill and the cross-correlation of krill and predators were calculated. Krill densities derived using this method were also used to determine the vertical structure of krill in depth bands appropriate to the predator foraging depth.

2. **Swarm method**: Krill swarms were identified using the shoal analysis and patch estimation system (SHAPES) as defined in Barange (1994) (see Section 2.2.3, Chapter 2 for methods).

4.2.2 Spatial overlap of krill and air-breathing predators

The acoustically derived grid of krill densities, integrated over depth horizons given in Section 4.2.1, was used to assess the spatial structure of krill and predators through the

application of three techniques:

1. **Correlation** between adjacent along transect aggregation intervals (0.5, 1, 2, 3, 4, 5, 6, 8 and 10 km) was calculated to determine spatial scale at which krill and predators were observed during the surveys.

2. **Spatial autocorrelations** at 0.5 km along-transect intervals were calculated for predators and krill to determine the characteristic scale and the variation in characteristic scale that occurred between core box and year.

3. **Cross-correlation** functions at 5 km along transect intervals were calculated to determine the spatial overlap between krill and different krill predator species (Table 4.2), and combinations of predator species to assess the possible existence of facilitative feeding.

The horizontal spatial aggregation scale, the scale at which observations were grouped of the three techniques varied (Figure 4.2) and were dependent on the results of previous techniques. Subsequent sections describe these techniques, with Figure 4.2 being included to provide an overview.

Grid method: correlations

The correlation between adjacent along-transect abundances of predator groups was calculated at aggregation intervals of 0.5, 1, 2, 3, 4, 5, 6, 8 and 10 km. Abundance within an aggregation interval was calculated as the total number of predators from each group sighted within a particular interval, for all surveys (Figure 4.3).

Grid method: auto-correlation functions

To calculate auto-correlation functions (ACF) of predator observations and acoustically derived krill density estimates, data for each survey were aggregated at common along transect intervals of 0.5 km, giving approximately 160 samples per transect. The 0.5 km aggregation interval was selected based on the results of the above correlation analysis. Within an aggregation interval $\hat{\rho}$ was calculated and the total number of predators (n) determined. Estimates of predator n were log-transformed prior to calculating the ACF. The ACF for each predator species with n >1,000 (Table 4.2), across all years, was calculated for each transect. The n >1000 threshold was selected to provide sufficient observations to calculate the ACF and to reduce the number of predator species for analysis. The mean inter-transect ACF was determined and the characteristic scale (L_s) estimated. In this study L_s was defined at the lag distance (k, km), or lag within which

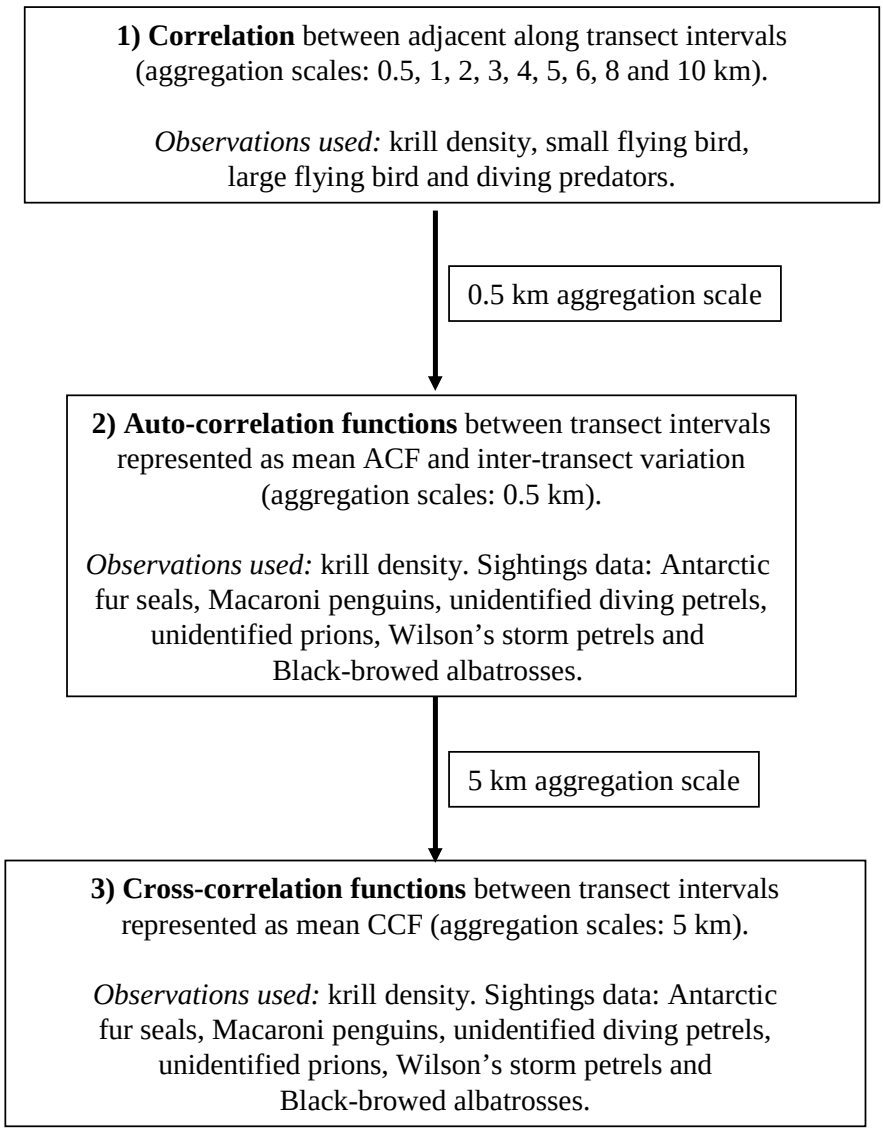

Figure 4.2: Analysis techniques used to identify the spatial scale of predators and krill. The aggregation interval used in technique two is dependent on technique one (0.5km) and the aggregation scale used in technique three is dependent on the results of technique two (5 km).

$ACF(k) \leq sig.ACF_{(n,k)}$, where:

$$sig.ACF_{(n,k)} = \pm\frac{\sqrt{2}}{n-k} \tag{4.1}$$

which is the significance level of ACF at lag k, given a total of n lags (see Box and Jenkins 1976). Within L_s the 0.5 km aggregated abundance of predators, and krill density, were more similar than expected from a random distribution.

To summarise, the ACF for a given transect, year and core box, e.g. transect 1,

Predator and group	number of sightings (n)
Small flying birds	
Black-bellied storm petrel (*Fregetta tropica*)	548
Blue petrel (*Halobaena caerulea*)	482
Cape petrel (*Daption capense*)	225
Soft-plumaged petrel (*Pterodroma mollis*)	179
Diving petrel(unid) (*Pelecanoides sp.*)	**2,158**
Prion(unid) (*Pachyptila sp. (desolata)*)	**30,311**
Wilson's storm petrel (*Oceanites oceanicus*)	**3,447**
Large flying birds	
Black-browed albatross (*Thalassarche melanophris*)	**1,271**
Grey-headed albatross (*Thalassarche chrysostoma*)	289
Light-mantled sooty albatross (*Phoebetria palpebrata*)	45
Wandering albatross (*Diomedea exulans*)	171
White-chinned petrel (*Procellaria aequinoctialis*)	**2,263**
Divers	
Antarctic fur seal (*Arctocephalus sp. (gazella)*)	**7,029**
Gentoo penguin (*Pygoscelis papua*)	789
King Penguin (*Aptenodytes patagonicus*)	160
Macaroni penguin (*Eudyptes chrysolophus*)	566

Table 4.2: Total number of predators sighted during six surveys. Predators were split by group and species with $n > 1{,}000$ are shown in bold.

WCB in 1998, was calculated at each 0.5 km aggregation interval (k). The mean ACF across transects, within a core box and year was calculated for each normalised, log-transformed, predator and krill density estimate and was used to determine L_s. For each of the five predator species with N >1,000: Black-browed albatross (*Thalassarche melanophris*); White-chinned petrel (*Procellaria aequinoctialis*); Wilson's storm petrel (*Oceanites oceanicus*); Antarctic fur seal (*Arctocephalus sp. (gazella)*); Prion (*Pachyptila sp. (desolata)*), and krill density, an estimate of the mean and variance of ACF at a given lag, for each core box and year was calculated giving six ACF curves per predator species or krill density.

Grid method: cross-correlations

To assess the spatial overlap between krill-predators and krill, and between krill-predators, cross-correlations (CCF) were calculated at 5 km aggregation intervals. The selection of 5 km aggregation interval was based on the results of the ACF analysis.

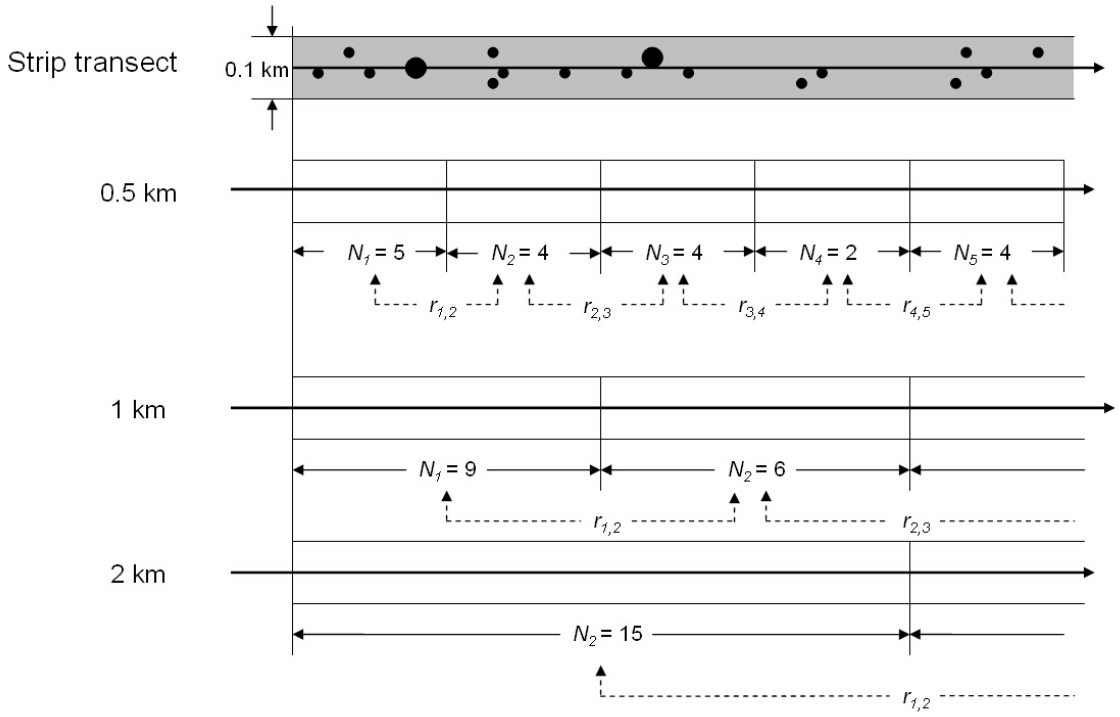

Figure 4.3: Pearson's correlation coefficient for adjacent along transect aggregation intervals. The top horizontal line shows in plan view predators sighted. Large black dots in the grey area (strip transect) are groupsize=2, small dots are groupsize=1. In this example the correlation coefficient for krill predator abundance (n) is calculated for pairs of 0.5, 1 and 2 km aggregations intervals.

Grid method: vertical distribution of krill

To determine the availability of krill to predators, the mean areal density of krill ($\hat{\rho}$) was determined from acoustic observations, in 10 m depth horizons, from a depth of 10 m to 250 m for each core box. The $\hat{\rho}$ for a given depth horizon and the variation in $\hat{\rho}$ within a depth horizon ($Var[\hat{\rho}]$) between transects within a core box was also calculated using the Jolly and Hampton (1990) technique. The full acoustic observation range was used so that the inter-survey differences in krill density could be examined outside of the acoustic observation range.

None of the 16 predator species considered in the auto-correlation analysis are capable of routinely diving to the full acoustic observation depth of 250 m. Consequently, the analysis of the spatial relationships between krill and predators have been confined to two vertical subsets of krill (Acoustic depth, Table 4.3).

Species	Dive depth (m)	Acoustic integration depth (m)
Prions (unid.)	5.5 ±1.4 Chastel and Bried (1996)	10 to 50
Antarctic fur seal	27±10.5 Boyd et al. (1994)	10 to 50
Wilson's storm petrel	2.5 Croxall et al. (1988a)	10 to 20
Diving petrels (unid.)	25.7±11.2 Prince and Jones (1992)	10 to 50
White chinned petrel	5 Huin (1994)	10 to 20
Black-browed albatross	2.5 ±1.3 Prince et al. (1994)	10 to 20

Table 4.3: Mean diving depths ±S.E. of krill predator species with n >1,000 sightings from 1997 to 1999. Acoustic integration gives the depth range over the acoustic data are integrated to calculate the areal krill density ($\hat{\rho}$).

4.2.3 Swarms method: krill swarms and air-breathing predator interactions

The effect of the spatial distribution and characteristics of krill swarms on the number of observed krill predators, n, in the vicinity of a krill swarm was examined, with n being calculated from the krill predator observations, rather than the gridded and summed predator observations. The length (l) of a krill swarm plus half the estimated sampling strip transect width (50 m, Figure 4.3) was used as the sampling region. Given that no distance data were collected for predators all sightings were considered to occur on the transect and n falling between the start geographical coordinates (φ_S, λ_S) and end geographical coordinates (φ_E, λ_E) was calculated. The correlation between n and krill swarm metrics volumetric density, length and depth was calculated. Additionally, linear and non-linear relationships were explained using generalized linear and additive models.

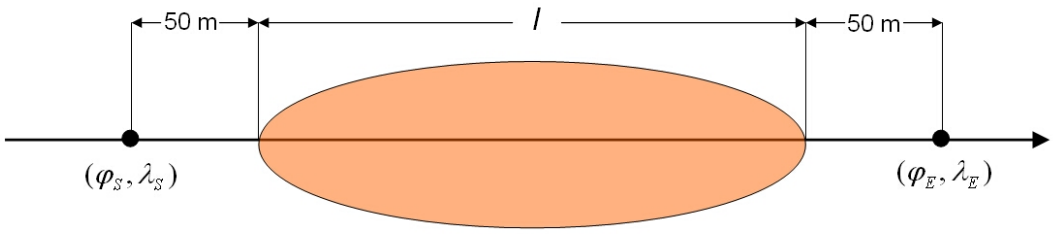

Figure 4.4: Plan view of the calculations used to determine the number of predators in the vicinity of a krill swarm (grey ellipse). The number of predators detected between the start of the sampling length, a point 50 m before the start of a krill swarm (φ_S, λ_S), of length l, finishing at a point 50 m beyond the end of the krill swarm (φ_E, λ_E).

4.3 Results

4.3.1 Summary spatial scales

All predator groups and krill showed significant, but varying, correlations between adjacent along-transect aggregation intervals, up to the 5 km aggregation interval (Figure 4.5). The small flying bird group, divers group and krill shared a common 5 km aggregation distance of significant correlation (Figure 4.5), suggesting either similar foraging scales, facilitative feeding or observation bias. The large flying bird group was significantly correlated from 1 to 10 km along transect aggregation scale, suggesting a larger foraging range. Given that the small flying bird group, divers group, and krill show significant spatial correlation at the smallest along transect aggregation interval (0.5 km), this range was used for the spatial-autocorrelation analysis.

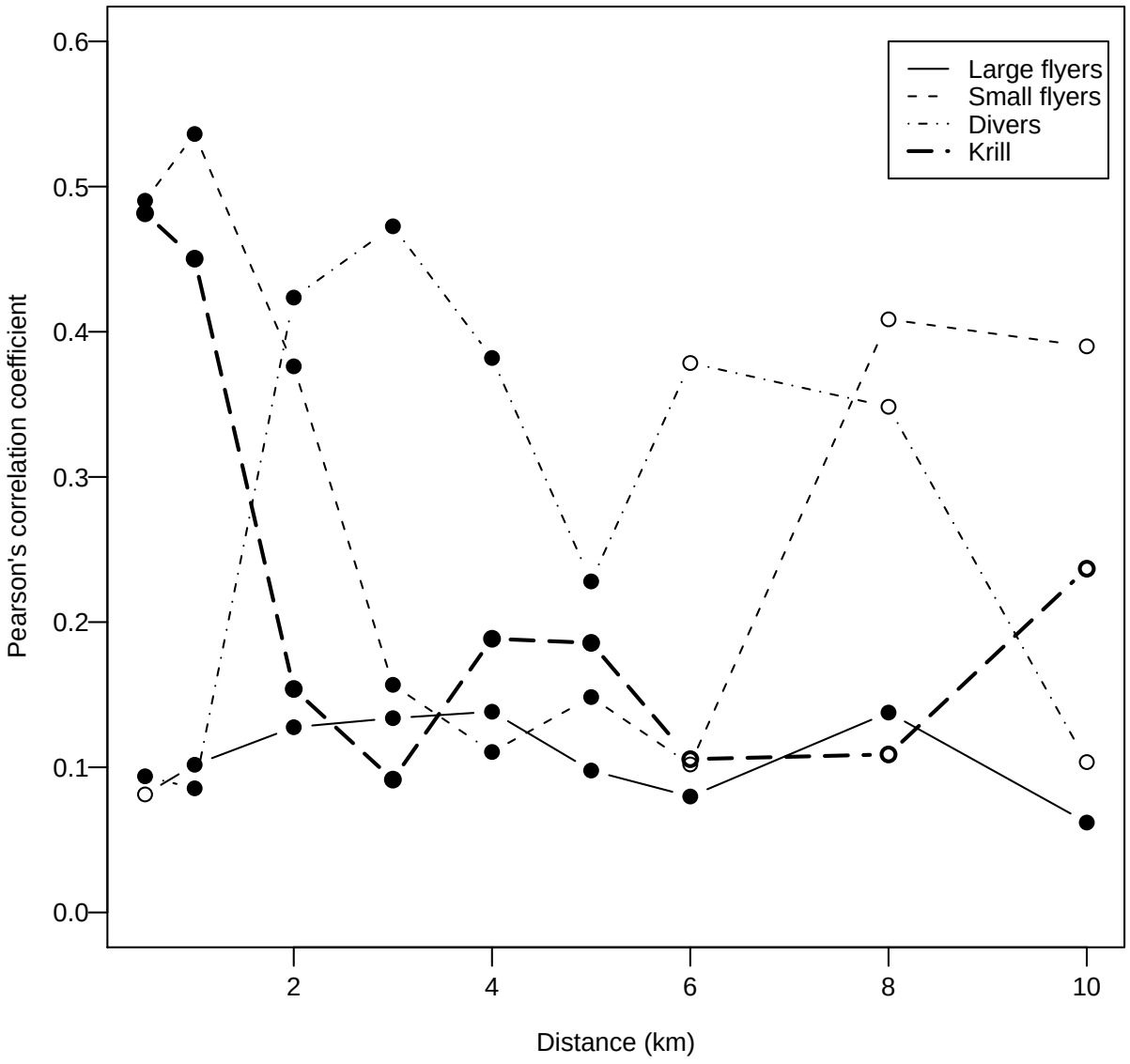

Figure 4.5: Variation in spatial auto-correlation in predator groups and Antarctic krill, for all years, in both boxes, aggregated at the scale of the x-axis, calculated using Pearson's correlation coefficient. Closed circles denote statistically significant (p <0.05, Bonferroni correction applied) correlations, open circles are not significant.

4.3.2 Vertical distribution of krill

There is considerable variation in the vertical distribution of krill density ($\hat{\rho}$) between study site and year, over the entire acoustic observation depth of 10 to 250 m (Figure 4.6). Also, there is large inter-survey variation in $\hat{\rho}$ between 10 m depth horizons. From the five predator species considered here, only diving petrels and Antarctic fur seals are capable of routinely diving below 20 m (Table 4.3). Consequently cross-correlations between krill and Antarctic fur seals and diving petrels were calculated using depth horizons between 10 to 50 m. For the other non-diving species krill density between 10 and 20 m was used.

In all surveys $\hat{\rho}$ in the upper 50 m of the water column was lower in the WCB, then the ECB (Table 4.4). Furthermore, to a depth of 100 m the WCB generally has lower $\hat{\rho}$ than the ECB. Also, the ECB generally showed a higher $\hat{\rho}$ in the top 100 m, compared to $\hat{\rho}$ in the ECB in the 100 to 250 m depth range, but the WCB did not (Figure 4.6).

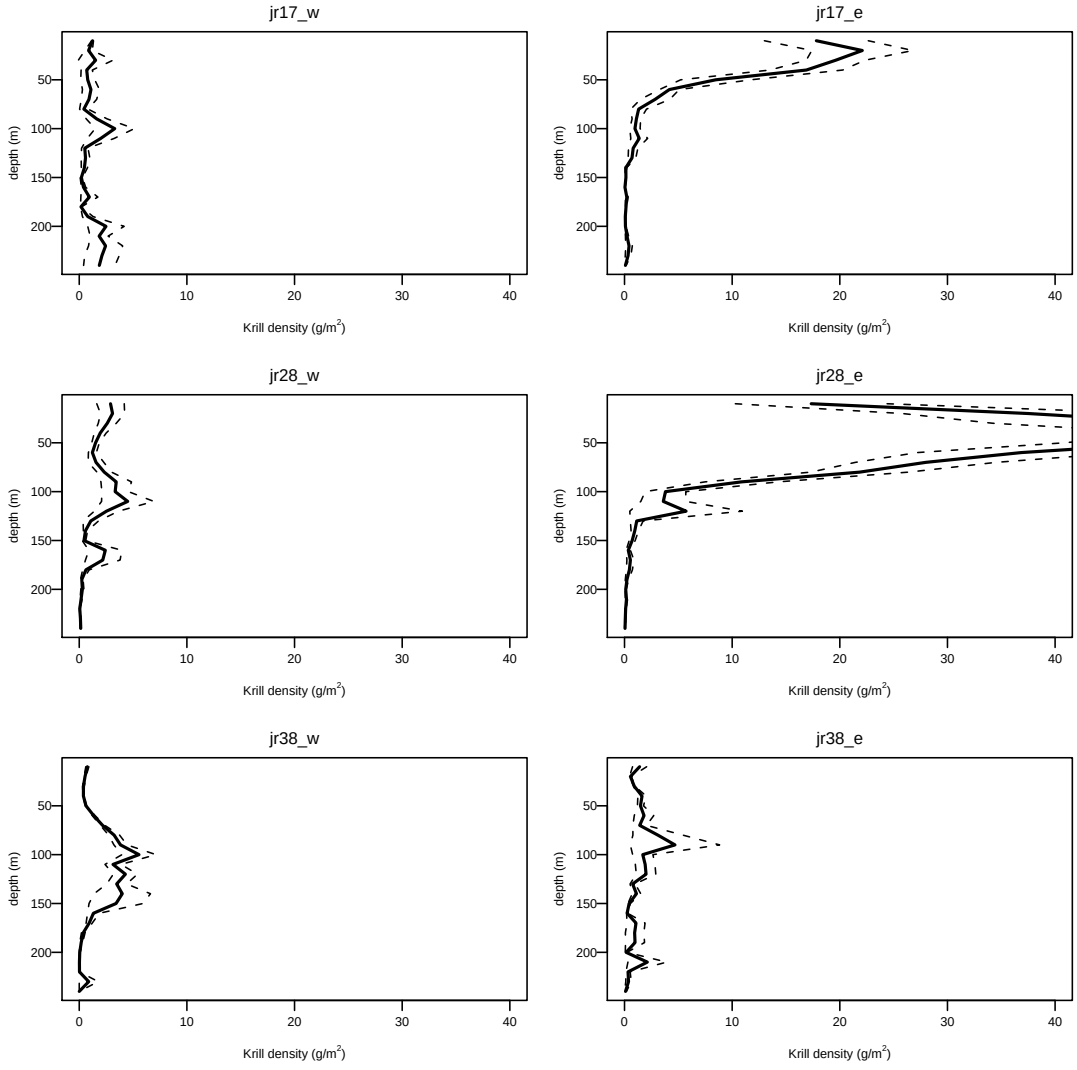

Figure 4.6: Areal density of krill ($\hat{\rho}$, g/m^2), in 10 m depth horizons from 10 to 250 m depth, by core box and year. The mean value of $\hat{p}$ for each 10 m depth horizon is given as a solid line. The dashed lines are ± 1 S.E., Both $\hat{p}$ and associated S.E, were calculated using the Jolly and Hampton (1990) technique. Note $\hat{\rho}_{max}$=78 g/m^2 in jr28_e

Depth (m)	Western core box ($\hat{p}$, g/m^2)			Eastern core box ($\hat{p}$, g/m^2)		
	JR-17	JR-28	JR-38	JR-17	JR-28	JR-38
10 to 20	1.23(0.05)	2.91(0.44)	0.75(0.19)	17.82(0.25)	17.34(0.4)	1.4(0.45)
20 to 30	0.87(0.13)	3.09(0.36)	0.54(0.16)	22.09(0.21)	37.48(0.31)	0.55(0.16)
30 to 40	1.52(0.32)	2.6(0.32)	0.39(0.2)	19.61(0.14)	52.73(0.35)	0.91(0.07)
40 to 50	0.69(0.17)	1.95(0.28)	0.39(0.14)	16.89(0.21)	69.23(0.27)	1.63(0.24)
50 to 60	0.79(0.19)	1.51(0.23)	0.62(0.08)	8.47(0.4)	50.99(0.2)	1.48(0.19)
60 to 70	1.09(0.22)	1.22(0.3)	1.34(0.1)	4.16(0.22)	36.86(0.26)	1.81(0.5)
70 to 80	0.9(0.24)	1.56(0.46)	2.17(0.1)	2.84(0.5)	27.99(0.23)	1.41(0.45)
80 to 90	0.43(0.25)	2.32(0.29)	3.24(0.16)	1.31(0.57)	21.86(0.21)	3.1(0.75)
90 to 100	1.62(0.34)	3.43(0.41)	3.83(0.16)	1.1(0.38)	10.85(0.31)	4.69(0.89)

Table 4.4: Inter-survey variation in the vertical distribution of mean areal krill density estimates ($\hat{p}$, g/m^2) within a core box from 10 m to 100 m in 10 m depth horizons, calculated using the Jolly and Hampton (1990) technique (coefficient of variation given as a proportion: 14% = 0.14). The 0 to 10 m depth horizon cannot be sampled using hull-mounted vertically downward looking echosounders.

4.3.3 Krill and predator spatial structure

Spatial autocorrelation

Generally krill had a larger characteristic scale (L_s, see Section 4.2.2) in the WCB than the ECB (Table 4.5). Also, in the WCB krill L_s generally increased as krill density from 10 m depth to to deeper depths was assessed. For example, during cruise JR28 (1998) in the WCB, krill L_s increased from 6.5 km for krill between depths of 10 to 20 m ($\text{krill}_{z=10to20m}$) to L_s=14.5 km for $\text{krill}_{z=10to250m}$. However, in the ECB krill L_s showed little inter-annual or depth-horizon variation for any group of depth horizons (Table 4.5).

Krill predators generally appear to form stronger spatial self associations in the WCB. Antarctic fur seals, prions and White chinned petrels had significant ACFs for 1997 to 1999 in the WCB, but not in the ECB. In the ECB only Wilson's storm petrels had significant ACF in all years.

With the exception of prions and Wilson's storm petrels, the L_s of predators was less than the L_s of $\text{krill}_{z=10to20m}$, suggesting that krill predators do not generally aggregate at the spatial scale of krill.

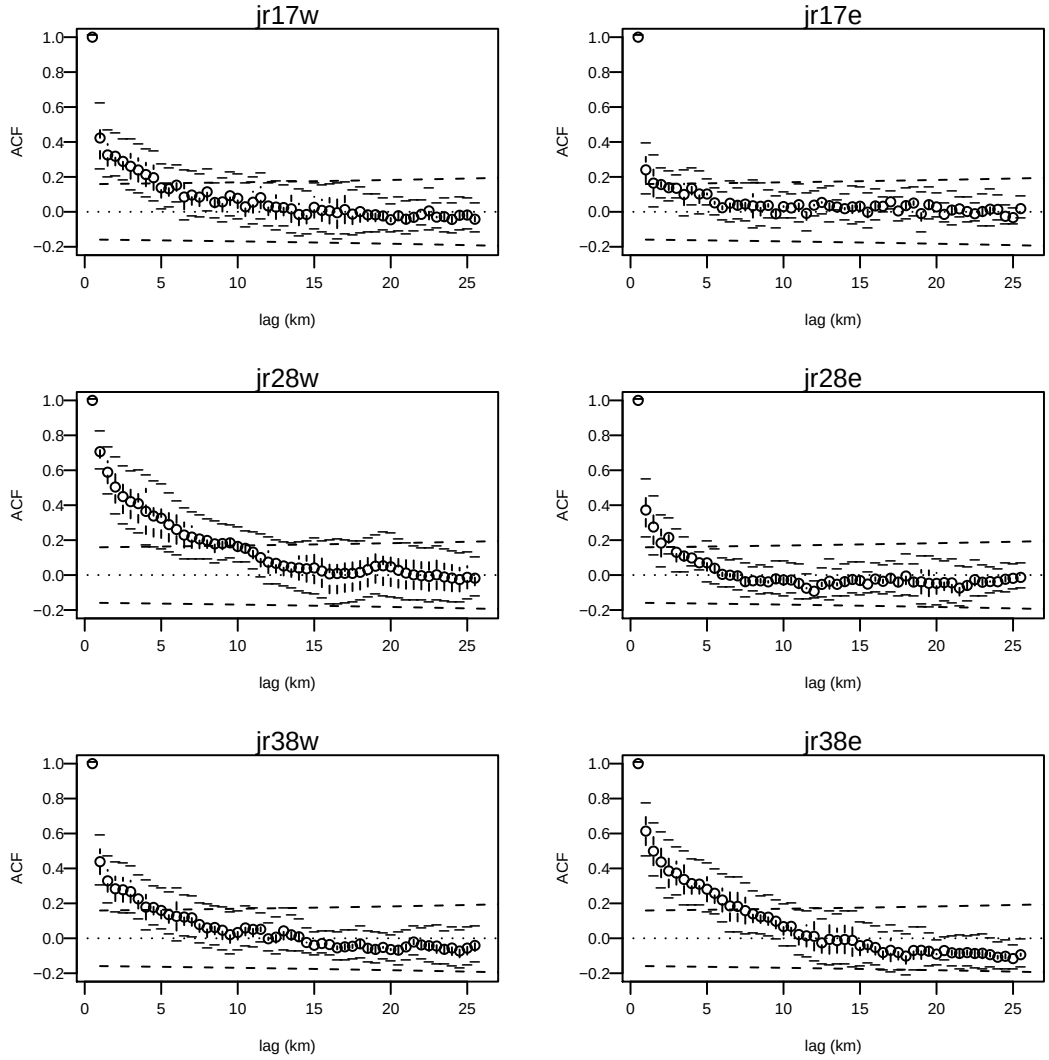

Figure 4.7: The mean autocorrelation function (ACF) of krill from 10 to 50 m, aggregated at 0.5 km intervals, calculated for each transect. Error bars are ±1S.E. determined from the inter-transect variation of ACF. The dotted lines denote significant ACF, calculated using Equation 4.1.

Species	Western core box						Eastern core box					
	JR-17		JR-28		JR-38		JR-17		JR-28		JR-38	
	L_s	r_{max}	L_s	r_{max}	L_s	r_{max}	L_s	r_{max}	L_s	r_{max}	L_s	r_{max}
$\text{Krill}_{z=10to20m}$	6.5	0.44	6.5	0.69	4.0	0.38	2.0	0.16	2.5	0.4	7.0	0.52
$\text{Krill}_{z=10to50m}$	5.0	0.43	10	0.70	4.0	0.44	1.0	0.24	2.5	0.37	7.0	0.61
$\text{Krill}_{z=10to100m}$	6.5	0.5	11.5	0.65	5.0	0.66	2.0	0.25	2.0	0.5	8.0	0.56
$\text{Krill}_{z=10to250m}$	3.5	0.5	14.5	0.64	6.5	0.71	2.0	0.27	2.5	0.39	7.0	0.59
FUSE	2.5	0.23	3.5	0.27	4.0	0.27	-	-	NS	0	NS	0.01
BBAL	NS	0.12	NS	0.15	0.5	0.20	NS	0.02	NS	0.04	NS	0.1
UNDP	NS	0.4	NS	0.2	NS	0.14	NS	0.25	NS	0.13	NS	0.2
UNPR	7	0.38	8	0.43	2.5	0.23	2.5	0.27	3	0.26	NS	0.13
WISP	NS	0.12	7.0	0.37	NS	0.13	7.0	0.41	3.5	0.29	2.0	0.24
WCPT	1.5	0.20	0.5	0.17	2.0	0.18	NS	0.02	NS	0.04	NS	0.1

Table 4.5: Characteristic scale (L_s) of all predator observations (km), from predator observation data aggregated at 0.5 km intervals along transect L_s is defined as the shortest distance at which the auto correlation function ceases to be significant (NS, Equation 4.1). r_{max} is the maximum autocorrelation function within L_s. No L_s or r values are given for fur seals in 1997 in the ECB because only one individual was sighted, and no significant ACF was apparent in 1998 or 1999 in the ECB.

Spatial cross-correlations

Given the mean L_s for $krill_{z=10to20m}$ across study sites and years was 4.75 km (Table 4.5), the spatial overlap between krill and predators was assessed using a 5 km along transect aggregation scale.

Only Black browed albatrosses and Antarctic fur seals had positive correlations with krill across sites and years (Table 4.5). Generally, Antarctic fur seals had the highest cross-correlation function at lag r ($CCF(r)$), but none of the spatial cross-correlations between krill predators and krill were significant. Other than high inter-site and year variability, there were no other discernable patterns in the predator-krill cross correlations.

The between predator CCF (denoted as X, Table 4.5) showed higher correlation than the predator-krill CCF, with all cross-correlations except White chinned petrels X Antarctic fur seals, and Blacked browed albatross X diving petrels. Also, with the exception of Black browed albatross X White chinned petrels, the significant correlations occurred in the WCB, and only White chinned petrels X prions show significant cross-correlations in two years.

Krill swarms

In all three years a higher volumetric density of krill occurred in the ECB (Table 2.6, Chapter 2), with mean horizontal nearest neighbour (NND) being lower in the ECB. However, the mean krill swarm length was larger in the WCB. Because swarms were, on average, larger in the WCB, once a predator had located a krill swarm there the predator was more likely to remain within the larger krill swarm boundary. Also swarms were shallower in the WCB, making them more detectable and accessible to predators.

No significant correlations, linear, or non-linear relationships (accessed using generalized additive models) were found between krill swarm metrics (Table 2.6, Chapter 2) and the number of predators occurring in the vicinity of a swarm.

4.4 Discussion

4.4.1 Summary of findings

From this and other investigations of krill-predator interactions (Harrison et al., 1991; Hunt et al., 1992a; Murphy, 1995; Fauchald and Erikstad, 2002), it is apparent that the at-sea distribution of air-breathing krill predators is dependent on multiple explanatory variables. Despite the complexity of at-sea distribution of krill predators, there is one characteristic that is evident from the observations of krill and the five krill predator

Cross correlation	Western core box 1997	1998	1999	Eastern core box 1997	1998	1999
	krill X predator					
Prion X $krill_{10,20}$	0.06	0.43	-0.02	-0.01	0.10	0.20
Wilson's storm petrel X $krill_{10,20}$	-0.08	0.19	-0.15	0.05	0.22	0.19
Unidentified diving petrel X $krill_{10,50}$	0.02	0.08	-0.08	0.08	-0.12	0.02
White chinned petrel X $krill_{10,20}$	0.17	0.30	-0.11	0.2	-0.05	0.08
Black browed albatross X $krill_{10,20}$	0.07	0.16	0.02	0.07	0.05	0.01
Antarctic fur seal X $krill_{10,50}$	0.36	0.23	0.38	-	0.04	0.20
	predator X predator					
Black browed albatross X Antarctic fur seal	0.18	0.42	**0.61**	-	0.21	0.29
Black browed albatross X White chinned petrel	0.46	0.26	0.56	0.19	0.43	**0.60**
Black browed albatross X Unidentified diving petrels	0.36	0.17	0.06	0.17	-0.18	0.10
Prion X Antarctic fur seal	0.43	**0.59**	0.55	-	0.19	0.22
Prion X Black browed albatross	**0.61**	0.38	0.40	0.21	0.38	0.38
Prion X diving petrel	**0.63**	0.14	0.05	0.32	-0.25	0.48
White chinned petrel X Antarctic fur seal	0.37	0.46	**0.59**	-	0.18	0.28
White chinned petrel X Prion	**0.61**	0.52	**0.58**	0.37	0.39	0.38
White chinned petrel X Diving petrel	**0.57**	0.18	0.17	0.03	-0.20	0.11
White chinned petrel X Antarctic fur seal	0.21	0.09	0.09	-	-0.02	0.17

Table 4.6: Cross correlation functions (CCF) for predators and krill aggregated to 5 km along transect intervals. CCF is given at lag 0, i.e. CCF here is a measure of the spatial similarity at a 5 km along transect scale. Significant CCF values (those greater than Equation 4.1) given in bold.

species assessed in this investigation: high variability in both study-area (core box) sightings and small spatial scale (0.5 to 10 km) interactions. The explanatory variables driving this perceived predator-prey system include: 1) the availability of krill; 2) the detectability of krill; 3) predator behaviour outside of foraging activity; and 4) interactions between different predator species, either by competition or facilitative feeding. Complexity in the predator-prey system is further increased by large variation in many explanatory variables, such as oceanographic fronts, at multiple spatial and temporal scales. In the following subsections the scale-dependent analysis employed in this investigation is used to describe quantitatively spatial and temporal distributions of krill and air-breathing krill predators, and the interactions between these air-breathing predator groups. This discussion ends with recommendations regarding future survey design.

4.4.2 Spatial variation in Antarctic krill

It is known that krill in the vicinity of South Georgia exhibits large spatial and temporal variability (Brierley et al., 1997b), and the surveys considered here from years 1997 to 1999 appear to be no exception. Results here show that there is considerable scale-dependent structure in the spatial distribution of krill around South Georgia, shown by the pattern in grouped core box and year spatial structure (Figure 4.5). The krill horizontal distribution auto-correlation of krill occurs to a mean along transect distance of 4.75 km. Ecologically this suggests that, on average, within these three years, predator foraging success will consistently occur when predators search for krill using a strategy that operates at a spatial scale of 5 km or less.

Whilst L_s does not describe krill patch quality it does describe krill density similarity. In the WCB in 1997 and 1998 krill had a larger characteristic scale (L_s) suggesting that it is easier for predators to locate and track krill of similar densities (Table 5.7, Chapter 3) which may drive the elevated number of predators in the WCB. Also, krill predators may have influenced the formation of krill swarms, either through anti-predation behaviour (Hamner and Hamner, 2000) or by predators herding krill (Hamer, 1984; Murphy et al., 1988).

There is considerable variation in the vertical distribution of krill between core box and year (Figure 4.7 and Table 4.4). Furthermore, there is variation in the spatial structure of krill between depth horizons in the same year and core box (Table 4.4). Together these facts suggest that simply integrating acoustic energy backscattered by krill through the water column from 10 to 250 m (as is typical for krill biomass surveys, Trathan et al. 2001) will mask small-scale krill structure, and thus mask interactions between krill and air-breathing predators. In addition, considering krill biomass outside of the foraging depth of air-breathing predators in conjunction with predator distribution will give a

biased estimate of the krill available to a predator and perturb krill/predator spatial association.

Considering the vertical distribution of krill exposes a major limitation of conventional hull-mounted echosounder transducers: an inability to sample the surface distribution of krill. Due to the depth of the echosounder transducer (6 m on *RRS James Clark Ross*), vessel motion and the acoustic nearfield, the region of water from the sea surface to a depth of *c.* 10 to 20 m cannot be consistently observed. The inability to acoustically observe krill in shallow water is a major limitation of this study and may decouple the acoustically derived estimates of krill density and visual observations of air-breathing predators, particularly for the shallow divers (Table 4.3).

4.4.3 Spatial distribution of krill predators

The differences in predator L_s (Table 4.5) expose inter-species variation in foraging activity which may have been caused by differences in predator foraging technique, which in turn may be due to predators attempting to avoid inter-species foraging competition. Differences in L_s show that the technique of grouping predators into functional groups for small-scale analysis would weaken any signal in predator spatial structure.

Another key characteristic of predator activity is of a consistent L_s of Antarctic fur seals in the WCB, while in the ECB there is no discernible spatial structure, which is replicated in the ECB by White chinned petrels (Table 4.5). The reasons air-breathing predators forage in the WCB, an area of generally lower krill density (Table 4.4, Brierley et al. 1997b, 1999b) are unclear. Potentially both the horizontal and vertical accessibility of krill may be important. Certainly in 1997 and 1998 krill L_s was greater in the WCB (Table 4.5). Also, krill flux into the WCB (Murphy, 1995) may be sufficient to sustain predators, as may local krill growth (Tarling et al., 2007).

Diving predators may have an advantage in foraging for krill since L_s increases with the thickness of depth horizon in the WCB and remains practically constant in the ECB (Table 4.5: 10 to 20 m and 10 to 50 m krill L_s). Consequently, if an Antarctic fur seal forages on a patch of krill in the WCB at a depth of 30 m, the Antarctic fur seal is more likely to remain within a patch of krill than a predator species that can only forage to a depth of 20 m.

Antarctic fur seals, may be able to adjust their diving behaviour in response to variation in the krill vertical distribution (Boyd and Croxall, 1992), which may enable them to reach deeper swarms than we have considered in this investigation. Nevertheless many other predator species, particularly the flying bird species, are constrained to forage in the top few metres of the water column (Table 4.3), so will exhibit low variability in diving depth.

4.4.4 Krill and air-breathing predator interactions

With the exception of Antarctic prions, the L_s of predators were less than the L_s of krill. This is because there is no requirement for predators to forage at the same L_s as krill, since foraging may be adequate at the edges of single krill aggregations, where the density of krill will drop at the edge of an aggregation (at the boundary between krill aggregations and empty water).

Harrison et al. (1991); Hunt et al. (1992b) suggested that negative association between krill and predators may be due to different bird species avoiding competition through spatial segregation. There is also the possibility of negative association between different flying bird species. For example Maniscalco et al. (2001) demonstrated that interference by Glaucous-winged Gulls (*Larus glaucescens*) was detrimental to the foraging success of Black-legged Kittiwakes (*Rissa tridactyla*), with the kittiwakes making fewer foraging attempts and confining their foraging efforts to the periphery of a gull's feeding aggregation.

In all instances in this investigation the Black browed albatross X other predator cross-correlation was stronger than the Black browed albatross X krill, providing qualitative evidence of facultative feeding, with Black-browed albatross using other predator species as a proxy for krill availability, rather than krill availability itself. Previous investigations have suggested facultative feeding between Antarctic fur seals and Black-browed albatrosses, with black-browed albatrosses using fur seal feeding as a foraging cue (Grënbaum and Veit, 2003).

The horizontal and vertical distribution of krill can be assessed through the identification and description of krill swarms. It is unlikely that swarms form independently of predation since the formation or splitting of swarms by krill anti-predation behaviour (Hamner and Hamner, 2000). Also, krill may be forced into dense swarms by herding krill (Hamner et al., 1988; Murphy et al., 1988). Unfortunately, there was no relationship between the number of predators, or type of predator in the vicinity of a krill swarm and krill swarm metrics. The absence of a relationship may have been caused by either the incorrect identification of krill swarms, or a spatial mismatch between krill and predator observations.

4.4.5 Conclusion

The small spatial scale (0.5 to 10 km) analyses conducted here have demonstrated that krill and air-breathing predator characteristic scales are highly variable (Table 4.5). At smaller spatial scales (5 km, Table 4.6), there is no direct relationship between predator density and krill. This is because there is not an equal number of predators and

krill swarms, which partially explains the weak krill X predator cross-correlations (Table 4.6), which may also explain the lack of concordance between krill swarm morphology and the number of predators. The stronger inter-predator cross-correlations suggest that facultative feeding was taking place.

4.4.6 Limitations

This subsection lists potential limitations with the data acquisition technique used to observed predators and the predator-prey analysis employed in this chapter.

This investigation has attempted to use a systematic approach to determining analysis scale but, in doing so, may have inadvertently aggregated data at biologically inappropriate spatial scale and masked relationships.

Predator observers recorded all predators within a parallelogram drawn onto a bridge window, which projected a square with 100 m long sides onto the sea surface, 100 m in front of the James Clark Ross bow (Figure 4.8) . This projected square was subject to ship's motion, so the observer was faced with either recording predators as seen in the observation box, even if the ship was pointing off transect, or estimating where the box would be if the ship was stable. Both methods are subject to error: recording predators sighted in the observation box irrespective of vessel heading meant that on average predators would be recorded on transect but, at small spatial scales (100 to 500 m), there could be a mismatch between acoustically derived estimates of krill and predator sightings. The second method, attempting to correct the observation box location for motion, introduces unquantifiable measurement error and was not used.

Sampling may potentially have been been biased by krill predator availability. Antarctic fur seals spend a significant proportion of their time diving (Boyd and Croxall, 1992; Boyd, 1996). The observation technique used cannot estimate the proportion of zero observations that are true predator absences rather than those caused by predators diving whilst engaged in foraging activity, thus rendering them undetectable to surface observations.

4.4.7 Recommendations

1. Integrated studies are useful for small-scale analyses for ecosystem monitoring (Atkinson et al., 2001; Boyd and Murphy, 2001). A combination of satellite tracking, acoustic moorings (Brierley et al., 2006) and ship-based predator and acoustic surveys are required to examine predator-prey interactions with a sufficiently high spatial and temporal sampling resolution to successfully elucidate predator-prey interactions. Such an integrated study could include predator diving activity as recorded from

(a) time 0 (b) time 1

(c) time 2 (d) time 3

(e) time 4 (f) time 5

Figure 4.8: The location of 100 x 100 m box (parallelogram above base of triangle) for observing predator observations from the *RRS James Clark Ross* was highly susceptible to ship motion, and is potentially a large source of error when spatially aligning predator and acoustic observations. Photographs are between 1 and 2 s apart.

biologging data to estimate availability bias in visual air-breathing predator surface observations. However, such corrections are not trivial and are outside the scope of this chapter, and cannot correct small spatial-scale observations.

2. Due to acoustic reverberation from wind and wave noise, the JCR hull mounted (depth 6 m) acoustic transducers cannot observe krill between the sea surface to a depth of c. 10 to 20 m. This prevents the acoustic assessment of krill density in this important shallow region, where many of the species in the large and small bird groups, and indeed many diving species, are constrained to forage. Consequently, it is not possible to observe krill air-breathing predator interactions using conventional hull-mounted acoustics, and this is potentially a severe limitation in determining krill X flying bird spatial overlap. An inclined or upward looking transducer could be used to observe this region (see Everson and Bone 1986; Hewitt and Demer 1996).

3. A simulation could be used to address the question of whether non-adaptive, ship-based, line transect surveys are useful for identifying marine predator-prey spatial interactions. This simulation could be used to investigate the recovery of predator-prey interaction using a simulated krill distribution and a predator distribution with a known spatial overlap. Various line-transect methods could be applied to these data to obtain estimates of the simulated spatial overlap parameters. If the observation technique used in this investigation doesn't successfully recover the simulated predator-prey relationships, but other techniques do, then these other techniques should be adopted for future investigations.

4. The probable existence of availability bias in the visual observations make the predator data considered here a $n > 0$ dataset. If no predators were sighted within a given transect length, it cannot be determined if this is a true absence of predators or caused by predators diving out of sight. This might also explain the increased cross correlation between predator species compared to predators X krill: since for facultative feeding to occur the predator species taking their foraging cue from the other predator species must be able to detect that predator species, which is impossible if the foraging species is underwater. There may be an abundance threshold at which a single predator species aggregation can be detected, since all the individuals in a larger foraging aggregation are unlikely to all be simultaneously underwater. Establishing a relationship between environmental covariates such as chlorophyll or sea surface temperature and predator abundance may allow the proportion of true absences in the sightings data to be estimated (see Zaniewski et al. 2002; Wintle et al. 2005).

5. The inter-survey variation in detectability of krill predators cannot be estimated. This research has implicitly assumed constant detectability. The collection of distance data (see Buckland et al. 2001) to diving species, such as Antarctic fur seals, would allow detectabilty to be quantified. When combined with dive behaviour mod-

els, detectability could be used to estimate availability bias and, combined, these two models would allow abundance to be estimated and predator krill consumption rates calculated.

6. The weak cross-correlations may have been caused by a mismatch in the sampling volumes between the predator and the krill echosounder observations. The next chapter will use a multibeam echsounder, that samples a much larger volume of water, to assess very small scale (<500 m) predator-prey interactions in an effort to overcome this limitation.

Chapter 5

Multibeam acoustic sampling of Antarctic krill swarms

The research in this chapter has been submitted us:
Cox, M.J., Demer, D.A., Warren, J.D., Cutter, G.R. and Brierley, A.S. (submitted). Multibeam echosounder observations of Antarctic krill (*Euphausia superba*) swarms provide new insight to interactions between krill and air breathing predators. *Marine Ecology Progress Series*.
Cox, M.J., Demer, D.A., Warren, J.D., Cutter, G.R. and Brierley, A.S. (submitted). Three dimensional observations of Antarctic krill (*Euphausia superba*) swarms made using a multi-beam echosounder. *Deep Sea Research II*.

5.1 Introduction

Antarctic krill play a pivotal role in the Southern Ocean ecosystem (Atkinson et al., 2001; Mangel and Nicol, 2000), but are difficult to sample because of their extremely patchy distribution: much krill biomass is contained in a relatively few high-density swarms (Brierley et al., 1999b; Hofmann et al., 2004). Efforts to understand interactions between krill and their predators at sea have been hampered because of an inability to sample krill over appropriate scales (Logerwell et al., 1998; Hewitt and Demer, 2000). Attempts to link krill and predator distributions from observations along survey transects have been largely unsuccessful because the downward looking echosounders used to estimate krill abundance fail to detect krill swarms just off the track line that predators observed in the vicinity of the research vessel may be feeding upon. Conventional echosounders sample only a narrow cone (typically 7 degrees) beneath the research vessel. For a research vessel with a draft of 5 m this provides a window of observation just 3 m wide at 30 m depth.

Multibeam echosounders (MBE) sample a wider swath, extending the window of obser-

vation to the sides of the survey track, and can effectively extend from the 2 dimensional view provided by vertical echosounders to 3 dimensions (Gerlotto et al. 1999 see Figure 5.1). This chapter describes field observations of krill made by a MBE, and reports 3D characteristics of krill swarms. The objective of the field observation programme was to assess the capability of a MBE system to sample krill. If MBE sampling is appropriate for krill, it may enable collection of data leading to improved understanding of krill predator-prey interactions, krill swarm morphology and behaviour and, ultimately, perhaps to improved acoustic estimates of krill biomass.

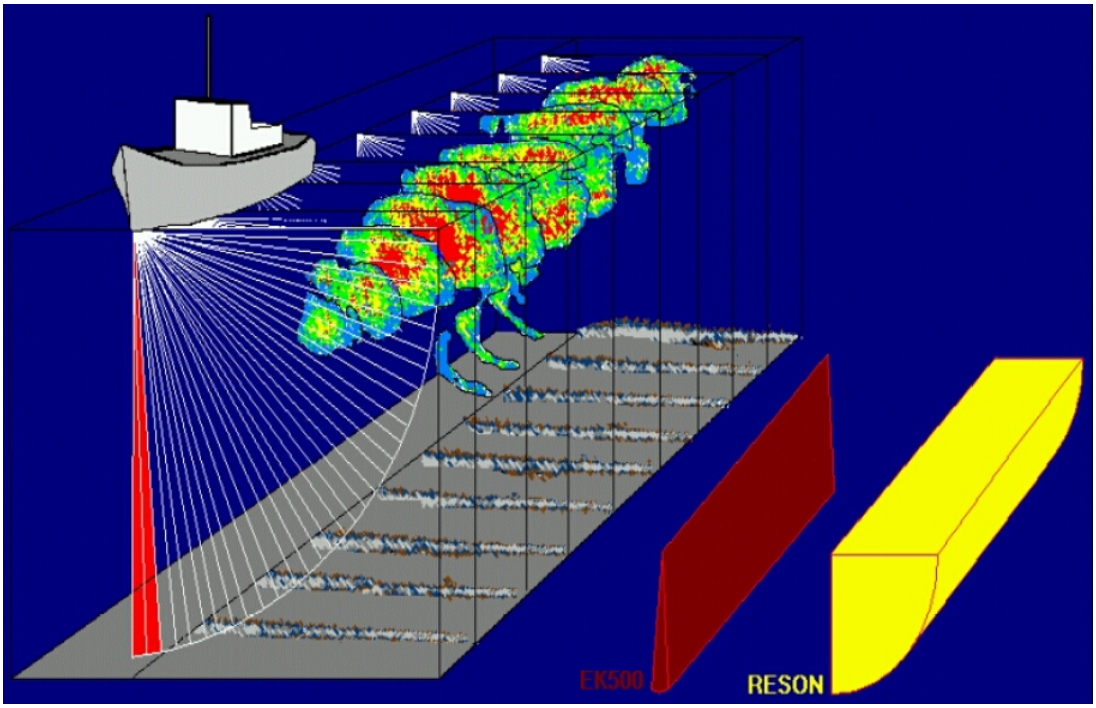

Figure 5.1: Illustration of variation between sampling volumes of a vertically downward-looking split-beam echosounder (EK500, Simrad, Norway) and a Reson multi-beam echosounder (MBE, Seabat 6012, Reson, Denmark) vertically mounted with a 90^o swath width (from Fréon and Misund 1999). Note the MBE used in the investigation reported in this thesis had a 120^o swath width, with the centre beam oriented vertically downward.

For the MBE to be a viable acoustic tool for biomass estimation, development of the current krill target strength (TS) models is required (Demer and Conti, 2003, 2005). TS models are used to scale acoustic observations to determine the numerical or biomass density of target organisms observed by an echosounder (MacLennan and Simmonds, 1992). In addition to body material composition, TS models are driven by animal length (l) and the dorsal angular orientation with respect to echosounder transducer face (θ) that is usually mounted looking vertically downwards. The varition of animal orientation relative to the various MBE beams means that so far it is not possible to estimate biomass using a MBE since for many species TS as a function of angle is unavailable.

5.1.1 Krill swarms

Aggregations of pelagic organisms may form to avoid predation, facilitate mating and feeding (Watkins et al., 1992; Hofmann et al., 2004) and convey an energetic advantage (Ritz, 1994, 2000). The swarm is considered to be the fundamental unit of krill ecology (Murphy et al., 1988). This investigation considered an individual krill swarm as the sampling unit, and swarm is used here to describe aggregations with both random and polarized orientation of krill (since krill orientation cannot be determined using this MBE). It is believed that swarms form so that individual krill are better able to respond to local changes in the environment conditions (Genin, 2004), thereby facilitating reproduction, reducing swimming energetic requirements, and as an anti-predation measure (O'Brien, 1987; Ritz, 1994, 2000).

Krill anti-predation behaviour can be thought of as acting at two scales, the larger scale being diel vertical migration (Demer and Hewitt, 1995), which has not been assessed in this investigation. At a smaller scale, individual krill swimming behaviour influences the risk of predation through two mechanisms: firstly, krill swimming behaviour partially influences krill visibility to predators and, secondly, krill swimming behaviour may aid the propagation of information of a predator attack through a krill swarm (O'Brien, 1987; Krakauer, 1995). Previous investigations of krill swarms have provided evidence of behavioural mechanisms for krill swarm formation, with anti-predation and reproduction being particularly important (Hewitt and Demer, 1993; Watkins and Murray, 1998).

Presently the use of conventional vertically mounted single- or split-beam echosounders (SBE), with limited sampling volumes, make it necessary to extrapolate from small sample sizes, which due to unknown spatial structure, have uncertain influence on biomass estimates (Mayer et al., 2002). It is anticipated the increased sampling volume of MBE compared to that of single-beam echosounders will improve the spatial matching between visual predator observations acoustic observations of krill swarms (Axelsen et al., 2001). The narrow sampling volume of the SBE may lead to the situation where predators (light blue circle, Figure 5.2) are observed foraging on a krill swarm (orange ellipse, figure 5.2) within the strip transect visual observation width (w_v), but remain undetected by the SBE. This occurs because the effective strip sampling transect width of the SBE (w_{sbe}) is less than w_v. This limitation cannot simply be overcome by making $w_v = w_{sbe}$ because, as the red cone (Figure 5.1) illustrating the EK500 sampling volume shows, w_{SBE} increases with depth. Compared to a SBE, a MBE samples a greater volume of water giving MBE a larger strip transect width (w_{MBE}), thereby reducing the probability of sampling mismatch between the acoustic observations of krill and the visual predator observations.

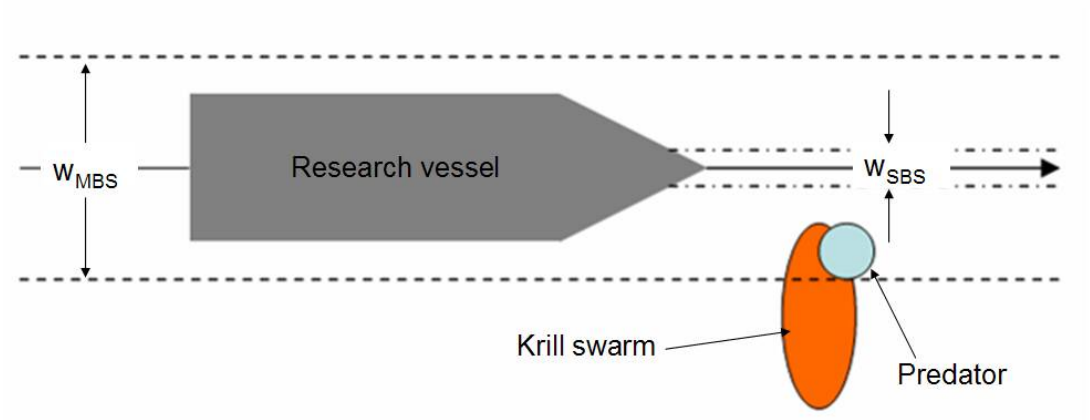

Figure 5.2: Conceptual effective across transect sampling widths (w) shown in plan view for acoustic and visual observations. The potential for mismatch to occur between single-beam echosounder observations of krill and visual observations of air-breathing predators is illustrated. A krill predator (light blue circle) is observed foraging on a krill swarm (orange ellipse), that is undetected by the SBE is a narrow w_{SBE}.

5.1.2 Split-beam and multi-beam echosounder observations

The volume backscatter (S_v) is used to represent the amount of acoustic energy returned from a group of aggregating organisms such as krill. Using a calibrated scientific echosounder it is possible to scale the S_v observations and determine the number or mass of organisms in a given water volume. Using conventional single or split-beam echosounders, S_v observations are observed in a single dimension. A single ping, comprising an echosounder transmit and receive cycle, contains multiple S_v samples, at constant time intervals (therefore depth) throughout the water column. One ping from a single- or split-beam vertically downwards oriented echosounder observes a single vertical strip through the water column, with sequential strips being combined to build up a two-dimensional matrix of water column observations (Reid and Simmonds, 1993).

When compared to hull-mounted vertically downward looking single- and split-beam conventional echosounders, MBEs ensonify large volumes of water, typically with a high resolution. The MBE samples in two instead of one dimension (Melvin et al., 2003), enabling areal coverage to be increased without decreasing spatial-resolution. A single ping from the MBE (Figure 5.3) is made up of multiple acoustic beams, with each S_v observation within a single ping or swath having a range and bearing. Each swath is an acoustic slice through the water column orthogonal to the direction of travel of the research vessel. Combining successive swaths builds up a 3 dimensional acoustic image of the water column (Figure 5.1).

The limitations of single-beam echosounders are caused by the narrow transducer beam width and the echosounder sampling volume increasing with range (see Figure 5.1).

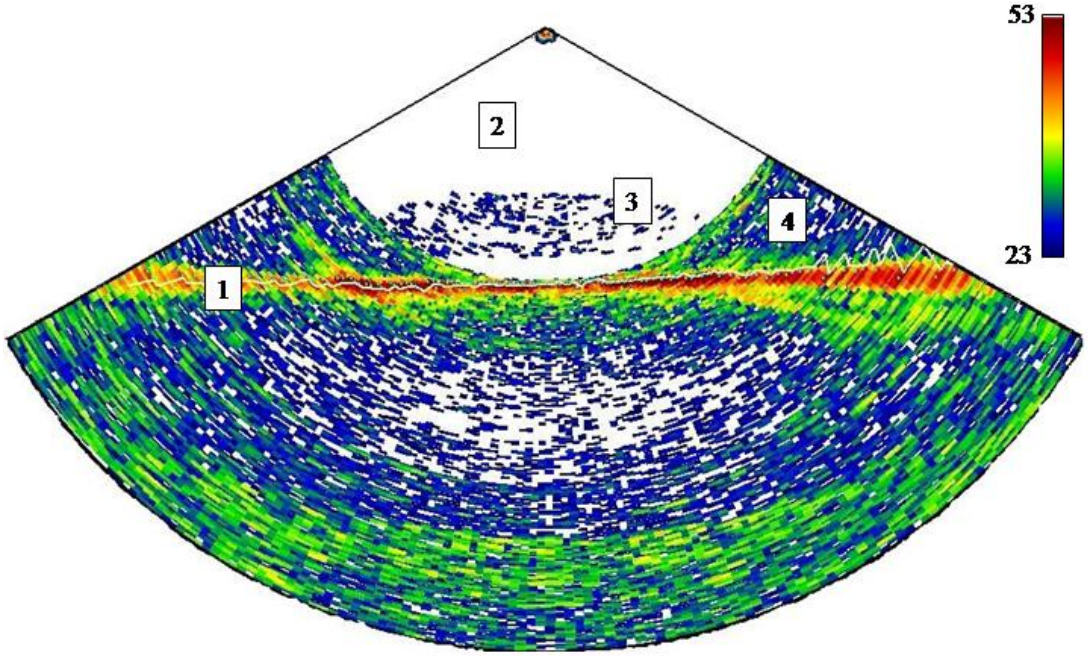

Figure 5.3: A single MBE swath, showing S_v, with uncalibrated S_v values from 23 to 53 dB. [1] the MBE seabed profile and sounder detected seabed, [2] effective sampling volume, [3] a krill swarm, [4] sidelobe seabed detections limiting the sampling volume. The 3D schools detection was performed at 23 dB and 3D regions were then repopulated with observed MBE data without a threshold applied

Given a typical transducer with a 7^o beam width, precision of swarm shape will decrease with increasing range from the echosounder transducer caused by the increased width of the ensonified cone. The location of an aggregation within the ensonified cone cannot be determined, causing the boundary of an aggregation to be smoothed and its horizontal dimension over estimated (Reid et al., 2000a; Diner, 2001). Some MBE also suffer from this aggregation boundary imprecision caused by large 10 to 30^o along transect beam widths. Vertical echosounders observe under the research vessel, so may be subjected to localised vessel avoidance that may occur. Also, it is difficult to detect avoidance behaviour using a single research vessel, equipped with a single beam echosounder, again because of the narrow beam transducer beam width. A MBE samples a larger volume of water at greater horizontal distances from the research vessel than SBE so are less susceptible to any avoidance behaviour (Gerlotto and Paramo, 2003).

5.1.3 South Shetlands study site

Since 1992 the US Antarctic Marine Living Resources (AMLR) programme has conducted acoustic surveys of Antarctic krill in the vicinity of the South Shetlands (Hewitt and Demer, 2003). These surveys were carried out to support management of krill fisheries, thus partially fulfilling the US portion of an agreement made with members of the Convention for the Conservation of Antarctic Marine Living Resources (CCAMLR).

The reproductive season of marine land breeding animals, such as penguins and Antarctic fur seals, located on the South Shetland Islands (Figure 5.4(c)) lasts from November to March. During the breeding season aggregations of Antarctic krill are advected past the South Shetland Islands on the Antarctic Circumpolar current, and approximately 0.83 million tonnes of krill are consumed by land breeding marine predators (Croll et al., 1998; Hewitt and Demer, 2003). The breeding success of these predator populations are known to be vulnerable to years of low area krill density (g/m^2). As part of the management programme, the effect of variation the South Shetlands krill density on land breeding seals and penguins was assessed. From 1992 to 2006, large changes in krill density (1 to 60 g/m^{-2}) at South Shetlands, and were correlated with fluctuations in predator breeding success (Hewitt and Demer, 1994; Hewitt et al., 2004; Reiss et al., 2008).

There is considerable potential for competition between the krill fishery operating in the South Shetland area (Figure 5.4(d)) and land-based predators. Despite the krill fishery in this area only taking an estimated 10% of the krill biomass taken by predators, 90% of the fishing occurs within 80 km of land (CCAMLR, 2000). Given that, during the reproductive season, the duration of foraging trips by land-based krill predators are constrained by rearing/feeding requirements (i.e. most foraging effort is close to land), it is important that the density and spatial distribution of krill in the near shore area is assessed. To investigate this, near shore oceanographic and biological studies of the waters surrounding Cape Shirreff, Livingston Island, have been conducted. Of particular interest are the two submarine canyons flanking Cape Shirreff which are believed to be a source of nutrient-rich water that increase productivity in the near shore region (Figure 5.4(c)).

5.2 Materials and methods

As part of the CCAMLR nearshore environment investigation, two inflatable boats (Mark V Zodiacs) were deployed in the vicinity of Cape Shirreff, from 2nd February until the 9th February 2006 (Figure 5.5(a)). One inflatable boat, *R/V Roald*, was equipped with a Simrad SM20 200 kHz MBE and conducted a high resolution seabed bathymetry survey

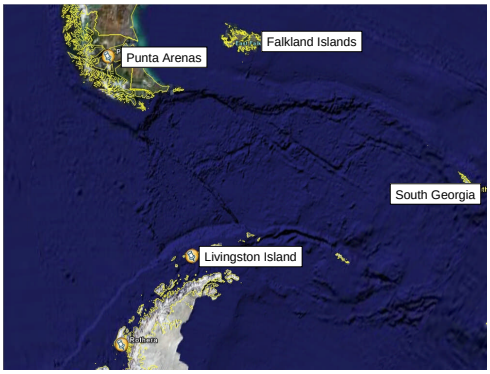

(a) General location (from Google Earth)

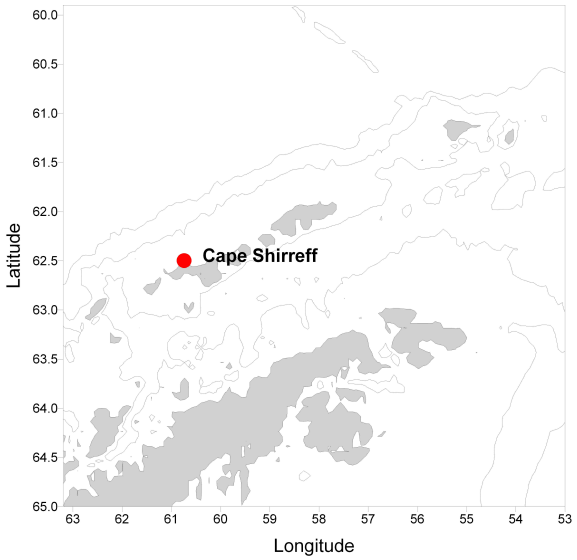

(b) The South Shetland Islandas

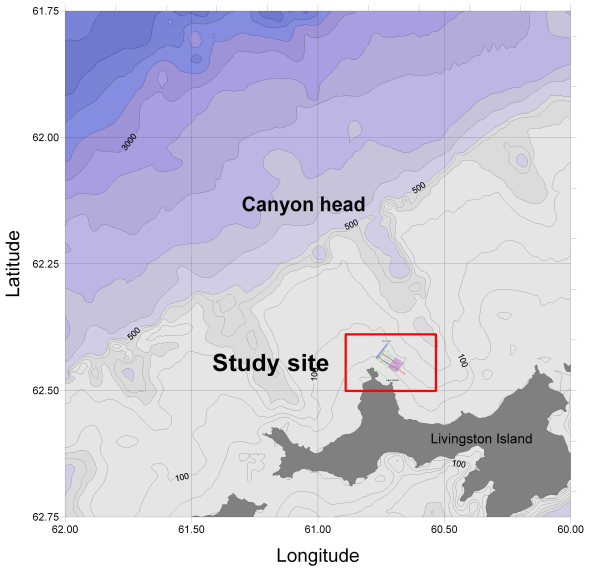

(c) Cape Shirreff, Livingston Island

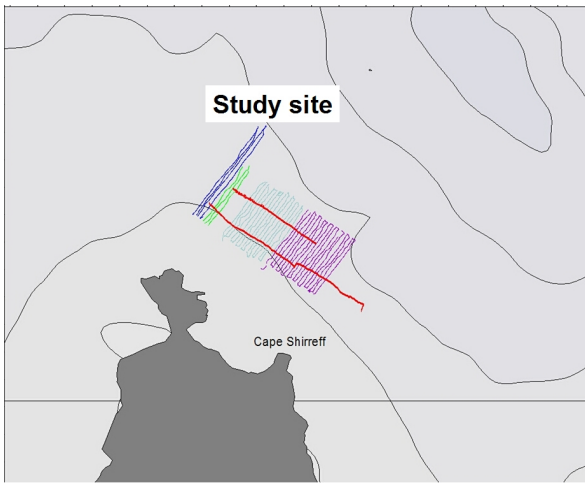

(d) Multibeam transects

Figure 5.4: The Cape Shirreff study site, Livingston Island, South Shetlands, Antarctica. MBE line transects are shown in image 5.4(d), colour coded by day. Note the two 'tie-lines' which were run perpendicular to the main survey.

(100 % seabed coverage, depth precision $\sigma = \pm 1$ m) with simultaneous water column sampling to acoustically sample krill swarms. The other, *R/V Ernest*,, was equipped with a Simrad (Norway) ES60 echosounder operating at 38 and 200 kHz. The MBE survey comprised of 35 2.5 km and 4 3.5 km line transects with a 120 m inter-transect spacing (figure 5.4(d)).

5.2.1 Multibeam equipment and data description

In 1997 Simrad introduced the SM2000 MBE, that enabled the acquisition of digital data for the entire acoustic swath observation range. Its primary purpose was the detection of divers for harbour defence. Up until this time many other multi-beam systems treated water column observations as noise and essentially ignored them, or were only capable of recording acoustic observations as video images. The digital recording of acoustic water column observations is vital for the quantitative assessment of pelagic organisms. The Simrad SM20 MBE is an upgraded SM2000 with a total swath width of 120^o, comprised of 128 receive beams, spaced at 0.96^o, from an 80-element transmit array, each with a 1.5^o across track and 20^o along track beam width. Assuming a flat seabed, the maximum swath width is approximately 3.5 times the water depth. An orthogonally-mounted external transmit, or profiling, transducer was used to reduce the along-track beam width from 20^o to 1.5^o, which improved the precision of locating targets in the water column and reduced between-ping along track volume overlap. The ping rate was between 1 ping every 1.5 to 3 s, TVG correction was set to $20\log r$ and the transmission power was 'medium'.

The MBE was housed in a blister fairing, mounted on a rotating frame, which when deployed positioned the SM20 head along the centre line of *R/V Roald*, with the centre beam of the MBE positioned vertically downwards, giving a 60^o swath either side of the boat, perpendicular to the transect (Figure 5.5(b)). This MBE orientation was selected to fulfil the dual requirements of simultaneously observing seabed bathymetry and water column targets. Also, the blister fairing mounting angle was constrained by the design of the rotating frame.

The MBE observations were logged continuously to the SM20 control computer. Two formats of MBE data were recorded: detected bathymetry profiles of the seabed were recorded using Triton ISIS v7.0 (Triton Imaging, Inc.), and acoustic returns throughout the observation range (200 m) were recorded using the Simrad SM20 control software. Water column data were converted to the SM2000 data format using a Simrad utility (MsToSm v1.0) and processed using Echoview v3.50 (SonarData, Hobart, Tasmania). Krill swarms were identified using the proprietary SonarData 3D school detection algorithm, and krill swarm descriptive metrics extracted. The sensitivity of the extracted swarm metrics to the selected 3D school detection parameters, minimum longest, middle and shortest dimensions and minimum data threshold, was investigated. The minimum data threshold is the minimum S_v that is included in the analysis.

(a) *R/V Ernest*

(b) SM20 blister fairing

Figure 5.5: Near shore survey equipment. Figure 5.5(a) shows *R/V Ernest* entering the protected anchorage at Cape Shirreff, Livingston Island. Note the protective dodge to shelter personnel and equipment from the elements. Figure 5.5(b) shows the SM20 multibeam echosounder, mounted inside a white blister fairing. The blister fairing was attached to a rotating frame that is mounted to the transom of *R/V Roald*.

5.2.2 Automated krill swarm detection

This investigation sought to examine individual krill swarms. A krill swarm boundary is defined as the interface between a densely packed aggregation of krill and empty water. Krill swarms were identified using the Sonardata 3D schools cruise scanning detection algorithm, implemented in Echoview v3.50. The algorithm identified contiguous groups of acoustic returns in each beam and places prisms to bound the extremities of each group. These prisms were triangulated, reducing each prism to two triangles. The perimeter of the 3D school was generated by retaining the visible vertices of the triangles, which were used to create a 3D bounding surface around the contiguous acoustic return. At this point the user-defined size parameters, minimum longest dimension, minimum middle dimension and minimum shortest dimension, were used to eliminate detected swarms with dimensions smaller than these minimum parameters (see following subsection). In addition, the minimum S_v threshold (dB) defined the minimum density of acoustic returns that were transferred to the 3D detection algorithm, hence defining the krill swarm boundary.

Acoustic observations of ranges less than 5 m were ignored due to sea-surface noise and near-field effects (Melvin et al., 2003). For the purposes of 3D target detection, the search volume for the 3D algorithm was constrained to water column targets by referencing a sounder detected seabed using the Sonardata MBE sounder detected bottom identification algorithm, offset by 0.5 m shallower. Based on MBE work by Gerlotto et al. (1999) it is assumed that the swarm speed was negligible compared to boat speed of 2.5 to 3.5 m/s .

Sensitivity analysis

In order to select a minimum threshold and minimum dimension parameters for swarm identification, sensitivity analysis of these parameters was conducted. Four transects, numbers 2, 17, 22 and 33, were selected at random from the 41 transects run. The value of each 3D schools detection parameter was varied sequentially across a range of biologically plausible values (given in the following paragraph) and the effect of these variations on the total number of detected swarms and swarm descriptive metrics was assessed.

The sensitivity of the 3D detection parameters was investigated in two stages. Firstly, the effect of varying the three minimum dimension parameters was investigated. Since there was no *a priori* available information about the 3D shape of krill swarms in the near shore study region, the same length was used for each of the 3D parameters. For example, during the first run of the 3D detection algorithm during sensitivity analysis, the minimum longest, middle and shortest dimension were all set to 2 m. This essentially assumed that krill swarms would be spherical. Subsequent 3D detections using the Sonardata algorithm were performed with all minimum dimensions set to 2, 3, 4, 5, 6, 10, 15, 30, 30 and 35 m, giving 10 sets of detections for the four randomly selected transects. During this section of the sensitivity analysis the minimum detection threshold was fixed at 24 dB.

The second part of the sensitivity analysis investigated the effect of varying minimum threshold. Based on results obtained from the analysis described in the previous paragraph, all the minimum school dimensions were set to 5 m, with a school detection performed at minimum threshold settings that ranged from 19 to 29 dB, in increments of 1 dB.

Assessment of swarm avoidance

Following Gerlotto and Paramo (2003), Soria et al. (2003) and Gerlotto et al. (2004) lateral avoidance of the research vessel by krill was assessed by testing the null hypothesis of a uniform distribution of schools with respect to horizontal distance from the transect to the geometric centre of a detected school ($d_{r,s}$), i.e. H_0: no lateral avoidance. Furthermore in Chapter 6 swarm detectability (see Buckland et al. 2001) was assessed across the survey area.

5.2.3 Viability of the SM20 to estimate biomass

Estimating calibrated multi-beam echosounder observations

To enable comparison between the SM20 and ES60, the empirical cumulative density function (ECDF) of S_v observations from the SM20 was mapped onto the ES60 200 KHz

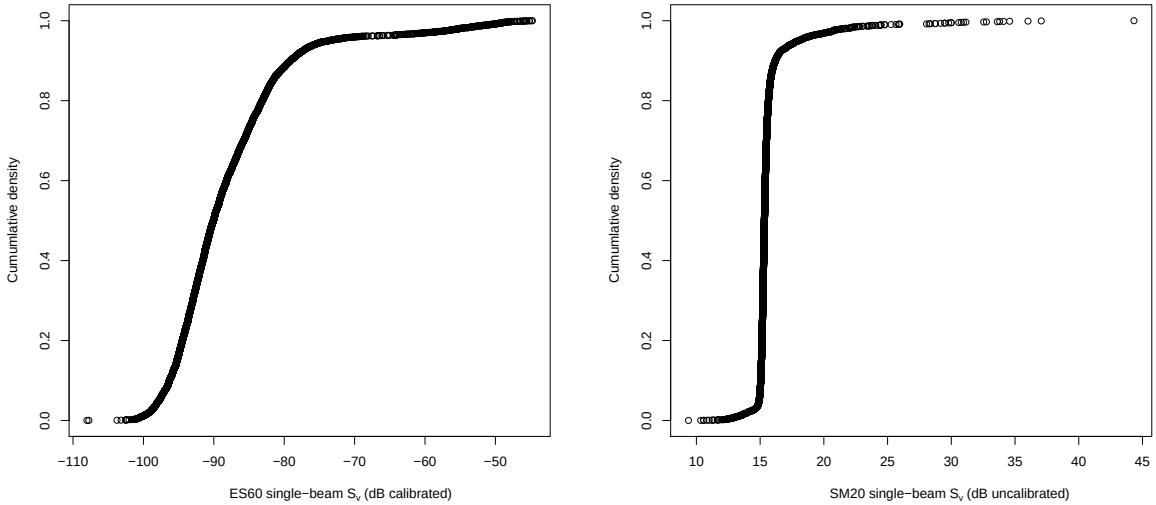

(a) ES60 S_v observations

(b) SM20 S_v observations

Figure 5.6: The Empirical cumulative distribution functions of S_v observations exported on a common vertical spatial grid for the ES60 (200 kHz transducer) and the SM20 beam number 64. Note the SM20 S_v values are uncalibrated.

S_v ECDF. The SM20 did not a have a nadir beam so, following Melvin et al. (2003), beam number 64 was used as the nadir beam. Data were exported for the SM20 and ES60 for both the tie lines run simultaneously by *R/V Roald* and *R/V Ernest* on 8 Feb 2006. To limit the spatial mismatch of S_v observations, the mean S_v from a time synchronised 5-ping horizontal by 5 m vertical grid was generated in Echoview for both data streams. The sea surface noise and seabed data exclusion regions from the ES60 system were used to limit the S_v observations to those only collected in the water column. The two sets of S_v observations were then mapped by determining which S_v values of both systems occurred at equal areas under the ECDF curves (Figure 5.6). The method uses the cumulative proportion of S_v observations of the SM20 to determine an equivalent ES60 S_v. For example, the calibrated ES60 equivalent of an SM20 S_v=19 dB, occurs at cumulative density of 0.95 on Figure 5.6(b). Transferring to the ES60 ECDF (Figure 5.6(a)) a cumulative density of 0.95 occurs at S_v=-76 dB. So using this ECDF mapping technique an uncalibrated SM20 S_v value of 19 dB is equivalent to a calibrated ES60 S_v=-76 dB.

To illustrate the ECDF mapping method the ES60 and the SM20 ECDFs are shown in Figures 5.6(a) and 5.6(b).

The purpose of mapping the uncalibrated SM20 S_v observations to the calibrated ES60 S_v observations (Figure 5.7) was to determine a calibrated S_v threshold at which the three dimensional schools detection was performed (see Section 5.2.2) so that the effect of this

threshold on biomass estimates could be estimated.

Currently, no TS model exists for lateral acoustic observations of krill (although Hewitt and Demer 1996 made lateral observations), so despite obtaining an S_v mapping function for the SM20 S_v observations from any other beam except the vertical beam cannot be used to estimate biomass.

The ES60 observations were used to estimate two sources of bias in biomass estimates:

1. The S_v threshold selected for three-dimensional schools detection may exclude lower density swarms, which will reduce the overall biomass estimate ($\hat{b}$).

2. Multi-frequency acoustic responses are often used to partition acoustic observations into specific species groups (see Madureira et al. 1993; Brierley et al. 1997b). Since the SM20 operates on a single frequency (200 kHz) this technique cannot be used. Consequently it was assumed that all acoustic targets observed in the water column were krill, this is likely to positively bias $\hat{b}$.

Swarm biomass estimates

The schools detection method given in Chapter 2 was used to extract krill swarms from the 38 and 200 kHz ES60 observations. Krill swarms within a 5 km radius of the centre of the MBE study site were used to calculate $\hat{b}$.

The irregular cruise track of *R/V Ernest* prevented density calculation using the standard Jolly and Hampton (1990) approach. Instead, the volumetric density ($\hat{p_v}$, g/m^3) of each krill swarm was calculated and scaled by the estimated swarm volume (V_i, see Diner 2001) to provide a point estimate of $\hat{b}$ for all krill swarms in a 5 km radius of the multi-beam study site using:

$$\hat{b} = \sum_{i=1}^{K} \hat{p_{v}}_i \cdot V_i \tag{5.1}$$

The $\hat{p_{vi}}$ was estimated by scaling the S_{vi} for swarm i by the TS determined using the Conti and Demer (2006) parameterised form of the SDWBA model (Figure 5.9(a)) and the Morris et al. (1988) krill length (l) to wet-mass relationship. The empirical distribution of l (l_{min} =32 mm and l_{max} = 55 mm, giving mean krill TS=-73.99 dB) was observed by near shore net samples conducted from the *R/V Yuzmorgeologiya* (Figure 5.9(a)).

Where applied to partition the ES60 observations, the dB difference window ($\Delta_{S_v:200-38}$) was determined using the (l)distribution data from the small scale survey. This gave $\Delta_{S_v:200-38}$=-0.72 to 13.34 dB using the Conti and Demer (2006) SDWBA krill TS model (Figure 5.9(b)).

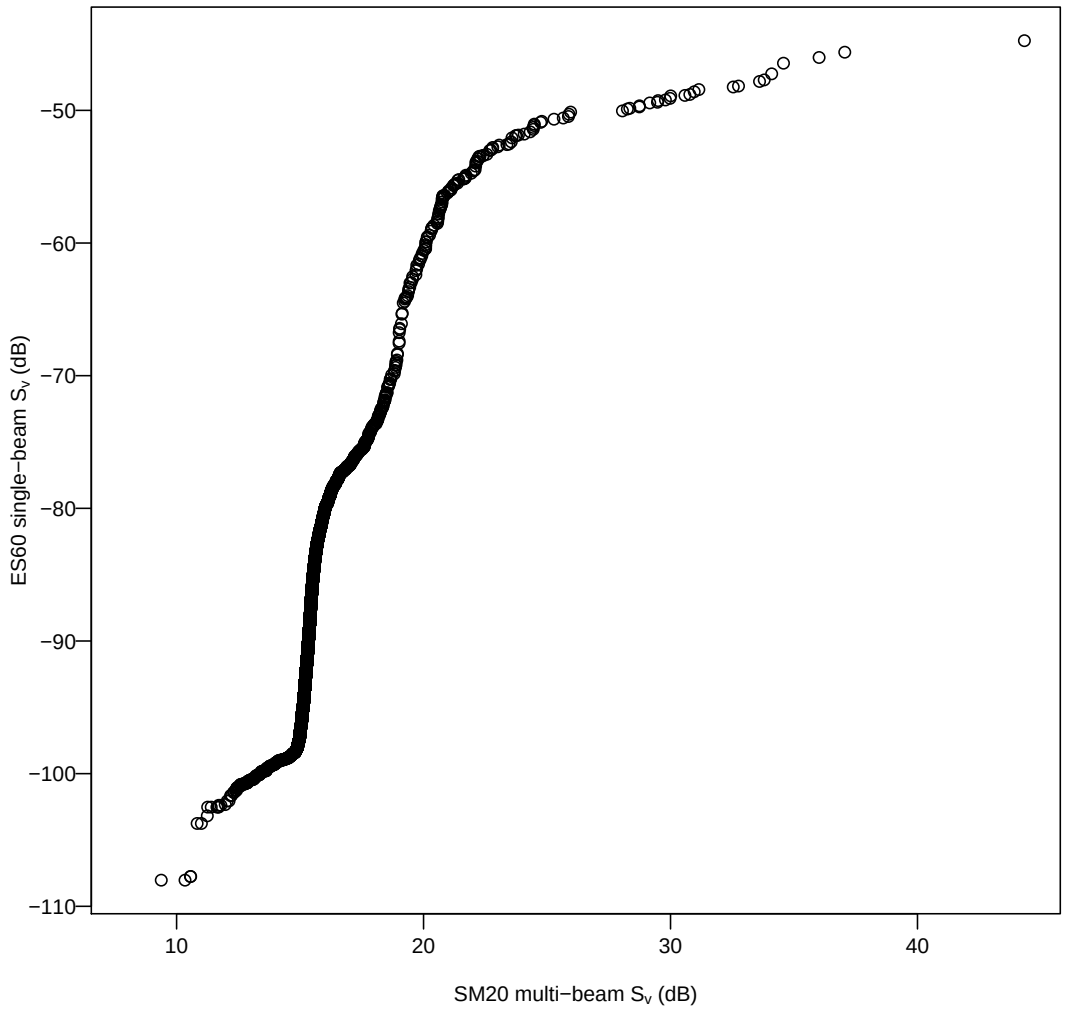

Figure 5.7: Empirical cumulative distribution function (ECDF) of SM20 S_v observations standardised to the ECDF of ES60 S_v observations to enable comparison between the calibrated ES60 single-beam echosounder and the SM20 multi-beam echosounder processing thresholds.

To investigate the two sources of bias, given above, the following $\hat{b}$ estimates were obtained from the calibrated ES60 observations:

1. All swarms detected using the ES60 200 kHz transducer, with the schools detection S_v threshold = -80 dB. This may, depending on the performance of the EDCF mapping technique (Section 5.2.3), give an overestimate of $\hat{p}$. The -80 dB threshold was selected based on Woodd-Walker et al. (2003).

2. Swarms falling within the 200-38 kHz dB difference range, with the schools detection S_v threshold = -80 dB. This will give the optimal estimate of $\hat{p}$.

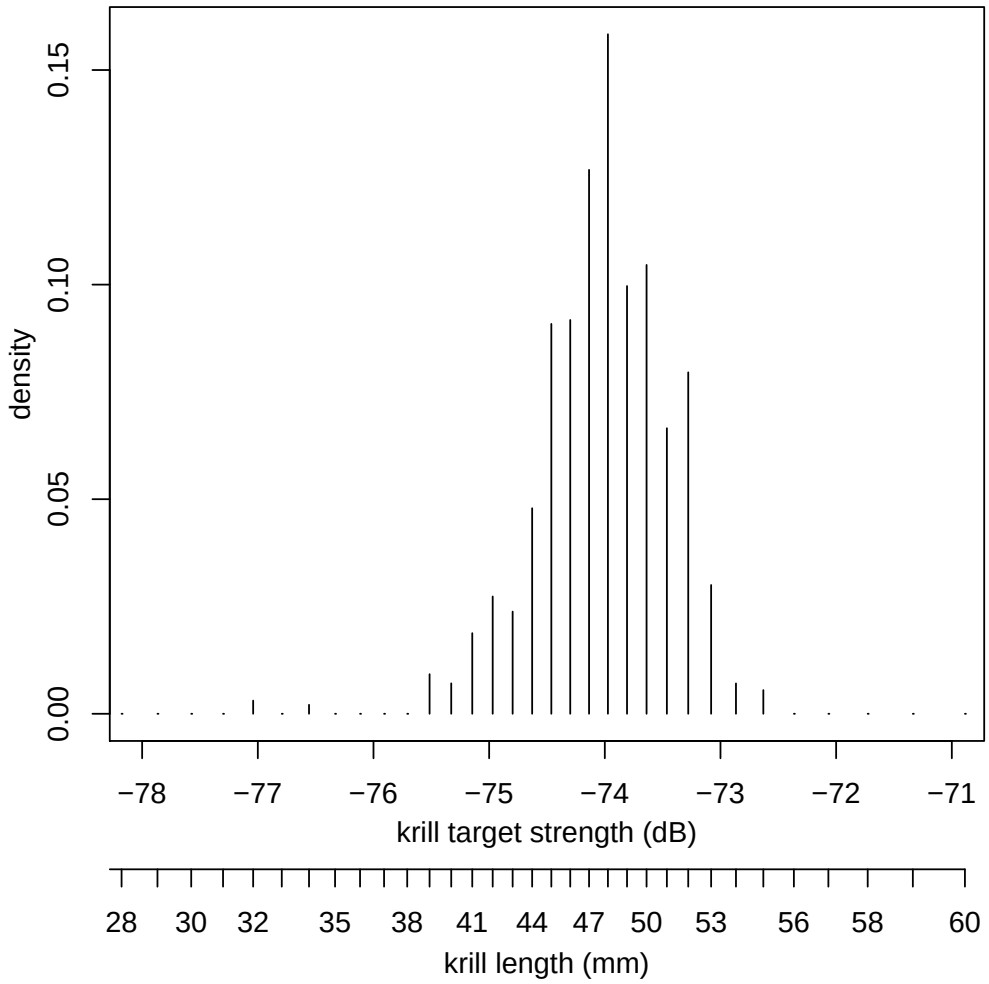

Figure 5.8: The empirical distribution of krill target strengths calculated using the Conti and Demer (2006) model from net samples conducted from the *R/V Yuzmorgeologiya* during the nearshore survey.

3. All swarms detected using the ES60 200 kHz transducer, with the schools detection S_v threshold = -57.2 dB (the ES60 threshold equivalent to the uncalibrated SM20 23 dB threshold determined from the ECDF mapping technique above. This will give an underestimate of $\hat{p}$.

5.2.4 3D krill swarm descriptors

All krill swarm metrics were calculated or derived from Echoview v3.5. Energetic measurements were limited to relative measures since the MBE was uncalibrated and the ECDF mapping technique is suitable for only for comparing thresholds at the centre of the MBE swath, so cannot be used alone to rescale MBE S_v observations that occur across

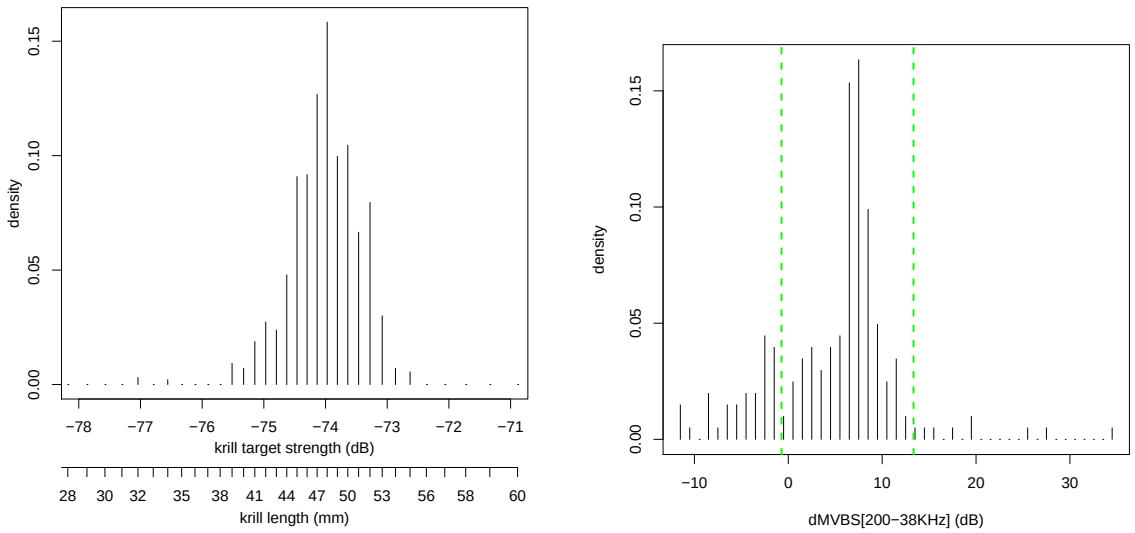

(a) Krill length frequency distribution

(b) 200-38 kHz dB difference

Figure 5.9: The empirical distribution of krill target strengths calculated using the Conti and Demer (2006) model from net samples conducted from the *R/V Yuzmorgeologiya* during the nearshore survey. Also the dB difference (200-38 kHz) with the upper and lower krill dB differences shown as grey dashed lines, calculated using the Conti and Demer (2006) TS model and the krill length frequency distribution.

a region of the swath. A complete list of krill swarm descriptive metrics are given in Table 5.1. Both morphological and energetic metrics were used in the multivariate analysis conducted that was carried out, along with partition analysis to determine if swarms can be classified into three types.

Metric name	Abbreviation	units	description
			Energetic and morphological metrics
Surface area	S	m^2	Surface area of the 3D krill swarm
North-south length	NSl	m	Maximum length of the 3D swarm along a north-south grid
East-west length EWl		m	Maximum length of the 3D swarm along a east-west grid
minimum swarm depth	z_{min}	m	Minimum swarm depth, corrected for multi-beam head depth
maximum swarm depth	z_{max}	m	Maximum swarm depth, corrected for multi-beam head depth
height	Ht.	m	Maximum swarm height ($z_{max} - z_{min}$)
volume	V	m^3	3D swarm volume
roughness	R	m^{-1}	$R = S/V$
object bounding box - 1	$OBBl_1$	m	Longest dimension of the object-aligned bounding box
object bounding box - 2	m	$OBBl_2$	Next longest dimension of the object-aligned bounding box
object bounding box - 3	$OBBl_3$	m	Shortest dimension of the object-aligned bounding box
Mean Sv	Sv_{mean}	dB re $1m^{-1}$	Mean of s_v (linear mean volume backscatter) within a swarm,$Sv_{mean} = 10log_{10}(\bar{s_v})$
Number of Samples	Samples	-	Number of samples within a 3D krill swarm.
Min Sv	Sv_{min}	dB re $1m^{-1}$	minimum of s_v within a swarm, $Sv_{min} = 10log_{10}(min(s_v))$
Max Sv	Sv_{max}	dB re $1m^{-1}$	maximum of s_v within a swarm, $Sv_{max} = 10log_{10}(max(s_v))$
position in water column[1]	$posn_{wc}$	-	$posn_{wc} = 1 - (\mid z_{max} - z \mid /z)$ giving $0 \leq posn_{wc} < 1$, when $posn_{wc} \simeq 1$ swarm on seabed.
proportion of water column occupied by krill swarm[1]	p_{wc}	-	$p_{wc} = (z_{max} - z_{min})/z$
			Positional metrics
geometric centre position	(ϑ_g, λ_g)	deg	Latitude and longitude of geometric centre of 3D krill swarm. Associated grid coordinates (E_g, N_g)[1].
geometric centre depth	z_g	m	Depth at the geometric centre of the 3D krill swarm.

Table 5.1: Description of 3D krill swarm metrics used in analysis. [1] metrics not obtained using Echoview v3.50.58 multi-beam module (Sonardata, Tasmania).

As pointed out by Gerlotto and Paramo (2003), linear measures of swarm dimensions may not represent accurately a swarm with a complex shape since linear measurements are generally based on a 3D bounding box placed around a swarm, which demarks the swarm's maximum dimensions. The roughness factor (R), defined by swarm surface area (A) divided by swarm volume (V), is a more useful metric that capitalizes on the 3D nature of multi-beam observations. Following the procedure given in Gerlotto and Paramo (2003), R was compared to that of three geometric shapes, sphere, cylinder and ellipse. Calculations of A for the sphere and cylinder were calculated using V from each swarm. Swarm height was used for cylinder height and the 3D bounding box dimensions, calculated using Echoview v3.5, were used to calculate ellipsoid volume and an approximation for ellipsoid area.

In order to determine which krill swarm metrics (Table 5.1) accounted for the largest inter-swarm differences in morphology a principal component analysis (PCA) was performed. The PCA was carried out on a matrix of normalised krill swarm metrics, and to aid interpretation of the PCA eigen vectors, Mardia's criterion was used to identify which swarm metrics had a significant influence on individual principle components, and make the greatest contribution to the inter-swarm variation (Jolliffe, 2002). A three group partition analysis was then performed in the reduced factorial space provided by the PCA results to determine if swarms form distinct types. Three swarm groups were selected based on the krill swarm classification devised by (Miller and Hampton, 1989; Hamner and Hamner, 2000). Also, the chosen number of groups (3) was based on the results of a pseudo F-test, to determine differences in the sums of squares of within cluster differences (Johnson, 1998).

5.2.5 Predator-prey interactions

Visual predator observations (predator sightings) were recorded from both *R/V Roald* and *R/V Ernest* in an attempt to assess the spatial overlap between air breathing predators and krill. Predator encounters forward of the protective dodger (1 m back from the bow, see Figure 5.5(a)) to a range 50 m were recorded by an observer on each of the inflatable boats. The predator species, group size, activity (e.g. feeding) and time of predator encounter was recorded and time and GPS position were subsequently merged enabling the predator positions to be determined during post-processing. Rapid, short term changes in boat heading due to waves often made it impossible to record off-transect distances to predators accurately.

The effect of predators on the external shape of krill swarms as determined from MBE data was investigated using a generalized additive model (GAM, R v2.4.0, mgcv library v1.3-19), with the response variable being observed krill swarm roughness R. A variety of

explanatory variables in different models were used and models were selected by Akaike's information criterion (AIC, Akaike 1974).

To compare the utility of MBE and SBE systems for investigating predator-prey interactions, the number of krill swarms detected for each transect by each sonar was calculated. This was carried out by comparing the number of krill swarms detected within a given area surrounding the position of a predator encounter. Since the MBE has the capability to detect krill swarms off transect (Figure 5.2) a sampling area must be used (Figure 5.10), rather than an along transect distance. This area was kept constant at the area of a circle of r=50 m (A=7,854 m^2, the position error in a predator encounter is estimated to be σ^2=50 m).

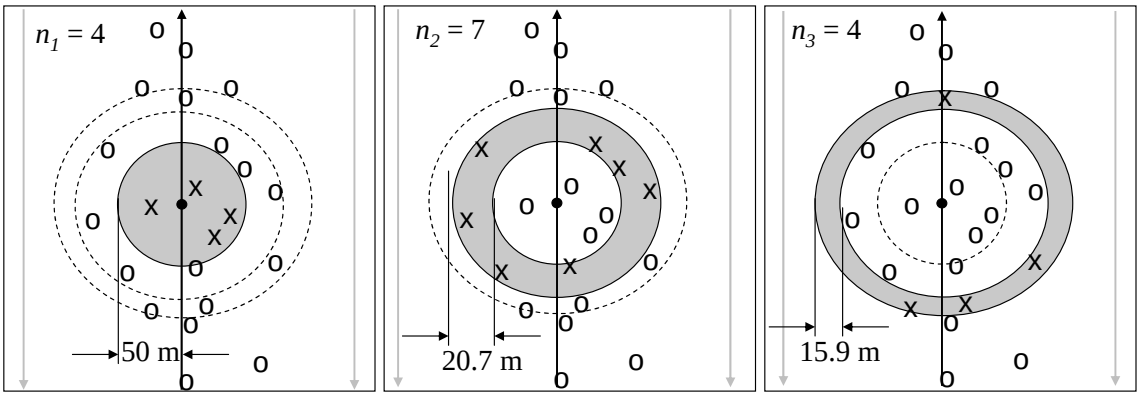

Figure 5.10: Plan view of the circle and annulus sampler (constant area= 7,854 m2) defined around predator positions. Left panel shows the circular sampling area (n1, radius=50 m) centred on the predator location in which 4 predators were seen and, sequentially, the first and 2nd concentric donuts (n2 and n3) in which 7 and 4 predators were seen respectively. In this example the current sampling area is shown in grey and krill swarms that fall in the current area are given as x, and those outside as o.

Only one transect at a time was considered in an effort to avoid bias that would be introduced by the different survey tracks followed by each vessel (Figure 5.23, page 145). The MBE equipped *R/V Roald* followed a narrowly spaced systematic line transect design, whereas the SBE equipped *R/V Ernest* followed a random line-transect design. Consequently if all swarms detected within a given comparison area (light blue area, Figure 5.10) was calculated the MBE would detect more swarms because the systematic, narrowly spaced transects, would result in an increased effort within the comparison area. Further, to minimise potential differences in geographical location specific krill predator foraging behaviour, only SBE detected krill swarms within a circle of r=5km from the centre of the MBE survey area were used.

To assess the potential of the multi-beam echosounder in investigating predator-prey interactions, the number of detected swarms in the vicinity of an air-breathing predator

encounter was determined. The number of detected swarms for both the multi-beam echosounder and single-beam echosounder detected swarms (threshold=-80 dB), out to a radius of 5 km (Figure 5.23, page 145) was calculated within expanding annulus areas around a predator encounter (Figure 5.10). The annulus width was selected so that each successive annulus had an equal area, with the initial circle having r=50 m (A=7,854 m^2), out to a range of 274 m from a predator encounter, giving a annulus radius of 274 m.

5.3 Results

Between 4 February 2006 and 8 February 2006 MBE surveying took place following a systematic line transect plan. Each transect was either 2.5 or 3.5 km long, with a line spacing of 120 m. The survey area extents were: 62.44^{o}S, 60.80^{o}W; 62.42^{o}S, 60.74^{o}W; 62.45^{o}S, 60.66^{o}W and 62.46^{o}S, 60.80^{o}W (Table 5.2). A total of 1,084 krill swarms were detected by the MBE, of which 1,006 were determined to be entirely within the MBE sampling volume, using the 3D detection algorithm described in section 5.2.2 with detection parameters given in section 5.3.1. Operational constrains meant that a different number of transects were sampled each day (Table 5.2). Seabed depth in the survey area ranged from 20 to 140 m. Variation in depth within the study site is an important consideration as depth determines the MBE sampling volume and maximum observable cross-track swarm width. In addition to seabed depth, MBE sampling volume was reduced by side lobe detections of the seabed (Figure 5.3) as krill swarms cannot be detected within the side lobe interference volume.

Date	No. of transects run	Other activities
4 Feb 06	4	None
5 Feb 06	3	2 transects run with *R/V Ernest* and *R/V Yuzhmorgeologiya*
6 Feb 06	15	None
7 Feb 06	17	None
8 Feb 06	0	2 tie-lines run with *R/V Ernest*

Table 5.2: Nearshore multi-beam transect disposition.

5.3.1 3D detection algorithm: sensitivity analysis

Minimum dimension sensitivity analysis showed that the number of detected swarms decreased with increasing minimum swarm dimensions (Figure 5.11). If the minimum swarm dimension was too small the detection algorithm will split larger swarms and increase the number of spurious side-lobe detections. Median swarm height, north-south and east-west

length, and swarm volume all increased with increasing minimum swarm dimensions. The 2D nearest-neighbour-distance (NND) was calculated using the geocentric latitude and longitude of a detected krill swarm. Median minimum NND increased with increasing minimum swarm size since fewer swarms were detected. The NND results at larger minimum swarm sizes indicate that remaining large krill swarms were not clustered: if the remaining large swarms were clustered, NND would not have increased.

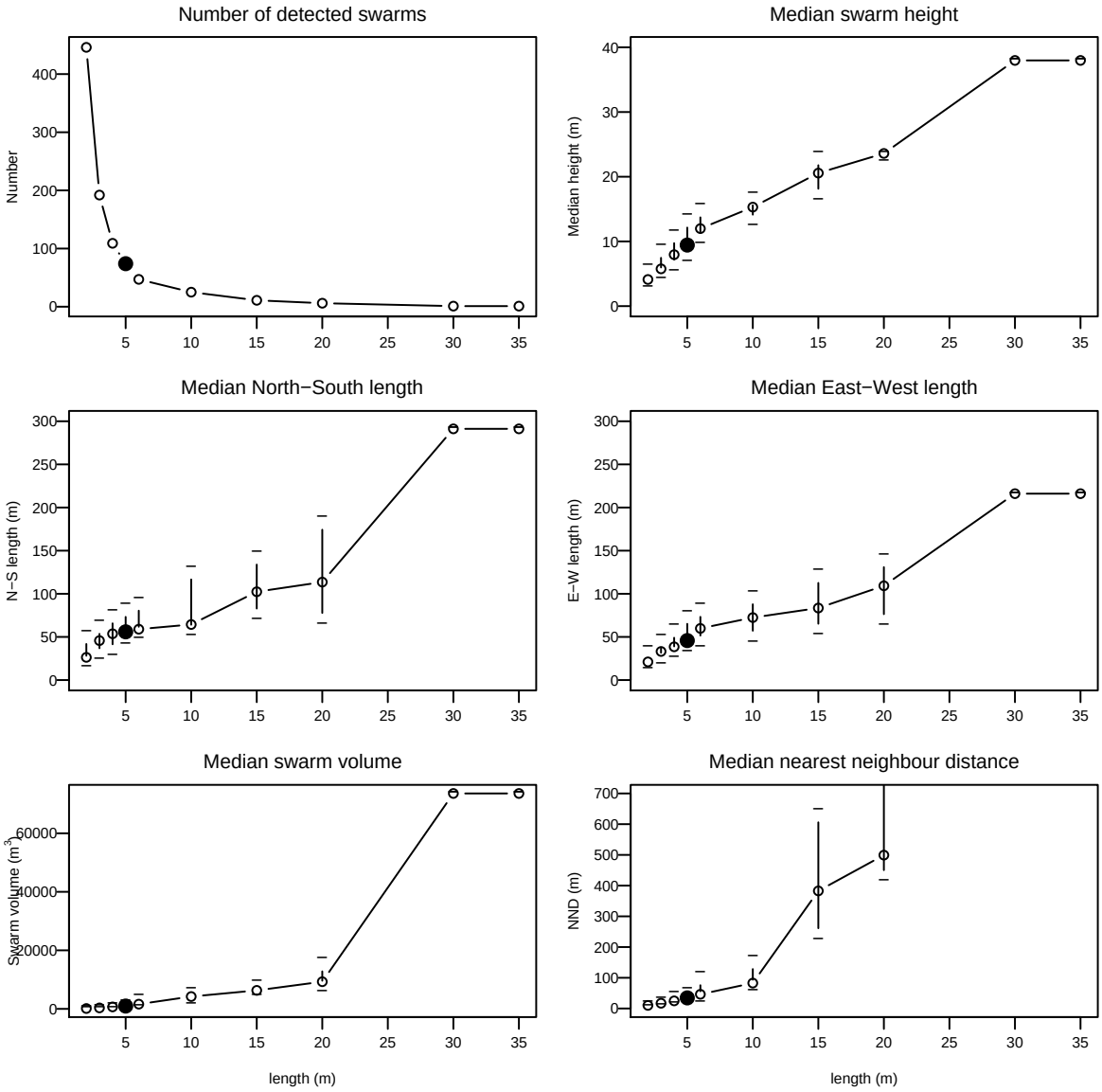

Figure 5.11: Sensitivity of krill swarm descriptive metrics to variations in the 3D school size detection parameters. Minimum threshold set to 24 dB throughout. Median values are given along with error bars at the 25 and 75 % quantiles. The selected school detection parameters (5m) are shown as black circles.

While the sensitivity plots (Figures 5.11 and 5.12) were informative about the relationship between krill swarm metrics and 3D school detection parameters, there is insufficient

information to decide on minimum dimension swarm detection parameters. Visual inspection of the 3D krill swarm boundaries generated using the detection algorithm showed that the 2 m minimum length resulted in many side lobe echoes being identified as krill swarms. The 5 m length reduced spurious identification of side lobe echoes whilst retaining krill swarm spatial structure, but did occasionally split krill swarms. The 10 m minimum length setting degraded the detected krill swarm spatial resolution and eliminated small swarms. The trend of degrading krill swarm spatial structure and eliminating smaller krill swarms continued with increasing minimum 3D length settings. The 5 m minimum length setting was selected as the processing minimum split swarms mentioned above were excluded by the algorithm at the 10 m setting.

The effect of varying the minimum S_v detection threshold on krill swarm descriptive metrics was investigated. Minimum detection thresholds of less than 19 dB (-71 dB, using mapping technique, Figure 5.7) were not used because the level of background noise detections prevented the 3D school detection algorithm from functioning correctly. The number of detected swarms vs. processing threshold shows that more swarms were detected at lower thresholds (Figure 5.12). Visual inspection of 3D krill swarm detections at the 19 dB and 20 dB minimum thresholds showed a large number of noise and side lobe detections. The maximum median swarm height and volume occur when the minimum threshold was 23 dB. At lower detection thresholds the 3D detection metrics contained data from side lobe and noise detections that generally resulted in 3D detections with smaller volumes than those attributed to 3D krill swarm detections. At thresholds greater than 23 dB the lower density edges of detected krill swarms were eroded, resulting in reductions in all median krill swarm metrics. The apparent spike in the median NND at the 27 dB threshold is caused by fewer swarms being detected. The median NND at minimum thresholds of 28 dB and 29 dB were calculated from only two swarms, creating the apparent spike at threshold 27 dB. The median north-south swarm length was again larger than the east-west swarm length, suggesting a non-random swarm orientation in the survey area or observation bias. Alternatively, this difference in swarm lengths may be due to variations in the MBE sampling volume and cross-track observation distance. Given that maximum swarm height and volume occurred at 23 dB, and that there was a fall in the number of spurious side lobe detections, 23 dB was selected as the S_v threshold for 3D schools detection of krill swarms. Therefore, for the purposes of this investigation, a krill swarm is defined as a collection of acoustic samples with $S_v > 23dB$ (uncalibrated SM20 observations, -57.2 dB, 48 krill/m^3) with dimensions $> 5m$.

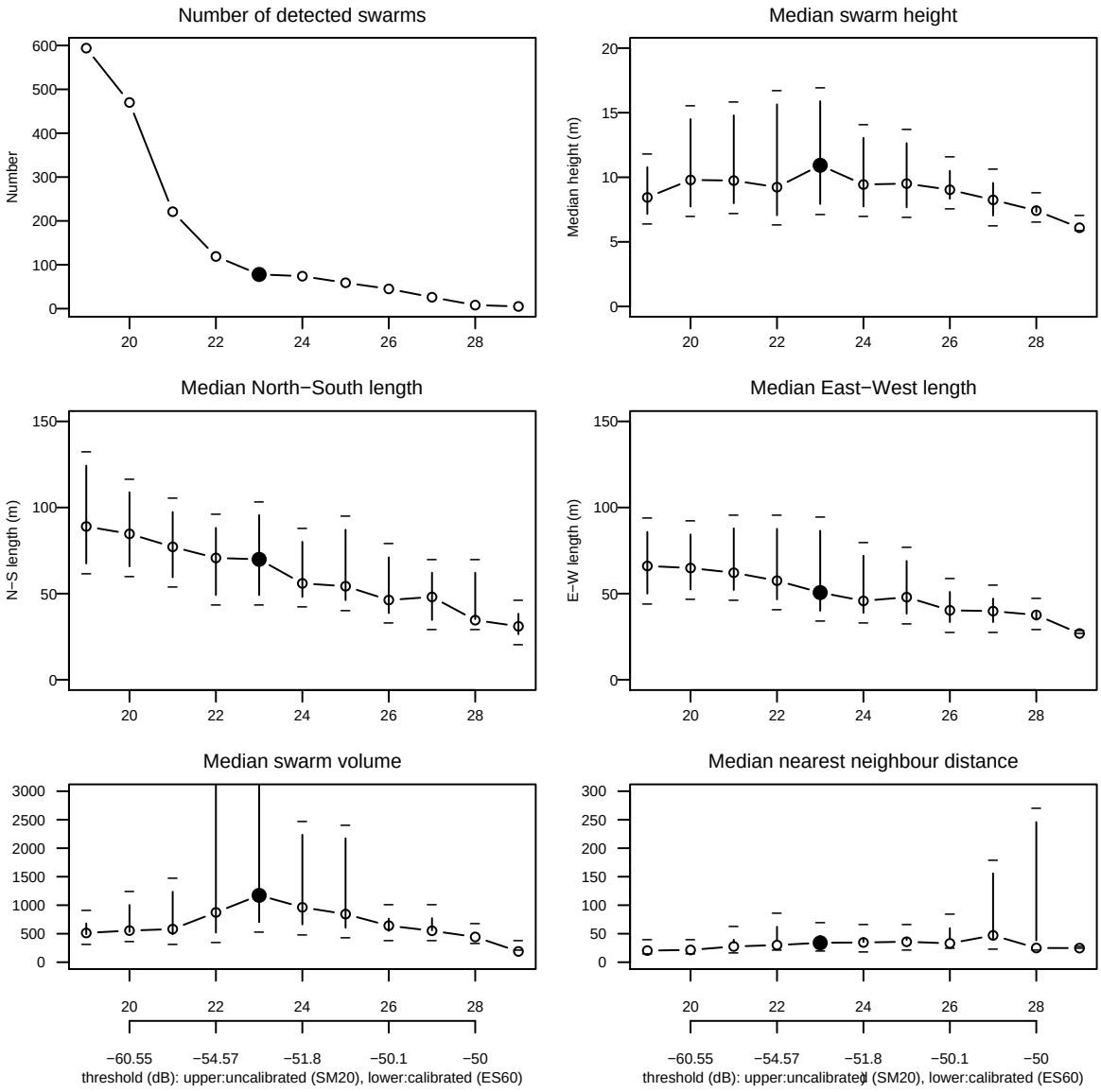

Figure 5.12: Sensitivity of krill swarm descriptive metrics to variations in the minimum detection threshold. Minimum 3D detection algorithm length parameters set to 5 m throughout the analysis. NND is nearest neighbour distance. Points are median values and the error bars are at the 25 and 75 % quantiles. The selected detection threshold (23 dB) is shown as black circles. The x-axis shows both the uncalibrated SM20 multi-beam echosounder thresholds and the equivalent calibrated threshold (see Figure 5.7 calibration map).

5.3.2 Krill swarm morphology

Krill swarms within the survey area exhibited broad variation of morphological metrics, particularly in volume, area and dimensions, with krill swarms generally being longer in the north-south direction, compared to east-west (Table 5.3). Height and swarm minimum and maximum depths did generally appear to be constrained by seabed depth since

swarms only occasionally occupied on average 40% of the acoustically observable water column (Table 5.3). The energetic measures showed less variation, which may be both a consequence of low biological variation and due to the lack of sensitivity of the SM20 MBE. Swarm roughness (R) had the lowest CV for the morphological parameters, suggesting some underlying biological constraint (Table 5.3), and is unlikely to be a sampling artefact, since only swarms that were entirely insonified by the MBE were analysed.

Metric	mean (CV)	range
Area (m^2)	11,024.7 (4.70)	218.6 to 1,222,048
North-south length (m)	120.2 (2.34)	9.9 to 4,793.6
East-west length (m)	86.22 (2.03)	9.22 to 2,959.5
Minimum depth (m)	51.8 (0.36)	6.1 to 114.5
Maximum depth (m)	68.4 (0.31)	12.3 to 119.6
Height (m)	10.6 (0.70)	3.9 to 77.5
Volume (m^3)	3,695.7 (4.59)	46.2 to 406,709.8
Object bounding box - 1 (m)	106.5 (0.72)	9.7 to 966.7
Object bounding box - 2 (m)	23.4 (0.80)	5.5 to 151.5
Object bounding box - 3 (m)	9.3 (0.72)	5.0 to 89.07
Roughness (m^{-1})	3.3 (0.23)	1.2 to 8.1
Sv_{mean} (dB re 1 m^2/m^3)	-56.17 (1.40)	-99.77 to -44.75
Sv_{min} (dB re 1 m^2/m^3)	-101.40 (14.75)	-108.03 to -51.62
Sv_{max} (dB re 1 m^2/m^3)	-51.04 (1.20)	-54.02 to -44.50
Depth (m)	94.6 (0.12)	45.3 to 134.2
position in water column	0.6 (0.32)	0 to 1.0
proportion of water column occupied	0.40 (0.49)	0.03 to 0.97

Table 5.3: Summary statistics for 3D krill swarms for the 1,006 swarms that were located entirely within the MBE swath during four days of surveying. CV is the coefficient of variation.

Following Gerlotto et al. (2004) the length/width (l/h) relationship of detected 3D krill swarms was investigated. The histogram (Figure 5.13) shows no obvious break point between different swarm types. A break point, as found by Gerlotto et al. (2004) would suggest distinct swarm types.

Krill swarm classification

The first three components of the PCA accounted for 22%, 15% and 13% respectively of the observed variance in krill swarm morphology (Table 5.4). Using Mardia's criterion, the first principle component was influenced significantly by krill swarm morphology, through the following metrics: volume, surface area, north-south length, east-west length and height. The second component was influenced significantly by the length to height ratio, and the third by geographical position and swarm energetics Sv_{mean} and Sv_{max}.

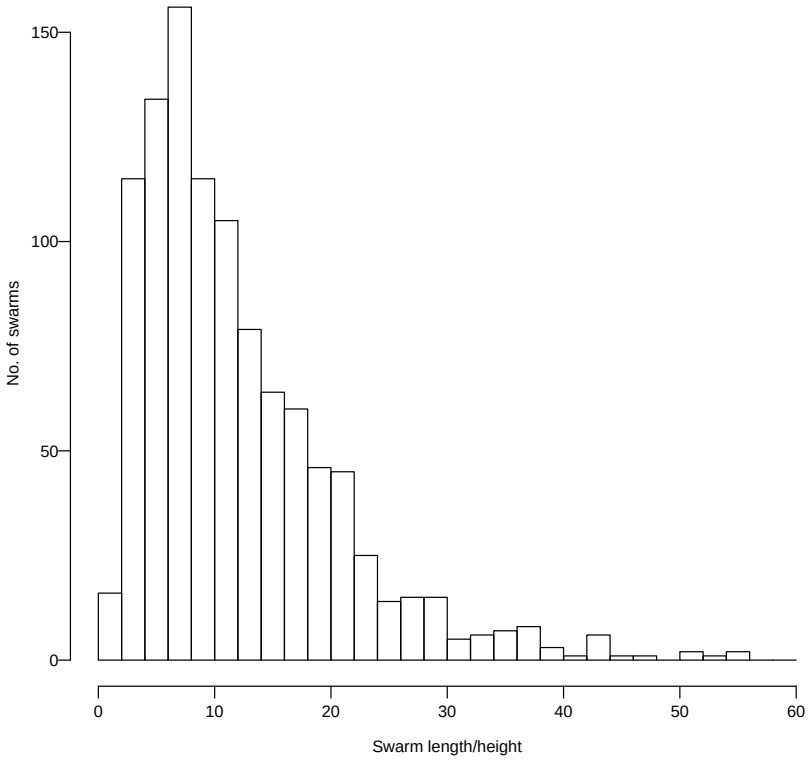

Figure 5.13: Histogram of length/height ratio of 3D detected krill swarms. Based on this ratio, there is no obvious pattern to allow the partitioning of the 3D krill swarms into morphological groups.

A three-class swarm typology (based on Miller and Hampton 1989; Hamner and Hamner 2000) was selected to partition the observed krill swarms into groups, defined by position, morphology and energy. The number of classes was determined using the pseudo F-statistic test for significant differences in the sums of squares of the within cluster distances between two possible clusterings. No significant differences were found between the three-class cluster and other n-class clusters (n=2 to 20). Further, visual inspection of the 3D krill swarm regions in Echoview suggested that there were three types of krill swarm: The partitioning was carried in the reduced factorial space determined by the above PCA (Figure 5.14). Group one contained 158 swarms, and groups two and three contained 431 and 417 swarms respectively (Table 5.5).

Variable	PC1	PC2	PC3
% variation explained	22.4	14.8	13.40
cumulative % variation	22.4	37.3	50.7
Mardia's criterion	0.278	0.328	0.361
Roughness (m^{-1})	-0.115	-0.264	-0.106
Volume (m^3)	**0.385**		0.280
Surface area (m^2)	**0.378**		0.278
North-south length (m)	**0.384**	-0.271	-0.163
East-west length (m)	**0.397**	-0.259	-0.140
Height (m)	**0.384**	0.147	0.217
Length/height	0.220	**-0.374**	-0.244
Latitude (deg)	0.127		**-0.403**
Longitude (deg)	-0.140	-0.180	**0.516**
Depth (m)		-0.266	0.275
Position in water column	0.185	0.214	
Sv_{mean} (dB)		**0.468**	
Sv_{min} (dB)	-0.206	0.148	-0.123
Sv_{max} (dB)	0.213	**0.393**	
Swarm nearest neighbour distance (m)		0.205	
Time of day	0.122		-0.347
cross track distance (m)		-0.192	0.172

Table 5.4: The first three principal components of krill swarm metrics. Principal component analysis was performed on the normalised correlation matrix of continuous krill swarm metrics. Swarm metrics with a significant influence on an individual principal component (j) are highlighted. Significant influence determined as eigenvector elements (u_{ij}) with a value greater than Mardia's criterion ($u_{ij} > 0.7max(|u_j|)$, Jolliffe 2002). Eigenvector elements <0.1 are not shown.

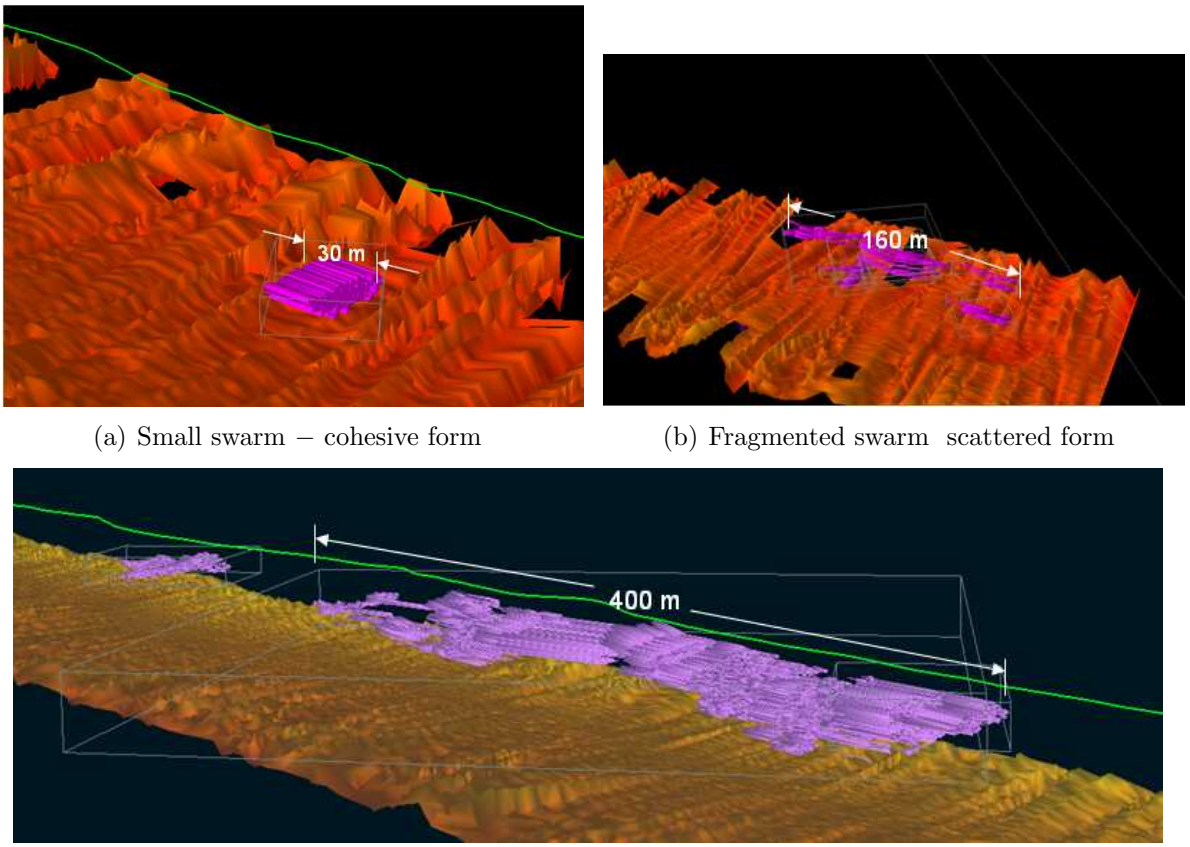

(a) Small swarm – cohesive form

(b) Fragmented swarm scattered form

(c) Large continuous swarm irregular form

Figure 5.14: Three krill swarm types as detected using SonarData's 3-D schools detection algorithm in Echoview v3.5. Swarms are shown in purple, along with a grey 3D wire frame bounding box. The multibeam detected seabed is shown in orange and the research vessel track in green.

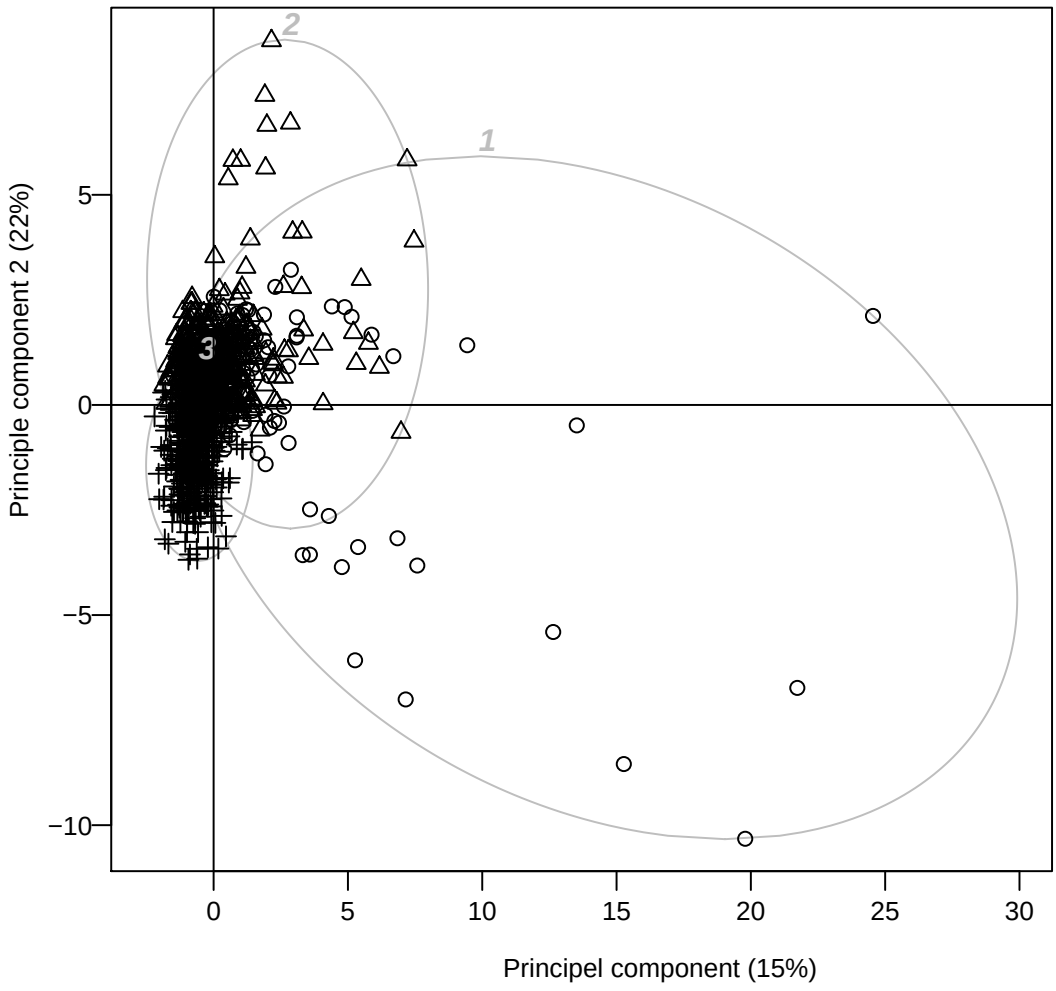

Figure 5.15: Three-class partition analysis of krill swarms performed in principle component analysis reduced factorial space. The grey ellipses delimit each of the krill swarm classes.

Swarm metric	Partition group 1	2	3
n	158	431	417
Roughness	3.23 (7.78)	2.96 (5.07)	3.65 (4.34)
Depth	88.02 (10.73)	90.82 (8.65)	101.00 (10.24)
Sv_{mean} (dB re 1 m^{-1})	-51.89 (11.57)	-51.65 (7.75)	-57.44 (8.96)
Position in water column	0.78 (6.32)	0.73 (4.46)	0.55 (2.83)
Nearest neighbour distance (m)	37.95 (1.39)	47.72 (1.11)	26.01 (1.16)
North-south length (m)	276.39 (0.41)	82.21 (1.17)	100.20 (2.06)
East-west length (m)	181.85 (0.43)	64.97 (1.22)	71.96 (2.02)
Height (m)	13.46 (1.21)	11.98 (1.57)	8.05 (2.24)
Sv_{min} (dB re 1 m^{-1})	-100 (0.00)	-99.51 (0.20)	-100 (0.09)
Sv_{max} (dB re 1 m^{-1})	-48.30 (11.88)	-48.32 (7.00)	-49.23 (13.75)
cross track distance (m)	33.87 (1.83)	29.80 (1.62)	40.42 (1.60)
Surface area (m^2)	29,197.01 (0.24)	11,554.54 (0.44)	3,591.56(0.84)
Volume (m^3)	9,237.07 (0.24)	4,220.67 (0.43)	1,053.37(0.86)
Length/height	19.46 (0.54)	7.24 (1.67)	13.80 (1.83)

Table 5.5: Summary statistics of the three partition groups for selected krill swarm metrics and associated coefficients of variation. The number of swarms (n) is given for each partition group. The coefficient of variation is given in brackets.

Examining the spatial position of partitioned swarms revealed that class one swarms were found entirely in the north-west of the survey area, whereas swarms of partition types two and three were found mixed throughout the remainder of the site, but particularly concentrated to the south-east (Figure 5.16).

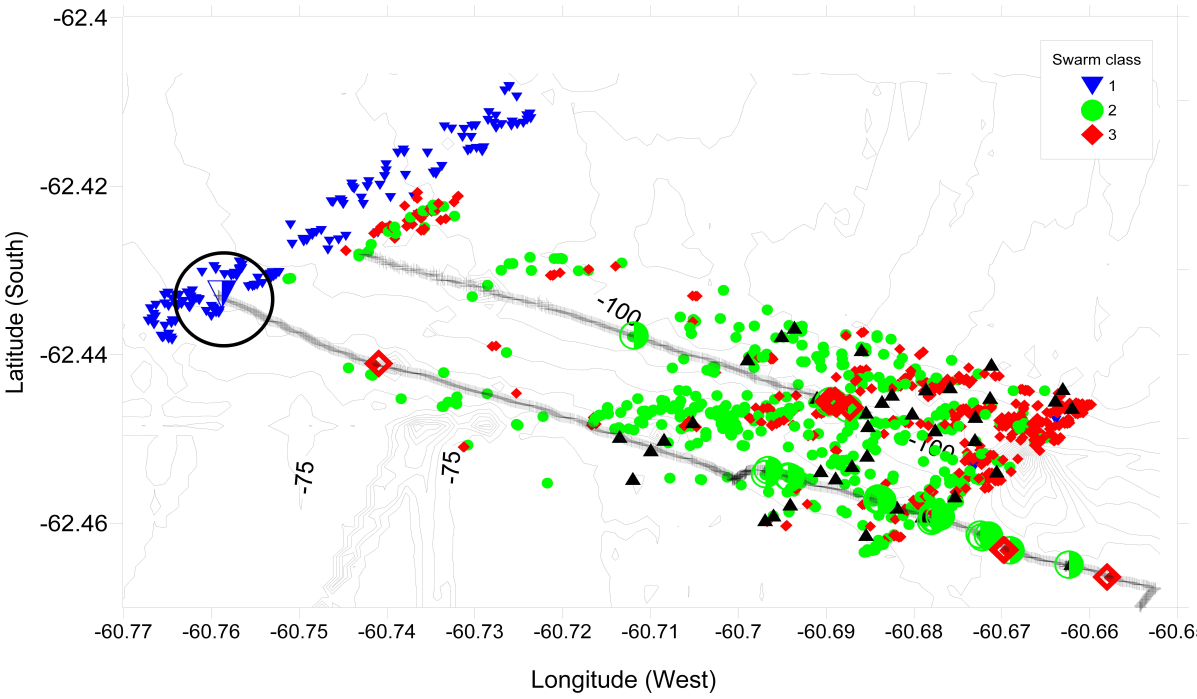

Figure 5.16: Spatial distribution of krill swarm types as classified using partition analysis. Seabed contours given in 5 m intervals, also derived from multi-beam echosounder observations. Predator sighting locations are marked as black triangles, and the positions of the two 'tie-lines' are marked in grey. The overlap between class-1 swarms detected along the survey transect proper and a class-1 swarm detected on the 'tie' line is shown as the enlarged ringed, type-1 swarm symbol.

Whilst analysis of the l/h ratio, as used by Gerlotto and Paramo (2003), failed to delineate Antarctic krill swarms into three distinct morphological groups, there were distinct differences in this ratio across the partitioned groups: group one had almost double the l/h ratio of group three (Table 5.5). Swarms in group one, whilst being smaller, exhibit a different morphological structure that isn't simply rescaled for larger swarms. For example, the north-south and east-west lengths are more than double that of swarm groups two and three.

Roughness

The observed roughness of 3D krill swarms did not conform to expectations for any simple geometric shapes. Spheres have the lowest roughness (i.e. the lowest surface area to

volume ratio), followed by the ellipsoid, and cylinders had the greater roughness (Figure 5.17) for the shapes considered. This suggests that krill swarms do not form simple geometric shapes, but are likely to form a variety of complex shapes that cannot be approximated by either the sphere, ellipsoid or cylinder. The low variation in roughness is interesting given the high variation in other krill swarm morphological parameters (Table 5.3). This low variation in R is not an observational artefact since the variation in swarm area and volume are both high (Table 5.3). The low variance of observed roughness suggests that krill within swarms are behaving in a way that maintains a similar roughness across swarms. This is apparently not driven by depth of water, since krill swarms were not seen to occupy more than one third of the water column. This group behaviour must in some way benefit an individual krill, but the mechanisms are unclear at this stage.

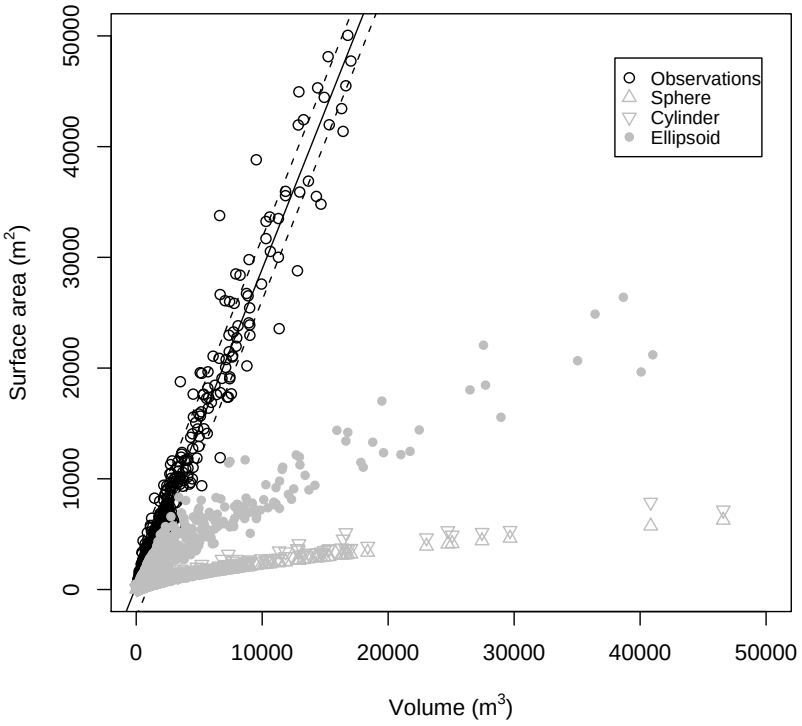

Figure 5.17: Krill swarm roughness (R) illustrated by observations (open circles) of swarm volume (V) and swarm surface area (A). Krill swarm roughness was compared to that of other geometric shapes. The area of sphere and cylinder was calculated from V and observed swarm height was used as cylinder height. Swarm bounding box dimensions were used to calculate ellipsoid volume and to approximate ellipsoid surface area. Observed krill swarms did not appear to comply to the expectation of these simple geometrical shapes.

The interactions between krill swarm roughness and predators were investigated using

Parameter	d.f.	F	p-value
distance to predator (km)	1.932	16.30	1.13e-07
NND (km)	1.744	6.229	0.0303
position in water column	1.989	280.92	<2e-16
S_v mean (dB)	1.948	21.28	9.49e-10

Table 5.6: explanatory variables used in the generalized additive model to model the response variable, krill swarm roughness R

predator sighting data observed from *R/V Roald* (Table 5.7). Since there was no *a priori* reason to expect a linear response between the roughness and explanatory variables, such as NND, a GAM was used to investigate potential drivers of changes in krill swarm roughness. The selected model was built of smooths of distance to nearest predator, NND between swarms and swarm position in water column (Table 5.6). Other combinations of explanatory variables were tried, but the selected combination gave the best model fit. Further, the selected model used a log link function and gamma error distribution, which resulted in a model that explained 50.3% of the deviance in R, with $R_{adj} = 0.54$ ($\gamma = 1.4$), AIC=1,612.40. A variety of link functions and error distributions were tried, but the above combination yielded the highest explanatory power and did not violate the model assumptions (Figure 5.22).

Species	Code	Number of individuals		
		R/V *Ernest*	R/V *Roald*	Total
Antarctic tern (*Sterna vittata*)	ANTE	8	10	18
Black-browed albatross (*Thalassarche melanophris*)	BBAL	9	8	17
Black-bellied storm petrel (*Fregetta tropica*)	BBSP	0	3	3
Chinstrap penguin (*Pygoscelis antarctica*)	CHPN	14	1	15
Antarctic fur seal (*Arctocephalus sp. (gazella)*)	FUSE	1	6	7
Grey-headed albatross (*Thalassarche chrysostoma*)	GHAL	6	0	6
Humpback whale (*Megaptera novaeangliae*)	HUMV	14	4	18
South Polar Skua (*Catharacta maccormicki*)	SPSK	0	2	2
Giant petrel(unid) (*Macronectes sp.*)	UGPT	9	1	10
Penguin(unid) (*Pygoscelis/Eudyptes sp.*)	UNPN	3	7	10
Wilson's storm petrel (*Oceanites oceanicus*)	WISP	12	12	24

Table 5.7: Predator observations in the vicinity of the multi-beam study site. Observations from R/V *Ernest* are within a circle (radius=5 km) from the centre of the study site.

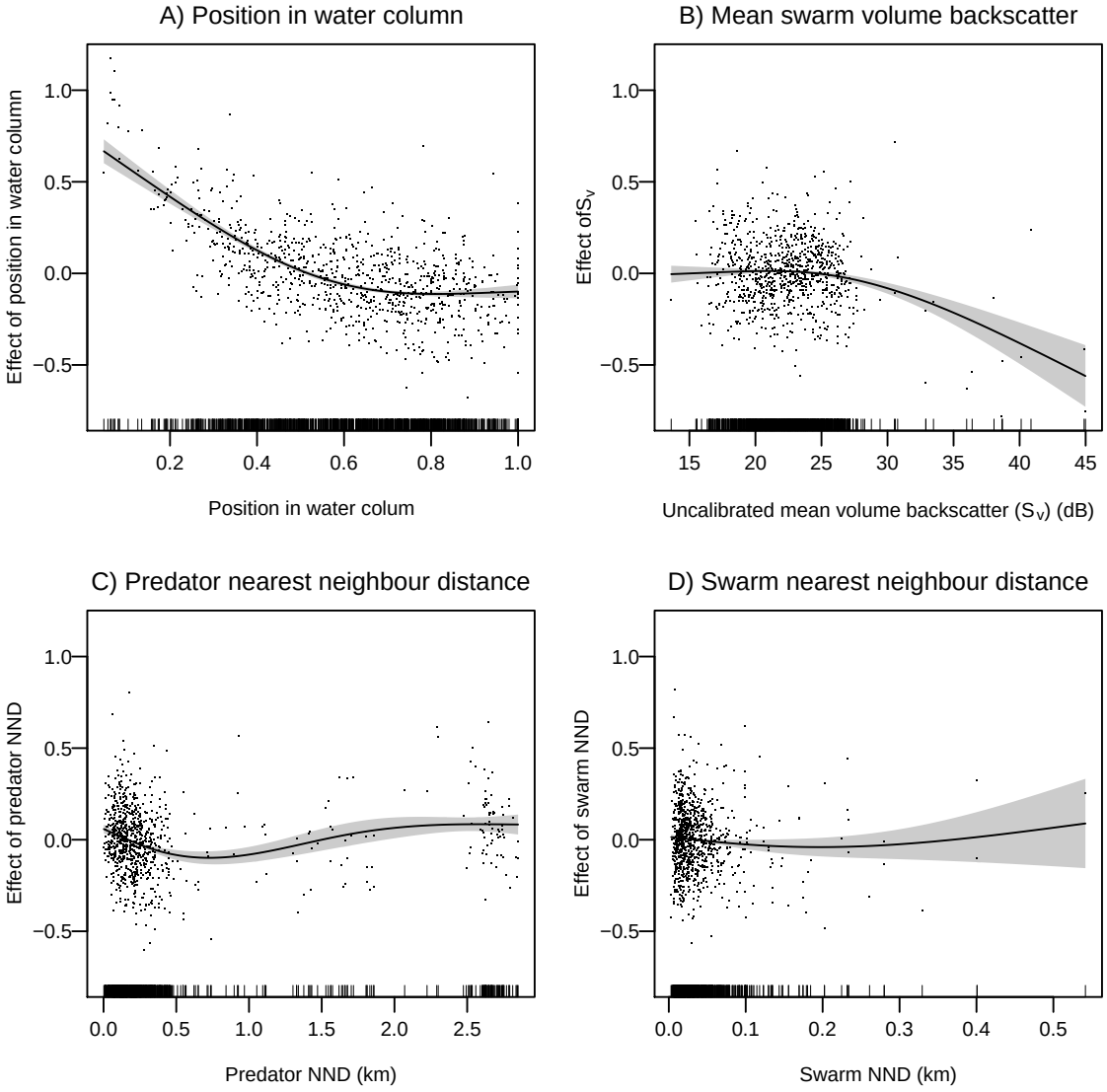

Figure 5.18: Smooths of generalized additive model terms showing the effect of various continuous variables on krill swarm roughness. Locations of observations are shown as vertical lines on the x-axes. The solid lines are the estimates of the smooths, the shaded areas are standard errors of the estimated smooths and the points are the observation partial residuals.

Of particular relevance to this investigation was the affect of the proximity of predators on the roughness (R) of krill swarms. The model output shows that up to a distance of 0.5 km to the nearest predator (p_d) there was a linear relationship between the distance to nearest predator and R (Panel C, Figure 5.18) and for p_d >0.8 km R begins to increase.

GAM predictions for the effect of swarm position in water column (posn_{wc}) show that as swarm depth increases R decreases (Panel A, Figure 5.18). As NND to swarm increases R decreases NND=0.2 km, after which R increases, but there is paucity of data at swarm NND>0.2 km (Panel D, Figure 5.18).

5.3.3 Assessment of multibeam performance

Predator-prey interactions

A comparison of the MBE and SBE for investigating predator-prey interactions found that around each air breathing predator sighting location the MBE detected an order of magnitude more krill swarms than the SBE. This is likely to be due to the increased sampling volume of the MBE, and demonstrates that the mismatch in the ES60 strip-transect width for sampling krill, and the visual predator strip-transect sampling width (see Figure 5.2) is weakening the signal in the predator-prey interactions.

The use of the MBE has enabled the assessment of krill predator foraging scale, there is an increased number of krill swarms closer to the locations of predator sightings, which decreases with increasing distance (Figure 5.19), suggesting that either predators are preferentially foraging in areas of high krill density or the presence of predators is causing swarms to fragment. Using the results of a GAM (Gaussian errors, identity link, r^2_{adj}=0.78, deviance explained=80.7%), the spatial-scale of the influence of krill predators is estimated to be approximately 220 m. This is the distance from a predator sighting at which the number of detected krill swarms reaches a minimum (Figure 5.19).

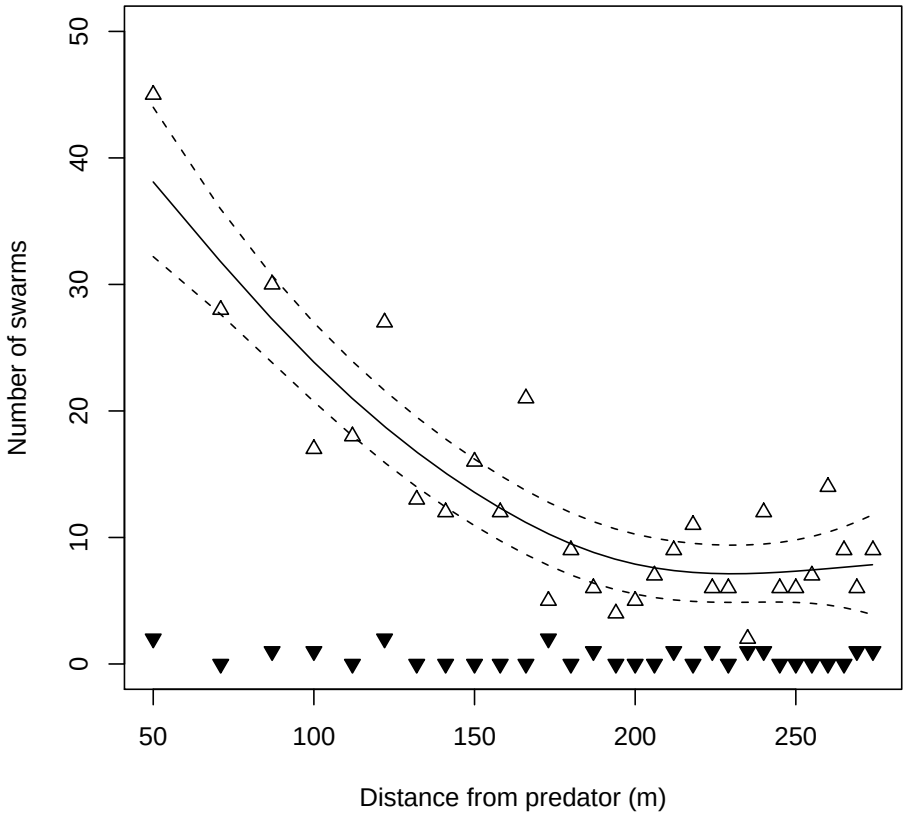

Figure 5.19: Comparison of the number of krill swarms detected by the SM20 multi-beam echosounder (triangles) and the ES60 single-beam echosounder (inverted, filled triangles). The number of krill swarms detected in constant area (A=7.854 m^2, with annulus ring widths diminishing to a minimum of 5 m at r=274 m) is shown. The fitted line and confidence intervals are from a GAM (Gaussian errors, identity link, r^2_{adj}=0.78, deviance explained=80.7%).

Potential for biomass estimation

Two sources of potential bias in MBE derived biomass estimates ($\hat{b}$) were investigated. Firstly, since the SM20 operated at a single frequency (200 kHz) it was not possible to apply the dB difference technique (see Madureira et al. 1993; Watkins and Brierley 2002) to partition the acoustic observations (S_v) to identify those arising from krill. This could potentially lead to an overestimate of $\hat{b}$ if many non-krill targets exist. Secondly, the 3-D schools detection used a detection algorithm threshold of 23 dB, which using the ECDF mapping technique (see section 5.2.3) was equivalent to a detection threshold of -52.7 dB (packing density of 48 krill/m^3) using the ES60. This meant that swarms with a density <- 52.7 dB would not be detected by the SM20, which would lead to an underestimate of $\hat{b}$.

To assess the magnitude of these biases $\hat{b}$ was obtained for krill swarms detected using the ES60 within a 5 km radius of the centre of the MBE study site. The optimal estimate of $\hat{b}$ gave 3,563 tonnes of krill (Table 5.8). Using only the 200 kHz ES60 transducer $\hat{b}$ was 7 % higher than the dB differenced estimate and the lower detection threshold resulted in $\hat{b}$ being 7 % lower.

Data Description	detection threshold (dB)	n	$\hat{b}$ (metric tonnes)	$\hat{b}$ % difference
200 kHz (dB difference)	-80	92	3,563.7	-
200 kHz	-80	109	3,830.6	+7.49
200 kHz	-54	85	3,535.1	-7.72

Table 5.8: Biomass estimates ($\hat{b}$) for krill swarms within a circle (r=5km) of the centre of the multi-beam study site. $\hat{b}$ calculated for schools detection thresholds of -54 and -80 dB, with acoustic energy threshold at -80 dB. The dB difference technique (200-38 kHz) has been used to identify Antarctic krill swarms from other organisms. This is considered to be the optimal estimate for krill swarm biomass.

The largest krill swarm biomass was estimated using the 200 kHz ES60 observations and the -80 dB detection threshold (Table 5.8 and Figure 5.20). For all krill swarm detection settings, approximately 80 % of the biomass was contained in four or five swarms (Figure 5.20). Individual krill swarm biomass appeared to be approximately 8% lower using the -54 dB detection threshold setting, which suggests that lower density regions of swarms are being excluded by the detection algorithm. Finally, the dB difference swarms (grey line, Figure 5.20) shows that one high-biomass swarm has been excluded, suggesting that this swarm/aggregation was not krill.

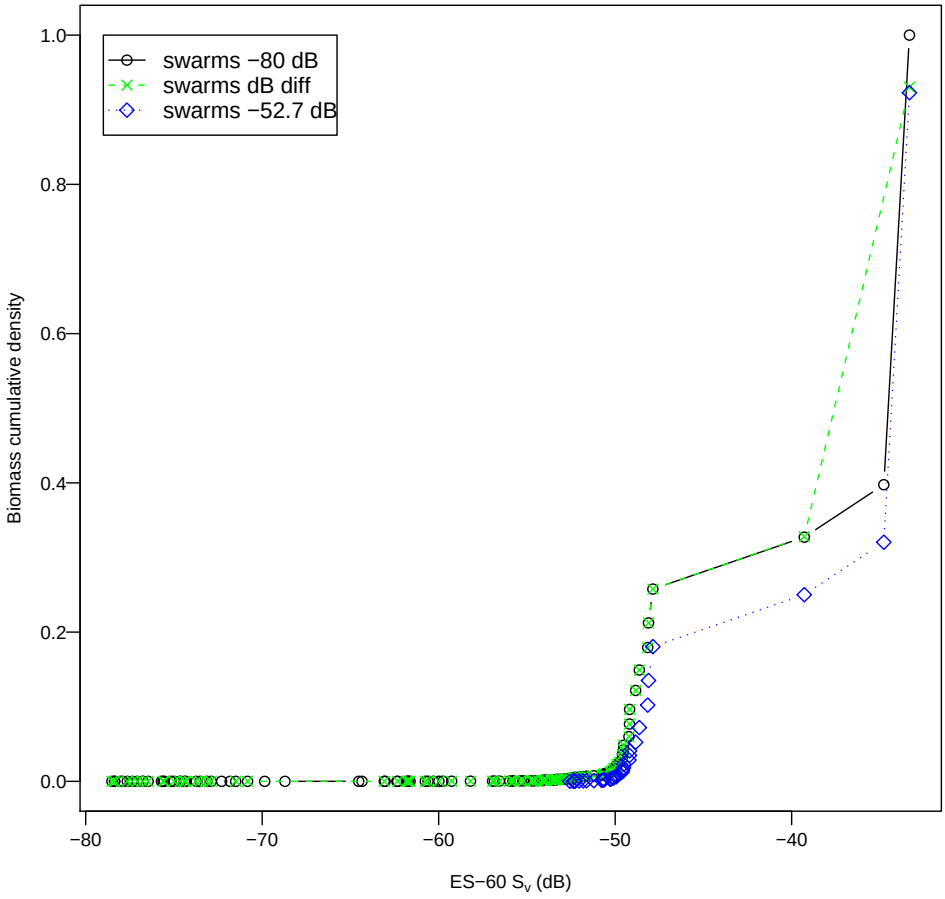

Figure 5.20: Standardised cumulative frequency plot of individual krill swarm biomass detected with the ES60 echo-sounder within a 5 km radius of the centre of the MBE study site. The plot has been standardised to the highest $\hat{b}$ (200 kHz, detection threshold: -80 dB).

Vessel avoidance

There is large variation in the number of detected schools with distance from *R/V Roald* (Figure 5.21 and Table 5.9). Certainly, changes in water depth cause the MBE sampling volume to vary across the survey region: sampling volume will be decrease in shallower water. The null hypothesis of a uniform distribution of detected swarms with horizontal distance from the boat (χ^2=814.743, d.f.=19, p-value<2.2e^{-16}) shows that there is a significant difference between the observed horizontal distance from krill swarm geometric centre to the boat. There are two potential causes of these differences: 1) avoidance, krill may be actively avoiding the boat, thus causing the observed difference in krill swarm characteristics with distance from the boat; 2) the orientation of the MBE, causing an increase in the number of krill swarms with range (Figure 5.21) may have caused these observed differences.

Metric	Horizontal distance classes (m)											
	(0,10]	(10,20]	(20,30]	(30,40]	(40,50]	(50,60]	(60,70]	(70,80]	(80,90]	>90	F-value	p-value
N	114	185	187	169	164	97	61	40	30	38	-	-
S	6337.3	6958.6	8111.8	10125.7	8650.4	15369.9	39129.6	6415.1	7465.7	32837.8	116,555	0.000
NSl	63.6	99.7	104.7	121.4	129.4	162.3	201.7	114.3	125.1	181.9	1.844	0.057
EWl	51.8	74.0	77.8	85.7	88.7	109.0	140.3	88.2	91.6	139.8	0.776	0.639
z_{min}	49.9	40.8	47.5	52.3	55.6	59.4	52.9	51.0	53.1	48.4	0.049	1.000
z_{max}	58.3	50.3	57.8	63.2	66.5	71.5	65.0	61.5	63.1	63.6	0.063	1.000
$Height$	8.4	9.5	10.3	10.9	10.9	12.1	12.1	10.5	10.0	15.2	0.003	1.000
V	2255.6	2306.4	2648.5	3450.7	2766.6	4635.0	12422.7	2178.2	2273.9	13022.3	13749	0.000
OBBl_1	73.5	85.1	101.0	98.8	102.8	135.6	170.9	139.6	151.8	223.0	1.765	0.071
OBBl_2	19.2	21.1	23.3	22.7	22.4	26.4	28.0	23.2	23.2	35.2	0.016	1.000
OBBl_3	8.1	9.0	9.2	9.2	9.1	10.0	10.8	8.7	9.0	14.0	0.002	1.000
R	3.4	3.6	3.4	3.1	3.1	3.2	3.3	3.4	3.7	3.5	0.000	1.000
Sv_{mean}	23.9	23.1	23.2	22.6	22.7	22.0	21.0	21.4	19.9	21.0	0.001	1.000

Table 5.9: Variation in mean krill swarm morphological parameters with horizontal distance to research vessel. Lengths in m, surfaces m^2, volumes m^3. Mean krill swarm surface area, and volume are significantly different ($p < 0.05$) across the distance classes.

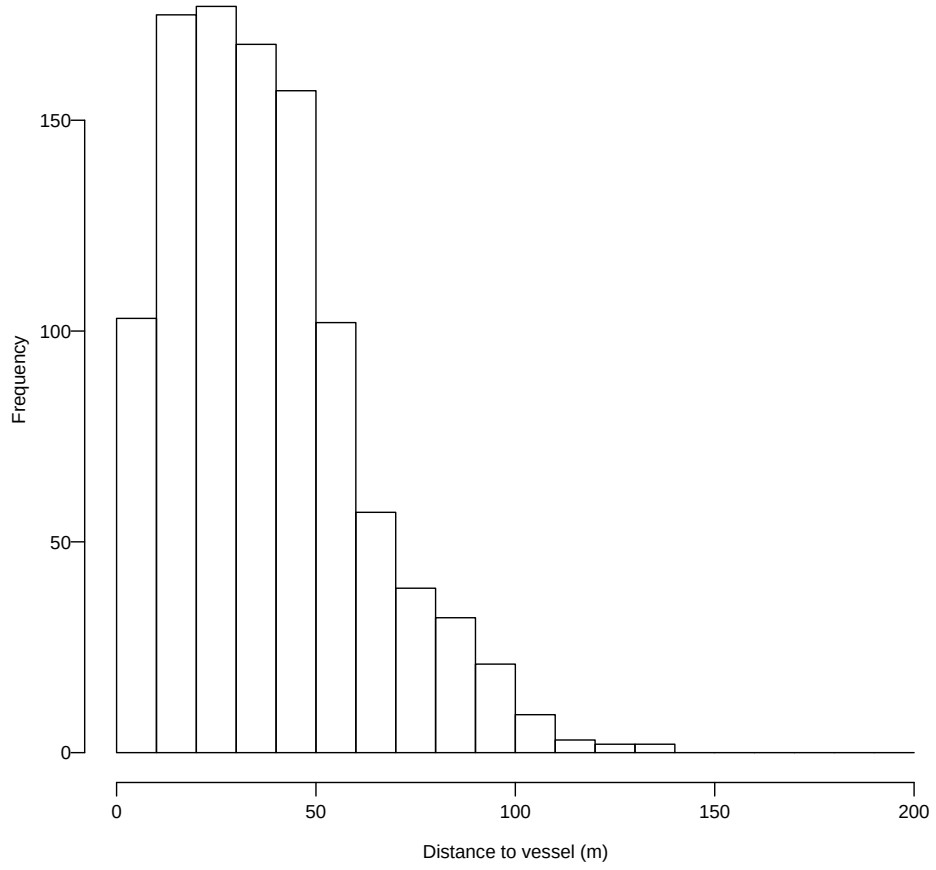

Figure 5.21: Horizontal range from detected krill swarms to the survey vessel as a frequency histogram of the number of schools in 10 m horizontal range bins. This non-uniform distribution arises from the multi-beam echosounder sampling volume and potentially from the avoidance of the research vessel by krill.

5.4 Discussion

This field investigation has successfully demonstrated that swarms of Antarctic krill can be detected using a 200 kHz MBE. After operational and logistic appraisal, assessment of the MBE system and the zodiac research vessel for sampling krill was made on the basis of a multi-variate analysis of the MBE detected krill swarms. If the metrics describing the characteristics of detected krill swarms had all been very similar then this would have suggested that the survey equipment was unsuitable, since previous investigations in this area, using conventional hull-mounted vertically downward looking echosounders, have demonstrated that there is large variation in krill swarm energetics and morphologies (Hewitt and Demer, 2000, 2003). In this instance detection of variability is indicative of some useful functionality.

5.4.1 Krill swarms

In these analyses krill swarms have been characterised by their external morphological characteristics. These morphological swarm metrics have been observed or calculated from a swarm envelope defined as the boundary between empty water and a densely packed animals (Reid et al., 2000a). This boundary was defined objectively using a 3D detection algorithm (Echoview v3.5, SonarData, Tasmania) and a sequentially varying set of parameters. Energetic swarm metrics (S_v) and water depth, determined from MBE bathymetry profiles, were calculated for each detected krill swarm. Using these metrics, the variation in the characteristics of krill swarms was determined for the study site. The variation in krill swarm metrics (Table 5.3) and visual inspection of the 3D krill swarm boundaries in Echoview show that the equipment used in this survey is suitable for sampling and obtaining information on krill swarms in 3D.

Krill swarms detected in this investigation, with a 23 dB S_v boundary threshold and 5 m minimum dimension exhibited a diverse range of metric values: there were large differences between the minimum and maximum values of krill swarm metrics (Table 5.3). Since group one swarms were found in one geographical area and groups two and three were mixed spatially, the examination concentrated on the differences between group one and the combined groups two and three, and the possibility that the difference was temporal, not spatial. Given that no predators were sighted in the group one spatial area, a potential explanation for the distinct identity of group one type krill swarms is that they represent undisturbed swarms. The most striking difference between partition group one and groups two and three was in size: swarms in group one were larger than groups two and three. North-south and east-west lengths, surface area and volume were at least double in group one compared to groups two and three (Table 5.5). Since group type one

krill swarms occurred in the absence of predators, the size differences observed between predator groups suggests that swarms may split in response to predation. Swarms in group two were the closest horizontally to *R/V Roald* and swarms in group three were found in shallower water. Interestingly the swarm data used in the multi-variate analysis include swarms that were detected along the two tie-lines (Table 5.2 and Figure 5.4), and since these tie-lines cut through both the south-east and north-west areas of the study site the apparent spatial segregation of partition swarm groups is unlikely to be an artifact of day-to-day variation. If this segregation was due to a day effect then it seems likely that swarm partition types two and three would have been detected in the north-east area that is exclusively type one swarms.

Watkins and Murray (1998) reported inter-swarm morphological differences as evidence of a size sorting mechanism, and this may be driving the differences between the groups seen here. Since the MBE is a single-frequency (200 kHz) system, it is not possible to use the dB difference technique (see Madureira et al. 1993; Brierley et al. 1997b) to identify krill swarms or to infer size. Fortunately, the other inflatable boat, *R/V Roald*, was equipped with a dual frequency (38 and 200 kHz) single-beam echosounder, which allows the dB difference of krill swarms within the MBE study site to be examined. Given that the dB difference of a krill swarm is proportional to the length frequency distribution of krill in the swarm, it is possible to examine the variation of inter-swarm mean krill lengths. Using this approach, there is strong evidence to suggest that there was inter-swarm variation in the mean krill length, within a 5 km radius of the centre of the MBE study site (Figure 5.9(b)).

A krill length sorting mechanism is important for predator foraging success (Barlow et al., 2002) and biomass estimates (Hewitt and Demer, 2000). Firstly, if a size storing mechanism exists then it is likely that juvenile krill are segregated into different krill swarms than older krill and these swarms of juveniles may be more vulnerable to predation: the response of a nïave school, comprised of juvenile krill may have ineffective behavioural responses to predation (O'Brien, 1989; Ritz, 1994). The transmission of information, by way of a wave of agitation (see Gerlotto et al. 2006) through a swarm, may be disrupted by for example a random orientation of escape swimming directions or a slow response to the presence of a predator. Secondly, should krill predators have a preference for a particular length of krill (Barlow et al., 2002), then predators will target those swarms. Also, some size classes of krill may be more vulnerable to being 'trapped' in particular geographical areas by physical forcing mechanisms, such as regions with rapidly varying bathymetry, or upwelling currents, thereby increasing their probability of detection by krill predators (O'Brien, 1987; Genin, 2004).

5.4.2 Swarm morphology

The 3D MBE data acquired during a study of anchovy and common sardine schools by Gerlotto et al. (2004), showed distinct structures, layers and schools that could be partitioned by an l/h ratio of 7. This l/h ratio does not seem to separate the krill swarms detected here, rather the MBE results suggest a continuum of swarm l/h ratios (Figure 5.13), making the l/h ratio unsuitable for delimiting swarm type. In agreement with other investigators studying pelagic species (*e.g.* clupeid schools, Gerlotto and Paramo 2003), this research discovered the krill data suggest that the external boundary of swarms are extended in the horizontal direction, compared to the vertical (l/h ratio>1, Table 5.5). Despite there being no pattern in the overall l/h ratio, there is considerable variation in l/h between partition groups. The variation in l/h ratio, combined with visual inspection of krill swarm boundaries in Echoview, and the analysis of swarm roughness, is evidence that krill swarms do not have spherical boundaries, since the expected krill swarm roughness in the study site differed from estimated spherical roughness. This l/h ratio was not generally caused by swarms being physically constrained by the sea surface or seabed (the mean height for all swarms detected within the survey area was just 10.6 m), with the mean minimum depth of the shallowest point of a swarm being 50.25 m, whereas mean seabed depth was 94.6 m.

5.4.3 Avoidance

Also of interest is the detection of horizontal and vertical avoidance of *R/V Roald* by krill. Results must be viewed with caution though because the mounting angle of the MBE makes horizontal avoidance of krill problematic to assess. The vertically downward mounting angle of the MBE head meant that the horizontal sampling distance, or the effective strip width, varied with depth. This meant that some horizontal distances were sampled more than others. The effective strip width also varied with seabed depth, so at this time it is impossible to disentangle the potential sampling artefact, caused by the MBE head orientation, from any avoidance behaviour of krill. Given that Brierley et al. (2003a) demonstrated using an autonomous underwater vehicle, the *Autosub*-2, deployed in the Weddell Sea and Bransfield Strait, that krill do not avoid the *RRS James Clark Ross*, then there is some evidence to suggest krill would not avoid a much smaller, quieter, inflatable boat. In a study of the behaviour of anchovy and common sardine schools, using an MBE Gerlotto et al. (2004) showed a difference between vertical avoidance due to physical protection, rather than a longer-range diving avoidance. Physical protection avoidance occurs when organisms move to avoid entering into close proximity or colliding with the hull of a research vessel, and unless the entire swarm moved, this would lead to

the vertical compression of the swarm (Soria et al., 1996). However, this is unlikely in this case since the survey was being conducted from an inflatable boat with a draught of less than 0.5 m and no swarms were visually observed close to the sea surface. Whilst no vertical avoidance behaviour of krill was detected, there were krill swarms detected close to *R/V Roald* at a depth of 5 m. If this behaviour is replicated in other locations it has implications for krill biomass estimates from conventional research vessels. Many conventional vertically downward looking transducers do not sample the water column until a depth of 10 to 15 m due to transducer depth and acoustic near field effects: if krill are located in this shallow water region this would negatively bias mean area krill density estimates. Due to acoustic nearfield effects and the 1 m deployment depth of the MBE head it was not possible to detect krill swarms at depths <5m. Currently, the MBE mounting angle prevents estimates of krill biomass with respect to depth from the MBE data set.

5.4.4 Swarm roughness and predation

A similar roughness of krill swarms observed in this investigation (R=3.3,CV=0.23, Table 5.3) was seen by Gerlotto and Paramo (2003) (R=3.15,CV=0.34) using MBE to observe clupeid schools (*Sardinella aurita* and *Sardinops sagax*) off Venezuela and Senegal. The reasons for the similar roughness between these species is unclear, but is not shared between all pelagic species. In another MBE investigation conducted by Gerlotto et al. (2004) into aggregations of Anchovy (*Engraulis ringens*) and common sardines (*Strangomera bentincki*) roughness (R) was 5.7 for schools, defined as aggregations with l/h <7 and R=6.4 for layers $l/h \geq$7. Both these values are similar to the predicted values for aggregations with a cylindrical shape (R=7.0, CV=0.78, see Section 5.2.4).

Krill swarm morphology appears to be influenced by predation. Since the results of the GAM (Section 5.3.2) showed that variation in swarm roughness is partially caused by proximity to predators. This change in morphology is perhaps due to krill swarms adopting anti-predation measures. These measure could either include the dilution effect, reducing the predation risk of an individual krill in response to attack by a whale, or alternatively, may be an attempt to confuse predators: group scattering would make it difficult for a predator such as a penguin or seal to take any individual krill (Landeau and Terborgh, 1986; Krakauer, 1995; Krause and Ruxton, 2002).

There maybe no standard response by individual krill in a swarm to the presence of predators. However, the change in R is evidence of a cohesive response to predation by a swarm, and therefore implicitly this response must be somehow communicated between individual krill within a swarm, perhaps through a wave of agitation (O'Brien, 1989; Hofmann et al., 2004).

The order-of-magnitude greater number of krill swarms detected by the MBE compared the SBE in the vicinity of air-breathing predator sightings showed that for the analysis of small-scale predator-prey interactions there is the potential for bias to occur when a SBE is used. The narrow sampling volume of the SBE meant that krill swarms located in shallow water, just off transect, were not detected. Further, it was determined that a MBE gathers more information regarding aggregations of pelagic organisms than a SBE. There are an increased number of swarms detected using the MBE compared to the SBE, this is because the sampling volume increased with MBE. A lower (-80 dB) threshold that was applied to the SBE gives this system an increased probability of detecting low density krill aggregations, where they exist within its beam pattern compared to the SM20. To summarise, the increased sampling volume of the SM20 makes this instrument the preferred device for studying predator-prey interactions.

5.4.5 Multibeam echosounder biomass estimates

Much of the biomass of krill in the study area is located in high density swarms (Table 5.3). High density swarms that are influential on biomass estimates are at least being detected by the MBE, but a great deal of further work is required before an MBE can be used for biomass estimates. One limitation of a single frequency acoustic system is that species cannot be identified. For example, during this survey, when a only the 200 kHz observations were used (lines 2 and 3, Table 5.8, page 131) from the ES60 single-beam echosounder, aggregations of other pelagic organisms were included in the biomass estimation. This resulted in a bias of approximately $\pm 7\%$ with respect to the 200-38 dB difference biomass estimated (Table 5.8). It may be possible to use a combination of SBE and MBE , deployed on the same platform to overcome the single frequency limitation of MBE. It is necessary to determine a lateral TS model for Antarctic krill (for *in-situ* see Hewitt and Demer 1996), so that S_v observations from an entire swath can be used to estimate swarm density. Thus far, a parameterised form Conti and Demer (2006) of the state of the art TS model for krill known as the stochastic distorted Born approximation (SDWBA) (Demer and Conti, 2005) uses a distribution of orientations of krill to the horizontal ($\theta = norm(u = 11^o, \sigma = 5^o)$). However, this TS model alone cannot be used to rescale MBE acoustic observations because the lateral TS of krill is known to be lower than the dorsal aspect TS (Hewitt and Demer, 1996). Since an MBE ensonifies the dorsal and lateral aspect it is necessary to develop lateral TS model for a distribution of lateral angular orientations and combine this model with dorsal TS models to scale MBE observations.

5.4.6 Limitations

The SM20 MBE has a narrower dynamic range and lower sensitivity than a conventional echosounder, such as the Simrad ES60. Given the narrow dynamic range of the SM20 MBE, determining the processing threshold sensitivity is important since acoustic observations (S_v) falling below this sensitivity will be excluded from the analysis. The target strength of krill in the survey area (at 200 kHz TS=-73.99 dB, mean, weighted by length frequency distribution of krill using Conti and Demer 2006 TS model, giving 48 krill/m^3) meant the MBE was detecting krill swarms at the lower limit of the system's dynamic range (Cochrane et al., 2003; Demer, 2004). It may have been possible to increase the detectability of krill swarms, by adjusting the MBE power and gain settings, but this would have effected the quality of the bathymetric data. The survey was a comprise between bathymetry and water column target data collection.

Whilst variation was observed in average krill density between swarms (S_v metrics Tables 5.3 and 5.5), it was not possible to examine the internal variation in the krill density within a swarm. This is because of both the MBE processing software used and the combination of low ping-rate and boat speed. This software limitation was countered by the delineation and selection of swarms from the MBE observations being automated, and therefore objective. Further the investigation of the sensitivity of these 3D school detection parameters was useful for selecting parameters for the detection of krill swarms used during these analyses.

The necessity to collect simultaneous water column and seabed observations was a limitation of the investigation. The orientation of MBE head (centre of the swath pointing vertically downwards), compared to other investigations (outer edge of the swath orientated parallel to the seabed), reduced the proportion of observations in shallow water, making it difficult to assess avoidance and the vertical distribution of krill swarms. In previous multibeam studies (eg Gerlotto et al. 2004 and Paramoa et al. 2007) the MBE system was mounted on one side of the research vessel and ensonified a volume of water from the sea surface to a plane vertically under the research vessel. The mounting configuration of the MBE head in these studies allowed direct observation of any lateral avoidance.

5.4.7 Conclusions

This investigation has demonstrated that krill swarms can be detected with an MBE, and that the external envelope of krill swarms cannot be described using simple geometric shapes. Based on these observations it is suggested that krill swarms attempt to maintain a constant roughness irrespective of shape, and the driver of the aggregation behaviour

that serves to maintain this constant roughness is potentially an anti-predation behaviour.

Through the use of a GAM it has been shown that the presence of predators influences the shape of a krill swarm. Additionally, swarm roughness is also influenced by the depth of the swarm and swarm nearest neighbour distance. Consequently, swarm shape is influenced by a combination of the presence of predators and environment. It is not possible to elucidate how krill detect the presence of predators from these observations.

When considering predator-prey interactions, an assessment of the interval structure of a krill swarm would be useful. Investigators have reported waves of agitation inside aggregations of pelagic species in response to predators (Axelsen et al., 2001; Gerlotto et al., 2006). Such data are difficult to observe, particularly from a small platform, such as an inflatable boat. Nevertheless a quantitative assessment of the variation of the internal structure of a krill swarm carried out using geostatistics, which is capable of describing interval swarm structure in two parameters, would provide a useful contrast of the interval structure in the presence/absence of predators, where predator presence/absence information could be obtained from visual observations.

A useful extension of the analysis of swarm roughness in response to predation would be the analysis of the variation in krill swarm morphology in response to oceanographic variables. As pointed out by Gerlotto et al. (2006), establishing a relationships between oceanographic variables and schools of anchovy would enable the acoustically-derived school shape to describe the condition of a school and enable inferences to be made about the anchovy population.

A1: Krill swarm roughness GAM model

This appendix summarises the selection of explanatory variables for modelling krill swarm roughness or R. A gamma error structure and log link function were chosen and the AIC used to determine the optimum model fit.

Intercept	Explanatory variables												AIC	r^2_{adj}	deviance
	Predator distance			Swarm NND			Position in water			Sv_{mean}					
	edf	F-value	p-value	edf	F-value	p-value	edf	F-value	p-value	edf	F-value	p-value			
1.215 <2e-16	1.407	41.72	<2e-16										2140.049	0.087	9.07
1.214 <2e-16	1.514	36.37	6.65e-16	1.96	15.35	2.79e-07							2107.923	0.14	12.7
1.202 <2e-16	1.948	15.30	2.95e-07	1.87	6.16	0.002	1.989	279.62	<2e-16				1645.915	0.529	48.2
1.201 <2e-16	1.932	1.63	1.48e-07	1.74	3.512	0.027	1.989	280.82	1.97e-08	1.948	21.276	< 2e-16	1612.402	0.541	50.3

Table 5.10: An example of combinations of explanatory variables tried in the GAM of krill swarm roughness.

Overall the diagnostics plots for the selected model show that none of the model assumptions have been violated. The response variable R is linear on the scale of the log-link function (Normal Q-Q plot). There is no apparent relationship between fitted values and residuals. The model fit residuals are normally distributed and model prediction show some over prediction of low R values and under prediction of high R values.

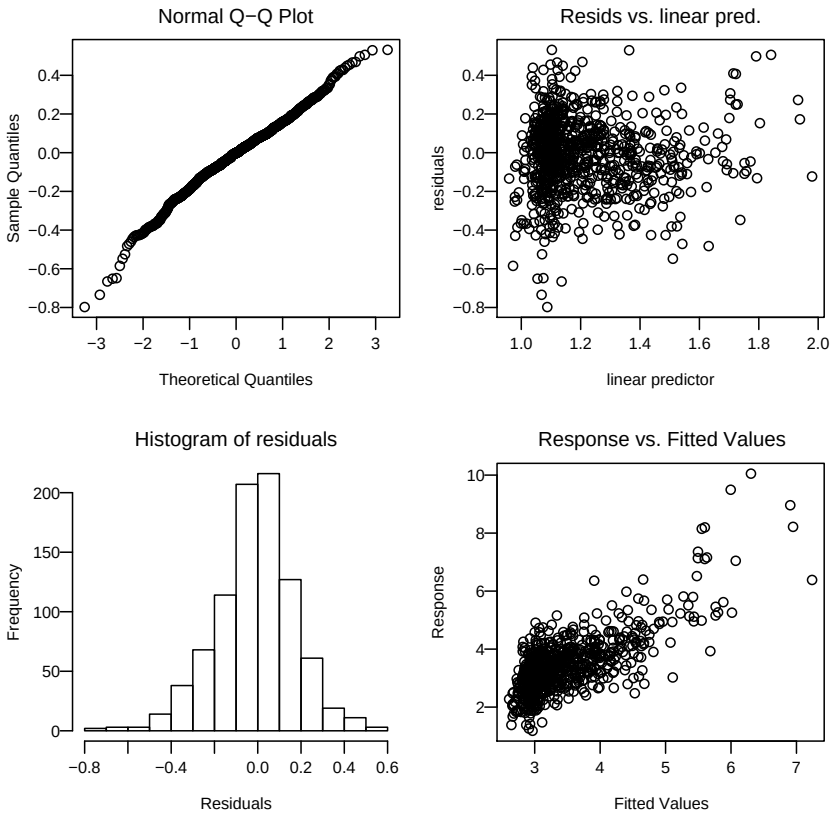

Figure 5.22: Diagnostic plots for the krill swarm roughness (R) generalized addictive model. The response vs. linear predictor plot suggests that the model is over predicting low values of R and under predicting high values.

A2: Calculation of krill biomass within the multibeam survey area

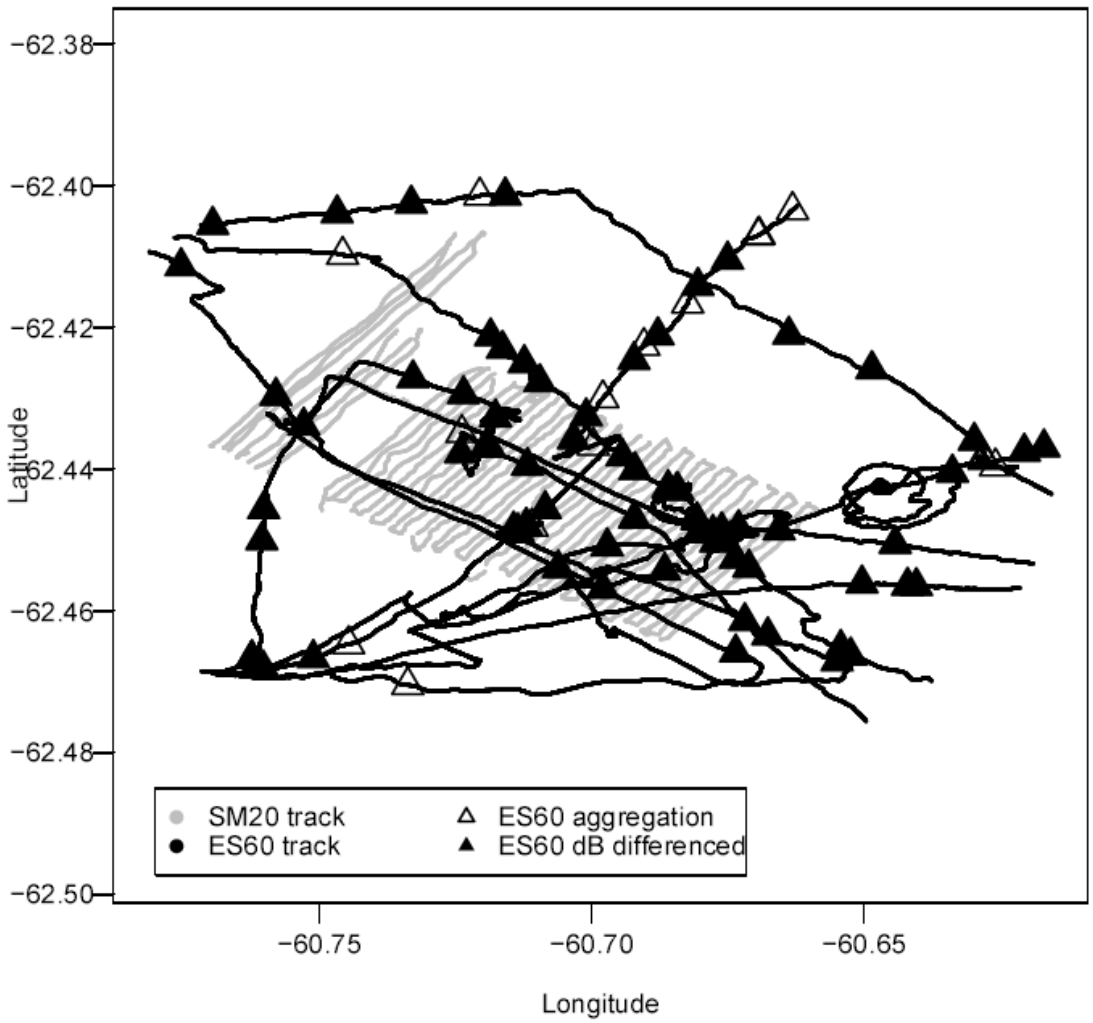

Figure 5.23: General location diagram showing the track lines of ES60 single beam echosounder (38 and 200 kHz) equipped *R/V Ernest* track line and the SM20 equipped (200 kHz) *R/V Roald*. Krill swarms detected are shown by the ES60 are shown as triangles. Swarms retained inside the dB difference window given as solid triangles

Chapter 6

Two-dimensional distance sampling of multi-beam echosounder detected krill swarms

6.1 Introduction

Krill are a key component in the Antarctic food web (Atkinson et al., 2001), which is illustrated by the classical short phytoplankton-krill-whale food chain (Siegel, 2000). Monitoring of the Antarctic krill (*Euphausia superba*) population is vital because of its role in the Antarctic ecosystem (Boyd and Murphy, 2001; Reid et al., 2005). The breeding success of land-based air-breathing marine predators has been shown to be dependent on krill availability (Brierley et al., 1999b; Mori and Boyd, 2004), and variation in krill population can influence the breeding of several predator populations over large spatial scales (Brierley et al., 1999a). Furthermore there is considerable potential overlap between krill predators and krill fisheries (Murphy et al., 1997; Reid et al., 2004) which requires careful management (Agnew, 1997). Monitoring of the Antarctic krill population is partially achieved using underwater acoustics, a remote-sensing technique that covers large survey areas and can provide krill density estimates (Hewitt and Demer, 2000).

Of particular importance to this investigation is the aggregative behaviour of krill: high density swarms are often detected acoustically and these swarms have a wide range of morphological characteristics, and exhibit a large range of densities, from 0.1 to 100,000 krill/m^2 (Hamner and Hamner, 2000). Determining the abundance, density and characteristics of krill swarms is important because: (i) an understanding of krill aggregation patterns will improve survey design, particularly, determining the required line transect spacing for mapping krill distribution (*cf* Hewitt and Demer 2000); (ii) the vertical distribution of krill is important for determining the accessibility of krill to land-based predators (Boyd et al., 1994), and for determining sampling bias in conventional acoustic surveys

of krill (Demer and Hewitt, 1995); and (iii) it will help determine links between swarms and physical oceanography (Barange et al., 1993; Cresswell et al., 2007).

6.1.1 Acoustic surveys

Acoustic surveys of krill are typically carried out from a research vessel following a line transect survey design, to estimate mean areal krill density ($\hat{\rho}$, see Hewitt and Demer 1991). Conventionally krill acoustic surveys use several frequencies of hull-mounted single- or split-beam transducers, oriented vertically downwards, that sample volume backscattering strength (S_v) at discrete intervals through the water column (Simmonds and MacLennan, 2005). When combined with a distribution of krill lengths obtained from net samples, measurements of S_v observed using a calibrated echosounder can be scaled to estimate krill density (see Demer and Hewitt 1995 for a description of this scaling process). Whilst useful for obtaining $\hat{p}$ single- or split-beam echsounders (SBE) are of limited use for observing krill swarms. The narrow beam width of SBEs, typically 7^o, effectively only sample a slice along the transect line through a krill swarm. This is because SBE S_v observations are only made in one-dimension (1-D), with each S_v observation having an associated time or range (r).

Multibeam echsounders (MBE) offer several advantages over SBEs, particularly if swarm shape is considered to be important. For example, with each ping (a transmit and receive cycle) the MBE used in this investigation sampled a 120^o swath width, allowing entire krill swarms to be acoustically sampled, with observations being made in two-dimensions (2-D). Each MBE S_v sample is associated with a detection angle (θ) was well as a time or range. The MBE sampling characteristics have enabled researchers to characterise aggregations, estimate the number of aggregations in a sampled region (Gerlotto et al., 1999; Reid et al., 2000a), assess aggregation distribution (Melvin et al., 2002), and examine school dynamics (Paramoa et al., 2007). In this research the 2-D observations made by an MBE are used to within a 2-D distance sampling framework to estimate: (i) the probability density function (pdf) describing the vertical distribution of krill swarms $v(z)$, where z is swarm depth and (ii) the abundance of swarms ($\hat{N}$) to be estimated within a survey region.

6.1.2 Objectives

This chapter describes analyses undertaken to estimate a range detection function and density gradient for Antarctic krill swarms in the vicinity of Livingston Island, South Shetland Islands, through the application of 2-D distance sampling theory to MBE observations of swarms of krill in order to estimate krill swarm abundance ($\hat{N}$) and the variance

of this estimate ($Var[\hat{N}]$). To summerise the research in this chapter will:

1. Build on recent developments in two-dimensional distance sampling by Marques (2007) to obtain $\hat{N}$ of krill swarms within MBE survey area.

2. Extend the 2-D distance sampling theory to include variation in detectability with sighting angle (θ).

3. Obtain a non-parametric bootstrap estimate of the variance of swarm abundance ($Var[\hat{N}]$).

4. Test the goodness-of-fit of the model.

This research does not provide solutions to all the steps required to obtain biomass estimates from MBE observations, rather this research provides a framework for estimating krill swarm abundance ($\hat{N}$) and variance ($Var[\hat{N}]$) swarm relative biomass (b) and area relative biomass (B), but does not provide a solution for estimating krill lateral target strength, which is required before MBE observations can be scaled. Hence the swarm and area biomasses in this investigation are relative rather than absolute.

6.1.3 Distance sampling

Distance sampling is a technique used to estimate the number of animals, or groups of animals, N, in a survey region, of area A, when N cannot be directly counted, which is the case for most wild animal populations. In most surveys a smaller area, a, is sampled and a subset of n animals detected. If all animals are detected in the sampled area the total abundance of animals in the survey area can be estimated from $\hat{N} = An/a$. However perfect detectability rarely occurs, and ignoring a reduced detectability will yield a negatively biased $\hat{N}$. A widely used method to estimate the probability of detecting an within a sampled area $\hat{p}$ is distance sampling (Buckland et al., 2001). Once estimated, $\hat{p}$ is used to scale the number of detected animals n to give the estimator:

$$\hat{N} = \frac{An}{a\hat{p}} \tag{6.1}$$

Generally it is simple to estimate both a and A, but obtaining an unbiased $1/\hat{p}$ is critical to obtaining a unbiased $\hat{N}$. In conventional line and point transect distance sampling $\hat{p}$ is obtained by recording the distances, at which animals are seen (animal i, observed at range r_i). The distribution of these observed distances is used to estimate a range detection function, $g(r)$, which is the probability detecting an animal at range r from a line or point, where $0 \leq r \leq w$ and w is the truncation distance, beyond which

detections are ignored. $\hat{g}(r)$ can be used to estimate $\hat{p}$ as follows:

$$\hat{p} = \int_0^w g(r)\pi(r)dr, \quad 0 \leq r \leq w \tag{6.2}$$

where $\pi(r)$ is the distribution of ranges of animals available for detection (see Buckland et al. 2001 for background and derivation).

In this investigation each MBE ping is analogous to a point transect sample, covering a $2\pi/3$ (120^o) arc, with r being the range from the MBE head to the geometric centre of a swarm. An important assumption of conventional distance sampling is that animals are uniformly distributed in the vicinity of the observer, which is known as the uniformity assumption (Buckland et al., 2001). It is this assumption which determines $\pi(r)$ and allows calculation of $\hat{p}$ using 6.2.

Previous research into the vertical distribution of krill provides strong evidence of a non-uniform distribution with respect to depth (Demer and Hewitt, 1995; Cresswell et al., 2007). This is a violation of the distance sampling uniformity assumption since the MBE can't be placed at a random depth. The incorrect assumption of a uniform vertical distribution of krill swarms could lead to strong bias in $\hat{p}$ caused by a incorrect $\pi(r)$. Further because $\pi(r)$ and $g(r)$ are a product in Equation 6.2 both cannot be estimated from range data alone.

It is reasonable to assume a uniform horizontal distribution of krill within the survey area, with respect to the MBE sampling, because transects are placed randomly. Using the uniformity assumption the 2-D observations, r and angle from the centre of the MBE swath to a krill swarm (θ) from the MBE can be used to estimate both the range detection function, $g(r)$, and the krill vertical density gradient, $\pi(r, \theta)$. This estimation is carried out by maximum likelihood (ML) using a method similar to that developed by Marques (2007). Details are given in Section 6.1.3.

6.2 Materials and methods

6.2.1 Multi-beam observations

A 200 kHz SM20 (Simrad-Mesotech, Vancouver, Canada) MBE was used in this research. A single ping insonifies a 120^o swath perpendicular to the line transect, with a ping rate of every 1.5 to 3 s. With a research vessel speed of 5 to 7 knots, this gave an inter-ping along-transect distance of 3.5 to 10.5 m. Within each ping there were 128 beams, and each beam comprises of 250 S_v samples. In this investigation the MBE range was set at 200 m giving an acoustic sample at 0.8 m intervals along a beam, with 32,000 samples in each ping.

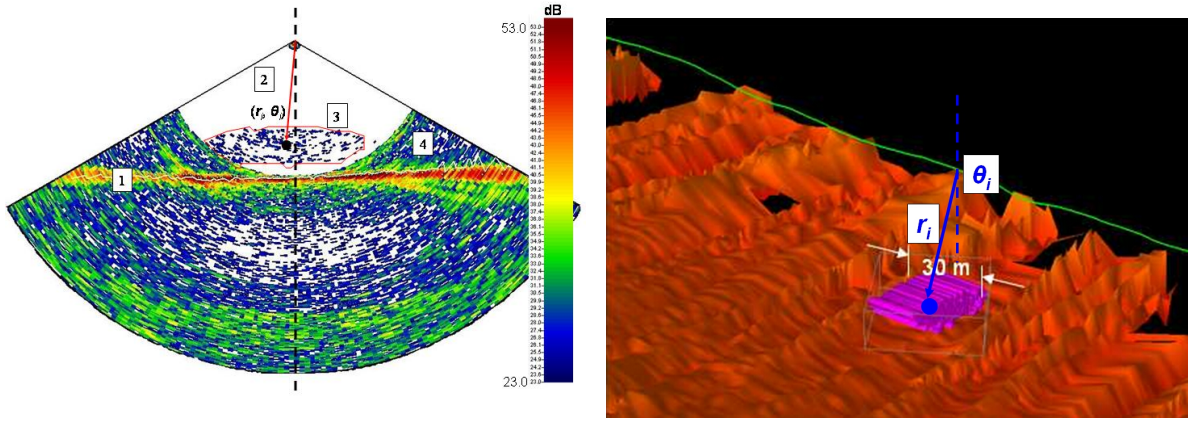

(a) Example multi-beam swath

(b) 3D krill swarm representation

Figure 6.1: Panel (a): Example multi-beam echosounder (MBE) swath (an across-transect acoustic slice), with higher intensity acoustic observations (S_v) shown in red. [1] MBE-detected seabed with cross transect bathymetry profile. [2] is the krill swarm observation volume, shown as the white area. [3] is an acoustic slice through a krill swarm, with the 3D detection algorithm shown as a red polygon line. The geometric krill swarm centre defined by (r_i, θ_i) [4] is the MBE side-lobe interference from the MBE sounder detected seabed. The black vertical dashed line is the centre or the axis of symmetry of the MBE swath. Panel (b) A 3D scene generated from combined MBE swaths using Echoview v3.5 (SonarData, Hobart, Tasmania). The research vessel track is shown as a green line, a krill swarm as a purple shape, and the 3D sounder detected seabed in orange.

Example multi-beam observations

Individual krill target strength (TS) models are used to scale S_v observations to determine the number of individual animals present in an S_v sample, or within a swarm. The example MBE swath in Figure 6.1(a) shows a single across-transect acoustic slice, or MBE ping, through the water column. Within this an acoustic cross section through a krill swarm is shown along with a graphical representation of the 3D detection algorithm boundary. Successive pings are combined to form a 3D representation of the krill swarm, which is comprised of multiple pings as shown in Figure 6.1(b). There are multiple S_v observations within the krill swarm that, with appropriate scaling i.e. a lateral target strength model, can be used to estimate krill biomass.

Data preparation

Only krill swarms that were detected while the vessel was on transect within the 41 line transects were included in the analysis. This is because the 3D detection algorithm (Echoview v3.5, Hobart, Tasmania) used to extract krill swarms from the MBE observation is only valid when the research vessel moves in a straight line, at a constant speed. The 3D detection algorithm parameters were selected from the sensitivity analysis described in the previous chapter (minimum longest, middle and shortest dimension all set to 5 m, the processing threshold was 24 dB (uncalibrated)). After krill swarm boundaries were determined krill swarm descriptive metrics (Table 6.1) were calculated and exported from Echoview.

Metric name	Abbreviation	units	description
geometric centre position	(ϑ, λ)	rad	Krill swarm geometric centre latitude and longitude.
geometric centre depth	z	m	Depth at the geometric centre of the krill swarm.
cross track distance	x	m	Perpendicular distance from MBE head to krill swarm geometric centre.
radial distance	r	m	Radial distance from MBE head to krill swarm geometric centre.
swarm angle	θ	radians	Angle from MBE swath centre to chord from MBE head to krill swarm geometric centre.
volume	Vol	m^3	Swarm volume.
mean S_v	S_{vmean}	dB re m^2/m^3	Krill swarm mean volume backscatter.
seabed depth	z_{sb}	m	Seabed depth under the krill swarm geometric centre.

Table 6.1: Description of multi-beam echosounder (MBE) detected krill swarm metrics used in this analysis. Krill swarm position can been defined by any two of z, r, x or θ.

Data manipulation

In conventional line transect distance sampling observations are conceptually folded along the expected axis of symmetry, which is the line transect direction (y-axis). In the case of 2D distance sampling the observations, in this instance Antarctic krill swarms, the observations are collapsed in the y-axis direction and folded across the axis of symmetry, the centre of the MBE swath, or a vertical line below the centre of the MBE (Figure 6.1a).

6.2.2 Model definitions

The models are defined in three stages, firstly the probability density function (*pdf*) of the availability of krill swarms within the survey site that can be detected by the MBE is

defined. Secondly the filter through which this underlying *pdf* of krill swarm availability is observed using the MBE. The filter is known as the detectability of krill swarms. Finally the modified 2-D distance sampling function as derived by Marques (2007) is given.

Krill swarm availability

The *pdf* of krill swarm centre coordinates, their availability, is dependent on the horizontal, $h(x)$, and vertical, $v(z)$, distributions of distances to the geometric centre of krill swarms an is defined by:

$$\pi(x, z) = h(x)v(z) \tag{6.3}$$

This assumes that the horizontal and vertical krill density distances are independent. Also, $h(x)$ is assumed to be uniform giving:

$$\pi(x, z) = \frac{1}{w\ sin(\pi/3)}v(z) \tag{6.4}$$

where $\pi/3$ is half the swath width (Figure 6.2). Equation 6.4 also assumes a constant seabed depth, although seabed depth throughout the survey region varied from 46 to 120 m. This effectively varied the survey effort with respect to depth: krill swarms cannot occupy depths greater the the seabed depth and not considering this attenuation effect may give a biased estimate of the krill density gradient. For example, consider a survey site that has a uniform distribution of krill with respect to depth, the site has two depths that occur equally across the site, 50 and 100 m. In this instance using the observed vertical distribution of krill (z) to estimate the krill *pdf*, $v^*(z)$, will lead to a depth gradient that estimates double the abundance of krill in the upper 50 m of the water column, which is biased. To correct for this bias the attenuation effect, $a(z)$, was estimated, allowing an estimate of the true krill density gradient unbiased by seabed depth, $v(z)$.

$$v^*(z) \propto \hat{a}(z)v(z) \tag{6.5}$$

The attenuation effect was estimated by fitting a logistic function to the proportion of depths (z) available over the survey area. The study site depths were measured using the mean observed seabed depth from the three centre beams of the SM20 MBE within 100 m line transect lengths. The seabed attenuation effect was incorporated into the krill swarm location *pdf* (equation 6.4), giving:

$$\pi(x, z) = \frac{1}{w\ sin(\pi/3)}v(z)a(z) \tag{6.6}$$

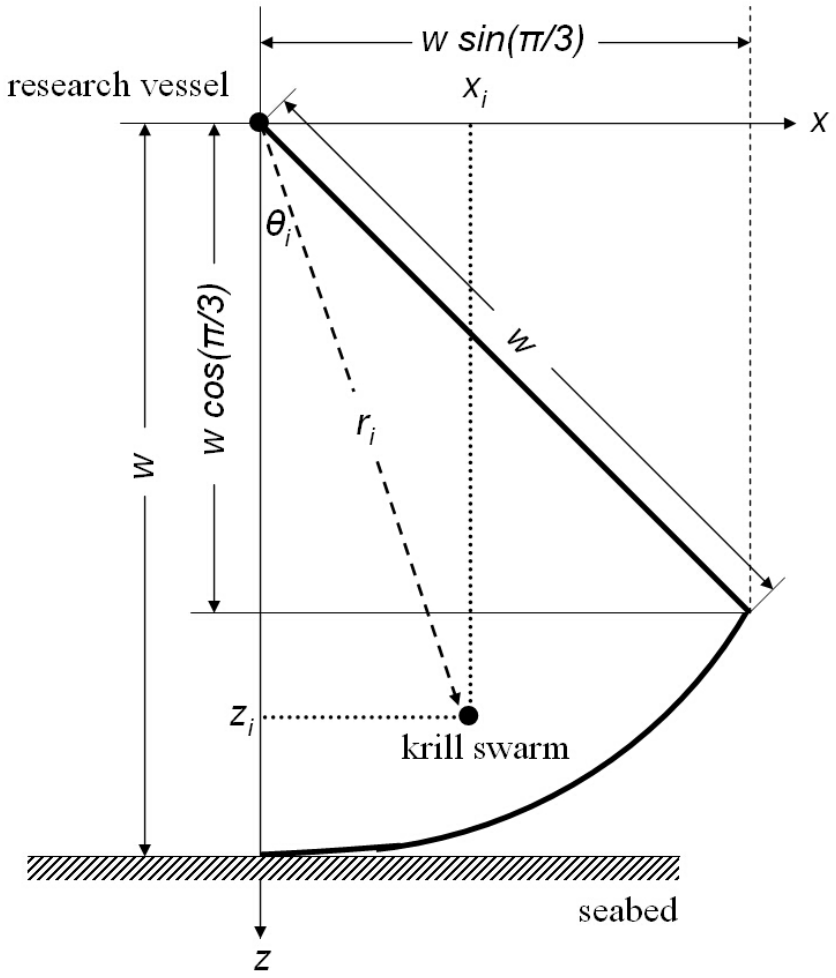

Figure 6.2: 2D swath geometry shown in the cross-track distance (x) and depth (z) dimensions, showing the maximum swath width $z = w\cos(\pi/3)$, where w is the seabed depth. Swarm i is located at $r_i = \sqrt{x_i^2 + z_i^2}$ and $\theta_i = atan(x_i/z_i)$. The thick line denotes the external swath boundary. The MBE swath has been folded about its axis of symmetry (a vertical line at the centre of the swath).

Krill swarm detectability

The detectability of krill swarms was determined using two independent detection functions. The first is the range detection function $g(r)$, where r is the radial distance from the MBE head to the krill swarm geometric centre. The second detection function is the angular detection function, $p(\theta)$, where θ is the angle from the centre of the MBE swath. These functions act as a filter on the available krill swarms (equation 6.6), consequently the krill location *pdf* cannot be observed directly. The range detection function was assumed to be half normal:

$$g(r \mid \sigma_d) = \frac{1}{\sqrt{(2\pi)\sigma_d^2}} e^{\left\{\frac{-r^2}{2\sigma_d^2}\right\}} \tag{6.7}$$

where σ_d is the scale parameter.

Krill swarms do not have equal detectability across the MBE swath. As with many MBE systems it is less likely to detected a *reference* swarm (a swarm with uniform characteristics) in the outer beams than in the centre beams whilst using the SM20 MBE. The variation in krill swarm detectability with θ was caused by changes in the across-swath MBE sensitivity, which is in turn caused by the beam pattern of the MBE transmitted acoustic pulse and the MBE head geometry (see Cochrane et al. 2003). The beam-by-beam sensitivity was estimated using observations of MBE beam-by-beam noise. Noise was assumed to be isotropic and estimated using mean volume backscatter (S_v) data that were collected 07/02/2007 in the Cape Shirreff study site. For this experiment the SM20 MBE was set to passive mode (no sound transmitted), with a 200 m observation range (r) and gain at $20log_{10}(r)$, which allowed the observation of MBE system noise. Krill were considered to have a lower detectability in beams with a higher S_v value, because a higher S_v meant there was more background acoustic noise over which to detect krill.

The beam-by-beam S_v observations were transformed to the linear domain ($s_v = 10^{\{S_v/10\}}$) and inverted, giving a relative measure of krill swarm detection probability, where it was less likely to detect krill swarms in the noisier beams. These data were rescaled so that the detection probability was one at the swath centre, $q(0) = 1$. Since the SM20 MBE does not have a nadir beam, minimum detectability of the three centre beams (Melvin et al., 2003) was used to rescale the inverted s_v observations. To accommodate the MBE observations in a distance sampling framework the sensitivity of the MBE was considered to be symmetrical about the swath centre, so only the angle from the swath centre was used (θ), rather than beam number was used. This approach meant that the data were folded, meaning the variation in across-swath sensitivity with respect to detection angle was $0 \leq \theta \leq \pi/3$. The across swath sensitivity was assumed to affect the detectability of a krill swarm and was modelled using a modified hazard rate detection

function with form:

$$q(\theta) = \gamma \left[1 - e^{-\left(\frac{\theta}{a}\right)^{-b}}\right] \tag{6.8}$$

The hazard rate model parameters were estimated using a non-linear least squares algorithm implemented in R v2.4.0 (Vienna, Austria). Given that the two detection functions $g(r)$ and $q(\theta)$ are independent the probability of observing a krill swarm, when it is present at (r, θ) is given by:

$$\begin{aligned} P(\text{observe} \mid r, \theta) &= \hat{g}(r)\hat{q}(\theta) \\ &= d(r, \theta) \end{aligned} \tag{6.9}$$

Where $d(r, \theta)$ is the combined range and angular detection function.

Likelihood: MBE observations

The *pdf* of the radial distance (r) and the sighting angle (θ) of detected krill swarms as derived by Marques (2007) is:

$$f(r, \theta) = \frac{\pi(r, \theta)g(r)}{\int_0^w \int_0^{\theta_{max}} \pi(r, \theta)g(r)d\theta dr} \tag{6.10}$$

where $\theta_{max} = \pi/3$, which is the limit of the MBE swath (see Figure 6.1(a))

Incorporating both the joint angular and range detection function $d(r, \theta)$ and the attenuation effect $a(z)$ gives a joint pdf for radial distances and sighting angles of detected swarms:

$$f(r, \theta) = \frac{\pi(r, \theta)d(r, \theta)a(r \sin \theta)}{\int_0^w \int_0^{\theta_{max}} \pi(r, \theta)d(r, \theta)a(r \sin \theta)d\theta dr} \tag{6.11}$$

This is the basis of a likelihood that can be maximised to estimate the unknown parameters of the vertical location *pdf* $\underline{\phi_1}$, and the range detection function $\underline{\phi_2}$, given the seabed attenuation detection function $a(r, \sin \theta)$:

$$L(\underline{\phi_1}, \underline{\phi_2} \mid r, \theta) = \prod_{i=1}^{n} \frac{\pi(r_i, \theta_i)d(r_i, \theta_i)a(r_i \sin \theta_i)}{\int_0^{r_{max}} \int_0^{\theta_{max}} \theta(r, \theta)d(r, \theta)a(r \sin \theta)d\theta dr} \tag{6.12}$$

Where the maximum observation range w is the seabed depth so $r_{max} = w$ and n is the number of detected krill swarms.

For the krill swarm analysis the vertical location *pdf* was considered to have either a beta form, normal, or a log-normal form each of which have two parameters to estimate

in $\underline{\phi_1}$. A uniform model, with no unknown parameters was also considered.

6.2.3 Probability of krill swarm presence with depth

As an extension to the current 2D distance sampling research the expectation of the vertical distribution of krill was calculated with respect to depth alone $v(z)$. This will allow visual inspection of the model fit, by plotting $v(z)$ and observed z of krill swarms, and also to permit a goodness of fit χ^2-test between $v(z)$ and observed z of krill swarms. The density $f(x,z)$ of observed krill swarm x and z is given by:

$$\begin{aligned} f(x,z) &= \frac{\hat{\pi}(x,z)\hat{d}\left(\sqrt{x^2+z^2}, \tan\frac{x}{z}\right)}{\int_0^w \int_0^{x_{max}} \hat{\pi}(x,z) \quad \hat{d}(\sqrt{x^2+z^2}, \tan\frac{x}{z}) \quad dxdz} \\ &= \frac{k_1(x,z)}{\int_0^w \int_0^{x_{max}} k_1(x,z) \quad dxdz} \\ &= \frac{k_1(x,z)}{\int_0^{x_{max}} k_2(z) \quad dz} \end{aligned} \tag{6.13}$$

where,

$$k_1(x,z) = \hat{\pi}(x,z)\hat{d}\left(\sqrt{x^2+z^2}, \tan\frac{x}{z}\right) \tag{6.14}$$

$\hat{\pi}(x,z)$ is the estimated *pdf* of swarm location and $\hat{d}$ is the estimated detection function.

Notice the probability of the MBE detecting a krill swarm is a function of the krill swarm depth, z, and cross track distance, x. However, to compare the model fit to the observed krill swarm depths the expectation of the proportion of krill with respect to depth alone is required. Given the swath geometry (Figure 6.2) it was necessary to calculate the *pdf* of observed of vertical distances between two sets of cross track distance limits. The first limit, $x_{max} = z\tan(\pi/3)$, occurs from the swath centre until the maximum swath width depth, $z \leq \sqrt{w^2 - z^2}$. The second limit from the maximum swath width to the seabed depth, $w\cos(\pi/3) < z \leq w$, giving a limit of $x_{max} = w\cos(\pi/3) < z \leq w$ hence:

$$x_{max}(z) = \begin{cases} z\tan\frac{\pi}{3} & : \quad z \leq w\cos(\pi/3) \\ \sqrt{w^2 - z^2} & : \quad w\cos(\pi/3) < z \leq w \end{cases} \tag{6.15}$$

The *pdf* of observed krill depth is:

$$v(z) = \int_0^{x_{max}(z)} f(x,z) \quad dx \tag{6.16}$$

where $x_{max}(z)$ is given by Equation 6.15.

6.2.4 Estimating krill swarm abundance

Krill swarm abundance in the covered area

In Section 6.3.5 it will be shown that the beta *pdf* gives the best model fit for describing the krill vertical distribution:

$$beta(\alpha, \beta, z) = \frac{\Gamma(\alpha+\beta)}{\Gamma(\alpha)\Gamma(\beta)} z^{\alpha-1}(1-z)^{\beta-1} \tag{6.17}$$

Consequently, the probability of detecting a krill swarm in the volume sampled, or covered by the MBE is estimated by:

$$\hat{p} = \frac{\int_{z=0}^{z=w}\int_{x=0}^{x=x_{max}} beta(\hat{\alpha},\hat{\beta},z)g(\sigma_d^2,\sqrt{z^2+x^2})q(atan(x/z))a(z) \quad dxdz}{\int_{z=0}^{z=w} c(z)beta(\hat{\alpha},\hat{\beta},z)a(z) \quad dz} \tag{6.18}$$

where, $x_{max}(z)$ is the maximum cross-track distance (x, in Figure 6.2) and is calculated using Equation 6.15. The model parameters $(\hat{\alpha}, \hat{\beta})$ are estimated using Equation 6.12. The swarm abundance in the covered region N_c was estimated by:

$$\hat{N_c} = \frac{n}{\hat{p}} \tag{6.19}$$

where n is the number of krill swarms observed using the MBE.

Krill swarm abundance in the survey area

Both krill swarm abundance $(\hat{N})$ and $(\mathrm{Var}[\hat{N}])$ were calculated. The krill swarm abundance in the survey area is calculated using:

$$\hat{N} = \frac{\hat{N_c}}{v} \times V \tag{6.20}$$

This equation scales the observed number of krill swarms (N_c) by the ratio of surveyed, or covered volume, v, by the survey area volume, V. The surveyed volume was calculated by:

$$v = \sum_{i=1}^{n_{seg}} z_{sb_i}\frac{1}{2}\pi[z_{sb_i}(1-cos(\theta))]^2 + z_{sb_i}^2(cos(\theta)sin(\theta)) \times l_i$$

where $\theta = \pi/3$, giving:

$$v = \frac{1}{8}z_{sb_i}^2 \sum_{i=1}^{n_{seg}} z_{sb_i}\pi + 2\sqrt{3}l_i \tag{6.21}$$

where n_{seg} is the total number of along transect segments used to calculate the seabed

attenuation effect (Equation 6.5) and z_{sb_i} is the water depth in segment i. In this investigation the along transect interval, l, was 100 m, so this procedure calculated the volume of water insonified in 100 m along-transect intervals. This volume is based on the swath geometry (Figure 6.2) and is simply the area of two right angled triangles and a semi circle. The total volume of the survey (V) was estimated using the volume of a water in each along transect interval, based the mean depth on a 100 m^2 grid overlaid on the survey area bathymetry.

Variance estimates of swarm abundance ($Var[\hat{N}]$) were estimated by non-parametric bootstrap, where the MBE krill swarm observations were resampled with replacement (1,000 replicates) at the transect (t) level ($n_t = 41$). The 95% confidence interval was estimated from the 2.5% and the 97.5% quantiles of the bootstrap $\hat{N}$ vector. For the purposes of this PhD thesis krill biomass was not estimated, but two candidate methods allowing relative biomass estimation are given in Section 6.4.4: further work.

6.2.5 Data simulator

Krill swarm MBE observations were simulated to examine the performance of the model estimators. Simulations were limited to the selected krill swarm vertical (depth) *pdf* (the beta distribution), and the half-normal range detection function, with the parameters determined by the MLE of Equation 6.12. The data simulator allowed the relative bias of the model to be assessed, using two techniques:

1. The data simulator was used to simulate a distribution of krill swarms of known covered area abundance (N_{sim}), which ranged from $N_{sim} = 200$ to 1800 in increments of 50. For each N_{sim} 120 simulations were performed and for each N_{sim} an estimate of covered area krill swarm abundance $\hat{N}_c$ was calculated.

2. The relative bias ($[N - \hat{N}]$/N) of the N_{sim} simulations was assessed. An unbiased model would, on average, return a relative bias = 0. Using relative bias standardises for the higher variance expected in the $\hat{N}$ distribution for larger N_{sim}.

6.3 Results

6.3.1 MBE swarm observations

The MBE head to swarm centre radial distances (r, Figure 6.4-a) is a function of swath width and the seabed depth of the MBE study site. The krill swarm detection angle shows two apparent clusters that occur in observation sectors 0.3 to 0.4 and 0.5 to 0.6 radians. These clusters are also seen in the across swath plot (Figure 6.4-c), the dashed line in

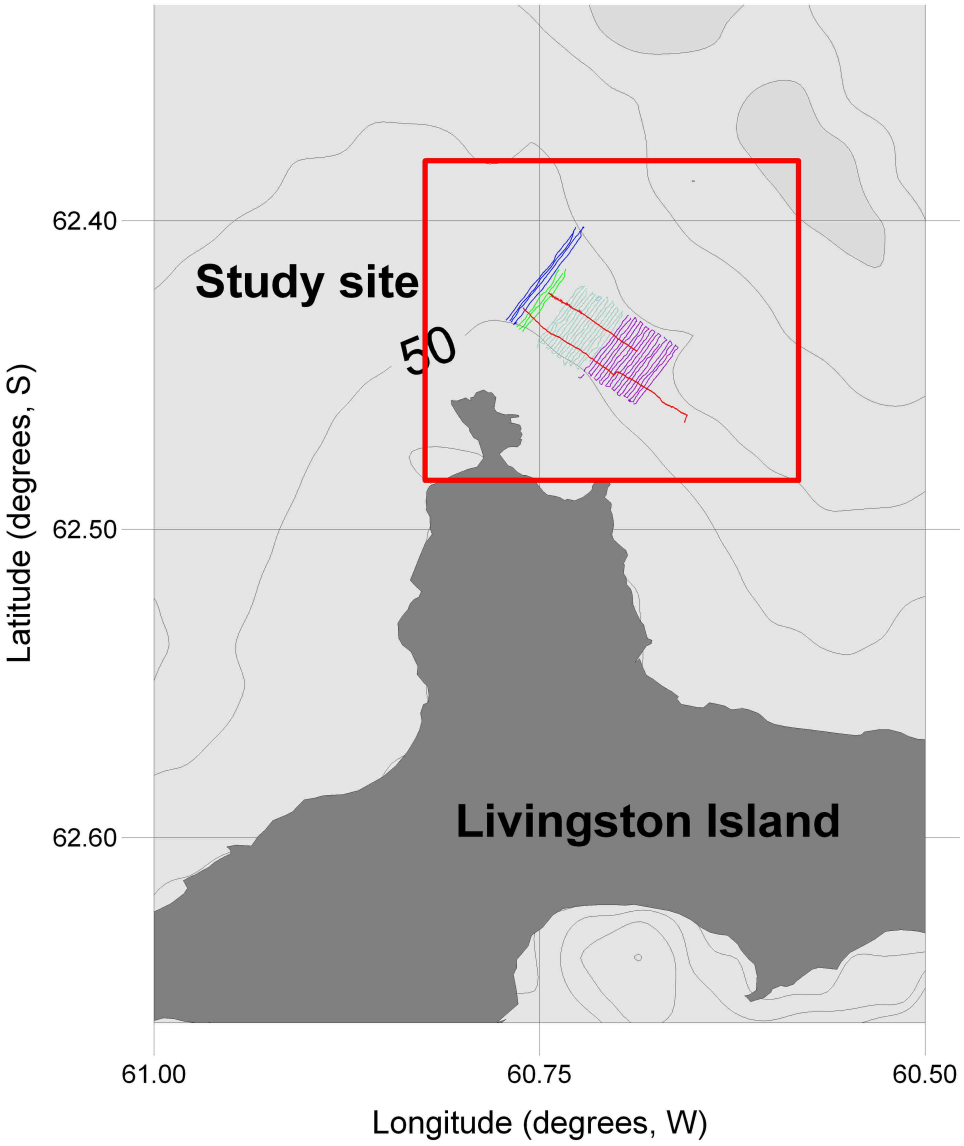

Figure 6.3: Multi-beam echosounder survey in the vicinity of Livingston Island, South Shetland Islands. Line transects are colour coded by day. Note transects 1 to 4 length is 3.5 km, transects 5 to 41 length are 2.5 km.

this plot shows the swath limit. The two swarm clusters within this plot extend from a depth of 20 to 90 m. The cause of these clusters are unclear. The vertical distribution of krill swarms (Figure 6.4-d) is a function of swath geometry, seabed depth and potentially a krill swarm vertical gradient.

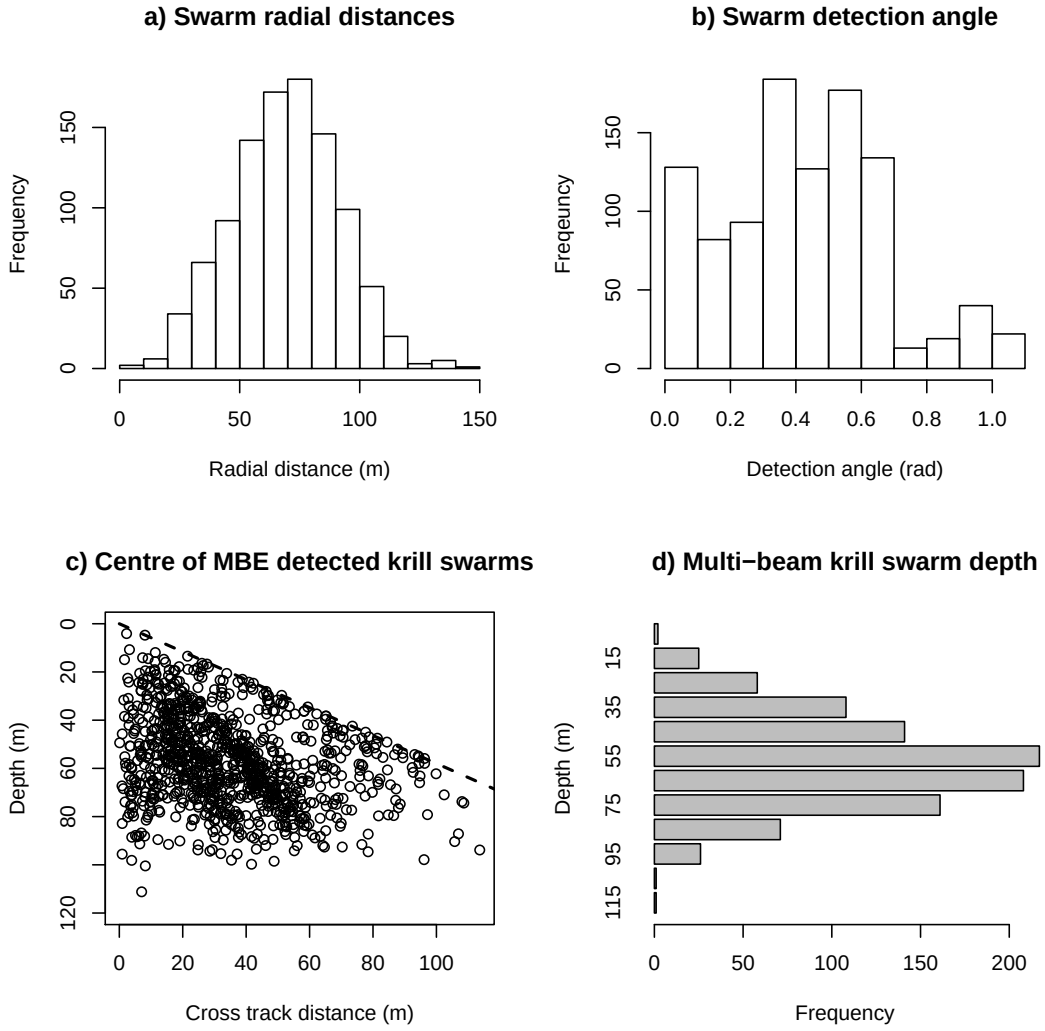

Figure 6.4: Krill swarms as detected by the SM20 MBE. All measurements are from the the MBE head to the geometric centre of a krill swarm. a) The radial distances to all detected krill swarms. b) The krill swarm detection angle after the transect had been folded about its centre. c) Two-dimensional plot of krill swarm centres after folding. d) As observed krill swarm depths.

Parameter	estimate	standard error (±)	p-value
γ	1.12	0.018	$<$ 2e-16
a	0.87	0.009	$<$ 2e-16
b	10.37	1.457	7.97e-11

Table 6.2: Non-linear least squares estimate of hazard rate model parameters for the across swath sensitivity, ($q(\theta)$).

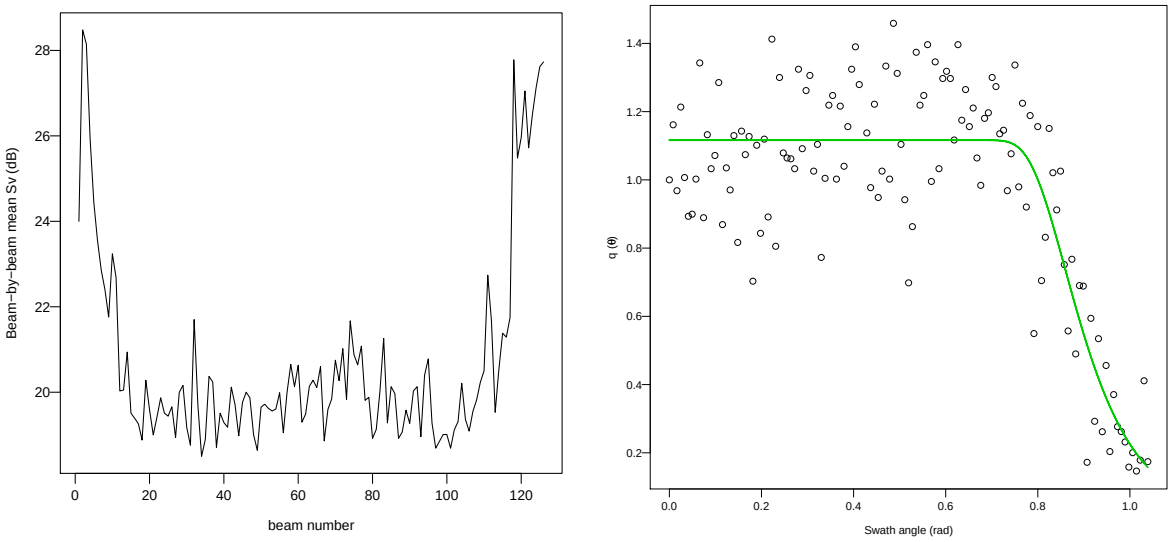

(a) Swath sensitivity

(b) Hazard rate model fit

Figure 6.5: Variation in beam-by-beam across sensitivity of the SM20 MBE used during the krill investigation. Panel (a) shows an increase in MBE noise (higher S_v) towards the edges of the swath. The large S_v values are due to the MBE being uncalibrated. Panel (b) shows the krill swarm detectability with respect to angle from the centre of the swath (θ). The hazard rate model fit is shown (grey line).

6.3.2 Angular detectability

Data collected during the SM20 calibration exercise conducted at Cape Shirreff showed increased noise on beams towards the edge of the MBE swath, Figure 6.5(a). The hazard rate model fitted well to the angular detectability (Table 6.2 and Figure 6.5(b)) and shows that the detectability of krill swarms caused by variation in across swath variability is uniform to 0.7 rad (or $\pm 40^o$ of swath centre).

Parameter	estimate	standard error (±)	p-value
m	-0.115	0.021	3.37e^{-08}
b	-5.920	0.018	$< 2\text{e}^{-16}$

Table 6.3: Non-linear least squares estimate of logistic curve parameters for the seabed attenuation ($a(z)$).

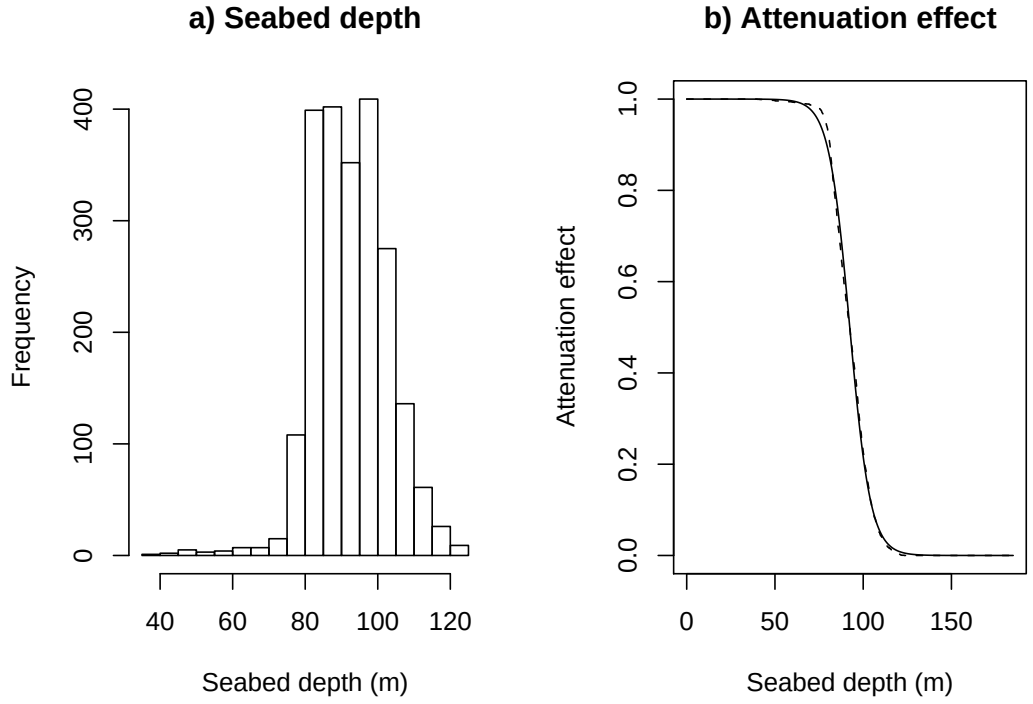

Figure 6.6: Estimated seabed attenuation. a) mean seabed depth for 100 m line transect depths in the MBE survey area b) The attenuation effect (proportion of MBE survey that sampled x-axis depths) shown as the dotted line, with the solid line a logistic curve fitted to the data.

6.3.3 Attenuation effect

The seabed attenuation effect, $a(z)$, was estimated for the study site, with a logistic curve (Equation 6.5) was fitted, using non-linear least squares (Table 6.3) to the empirical distribution of mean seabed depths (Figure 6.6), which show that seabed attenuation has little influence over model estimates of $\hat{N}_c$.

$$a(z) = \frac{1}{1 + exp(-(z - m)/b)} \tag{6.22}$$

Density gradient	parameter 1	parameter 2	$\sigma_r(m)$	log-likelihood	AIC	Δ AIC
Beta	$\alpha = 2.62$	$\beta = 2.41$	365.00	-7,701.66	15,409.32	-
Normal	mean = 54.31 m	sd = 23.39 m	132.1	-7,706.85	15,419.71	10.59
Log-normal	ln mean = 4.26	ln sd = 0.64	99.8	-7,731.50	15,469.00	59.68
Uniform	-	-	123.76	-7,779.80	15,561.59	152.27

Table 6.4: Selection of vertical distance functional form. With the exception of uniform, krill swarm vertical distance had two parameters. The ΔAIC is with respect to Beta distribution vertical distance model. In all cases the standard deviation (sd, σ_r) of the range detection function is estimated.

6.3.4 Range detection function

The σ_d parameter for the half-normal range detection function varies with each krill swarm vertical distance model used (Table 6.4), this may be due to confounding between the range detection function and vertical distance models. The σ_d parameter for the selected beta vertical distance model shows the highest range detectability of all the models (solid line, left-panel, Figure 6.10, page 170). The reduction of σ_d for the uniform vertical distance does not mean that this is the underlying range detection function, rather this is the range detection function confounded with the the krill vertical distance. Within the survey area the range detectability of krill swarms is high, considering the lowest σ_d = 99.76 m, calculated for the log-normal distribution, suggesting that at the truncation distance (w= 100 m) 60% of krill swarms being detected.

6.3.5 Vertical distance selection

The model fit of four vertical distance functional forms were assessed using four vertical distance models: (i) beta distribution; (ii) normal distribution; (iii) log-normal distribution; and (iv) uniform distribution. The Akiake's information criteria (AIC) for each vertical distance model fit was used for model selection, and a χ^2 test was used as a goodness-of-fit test (GOF). Using these AIC the beta vertical distance model was selected as the optimal model (Table 6.4).

The χ^2 goodness-of-fit test (GOF) was calculated for each of the model fits and again demonstrated that the beta vertical distance model gave the best fit, with all other vertical distance models being rejected as not representing the underlying 'true' krill swarm vertical distance distribution (Table 6.5). Consequently the selected beta vertical distance model was used in subsequent sections to estimate swarm abundance.

A graphical output of the candidate models, with respect to depth (Figure 6.7), is useful for providing a qualitative assessment of model fit, and this graphical output also shows the beta gradient is giving the best fit (Figure 6.7(a)).

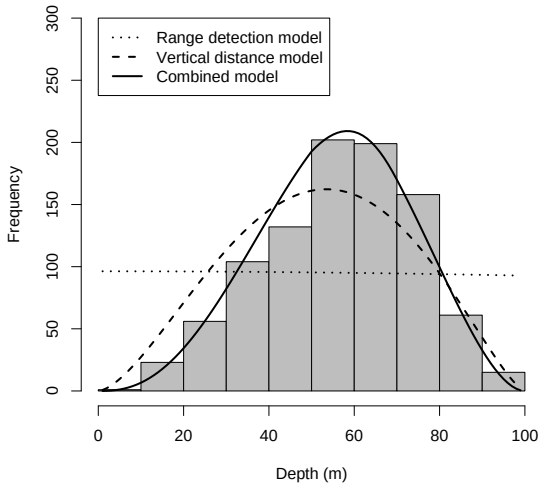

(a) Beta vertical distance ($\alpha = 2.61, \beta = 2.41$), σ_d=365.0 m

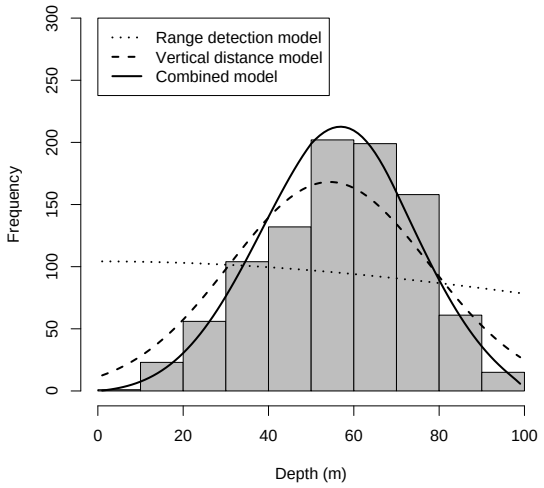

(b) Normal vertical distance ($\mu_g = 54.31, \sigma_g = 23.39m$), σ_d=132.1 m

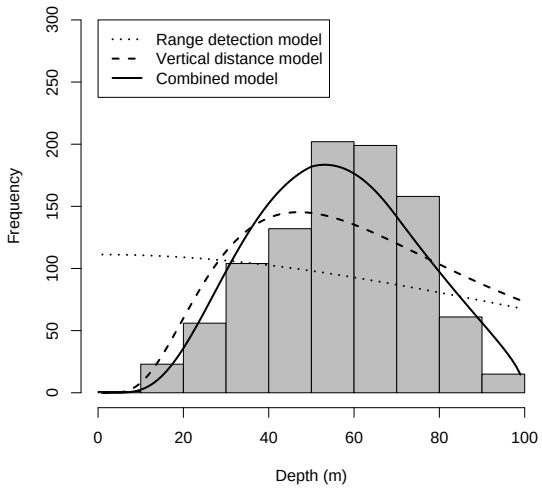

(c) Log normal vertical distance ($ln\ \mu_g = 4.26$, $ln\ \sigma_g = 0.64$), σ_d=99.8 m

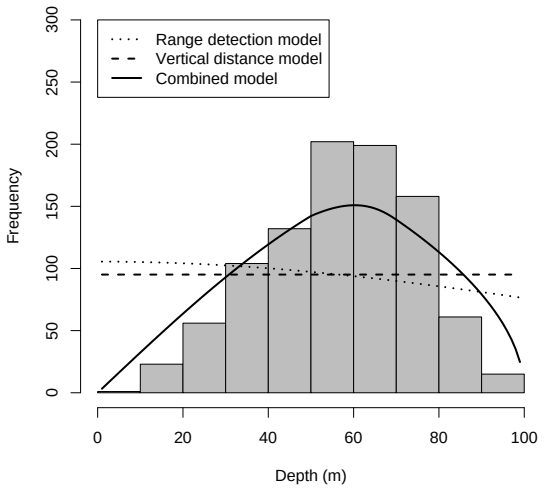

(d) Uniform vertical distance σ_d=123.8 m

Figure 6.7: Model fit with various vertical distance models. The combined density and range detection model, vertical distance model along and half-normal range detection model. All are shown separately all shown with respect to water column depth. A histogram of the frequency of geometric centre krill swarm depths is also shown in grey (10 m depth bins). The beta distribution (Panel a) gave the best model fit.

Density gradient	χ^2	p-value
Beta	16.048	0.065
Normal	23.041	0
Log-normal	57.853	0
Uniform	123.678	0

Table 6.5: The χ^2 goodness-of-fit (GOF) test for each vertical distance model (H_0: krill swarms have a vertical distance used in the model; H_1: krill swarms do not have a vertical distance used in the model). Based on this GOF test the beta vertical distance model was the only model that fitted the underlying krill density adequately.

Using the inverse of the hessian matrix, the covariance matrix, the precision with which the parameter estimates for the krill vertical distance model and the range detection model was estimated to be: $CV_{\hat{\alpha}} = 18.70$ %; $CV_{\hat{\beta}} = 14.75$ % and $CV_{\widehat{\sigma_d}}$=15.90 %.

6.3.6 Krill swarm abundance

Krill swarm abundance estimation took place in three steps: (i) the probability of detecting a krill swarm in the insonified region was estimated ($\hat{p}$); (ii) the number of krill swarms in the insonified (covered) region within the survey was estimated ($\hat{N}_c$): and (iii) the number of krill swarms in the survey area wass estimated ($\hat{N}$).

The $\hat{p}$ was calculated using Equation 6.18, which resulted in $\hat{p}$=0.721. Given the number of swarms detected in the covered region n=998, $\hat{N}_c$=1,384.7 (Equation 6.20). The variance of covered region abundance ($Var[\hat{N}_c]$) was estimated by non-parametric bootstrap (Section 6.2.4).

The covered volume (v) was calculated by determining the volume of water insonified by the MBE in each 100 m along transect length (Equation 6.21). The total transect length, L, for the survey area (Figure 6.9) was 106.5 km, which gave 1,065 100 m line transect depth intervals with which to calculate the v = 461,259,582 m^3. Using a volume calculation (Surfer v8, Golden Software) for the survey area held V=1,686,071,886 m^3 of water, so the MBE covered 27.36 % of the water volume within the survey area.

The survey region krill swarm abundance was estimated from:

$$\begin{aligned}
\hat{N} &= \frac{\hat{N}_c}{v} \times V \\
\hat{N} &= \frac{1,384.7}{461,259,582} \times 1,686,071,886 \\
\hat{N} &= 5,061.6
\end{aligned}$$

The variance of the krill swarm encounter rate (n/L), $\hat{p}$ and $\hat{N}$ were estimated by non-parametric bootstrap (1,000 replicates, Table 6.6). The variation in the swarm encounter rate is a useful measure of the spatial heterogeneity of swarms, which influences the precision of the model: the bootstrap estimate of $Var[\hat{N}]$ will not be less than encounter rate variance, since encounter rate variance is caused by krill biology.

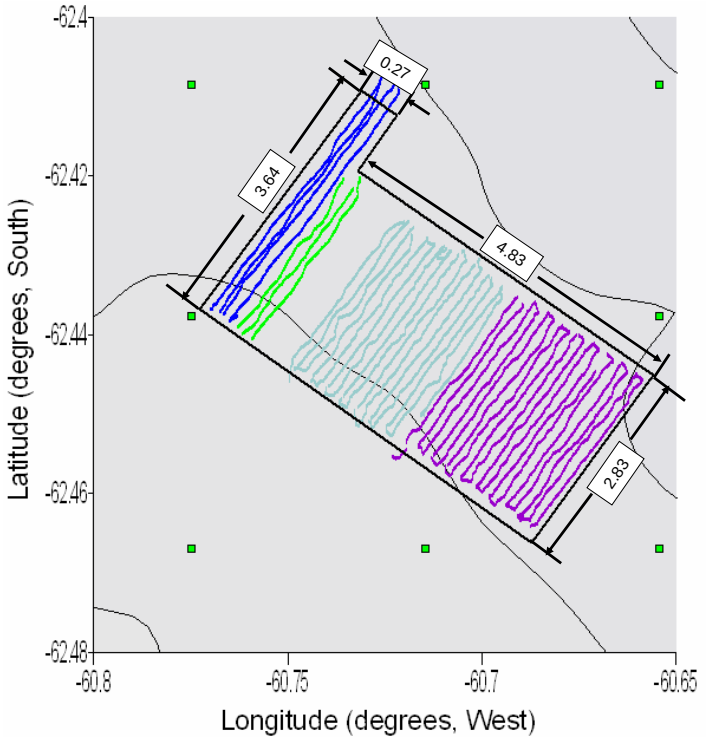

Figure 6.8: Plan view of the multibeam echosounder (MBE) line transect survey in the vicinity of Livingston Island, South Shetland Islands. The limits of the survey region are shown as a solid black line (dimensions in km). Within this region the MBE sampled 26.71% of the water volume. Note the line transects are colour coded by survey day.

encounter rate ($CV[n/L]$)	detection probability ($CV[\hat{p}]$)	abundance ($CV[\hat{N}]$)
0.348	0.205	0.352

Table 6.6: Coefficient of variation (CV) as determined by non-parametric bootstrap (n=1,000). Variation in encounter rate n/L contributes to the majority of the variation in the abundance estimate ($Var[\hat{N}]$).

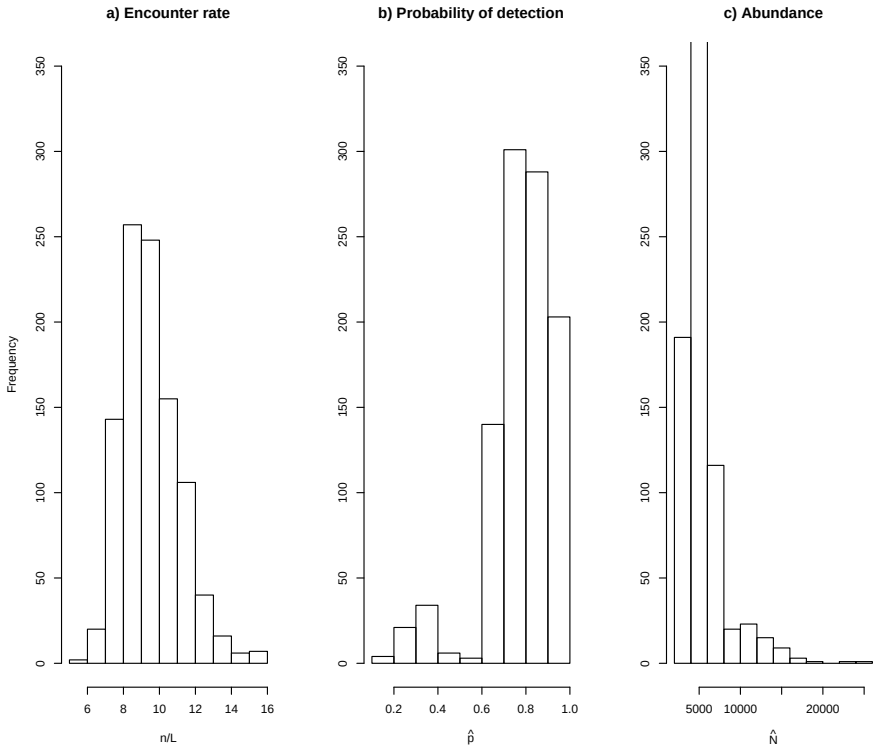

Figure 6.9: Bootstrap results for swarm encounter rate n/L, the detection probability $\hat{p}$ and the abundance of krill swarms within the survey area $\hat{N}$.

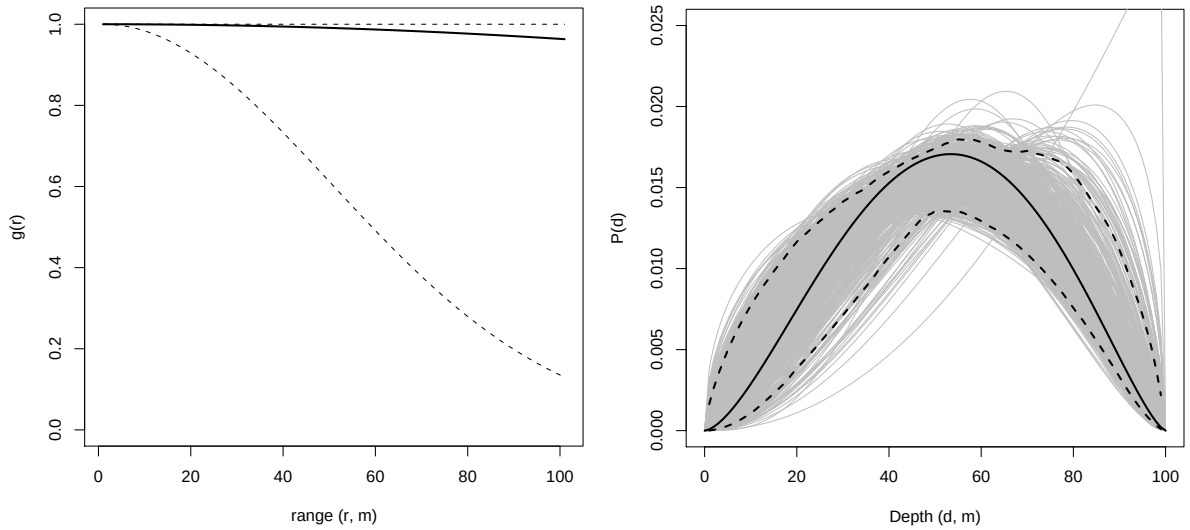

(a) Half normal range detection function

(b) Beta swarm vertical distance

Figure 6.10: Model estimates of swarm range detection function (upper panel) and swarm vertical distance model (lower panel), solid black line. Range detection function 95% confidence intervals (dashed black lines) determined by the 2.5% and 97.5% quantiles of the bootstrap $\hat{\sigma_r}$. The density gradient 95% confidence intervals were determined by the 1 m depth band 2.5% and 97.5% quantiles of each bootstrap realisation of the beta swarm density gradient (solid grey lines).

From the non-parametric bootstrap the 95% confidence intervals, determined from the 2.5% and 97.5% quantiles for $\hat{N}$ were 4,052 and 12,281. Using the $\hat{\sigma_r}$ determined during each bootstrap the variation in the shape of half-normal range detection function curve was estimated, and the 95% confidence intervals calculated, using the $\hat{\sigma_r}$ 2.5% and 97.5% quantiles, Figure 6.10(a). This procedure was not used for plotting variation in the beta vertical distance shape because this distribution requires two parameter estimates, which are not independent, so to determine the confidence intervals in Figure (6.10(b)) the 2.5% and 97.5% quantiles, of the 1,000 realised beta distributions were determined at each 1 m depth band. These results showed that both the range detection function and the depth gradient exhibited large variation.

Additionally the variation in the model parameter estimates was investigated. This shows the sensitivity of the MLE framework to biologically plausible realisations of the MBE survey. The small differences between mean parameter values obtained by non-parametric bootstrap (Table 6.7) and the point estimates (Table 6.4) suggest that the bootstrap was unbiased and the low CVs demonstrate the MLE framework was robust across a range in biologically plausible surveys.

Parameter	mean	CV	95% confidence interval
$\hat{\alpha}$	2.31	0.156	1.69 to 3.04
$\hat{\beta}$	2.11	0.113	1.69 to 2.61
$\hat{\sigma_r}$	343.69	0.230	49.49 to 365.00

Table 6.7: Statistics of model parameter estimates determined by non-parametric bootstrap (n=1,000).

6.3.7 Model performance

Using the data simulator with parameters estimated for the krill swarm vertical distance distribution and range detection function (Table 6.4) resulted in two model performance tests: assessment of absolute model bias and relative model bias. Assessment of the absolute model bias provides strong evidence that the model was not biased based on a range of simulated krill swarm abundances (N_{sim}=200 to 1800, each N_{sim} group comprised of 120 simulations, Figure 6.11). Visual inspection of the assessment for absolute model bias (Figure 6.11) showed no obvious signs of bias. The increase in the variance of $\hat{N_{sim}}$ with increasing N_{sim} is also excepted, but this is accounted for the assessment of relative bias (Figure 6.12). Again, the box plot of relative bias ($[N_{sim} - \hat{N_{sim}}]/N_{sim}$) provides no evidence of bias with respect to increasing N_{sim}.

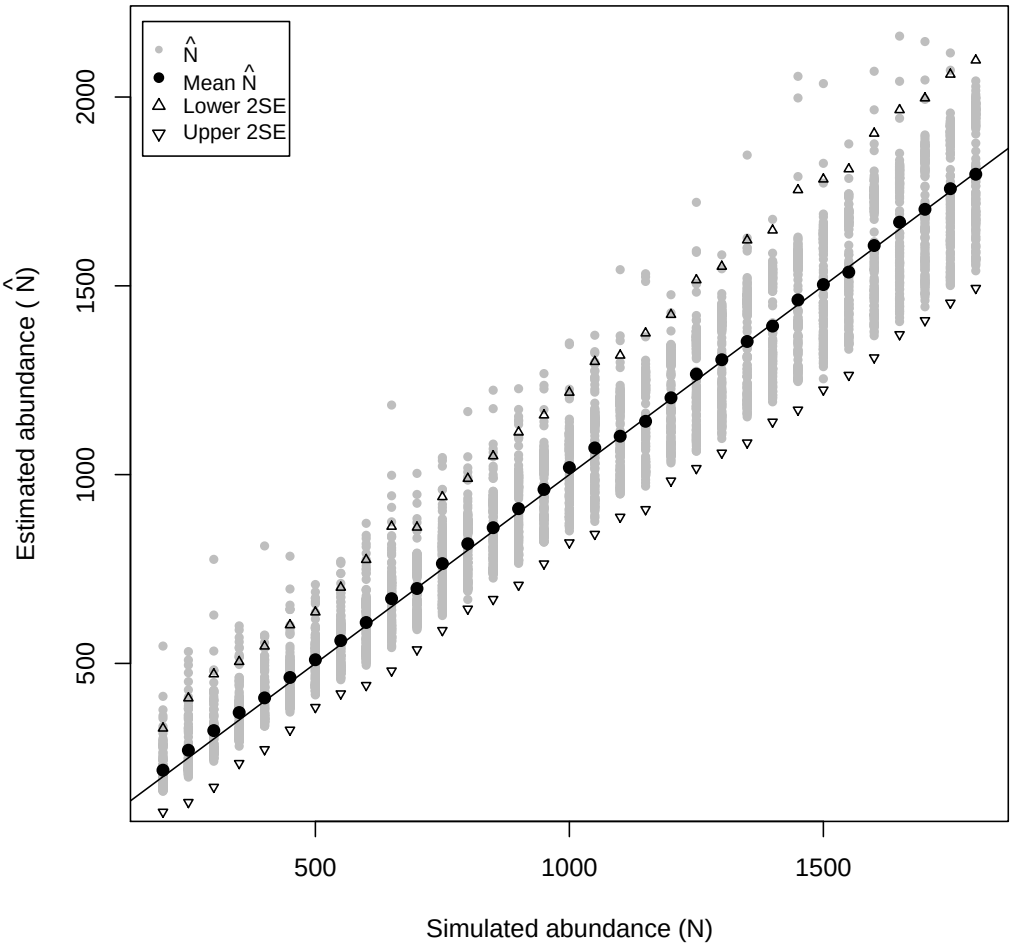

Figure 6.11: Assessment of model performance using simulated data. The underlying abundance of simulated krill swarms ($\hat{N_{sim}}$, see Section 6.2.5) is estimated by equation 6.20. $\hat{N}_{sim}$ was determined for a range of N_{sim} from N_{sim}=200 to 1800 in increments of N_{sim}=50, giving 33 groups of N_{sim} (x-axis). Each N_{sim} group contained $\hat{N}_{sim}$ (solid grey circles).

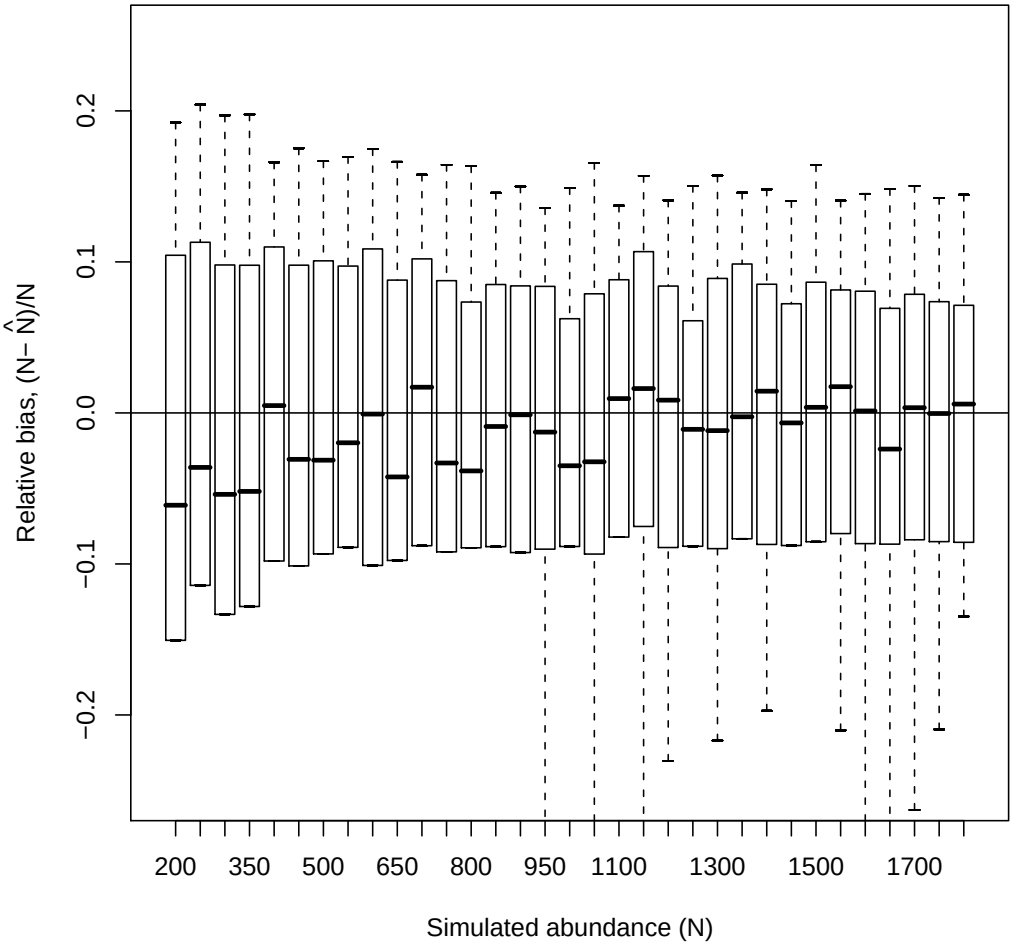

Figure 6.12: Assessment of model bias using simulated data. Boxplot of the relative bias ($[N_{sim} - \hat{N}]/N_{sim}$) for each of the N_{sim} groups. This relative bias corrects for increasing variance with N, and again shows that the model is unbiased for the N_{sim} considered here.

6.4 Discussion

This research has developed the 2-D distance sampling theory derived by Marques (2007) through: (i) incorporating angular detectability into the model and (ii) modelling the vertical distance distribution with respect to depth given the pre-sampled region and developing GOF test for the vertical distribution of krill. Whilst there is still some development required, the technique presented here provides a useful basis for biomass assessments once a formal lateral krill target strength model is devised.

6.4.1 Model components

The model components considered here are those specific to the model extensions undertaken during this research, see Marques (2007) and Marques et al. (2007) for a complete description of the maximum likelihood framework.

Range detection function

There is considerable variation in the range detection function between models (Table 6.4. The half normal range detection function assumes a loss of krill swarm detectability with range, but this distribution has considerable flexibility and only assumes certain detectability at $r = 0$. It is a reasonable functional form to model acoustic transmission loss with spherical spreading, $20 \times log_{10}(r)$, and only requires one parameter to be estimated (σ_r, Table 6.4). Across all models the estimates of σ_r suggest that within the depth of water encountered in the survey site there is little loss of detectability of krill swarms with range. This is as expected because it is whole krill swarms that are being detected, not individual krill. Further, we are only detecting high-density swarms because the 3D detection algorithm employed in the previous chapter is set to detect high density krill swarms.

Angular detection function

Cochrane et al. (2003) demonstrated that there is reduced acoustic detectability with increased beam angle (θ) whilst using the SM2000 MBE. Melvin et al. (2003) who used a SM2000 MBE and single-beam echosounder to monitor Atlantic herring within a weir, also found a reduction in acoustic detectability with increasing θ. Despite the SM2000 MBE system used by (Cochrane et al., 2003) and (Melvin et al., 2003) having a swath width of 180^o, rather than 120^o as used in this investigation, it is fair to assume that the pattern of reduced acoustic detectability with respect to θ will be similar using the SM20 MBE system with a 120^o swath width. Consequently the beam-by-beam $\overline{S_v}$ collected during the

passive data-logging exercise were used to estimate the reduction in acoustic detectability with respect to θ ($q(\theta)$). Another assumption was made for the purposes of estimating $q(\theta)$: the increase in $\overline{S_v}$ is inversely proportional to detectability. Consequently, this angular detection model allows the estimation of the reduction in acoustic detectability of swarms with detection angle.

For the purposes of implementing this MLE framework, θ, was calculated from the centre of the MBE swath (Figure 6.2) to the geometric centre of a krill swarm. However, it is possible that large krill swarm will be insonified by many beams in the MBE swath, so a single measure of angular detectability per krill swarm, may not be representative of the angular detectability of an entire swarm, spanning multiple beams. However, examination of the hazard-rate model fit for angular detectability (Figure 6.5(b)) showed that for swarms spanning up to θ=40^o there was constant, full detectability.

6.4.2 Model selection

The estimation of the krill vertical distance is an important component of the model. Investigations into the spatial distribution of krill at the South Shetland Islands, have shown that krill undertake diel vertical migration (DVM, see Demer and Hewitt 1995) that can significantly bias biomass estimates for surveys conducted during day and night. To the west of the Antarctic Peninsula seasonal variation in krill biomass has been shown, with a krill biomass being located in deeper water in the winter, and shallower in the summer (Lascara et al., 1999). A krill vertical distribution gradient also occurs at other locations. For example, around South Georgia krill have been shown to undertake DVM that varies with location: on, at, or off continental shelf (Cresswell et al., 2007) and there is significant variation in the observed vertical krill density distribution (see Section 4.3.2, Chapter 4). Consequently, it would generally be biologically unrealistic to assume a uniform krill swarm vertical distribution, but given the high variation in krill vertical distribution it would be unrealistic to pre-specify the depth distribution model. Given that the results of the Cresswell et al. (2007) study suggest that the vertical distribution of krill varies with location then it may be useful to stratify surveys based on the criteria of: on, at, or off continental shelf. These criteria however, may be subject to seasonal and geographic variation.

Model selection was conducted using AIC, the results of which showed that the beta vertical distance model and was better (between model $\Delta AIC > 6$) than the alternative models considered (Table 6.4). Furthermore, the χ^2 GOF test supported the hypothesis that the vertical distribution has a beta distribution form (Table 6.5).

The beta distribution is more flexible than the other distributions considered here. It can accommodate unimodal peaks in vertical krill swarm distributions that occur at any

depth, and can also model a uniform distribution (α=1; β=1). It is recommended that the beta distribution is included as a candidate distribution in any future modelling of krill swarm depth distribution.

6.4.3 Model performance

The largest component of the $CV[\hat{N}]$ came from encounter rate (n/L), which is due to the underlying krill biology, i.e. the high spatial heterogeneity in the distribution of swarms throughout the study site, and because this is a biological not a sampling process, nothing can be done to reduce the $CV[n/L]$.

The 95% confidence interval of the bootstrap estimates of $\hat{\sigma_d}$ show high variability, Figure 6.10(a), and within the 95% confidence interval there are $\hat{\sigma_d}$ values that are biologically and acoustically unrealistic, which suggests the range detection function and the density gradient functions are confounded. The 95% confidence intervals for the density gradient detection function are biologically plausible, and are narrower at $z \simeq 0$ m and $z \simeq 100$ m because there were few krill swarms observed close to the surface and the swarm data have been truncated at $z = 100$. The confounding of the density gradient and range detection functions may potentially be overcome using SBE observations (Section 6.4.5).

From the assessment of model performance (Section 6.3.7) the model appears to be unbiased, with all but one of the simulated krill swarm abundance groups ($N_{sim} = 350$) falling within $\bar{N} \pm 2S.E.$, which is as expected given the number of trials performed. Given that the non-parametric bootstrap took approximately 1.5 days of computer time it is unrealistic to obtain a non-parametric variance estimate for each of the $\hat{N}$ calculations carried out to assess $\hat{Var}[\hat{N}]$.

There were many potential simulations that could have been carried out for any vertical distance functional form, for any range of plausible functional form parameter values, it was decided to limit simulations to the beta vertical distance, since this *pdf* was the best AIC of those considered (Table 6.4). The parameter values obtained from MLE (Table 6.4) were used in the simulation model.

6.4.4 Biomass estimates

The estimation of krill biomass for the survey region requires considerable further work and several key assumptions to be made. The principle assumption and limitation is the calibration of the SM20 S_v observations. In the previous chapter a procedure was developed for mapping the empirical distribution function (EDF) of the SM20 MBE onto the EDF of a calibrated, conventional SBE. Currently, to calculate a biomass estimate

($\hat{B}$), it is necessary to assume that this EDF mapping technique gives a calibrated SM20 S_v observations with no transformation error. It is reasonable to suggest that this is valid for S_v observations for the three centre beams of the SM20, but this technique cannot extrapolate over other SM20 beams.

Mean volume backscatter scaling from centre beams

Where the SM20 centre beams insonify a krill swarm, a uniform krill density within the swarm could be assumed. SM20 S_v observations from these three centre beams could be rescaled using the EDF scaling technique described in the previous chapter. Assuming a constant within swarm density the scaled (calibrated) mean S_v from the three centre beams is used, with the swarm volume, to estimate swarm biomass. Using only S_v detections that are both within a krill swarm boundary and the centre beams keeps the EDF mapping within a valid range of S_v observations; S_v values derived from single target detections outside of the centre beams cannot be used because of S_v variation with respect to observation angle (θ). Mean volume backscatter (S_v) varies due to: (i) target strength (TS) model of krill with a lower amount of acoustic energy is reflected by a krill when it is ensonified laterally (Hewitt and Demer, 1996), and (ii) S_v is reduced with increasing MBE beam angle Figure 6.5(b).

A key limitation of this technique is that not all krill swarms are insonified by the MBE centre beams. This is a difficult limitation to overcome, but a simple method would be to use the geometric mean swarm S_v that have been rescaled using the ECDF mapping technique (Figure 5.6(a), page 107, Chapter 5). Depending on the inter-swarm variation in S_v this could introduce bias. Assuming a uniform internal swarm density the numerical abundance of krill in an individual swarm could be incorporated into the 2D distance sampling likelihood (Equation 6.12. This would allow the variation between the number of krill in a swarm (that is related to S_v) and θ could be established.

The assumption of a uniform interval swarm density may not be valid. Acoustic data collected during the First International BIOMASS Experiment (FIBEX) Barange et al. (1993) examined the internal structure of more than 3,000 krill swarms found in the Indian ocean (60 to 70^{o}S; 15 to 30^{o}E) detected using a Simrad EKS 120 kHz calibrated single-beam scientific echosounder. This research found that there was significant variation in the internal structure of krill swarms. However, this does not necessarily mean that there is variation in the internal krill swarm density in swarms detected this 2006 nearshore survey. Further, the uniform density assumption can be tested by taking a narrow, along transect acoustic slice, *e.g.* the 30 m along transect length in Figure 6.1(b), through a krill swarm, which is orthogonal to the MBE swath. If this slice has a uniform distribution of S_v observations then it likely that krill swarms do indeed have a uniform density in all

directions. The results of this model would give the variation in the S_v with θ, where the variation would be caused by the decreasing sensitivity of the MBE,Figure 6.5(b), and the variation in krill acoustic target strength (TS) with lateral angle, also θ. The resultant model would be species and MBE system specific.

The use of a krill lateral TS model (see Hewitt and Demer 1996) would enable the proportion of $S_v(\theta)$ due to TS to be estimated, thus leaving the variation $S_v(\theta)$ that caused by the reduction in MBE sensitivity with θ, allowing the validity of the angular detectability function, $q(\theta)$ Figure 6.5(b), to be assessed.

Krill density estimates

The estimate of the per unit volume density, $\hat{p}_v$, of a given krill swarm is calculated using standard acoustic processing techniques, see Demer and Hewitt (1995) for krill and more generally for aggregating pelagic organisms see Simmonds and MacLennan (2005). Both the empirical distribution, $\hat{\pi}_l$, of krill length (l) and swarm $S_{v_{mean}}$ are required. The biomass of an individual krill swarm is simply calculated from:

$$b_i = V_i \rho_i \tag{6.23}$$

where vol_i is the krill swarm volume. Buckland et al. (2001) showed that using the mean of group size is a robust way to estimate survey region abundance, so the mean swarm biomass in the survey region is calculated by:

$$\bar{b} = \sum_{i=1}^{n} b_i \frac{1}{n} \tag{6.24}$$

where, n is the number of krill swarms in the survey area. Mean swarm biomass is scaled to estimated the total biomass in the survey area:

$$\hat{B} = \frac{\hat{N}_c \times \bar{b}}{v} \times V \tag{6.25}$$

where, v is the volume insonified by the MBE, and V is the total survey area volume. With the $Var[\hat{B}]$ being estimated by non-parametric bootstrap (using transect as the sampling unit).

with the variance of krill survey region biomass ($Var[\hat{B}]$) is estimated using the delta method, as derived by Buckland et al. (2001):

distance sampling technique will be useful for correcting the acoustically weak jelly fish targets to obtain an abundance estimate.

6.4.5 Further work

The MBE used in this investigation had a 120^o swath width that was oriented so the centre of the swath pointed vertically downwards (Figures 6.1(a) and 6.2), which meant that shallow water was sampled less intensely than deeper water. Also this MBE head arrangement meant that due to the depth of the MBE head, and the acoustic nearfield (the upper 5 m of the water column) was not sampled at all. For future surveys we recommend that the MBE is inclined 30^o to the vertical so that the outer limit of the swath is coincident with the sea surface, which would allow the same across transect width of water column to be sampled and would limit the effect of the acoustic nearfield on cross track length insonified, *i.e.* all depths can be sampled equally.

There is additional source of information available to determine the distance distribution of krill swarms: those detected using a vertically downward looking SBE. If constant detectability is assumed for krill swarms detected by an SBE with respect to range, then trend in the number of krill swarms detected using a SBE is due to the vertical gradient of krill, which could be used in the MLE (Equation 6.12). During the krill survey another inflatable boat was deployed within the survey region that was equipped with an SBE. Given that these data were obtained from a different boat an additional assumption is required: krill behaviour is not influenced by boat i.e. the second SBE boat samples from the same vertical distribution of krill as the MBE boat. This seems a reasonable assumption to make since both boats were equipped with the same engine, were the same size, and were driven at similar speeds. The incorporation of SBE observations into the MLE would be useful for acoustic surveys generally since other research conducted with an MBE using often carried out from research vessels equipped with both an MBE and SBE (*e.g* Gerlotto et al. 2004).

Another advantage of incorporating SBE data with MBE data is species identification. In the case of Antarctic krill multi-frequency acoustics has been used to partition acoustic data into species-specific acoustic observations, Madureira et al. (1993) recommended the use of the difference between 38 and 120 kHz frequencies, (120-38 kHz), with a range of 2 to 12 dB, which was adopted by British Antarctic Survey (BAS, see Brierley et al. 1999b). However, this approach is not possible using a single-frequency (200 kHz) MBE system. Assessment of net samples collected from R/V during the 2006 nearshore survey showed that krill was the dominant scatterer in the nearshore area, thus partially validating our assumption that all pelagic aggregations detected by the MBE were krill. For future surveys we recommend that a MBE and multi-frequency SBE are installed on the same research vessel. Recently advances in MBE technology have allowed the introduction of broad-band fisheries MBE (Simrad ME70), which would enable acoustic targets to be identified using a dB difference technique, from MBE observations alone. However, this

MBE system is expensive and must be permanently installed on an ocean going research vessel. This means that the use of small MBE systems and conventional SBE will continue, and further development of the 2-D distance sampling technique is important.

6.4.6 Conclusion

This research has taken the initial steps to pelagic biomass estimation using a MBE. Using 2-D distance sampling theory parameters for a half-normal range detection function and a beta density gradient for krill swarms in the vicinity of Livingston Island, South Shetland Islands, were simultaneously estimated, thereby allowing point and variance estimates of swarm abundance to be determined ($\hat{N}$ = 5,061.6, 95% CI = 4,052 to 12,281). We believe 2-D distance sampling theory to be widely applicable to MBE surveys, but requires further work to include SBE data in the MLE to disentangle the range detection and vertical gradient functions. More work is also required on acoustic lateral TS models to allow unbiased scaling of acoustic data for off-centre S_v observations and the calculation of biomass.

Chapter 7

A spatially adaptive multidimensional smoother for biological applications: An example using Antarctic krill density estimation

Elements of research chapter were published as: Cox, M.J., MacKenzie, M.L., Watkins, J.L. and Brierley, A.S. (2006) The effect of missing acoustic observations (dropped pings) on mean area density estimates of Antarctic krill (*Euphausia superba*). ICES CM 2006/I:16.

7.1 Introduction

Antarctic krill (*Euphausia superba*) is a key stone species in the short Southern Ocean food chain which, at its most simple, can be described as comprising of three trophic levels; primary production; krill; and krill predators (Reid et al., 1999a; Atkinson et al., 2001). Krill is the primary prey item for many species of marine birds and mammals, notably the large populations of central place foragers located at South Georgia and the South Shetland Islands (Boyd and Murphy, 2001; Reid et al., 2004). The reproductive success of these species has been linked to krill availability (Croxall et al., 1988b; Murphy et al., 1998; Croxall et al., 1999; Boyd, 2002). Because of the vital ecosystem role krill plays, for the last 20 years it has been the subject of international long term monitoring programmes (see Hewitt and Demer 1994; Agnew 1997). Currently, several nations conduct annual surveys of krill, the results of which contribute to krill fisheries management models (Trathan et al., 2001; Hewitt et al., 2004).

Antarctic krill form aggregations and exhibit a spatially patchy distribution, both horizontally and vertically through the water column (Watkins, 2000; Watkins and Brierley,

2002). Aggregations vary in size from 20 m to larger than 20 km, and density, with diffuse aggregations, known as layers, having an internal density of 1 or 2 g/m^3 and higher density aggregations, or swarms, having internal densities of 100 g/m^3 to 1 kg/m^3 (Brierley et al., 1998; Watkins and Murray, 1998; Woodd-Walker et al., 2003). During research cruises conducted by British Antarctic Survey (BAS) at South Georgia (54^{o}S 35^{o}W) up to 20% of krill biomass has been observed in a single swarm (Brierley et al., 1997b). The large variation in the spatial structure and density of krill make spatial modelling problematic which is confounded by measurement error (Hewitt and Demer, 2000; Demer, 2004).

Recently, it has been suggested that management models be extended to limit the spatial overlap between krill predators and krill fisheries, since it is believed that many species of krill predator return to the same area to forage (Reid et al., 2004). Because these predators show fidelity to specific foraging sites and when rearing offspring are constrained in their foraging range this creates the potential for krill fisheries to have a disproportionately detrimental impact on krill predator populations: an identical biomass of krill caught by a fishery within or outside of the foraging range of a krill predators would have a different effect on the krill predator population (Murphy et al., 1997; Boyd et al., 2002). The need to assess the potential for competition between krill fisheries and predators has given rise to krill populations being assessed at the level of individual aggregations (Reid et al., 2004). Krill density, either at the scale of an individual aggregations or at the larger transect scale is often calculated from acoustic data that are generally observed from research ships, steaming line transect surveys, equipped with scientific echosounders (see Brierley and Watkins 1996 for Antarctic krill survey techniques, and more generally Simmonds and MacLennan 2005).

The use of scientific echosounders provides a non-evasive remote sensing technique that allows the observation of krill through the water column over a large area, often to a depth of 250 m. Typically, scientific echosounder transducers are mounted facing vertically downwards on the hull of a research vessel that carries out a line transect survey through the study site collecting acoustic observations of krill (*e.g.* Brierley et al. 1999b). These observations are then partitioned to identify those returns coming from krill which are scaled to determine krill density (Simmonds and MacLennan, 2005).

Acoustic analysis of krill can be broadly divided into two groups: (1) those that consider krill in arbitrary along transect intervals, known as elementary distance sample units (EDSU, Reid et al. 2000a), and are typically from 100 m to 1 nautical mile long and (2) those that assess krill at the individual krill aggregation, or swarm scale (Barange et al., 1993; Brierley et al., 1999b; Woodd-Walker et al., 2003). Historically, krill have been assessed in EDSUs because until relatively recently it has not been possible to objectively identify aggregations nor has it been required for all surveys (Reid et al.,

2000a). For example, large scale acoustic surveys, which are often used to estimate mean area biomass ($\hat{\rho}$), use EDSU. However, alternative ecosystem approaches use the shape of aggregations to predict the species composition and provide indicators of environmental variability (Paramoa et al., 2007).

A single data observation cycle from an echosounder is known as a ping and comprises of transmit and receive components. A pulse of sound, with known characteristics, is transmitted into the water column and returned, (or backscattered) sound is received at discrete intervals by the same transducer. This backscattered sound is proportional to the density of krill in the echosounder sampling volume. Thus, one ping is a vector containing backscattered acoustic energy from discrete intervals, standardised for sampling volume from a narrow cone in the water column directly under the research vessel. Vectors arising from sequential pings are combined in a matrix that is used for further analysis, that includes the identification of acoustic returns arising from krill and the scaling of these returns to determine krill density (Reid and Simmonds, 1993).

Krill are generally identified using a multi-frequency acoustic approach (for Antarctic krill see Madureira et al. 1993; Brierley et al. 1998; Watkins and Brierley 2002), in which two or more frequencies of sound are used to sample the water column. Since the amount of energy backscatttered by a krill aggregation is proportional to the acoustic frequency of the echosounder observing it and the length of the krill, these are used as arguments in theoretical models to predict the acoustic energy backscattered by krill (target strength models, *e.g.* Demer and Conti 2003, 2005). The results of these models are used to set the upper and lower bounds of the acoustic energy that can be expected to be returned, for each acoustic frequency by aggregations of krill within the study site. The difference in acoustic backscatter between frequencies is then calculated and used to separate the acoustic observations into those arising from krill and those from other scatterers. Conventionally, two frequencies 38 and 120 kHz have been used to observe the water column during krill surveys and the krill length frequency distribution within the survey site is estimated by net sampling (Brierley et al., 1998; Reiss et al., 2008).

Where the multi-frequency technique identifies an acoustic sample as being krill the sample from a single frequency, typically 120 kHz at that sample location, is used to calculate krill density. Target strength models are used to estimate the number of krill in the observation and length-wet mass models (*eg* Morris et al. 1988) are used to calculate the mass of krill in the samples. Krill density estimation can take place at a variety of spatial scales which is dependent on the purpose of the survey i.e from small-scale predator prey interactions to large-scale biomass estimates (Hewitt and Demer, 2000).

Acoustic surveys of krill are generally performed from research vessels and are often conducted in rough weather since there is considerable time and financial pressure on

ship operations. The quality of acoustic observations is influenced by weather conditions. As weather conditions deteriorate vessel motion increases, this in turn decreases the detectability of krill aggregations. Beyond a range of vessel motion, that is unique to the scientific echosounder, the detectability of krill will drop to zero. Zero detectability occurs when either the pulse of acoustic energy transmitted by an echosounder fails to propagate through the water column, or when reception of the acoustic energy backscattered by water column targets fails. The transmitted acoustic pulse may fail to propagate correctly when the water surrounding an echosounder transducer becomes aerated. Excessive vessel motion causes pings to be dropped and entire columns in the acoustic observation matrix will record the acoustic backscatter of krill as zero and are unrepresentative of krill in the the echosounder sampling volume.

In many cases, the issue of missing pings is ignored and missing pings are therefore assumed to contribute zero intensity (*e.g.* Brierley et al. 1997a) and thus transect krill density can be drastically underestimated when the number of missing pings is large. A more realistic approach estimates krill density for the missing pings using the mean of the non-missing pings. This approach is not ideal. For example, a threshold intensity is used to determine if surface intensities are krill and a block of missing pings located in a low intensity area may falsely indicate a krill swarm is present. Conversely, blocks of missing pings located within krill swarms may falsely ignore one or more krill swarms, or will split a single swarm into multiple swarms.

Krill intensity values are spatially correlated - values from adjacent pings tend to be more similar than values from distant pings. For this reason, krill intensities from nearby pings should be used to estimate the intensity of missing pings. A smoother-based method can use neighbouring pings to estimate those which are missing. However the extent of the smoothing should be determined locally. For instance, areas of water absent of krill only require a rigid flat surface, while areas with swarms will exhibit rapid changes in surface intensity and require a relatively flexible surface.

To make use of information on krill distribution surrounding a missing ping this research uses a smoother-based method that employs thin-plate regression splines (TPRS) with locally determined flexibility. This method permits surface flexibility to be targeted so that the smoothness permitted in each area of the surface is appropriate. This smoother based method uses the spatial structure of krill distribution to estimate the intensities of missing pings and the predictions from the fitted surface are used to reconstruct krill density within missing pings to allow more accurate quantification of krill density.

7.2 Methods

7.2.1 Thin-plate regression splines

Thin-plate regression splines (TPRS) are a two-dimensional smoothing technique, that have the same basis as the more commonly used thin-plate splines, but with different knot selection criteria. The basis matrix is made up of one row for each observations, and one column for each radial basis function. The radial basis functions are centred at knots. The selection of knot locations is an important part of the TPRS fitting procedure. The TPRS approach employed here uses locally-defined smoothing, as opposed to globally-defined smoothing, as used in most smoother based methods; the MGCV generalized additive model (GAM) technique is one example. Local-smoothing allows the TPRS to estimate areas of local complexity, so is applied here to model highly spatially variable acoustic observations of krill.

TPRS have been used with a global smoothing parameter in a variety of ecological areas such as to combine direct ship sampling and remotely sensed chlorophyll-a data (Clarke et al., 2006), which was also used to model copepod (*Calanus finmarchicus*) abundance (Speirs et al., 2006). TPRS have also been used to estimate species abundance, e.g. shorebirds (Granadeiro et al., 2004) and crabeater seals (*Lobodon carcinophaga*) (Southwell et al., 2007). The work presented in this chapter is different to theirs because this approach is local; different numbers of knots are chosen in different areas to accommodate local changes in the smooth surface. As a graphical example, the results of radial basis functions that make up a column in the basis matrix are shown in panels 1 to 3, Figure 7.1, and the combination of these basis functions in panel 4, Figure 7.1. Note the basis functions are additive and each function is scaled by model coefficients (see Equation 7.4, page 189)

In this modelling framework the candidate knot locations (x,y coordinates, where x=ping number, y = depth sample) were selected randomly from available acoustic volume backscatter (S_v) sample locations in the echogram (Figure 7.2). Selection of candidate knot locations was weighted by the empirical distribution of the S_v values, meaning that high value S_v locations were more likely to be chosen than low S_v values. Also, S_v locations could only be chosen once as a candidate knot location and due to computational reasons 30 candidate knot locations were selected for each model fit.

7.2.2 The branch and bound algorithm

Branch and bound algorithms are used to solve global optimisation problems. The branch and bound algorithm achieves this by partitioning and sampling from the optimisation

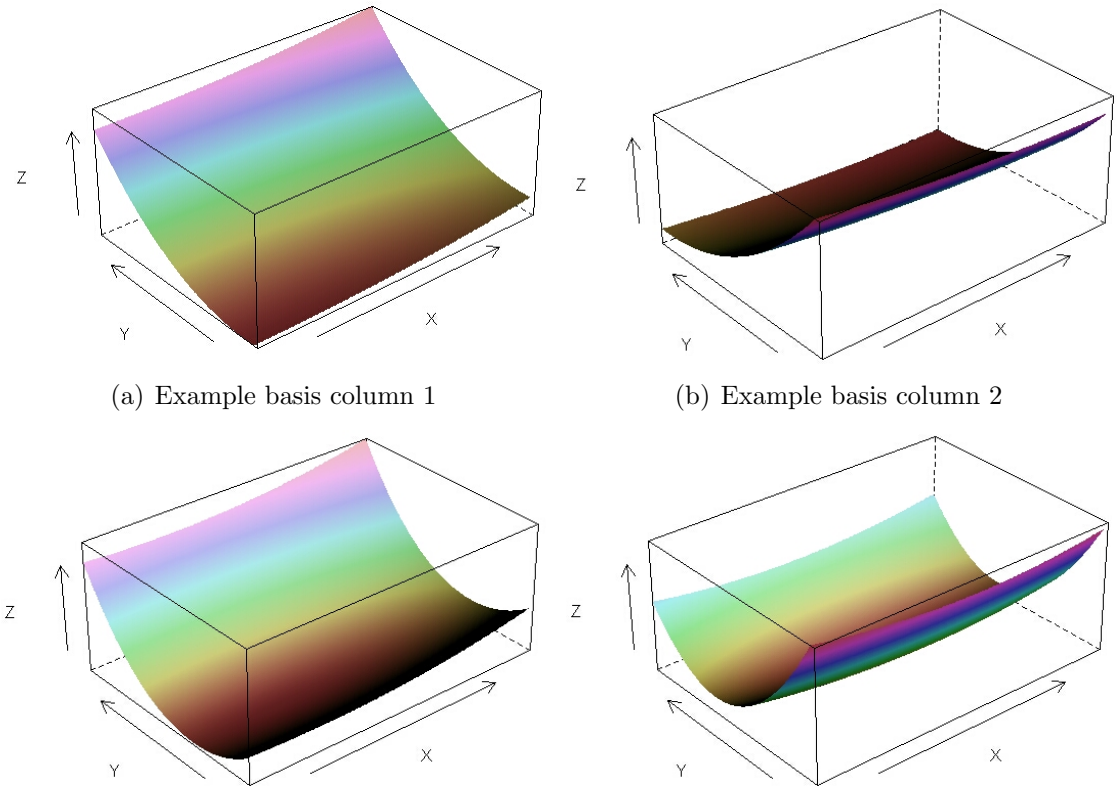

(a) Example basis column 1

(b) Example basis column 2

(c) Example basis column 3

(d) Combined basis columns

Figure 7.1: Example of thin plate regression splines. From upper left to lower left panels the surfaces are from one column of the example basis matrix. The lower right panel is a combination for the three basis surfaces. Note, basis surfaces (panels 1 to 3) are rescaled in the modelling framework (Section 7.3.2).

problem parameter space (Θ). The branch and bound algorithm partitions Θ into a number of subsets. In the linear modelling case each of these Θ subsets contain different combinations of explanatory variables. Each subset is then solved, providing a solution to the optimisation problem for selected parameter values (explanatory variable coefficients for linear models), in the current partition of Θ. The branch and bound algorithm performs what amounts to an exhaustive search of combinations of explanatory variables, whilst avoiding the need to search through all possible combinations of explanatory variables. Often searching all possible solutions, for an optimisation problem is impractical due to the time required.

At the start of the branch and bound algorithm only one solution exists: the entire parameter space (Θ), and each iteration of the branch and bound algorithm examines a portion of the unexplored solution space. At any time in the branch and bound procedure the current solution can be described in terms of: (1) the best solution so far and, (2) the regions of Θ that have yet to be explored.

One iteration of the branch and bound procedure has three main parts: (i) the selection

of the Θ partition to process; (ii) the bound calculation; and (iii) branching. The order in which these procedures are carried out differs with the branch and bound algorithm used. The first operation of the algorithm may be to determine if the current partition should be split into two or more further partitions. One of these newly created partitions is checked to see if it contains a single solution, if so, this is checked against the current optimum solution and the best of these is retained. If the current partition contains more than one solution the range of these solutions for the current partition are calculated. If the partition bounding determines that the partition cannot contain the optimum solution, then the partition is discarded. The discarding of bounded partitions means that not all of Θ needs to be explicitly searched, reducing the time required to obtain an optimal solution. Using a branch and bound algorithm in this multi-dimensional surface fitting application is particularly useful because it effectively allows an exhaustive search of combinations of candidate knot locations, without having to explicitly search all potential combinations, thus reducing computation time.

7.3 Spatially adaptive krill modelling using TPRS and a branch and bound algorithm

7.3.1 Data description

Acoustic data are often displayed as echograms (Figure 7.2), and in the case of Antarctic krill the data displayed are volume backscatter (S_v). Volume backscatter will either be in the logarithm domain (S_v) or in the linear domain (s_v) and are related by $S_v = 10\log_{10}(s_v)$. Echograms can be thought of a matrix with the columns comprising of S_v samples arising from a single echosounder ping and rows are S_v samples are fixed, discrete depths. Echograms are made up of successive pings as the research vessel travels along transect.

To assess the modelling framework described in Section 7.3.2 two types of acoustic data were used. Both data types were sampled during BAS acoustic surveys. The first acoustic data set was taken from a portion of acoustic data from a region of exceptionally high krill density around South Georgia (Brierley et al., 1999b), the second is from a region of lower krill density (Table 7.1). These data were used to determine the model performance during two extreme, but biologically plausible situations.

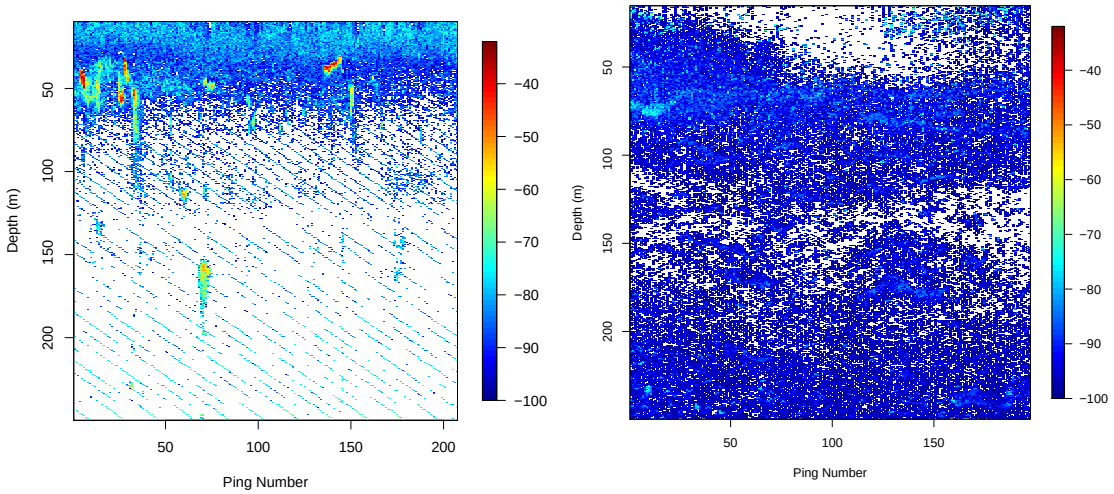

(a) 120 kHz high S_v data

(b) 38 kHz low S_v data

Figure 7.2: An acoustic echogram of the 38 kHz volume backscatter (low-density, low-variability) and 120 kHz volume backscatter (high-density, high-variability,S_v, units: dB). The data were sampled over 208 pings, each comprising of 480 volume backscatter (S_v) samples with higher acoustic intensity returns being displayed in red and lower in blue. In these echogram acoustic returns from krill swarms are shown in the upper left-hand corner. In the 120 kHz echogram a diffuse, low intensity, scattering layer that extends from a range of 0 to approximately 70 m. The diagonal banding seen on the 120 kHz echogram is electrical noise from the research ship.

Data type	Observation date	Frequency (kHz)	transect length (L, km)	S_v (dB) mean	S_v (dB) range
High-density high-variability	25/01/1998	120	2.58	-64.55	-99.91 to -41.05
Low-density low-variability	27/01/1998	38	2.45	-91.52	-100 to -61.90

Table 7.1: Description of the two acoustic data sets used in this investigation. The length of transect sub-sampled for this investigation is given and mean volume backscatter (S_v) is that of the underlying data.

7.3.2 TPRS model framework methods

Model specification and fitting

The candidate knot locations for the radial basis functions were data-driven. Computational restrictions prohibited considering all intensity values as candidate knot locations so for practical reasons a maximum of 30 knots were considered for selection. Knots at spatial locations within and around krill swarms were given higher priority; intensities

within and around krill swarms exhibit abrupt intensity changes and knots in these areas would help capture these changes. For this reason, candidate knot locations were randomly sampled from all spatial positions with weights in line with the observed intensity at each location. These weights are the intensity at each spatial location divided by the total intensity of each transect portion (Figure 7.2) giving:

$$w_i = \frac{s_{v_i}}{\sum_i s_{v_i}} \tag{7.1}$$

Radial basis functions are formed using the radial distances (r) between each knot location and each S_v observation in the following way:

$$r_{ki}^2 = (x_i - x_k)^2 + (y_i - y_k)^2 \tag{7.2}$$

where (x_i,y_i) are the coordinates for observations where $i = 1, 2 \ldots, n$,where n is the number of the acoustic data observations (S_v samples). The knot coordinates are specified by (x_k,y_k), where $k = 1, 2, \ldots, K$, and K is the number of knots. Since radial basis functions are linear in their parameters, a linear model framework can be used (Equation 7.4). The branch and bound algorithm was used to select a subset of these candidate knots and yield the optimum model fit. The Mallow's C_p statistic was used to select the optimum number of knots. Mallow's C_p statistic is a penalised measure of fit i.e. model fidelity to the data is penalised by the number of estimated parameters p, which for the linear model in Equation 7.4 gave $p = K + 3$. Like the AIC statistic (Akaike, 1974), the C_p statistic has a penalty of 2 units per parameter (p):

$$C_p = n \log \frac{RSS}{n} + 2p - n \tag{7.3}$$

where, n is the number of observations, and RSS is the residual sums of squares.

The C_p was calculated for each potential number of knots, K, from 1 to 30. Within each K the combination of knot locations that gave the lowest the C_p was selected. The final branch and bound solution gave the lowest C_p statistic, one for each K, based on the optimum knot locations.

Based on these selected knots a thin-plate regression spline basis was generated and least-squares was used to fit a linear model using the selected knot locations (columns in the radial basis function matrix). In this case the s_v was used as the predictor variable along with the position (x, y), and the columns of the radial basis function:

$$s_{v_i} = \beta_0 + \beta_1 x_i + \beta_2 y_i + \sum_{k=1}^{K} \beta_{k+2} r_{ki}^2 \log r_{ki}^2 + \epsilon_i \tag{7.4}$$

Normal errors (ϵ_i) were assumed for these models which was found to be reasonable in practice. Note, only one parameter is required for each of the K radial basis functions used.

Model Assessment

The method proposed is heavily data based; the candidate knot locations were selected using weights in line with observed intensities and the branch and bound algorithm seeks knot locations which result in the best fit to the data. While model fit is clearly important, is necessary to ensure that the number and location of knots chosen gives appropriate estimates for pings unseen by the model. For this reason the performance of this approach was assessed by simulating missing pings from complete transects and comparing the volume backscatter for these missing pings with the intensities observed, but unseen by the model. This cross-validation exercise meant that 20% of the data were discarded at the ping scale, i.e. if selected, all the samples in an individual ping were discarded. The branch and bound TRPS model framework was then fitted to the remaining 80% pings, and predictions from this model were made to the dropped pings.

The sum of the squared differences (RSS) between the observed intensities unseen by the model (S_{vi}) and the model predictions(S_{pvi}, see Equation 7.4), the model R^2 and the estimated intensities formed the basis of model assessment, since these S_v gave the cross validation or CV score (CV):

$$CV = \sum_{i=1}^{N} (S_{vi} - S_{pvi})^2 \tag{7.5}$$

Since missing pings do not appear at random along a transect, but often present in succession, the horizontal locations of the simulated missing pings were chosen using those observed for randomly chosen transects with missing pings. While this method assumes that missingness is random with respect to krill density, this appears to be reasonable for these data. Missing pings primarily occur in bad weather when the sea surface is rough and exploration of the data revealed that there is no evidence to suggest this affects krill density in the water column.

Comparison with an alternative smoothing method

For comparison with an alternative smoothing-based method the TPRS method was compared to a penalised thin-plate regression spline method with smoothness estimated using the MGCV R library, see Wood 2006. For comparison, both methods were applied to the transect portion with simulated missingness, and both approaches were compared using

the CV score.

7.3.3 Model fit example using high-density data

This section provides an example of the modelling framework carried out on the 120 kHz data (Figure 7.2, page 188 and Table 7.1, page 188). Under cross validation 20% of the pings were removed from the echogram (Figure 7.3) and the 30 candidate knot locations were based on the distribution of the remaining S_v values (Equation 7.1, page 189), and since knot selection was weighted by relative S_v at each location (left and centre panels, Figure 7.4, page 192), acoustic samples with a high S_v were more likely to be selected as candidate locations (right panel, Figure 7.4). In this example the S_v at the 30 candidate knot locations (shown as black circles, Figure 7.3) were taken from the upper 2% of the S_v distribution (right panel, Figure 7.4).

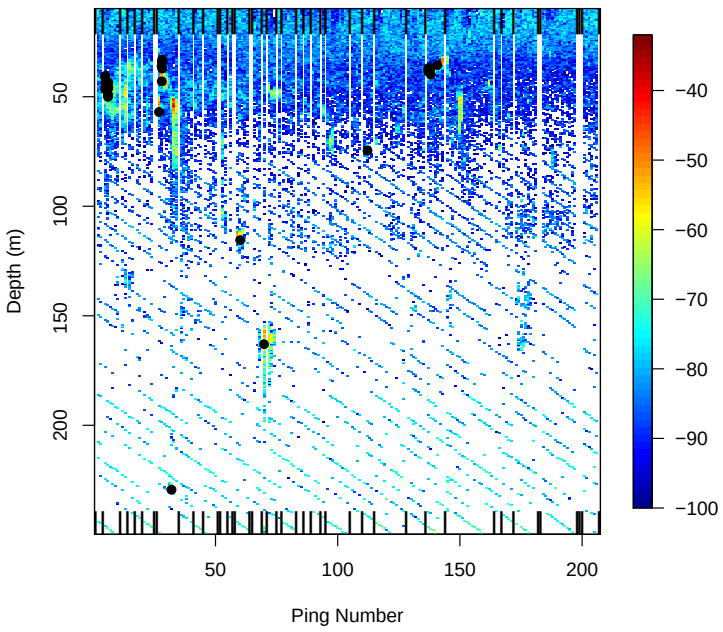

Figure 7.3: An example 120 kHz (high-density, high-variability, volume backscatter, S_v, data) acoustic echogram during cross-validation. To simulate missing pings 20% of the pings were removed. These are marked by short black vertical lines on the x-axis. The data within these pings are set to 0, which results in the white vertical lines. The 30 candidate knot locations, shown as solid black circles are based on the empirical distribution of S_v values.

In the example model fit 29 of the 30 candidate knots were placed within krill swarms (Figure 7.5, page 193) and the boundaries of which were identified using the validated dB difference (120kHz-38kHz = 2 to 12 dB, see Madureira et al. 1993; Watkins and Brierley

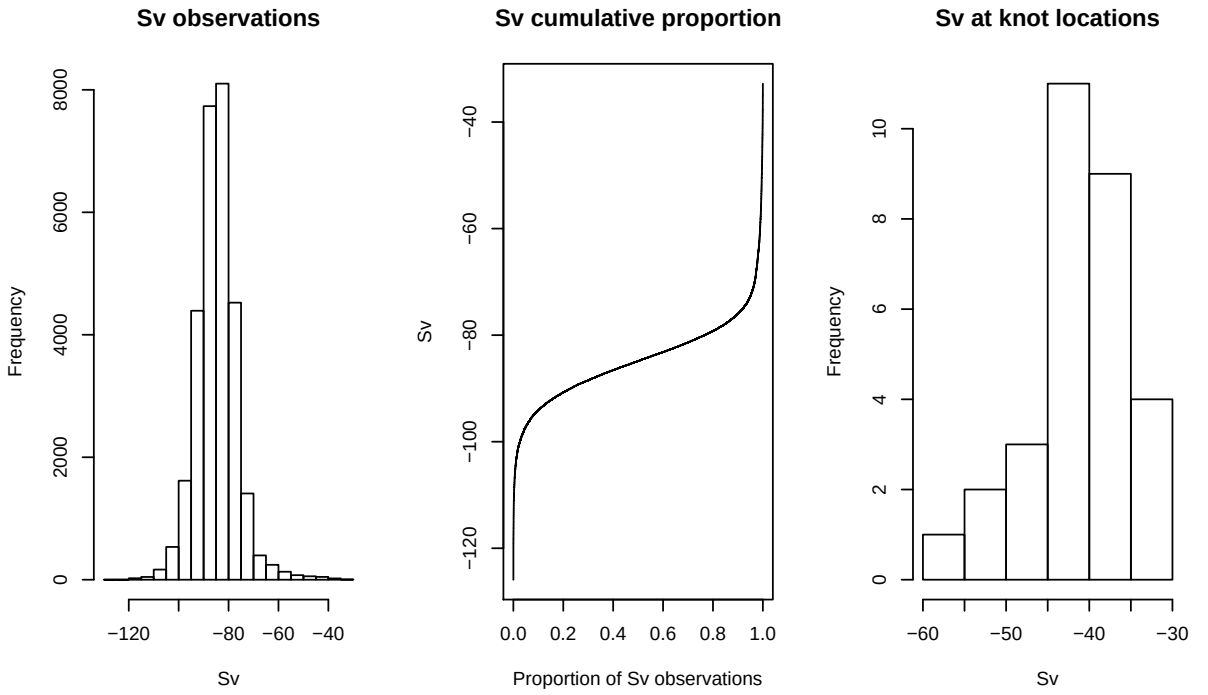

Figure 7.4: Candidate knot locations from one cross validation procedure. Left panel: Distribution of S_v observations . Centre panel: Cumulative frequency distribution of the S_v observations. Right panel: S_v observations at the candidate knot locations, which in this iteration are all drawn from the upper 2% of the cumulative distribution function of the S_v observations.

2002) technique (Figure 7.5). In this instance the 28 knot model was selected (Figure 7.6, page 193) using the C_p score and retained knots which were all within krill swarms.

The MGCV GAM was then fitted to the seen data and predictions made to the missing data. The performance of both the TPRS and MGCV GAM models were then compared (graphically Figure 7.7), and in this example, the TPRS GAM outperformed (CV score = 159506) the MGCV GAM (CV score = 160551). The relative bias ($r_b = (s_v - s_{vp})/s_v$) for the TPRS GAM was 0.626 and 0.629 for the MGCV GAM. The cumulative frequency distributions of each of the model fits demonstrates that, in this example, both models have under predicted krill density and the very high S_v values were very difficult to predict (Figure 7.8).

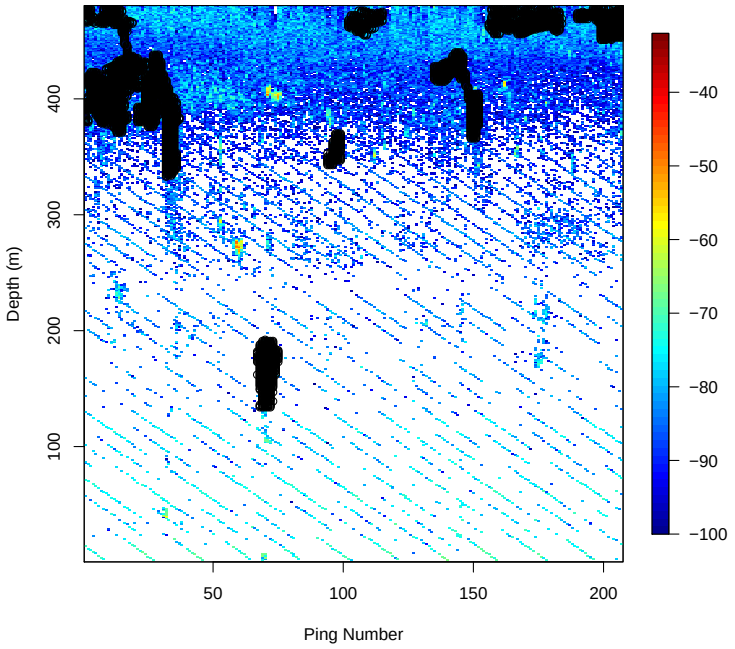

Figure 7.5: Krill swarm locations. The black circles show mean volume backscatter samples (S_v) that occur from krill swarms in the 120 kHz (high- density, high-variability) example data. The krill swarm boundary was identified using the dB difference technique (120kHz-38kHz = 2 to 12 dB).

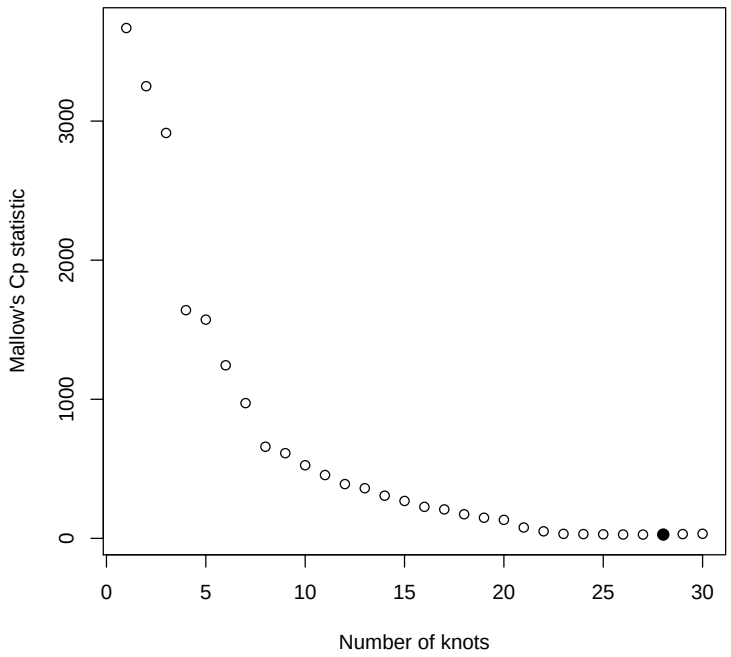

Figure 7.6: The Mallow's C_p statistic for the optimum combination of knots from each possible number of knots (from 1 to 30). In this instance the 28 knot model was selected as the best overall model.

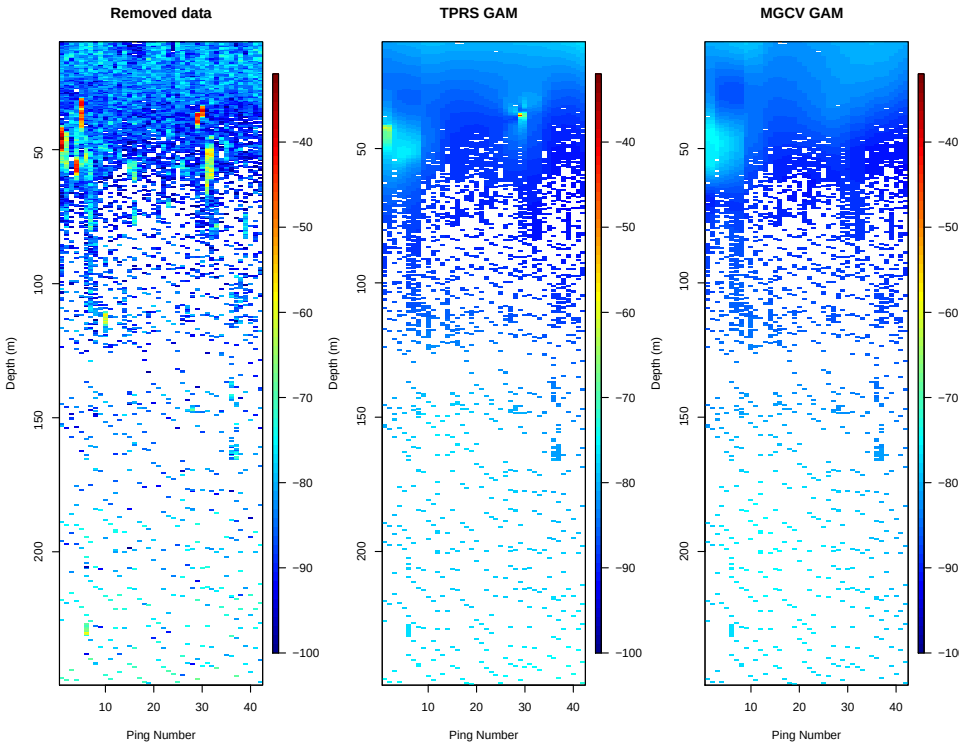

Figure 7.7: Left panel: The removed acoustic data under cross validation (20%). Data were removed on a ping-by-ping basis, at the locations shown in Figure 7.3 to simulate missing pings. Note, these missing pings are not necessarily consecutive. Centre panel: Missing data predictions made using the TPRS GAM. Right panel: Missing data predictions made using the MGCV GAM.

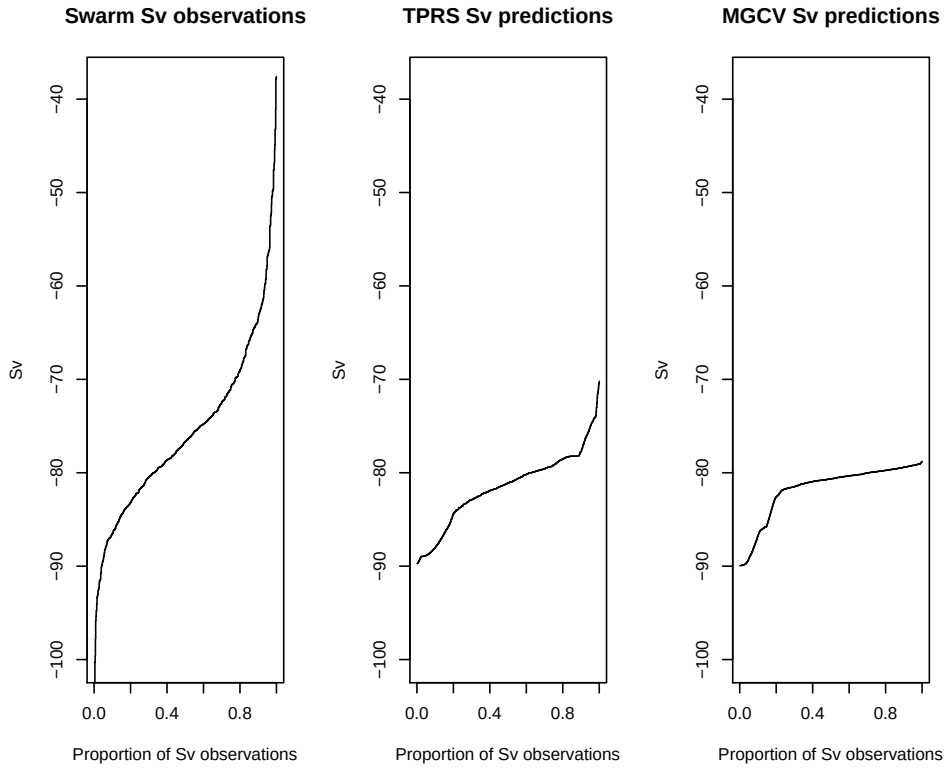

Figure 7.8: Empirical distributions of the unseen data (20% of the pings, left panel), the TPRS GAM (centre panel) and the MGCV GAM (right panel).

7.3.4 Large scale cross validation results

Model specification and fitting

Cross validation was performed 1,000 times for both the high-density, high-variability (120 kHz) and low-density, low-variability (38 kHz), volume backscatter data sets (S_v, Table 7.1, page 188).

Model selection was carried out using Mallows's statistic (C_p) which resulted in a 'best' model for a given number of knots ranging from one to thirty. Subsequently, the optimum number of knots was selected by the combination that had the lowest C_p. The number of knots selected for the 'best' model fit ranged from 20 to 29 knots for the 1,000 cross validations (Figure 7.9).

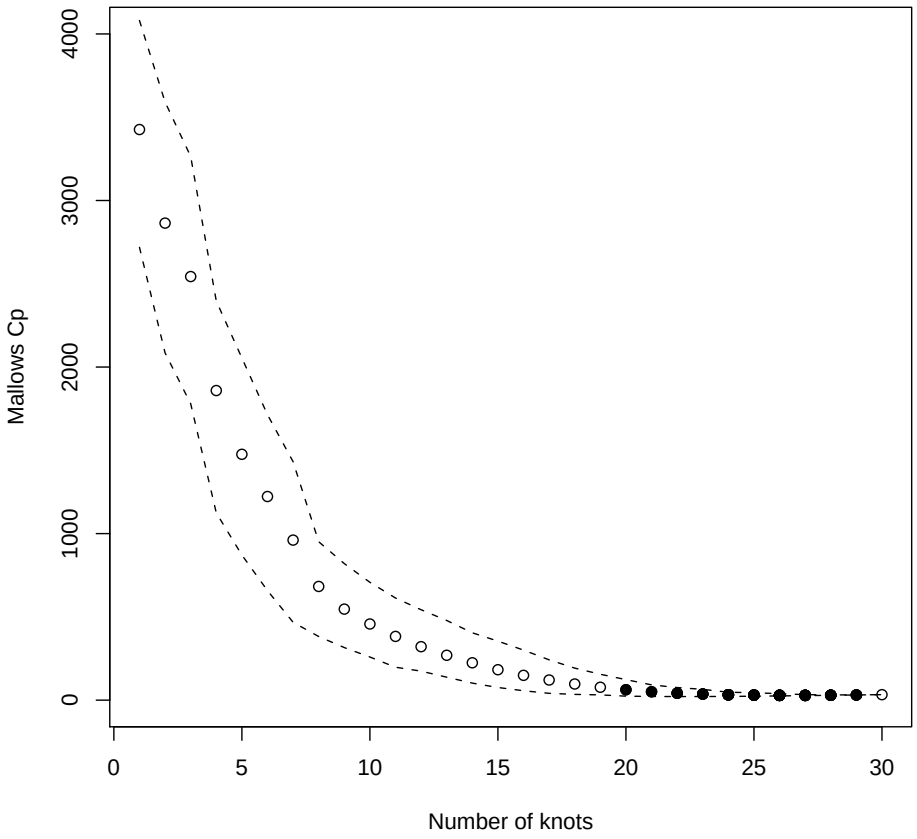

Figure 7.9: Mean Mallows's C_p model fit statistic for 1,000 cross validations of the high S_v 120 kHz data. Open circles are the mean C_p across 1,000 cross-validations at each potential knot number. Dashed lines are the 5 and 95% C_p bounds. Closed circles show the number of knots used in model fits, from 20 to 29.

A fundamental component of the all-possible subsets TPRS framework is the selection

of both the candidate knot locations and the optimal subset of these knots. Using krill swarm boundaries (determined using the dB difference technique) the variability of the candidate knot locations was determined to be small; approximately 92% of knots were found inside krill swarms on average. During cross validation of the high-density, high-variability S_v 120 kHz acoustic data (Table 7.1, page 188), the number of optimal knots selected ranged from 20 to 29, with approximately 28 being selected on average. Similar results were obtained when cross validation was carried out on the low-density, low-variability S_v acoustic data, when on average 27 knots were used, with a range of 20 to 30 knots being selected. Importantly 8% of the cross-validation procedures for the low S_v data set resulted in 30 knots being selected as the optimum knot combination, suggesting that 30 knots may be insufficient to obtain the optimal fit of the low-density, low-variability 38 kHz S_v data.

The low variation in candidate knot locations is illustrated by examining the distribution of S_v observations in the high-density, high-variability S_v dataset during one iteration of the CV exercise (right panel, Figure 7.4). The distribution of S_v observations in each cross validation will vary depending on which pings were dropped, as will the cumulative frequency distribution of S_v (centre panel, Figure 7.4, page 192). Generally S_v observations for candidate knot locations were chosen from the upper 2% of S_v distribution. On average, one of the thirty candidate knot locations was selected outside of the krill swarms for the high-density, high-variability 120 kHz data set. In the low-density, low-variability 38 kHz dataset two candidate knot locations, on average, fell outside of krill swarms.

Model assessment

Based on the CV score, the TPRS is, on average, out performing the MGCV GAM for both the high-density, high-variability and low-density, low-variability S_v data sets (Table 7.2, page 198). Furthermore, the volume backscatter bias measure ($s_{vb} = (s_v - s_{vp})/s_v$, Table 7.2) shows that TPRS model is out performing MGCV for both types of S_v data, but both models are under predicting the high S_v observations in both the high-density, high-variability and low-density, low-variability, S_v data sets. The lower CV scores and lower s_v bias show that both the MGCV and the TPRS GAMs both perform better with the high-density, high-variability S_v data set, than the low-density, low-variability S_v data set (Table 7.2). The gap between the performance of the two models is narrower for the low-density, low-variability S_v dataset (Table 7.2), with the TPRS out performing MGCV 57% of the time for the low-density, low-variability dataset, as opposed to 89% of the time for the high-density, high-variability dataset.

Data type	Frequency (kHz)	Method	CV Score	s_v bias
High-density, high-variability	120	TPRS	220514 (89%)	0.627
		MGCV	223332	0.632
Low-density, low-variability	38	TPRS	315501 (57%)	0.750
		MGCV	317692	0.755

Table 7.2: Average model performance results for the thin-plate regression splines (TPRS) GAM and the MGCV GAM model performance for both the lower and higher acoustic intensity (S_v) data. The percentage that TPRS out performs MGCV is given in the CV score column. The s_v bias, is the bias in predictions made within krill swarms was determined from $s_{vb} = (s_v - s_{vp})/s_v$, where $s_{vb} = 0$ is unbiased; $sv_{vb} > 0$ is negatively biased; $s_{vb} < 0$ is positively biased.

7.3.5 Discussion

The cross-validation results have shown that the TPRS model has, for both the acoustic data sets used here (Table 7.2), improved on the current MGCV based GAM fitting technique. Generally, the TPRS GAM performs well particularly for the high-density, high-variability S_v datasets (Table 7.2), showing that this model capable of capturing the behaviour of complex, highly variable surfaces. However, the TPRS and MGCV models perform similarly for the low-density, low-variability S_v dataset (Table 7.2). This difference in performance was due to the differing dataset characteristics. The high-density, high-variability S_v observations had a range of S_v values that is three times greater than the low-density, low-variability S_v dataset (Table 7.1, page 188). The high-density, high-variability S_v dataset also has different spatial variation, with extremely high S_v values that have a limited spatial extent (*e.g.* ping number 45, depth 75 m, left panel, Figure 7.2, page 188). In comparison, the low-density, low-variability S_v dataset had a far more spatially homogenous distribution of S_v values (right panel, Figure 7.2).

The ability of the TPRS GAM framework to capture areas of high complexity is illustrated in the example CV exercise (Section 7.3.3, page 7.3.3). At ping number 28 (x-axis), at a depth of 40m the TPRS GAM predicted large S_v observations from within a krill swarm (centre panel, Figure 7.7, page 194), but the MGCV GAM did not (right panel, Figure 7.7). It is suspected that the improved performance of the MGCV GAM relative to the TPRS GAM for the low-density, low-variability S_v data set is due to the MGCV GAM global smoothing parameter. So for surfaces that are spatially homogenous, such the low-density, low-variability S_v echogram (right panel Figure 7.2, page 188), there is less need for a local smoothing parameter. This makes the predictions of the simulated missing pings, by the MGCV, representative of a surface that has lower spatial variance. However,

the TPRS GAM still out performed the MGCV GAM, but the difference in performance between the two models was less for the low-density, low-variability S_v dataset than that seen with the high-density, high-variability S_v dataset (Table 7.2, page 198). This suggests that less local flexibility was required to model the low-density, low-variability S_v dataset.

The main advantage of the TPRS GAM is that the method is capable of modelling areas of high S_v. This is because the method targets its knots at these locations. Furthermore, the method is also parsimonious, with each knot apparently only costing one parameter. The knots are optimally placed however, so one could argue that each knot ought to "cost" >1 parameter. Like all methods, the branch and bound algorithm has limitations. In the case of modelling Antarctic krill echograms, the number of knots places an important constraint on knot selection: a maximum of 30 knots could be selected. This is because currently solving the TPRS model using the branch and bound algorithm is very time consuming for more than 30 candidate knot locations, so is outside the scope of this PhD research. Should the TPRS technique be implemented for acoustic data in the future this limitation could be overcome by dividing the echogram into shorter EDSUs. Also, developments in the computational efficiency of the branch-and-bound algorithm will allow >30 candidate knot locations to be selected, eventually allowing all the S_v data points, in an EDSU, to be used as possible candidate knot locations. The selection of the optimum number of knots in the TPRS is highly data driven, which in turn makes the TPRS framework used here data driven. This is partly because the empirical *pdf* of the S_v observations is used to determine the knot locations (Figure 7.4). Also, the number of knots, selected from the candidate knots, used in the selected TPRS model fit is determined by the size and complexity of the data. Consequently, we are unable to give general quantitative rules regarding the minimum number of knots that could be applied to all potential acoustic data sets.

Since the probability of a knot location being selected is by S_v, fitting the TPRS model to the same data could result in different model fits. Determining how many model fits are on average required, to given the best model fit, may improve the performance of the TPRS framework, although this is likely to be data dependent: it is likely that complex data sets will require an increasing number of model fits to obtain the optimum solution. It is also important to determine the practical significance of these additional model fits. As an initial investigation 50 model fits were carried out on the high-density, high-variability S_v 120 kHz data set. The number of knots ranged from 20 to 29 and mean CV score 221984. The minimum CV score was reached after 29 iterations, which was only approximately 2% less than the first model fit CV score. These results should not be considered representative of the TPRS technique generally, but do show that for the high-density, high-variability 120 kHz high S_v data set, multiple TPRS model fits within

each cross validation iteration would not have practically improved model performance.

Interesting the MGCV GAM had, on average, 32 effective degrees of freedom, compared to a maximum of 30 for the TPRS GAM, so even with the potential increase in flexibility the MGCV GAM did not out perform the TRPS. Although the data were used to select the knots so the degrees of freedom for each knot used in the TPRS model were likely to be >1.

There is no evidence that the TPRS GAM is overfitting for these data. Given the restraint of a maximum of 30 knots and the fact that the C_p score decreases as the number of knots increase, it is believed that overfitting is unlikely (Figure 7.9, page 196).

The results of this research show that the TPRS model framework shows promise, by improving the current industry standard fitting procedure. However, the technique requires additional work prior to being used to predict krill density within missing pings. For the acoustics user the technique will be assessed on how well it estimates S_v, hence krill density. Currently the TPRS model is under predicting large values of krill density (Table 7.2, page 198), and improving this prediction is a priority for this work.

7.3.6 Further work

1. Currently it is assumed that the location of the missing pings in the acoustic data are known. In the example given here it is obvious which pings were removed in cross-validation, because the entire ping was removed and the underlying data replaced with zeros. In reality, missing pings are not always so obvious to detect. Consequently, techniques to identify when a ping is missing should be established. Also, pings are not always completely missing, rather acoustic detectability within a ping may be reduced, making some acoustic targets appear weaker than truth, with others remaining undetected.

2. The identification of missing pings is important for biomass estimation: ignoring missing pings will negatively bias biomass estimates. Simulations could be used to determine the effect of different treatments of missing pings on biomass estimation. When acoustic echoes are identified using multi-frequency acoustics, possibly to species level, the effect of missing pings is unclear - simply marking pings as missing may bias biomass estimates in either direction, so interpolation techniques may be required.

3. To select candidate knot locations an echogram could be divided into squares, and selected at random as a candidate knot location. Again the squares could be weighted by the proportion of echogram s_v that falls in them. This would lead to less clustering in candidate knot locations, but might mean lower flexibility.

4. Both models were under predicting the large values of S_v, suggesting that neither GAM was sufficiently flexible enough to capture the high local variability of the 120 kHz S_v data set. In the case of the MGCV GAM this was caused by the model using a global smoothing parameter. For the TPRS GAM this under-prediction may have been used by the radial basis functions not having enough flexibility to accommodate the data. It may be possible to increase the flexibility of the radial basis function, thus improving the TPRS model performance in regions on the echogram surface of rapidly varying S_v. This could potentially be achieved by modifying Equation 7.4, for example from:

$$s_{v_i} = \beta_0 + \beta_1 x_i + \beta_2 y_i + \sum_{k=1}^{K} \beta_{k+2} r_{ki}^2 \log r_{ki}^2 + \epsilon_i$$

to:

$$s_{v_i} = \beta_0 + \beta_1 x_i + \beta_2 y_i + \sum_{k=1}^{K} \beta_{k+2} r_{ki}^4 \log r_{ki}^4 + \epsilon_i \tag{7.6}$$

7.3.7 Summary

The large spatial variation in krill S_v values provide a complex, challenging biological data set to test surface fitting functions. The rapidly varying S_v require a local adaptive smoothing technique with a high level of flexibility and the TPRS method certainly offers this, but is currently constrained by the number of candidate knots that can be searched by the branch and bound algorithm.

Chapter 8

General discussion

This thesis (Chapters 3, 4 and 5) has reaffirmed (*cf* Hunt et al. 1992a; Veit et al. 1993; Reid et al. 2004) that observing predator-prey interactions, particularly at-sea in the Southern Ocean, can be difficult, and fraught with technical problems. Nevertheless the practical and numerical work described in this thesis has successfully characterised, at least in part some of the spatial interactions between Antarctic krill and some of their air-breathing predators. Here I attempt to draw together the various research components conducted at different sites using different methods, in a common spatial/temporal framework, that operates at various scales.

Scale has long been recognised as an important quantity in ecology (Horne and Schneider, 1995), since the scale at which data are collected, or grouped during analysis, influences investigation results. Selecting an appropriate spatial scale to address the characteristics of the organism being studied is vital for successful analysis. For example assessing predator-prey interactions at large spatial scales reveals little about smaller scale interactions.

Scale in ecosystems has been described as hierarchical, or nested (see Fauchald 1999 and Figure 1.2, Chapter 1). Hierarchical scale has been used to describe interactions between organisms and energy dissipation in ecosystems, and may explain stability in complex ecosystems (Allen and Hoekstra, 1982). For example, Van de Koppel et al. (2005) devised a theoretical framework to explain the spatial-scale and overlap of predators and prey. That framework was used to examine and explain the gap between theoretical food chain models, including predator-prey interactions, and the dynamics of natural ecosystems. Without considering scale, theoretical models are often unstable and cannot replicate real-world food webs (Wu and Louckes, 1995; Kneitel and Chase, 2004). The consumption rate of prey, that is partly dependent on predator and prey spatial scales (Sims et al., 2006) has also been shown to affect the stability of food webs (Hassell et al., 1994).

Differences in spatial-scale between predator and prey aggregations do not have to be large for ecosystem stability to occur. Studies of krill-phytoplankton predator-prey interactions (*e.g.* Martin 2003, and references therein) suggest that zooplankton exhibit additional small-scale spatial structure compared to phytoplankton. This additional small-scale zooplankton structure, caused by diel vertical migration and swarming, provide food web stability. Oceanographic processes can also reduce spatial overlap and thus reduce competition between predator species. For example, upwelling and alongshore transport in the northern Benguela was shown by Barange and Piller (1992) to reduce competition between *Nyctiphanes capensis* and *Euphausia hanseni* euphausiid species, by separating the species into patchy, spatially discrete zones.

A scale dependent approach was also adopted in this PhD research because the environment an organism inhabits can often be described at multiple spatial scales and the environment may induce positive and negative associations between predators and prey. For example, Rose and Leggett (1990) studied the spatial interactions between Atlantic cod (*Gadus morhua*) and its prey, capelin (*Mallotus villosus*). They found that these species were associated in a hierarchical patch structure that ranged from 2 to 30 km, within which associations were positive and were caused by foraging cod. Within this larger scale, negative associations were caused by capelin occupying thermal refuges, within which no cod were observed.

The importance of considering the multiple scales of drivers for the aggregation of pelagic organisms was illustrated by Lavoie et al. (2000). During their study, observations were collected from a "quasi-permanent" dense aggregation, at the head of the Laurentian Channel (48^o50'N, 68^o45'W). This aggregation of euphausiids *Thysanoessa raschi* and *Meganyctiphanes norvegica* was demonstrated to be driven by events that occupied a broad-range of scales. At the smallest scale krill responded to light levels and at the largest scale, estuarine circulations ($\simeq$ 2 weeks, $>$ 100 km) influenced the aggregation characteristics. These multiple scale drivers determined when the krill aggregation met the feeding requirements of pelagic fish and baleen whales. Thus indirectly krill behavioural responses and physical processes, that operate at different scales, were driving predator distribution.

Because ecosystems may be large and patterns often occur over decades, understanding the hierarchical scale of ecosystem structures is generally limited by data collection and analysis methods. This is because measurements can usually only be made over small areas, and extrapolating small-scale observations to large-scale processes in many instances cannot be done. For example, after the collapse of the Atlantic cod on the north-eastern continental shelf of North America, first year juveniles were confined to coastal waters. However, even with the reduced habitat, because of spatial heterogeneity scaling

seine fishing catches of cod juveniles could not be extrapolated to estimate abundance (see Schneider 2001).

In this chapter I use a Stommel diagram modified from Haury et al. (1985) and Kaiser et al. (2005) (Figure 8.1), to display the overlapping scales of my PhD research in relation to the spatial and temporal scales of krill biomass variability and various observation platforms, such as research vessels and moorings.

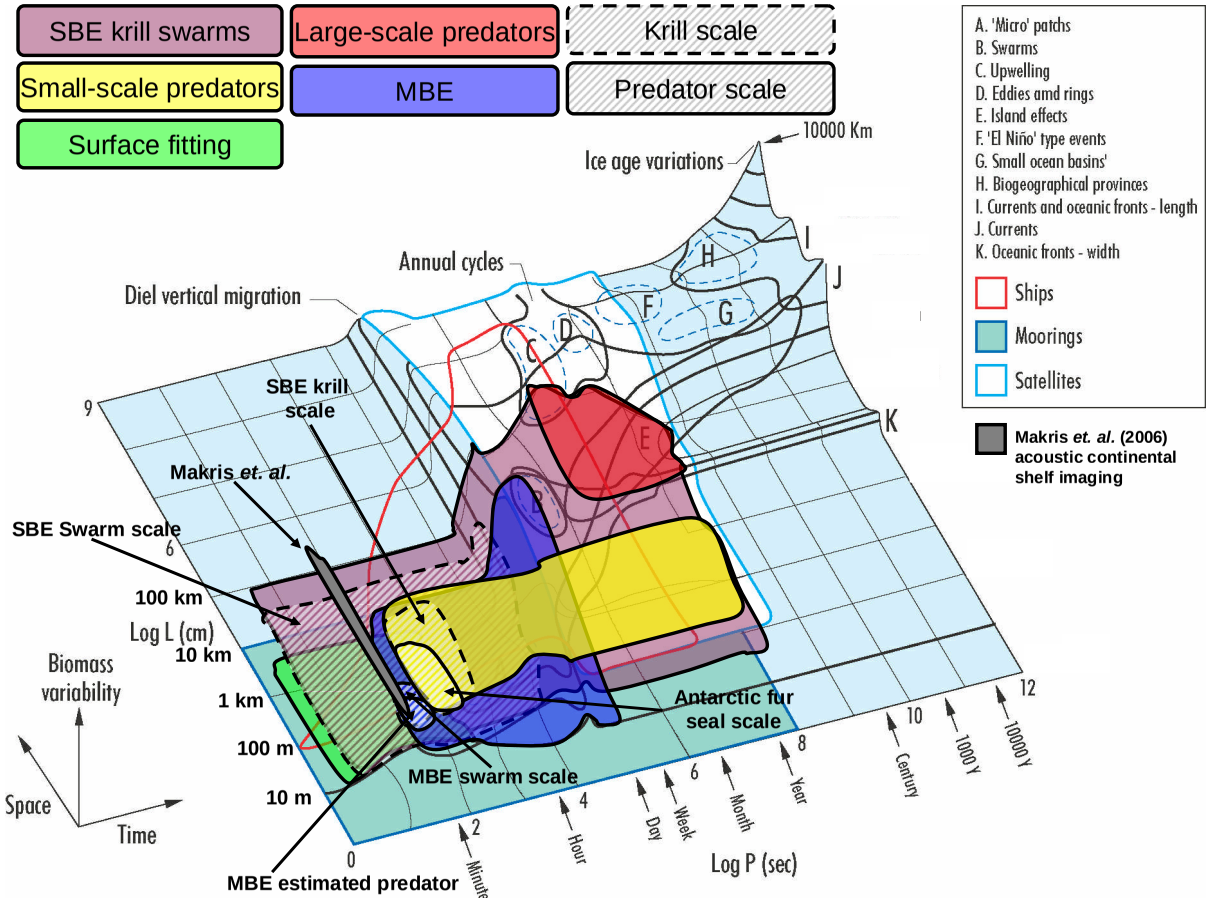

Figure 8.1: Stommel diagram from Haury et al. (1985), modified from Chapter 6 Kaiser et al. (2005). Using logarithmic axes, the purpose of this diagram is to illustrate the spatial and temporal scales of Antarctic krill and predator aggregations. The underlying diagram shows the scales of abiotic forcing mechanisms (legend top-right), and colour coded observation platforms and they have . Types of analyses that have been conducted in this PhD are shown. Note the predator foraging areas (hatched areas, bounded by a solid line) are found within the appropriate krill region (hatched areas, bounded by a dotted line) of the diagram i.e. the characteristic scale of krill predators is smaller than that of krill.

8.1 Krill swarms

Krill swarms are a fundamental unit of krill ecology (Mangel and Nicol, 2000). During this research krill swarms (length 19 m to 49 km; volumetric density 0.04 to 1,290 g/m^3) were observed and described quantitatively at both South Georgia and the South Shetland Islands.

8.1.1 South Georgia krill swarms

At South Georgia krill swarms were sampled using a standard split-beam (SBE) scientific echosounder (EK500) and identified objectively, using the SHAPES algorithm (Barange, 1994). This study was the first time that variation in krill swarm metrics at South Georgia was assessed. At the larger inter-survey scale the krill swarm research conducted in this thesis showed that krill swarm abundance (n_s) was strongly correlated with mean areal krill density ($n_s \sim \hat{\rho}$, r =0.88, p =0.02, 95% C.I.= 0.24 to 0.99). For krill predators, the positive correlation found here between $n_s \sim \hat{\rho}$ is important, because as the $\hat{\rho}$ decreases so will n_s. A decline in n_s causes the probability of a predator encountering a swarm to decrease, suggesting an adaptive foraging strategy is required if optimal foraging is to be maintained. This result is unexpected because for another pelagic species no relationship was found between $n_s \sim \hat{\rho}$ for North Sea herring (Petitgas et al., 2001). The strong $n_s \sim \hat{\rho}$ correlation for krill also suggests that it is appropriate to use $\hat{\rho}$ as a proxy for swarm availability as proposed by Mori and Boyd (2004). The variation in n_s (Figure 2.4, page 27) suggests that for systematic net sampling the catchability of krill will vary between surveys, and if inter-swarm krill length segregation occurs (see Watkins et al. 1986) then this will bias krill bias estimates.

At South Georgia both intra- and inter-survey swarm variation in swarm morphology and density, shown in Chapter 2, has important implications for krill predators: a consistent, non-adaptive, foraging strategy will rarely be optimal (foraging being defined as both searching and feeding) in a varying prey field (Sims et al., 2006). Significant inter-survey differences were found in quantitative krill swarm descriptors or metrics (purple hatched area, Figure 8.1).

8.1.2 South Shetland krill swarms

The small-scale analysis, using data from a multibeam echosounder (MBE), at Livingston Island (Chapter 5 and blue area, Figure 8.1) highlighted the limitations inherent with the small volume of water sampled by conventional split-beam (SBE) echosounders: swarms are effectively only observed by SBE in 2D. Sampling krill swarms in 2D imposes two major limitations. Firstly, only 2D swarm characteristics can be identified. Secondly,

visually observing predators in a narrow, fixed width, strip transect using a SBE creates a fundamental strip transect width mismatch between the SBE observations of krill and the visual observation of predators. The SBE strip width is much narrower than that of the visual observations (Figure 8.2). The visual observation and SBE spatial mismatch may explain why, at the krill swarm scale, no relationship was found between the number of foraging predators in the vicinity of a krill swarm and variation in swarm metrics, such as volumetric density and length (Section 4.3.3, Chapter 4).

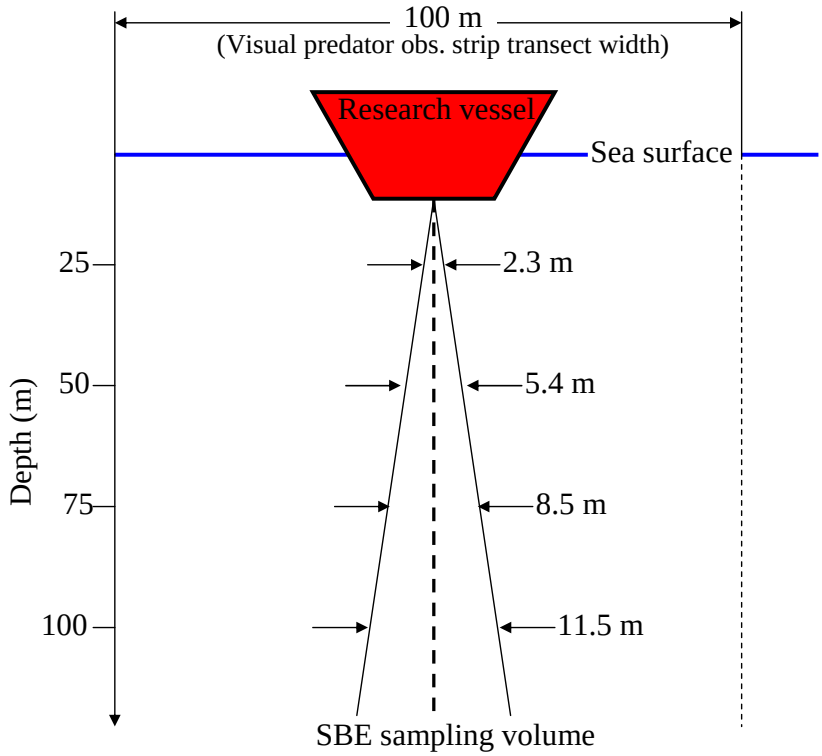

Figure 8.2: Cross-section view of line-transect sampling. The cross-section shows an across transect slice, with the research vessel following a line transect into the page. The across-transect sampling width for a typical split-beam echosounder (SBE), with a 7^o beamwidth is shown. The 100 m wide strip transect for visual observations of air-breathing predators is shown above the sea surface (see Section 4.2.1, Chapter 4). The effective across transect sampling width for the SBE is given at 25 m depth intervals that shows a large across-transect mismatch between the visual observations of air-breathing predators and SBE observations of krill.

This MBE research was the first time that an MBE had been used to examine pelagic invertebrate aggregations in 3D. It was also the first time that aggregations were objectively identified using a 3D detection algorithm. It was found that krill swarms maintain a similar roughness (R, the ratio between swarm surface area and swarm volume) of R=3.3 (CV=0.23) to aggregations of clupeids (*Sardinella aurita* and *Sardinops sagax*; R=3.0 to 3.2, Paramoa et al. 2007). Despite krill swarms having amoeboid shapes, it is now appears that individual krill in a swarm interact so as to maintain a constant R irrespective of

swarm size. The biological mechanisms underlying this are yet to be elucidated, but offer a fruitful area for future research. Furthermore, the observation of irregular swarm shape strongly suggests that krill swarm volume should not be calculated from SBE observations using the procedure given in MacLennan and Simmonds (1992), where a cylindrical aggregation shape is assumed.

Theoretical individual based models (IBM) of krill swarms, such as the 2D Lagrangian particle model developed by Hofmann et al. (2004), could be extended into 3D using MBE observations. These models are important because of the potential to incorporate them into ecosystem simulations, that can be used to assist in ecosystem management decisions. In such IBMs R and Var[R] could be included as model parameters. Further, MBE swarm observations could be used to validate the output of theoretical models, and may allow improved (both in precision and biologically plausible) model parameters, such as swarm nearest neighbour distances. Incorporating new parameters into swarm IBMs, or constraining current model parameters, may improve the estimation of elusive parameters such as biological attractive force (Okubo, 1986) and may allow density dependence to be incorporated into model parameters (Hofmann et al., 2004).

Using the MBE an elevated number of swarms within 200 m of a predator was detected (blue hatched area, Figure 8.1). The elevated number of krill swarms may either have been caused by predators actively selecting areas of higher krill swarm abundance, or larger krill swarms splitting into smaller swarms in response to predation attack (O'Brien, 1987; Hamner and Hamner, 2000). Again this finding highlighted the problem of sampling volume mismatch between krill distribution, observed using a SBE, and krill predators: at smaller scales (<1 km, Figure 8.2) this spatial mismatch will weaken, or possibly mask, any relationship between local predator and krill abundances. Prior to this research, estimating the smallest characteristic spatial scale of krill predators using krill swarm abundance derived from SBE observations used during conventional biomass surveys (with a 10 km line-transect spacing) would have been impossible. Determining this scale (200 m, Figure 5.19, Chapter 5) is important because it indicates the minimum spatial scale at which marine predators need to forage. The 200 m krill predator-prey interaction scale could be used in the planning of future MBE investigations as the scale at which the relationship between krill predators and environmental variables be analysed.

8.2 Predator-prey interactions

The small spatial scale (0.5 to 10 km) predator analysis again revealed high variability in the South Georgia ecosystem (yellow area, Figure 8.1). The use of auto-correlation functions showed higher spatial correlations between predator species than between preda-

tors and krill (yellow hatched regions, Figure 8.1). This is indicative of facilitative prey location and feeding, where predators cue on other predator species, rather than on the underlying prey distribution (Veit et al., 1993; Grënbaum and Veit, 2003). Predominately facilitative location and feeding occurred in the western core box (WCB, Figure 2.1, page 19) and most frequently in 1997.

At small spatial scales, positive correlations are expected only if krill cannot, or do not, avoid predators. Given that it is known that krill exhibit anti-predation behaviour, it is perhaps unreasonable to expect positive predator-prey correlations (Schneider, 2001). Certainly, without analysing environmental covariates it would have been difficult to interpret the negative correlations between cod and capelin, observed by Rose and Leggett (1990) as caused by refuges due to differences in water temperature.

No spatial overlap occurred between the small scale MBE and SBE studies (blue and yellow crossed-hatched areas, Figure 8.1). This may merely have been caused by boat speed (5 knots during the MBE study and 10 knots during the SBE), rather than there being no temporal persistence of krill swarms. Attempting to determine krill swarm temporal scale exposes a limitation of line-transect surveys, the evolution of individual krill swarms cannot be investigated, and analyses have to assume a stationary spatial distribution of predators and prey. There is no way to determine the persistence of an individual swarm without acoustically monitoring it, so the vessel speed and spatial scale were used to estimate temporal scale of the crossed-hatched areas in Figure 8.1. The same problem occurs for determining the temporal scale of predators.

At a larger-scale the research conducted at South Georgia showed that core box was more important as an explanatory variable of air-breathing predator sighting numbers than year. Despite there being a higher $\hat{\rho}$ in the eastern core box (ECB, Figure 2.1, page 19), more predators consistently foraged in the western core box (WCB), but the cause of this was not determined. At this larger scale several anolomous events occurred in 1998: (1) there was an exceptionally high $\hat{\rho}$ in the ECB; (2) an absence of Blue petrels, the cause of which is unknown, and demonstrates how little is known about the ecology of this species; and (3) elevated numbers of Antarctic fur seals were encountered. Analysis of a sea-surface temperature (SST) time series for the South Georgia region and Antarctic fur seal counts at the Signy Island research station, suggest that temperature may be driving, or be a proxy for the drivers of, inter-survey variability in predator sightings numbers at South Georgia. This agrees with research by Trathan et al. (2003) that demonstrated, at the transect scale, that an inverse relationship between $\hat{\rho}$ and temperature existed during the 1997 to 1999 BAS surveys.

Murphy (1995) showed that whilst high density areas of krill were not required to be available locally to support predators at South Georgia, concentrating factors, such as krill

transported to the South Georgia region by the Antarctic Circumpolar Current (ACC) were necessary. The results of this PhD research suggest that predator-prey processes in the waters around South Georgia are influenced by large-scale ocean wide events, such as El Niño (Meredith et al. 2005; temporal overlap between effect, labelled F, and large scale predator analysis, Figure 8.1). Given that it is believed that krill are advected into the South Georgia region by the Southern Antarctic Circumpolar Current Front (SACCF, Atkinson et al. 2001; Thorpe et al. 2002; Murphy et al. 2004) it is important to use data outside of the South Georgia region to interpret ecosystem variations, *e.g.* Signy Island Antarctic fur seal counts and the SST time series (frontal systems are shown to interact with the large scale predator analysis in Figure 8.1). Meredith et al. (2007) linked variation in the ACC to physical forcing, by El Niño/Southern Oscillation, that was characterised by changes in SST. Also, events that influence the krill population upstream of South Georgia, particularly around the Antarctic Peninsula, may cause changes in the South Georgia krill population (Tarling et al., 2007). In addition to influencing water temperature around South Georgia, large scale events such as El Niño, may induce lagged changes in South Georgia krill recruitment by affecting sea ice extent (Meredith et al., 2005; Murphy et al., 2007). Incorporating such lagged explanatory variables of the South Georgia krill population into population models may assist in the management of the South Georgia krill fishery (Constable et al., 2000).

Ultimately, a research vessel steaming a line-transect survey, as per the *RRS James Clark Ross*, at South Georgia, does not sample the spatial distribution of prey in the same way as a marine predator does. The line transect survey is non-adaptive, i.e. the sampling strategy is fixed irrespective to the amount of prey that is sampled. Marine predators, however, are capable of adapting their foraging strategy in response to local prey availability, determined by sensory information (Sims and Quayle, 1998; Sims et al., 2006).

8.3 Observation scale and observation bias

The research conducted in this thesis has shown that predator-prey interactions occur at multiple spatial and temporal scales, nested in a hierarchical structure. In all cases krill predators were shown to aggregate at smaller scales than krill (hatched areas, Figure 8.1). Bias has been shown to exist in the number of predators encountered, caused by availability and detectability, but techniques have been proposed to overcome this. However, bias remains in both the number of krill swarms detected (n_s) and some of their metrics. Bias in n_s can be overcome by using a MBE and the 2D distance sampling framework detailed in Chapter 6 (see also, blue area, Figure 8.1).

The newly developed 2D distance sampling framework used a goodness-of-fit test to select a vertical *pdf* of krill swarm distribution and accounted for MBE swath width, and range and angular detectability. The MBE 2D distance sampling research allows the abundance of krill swarms to be estimated across a (stratified) survey area, which when combined with conventional distance sampling of visual predator observations, may allow improved estimation of survey scale predator-prey interactions. Furthermore, estimating a *pdf* for the vertical distribution of krill allows, at the survey scale, estimation of swarm abundance in the acoustically inaccessible near surface region. The 2D distance sampling technique could be applied to any MBE equipped ship (area enclosed by a red line, Figure 8.1).

Single frequency MBE cannot be used to identify acoustic targets using the dB difference technique (see Section 5.2.3). Advanced MBE technology such as the Simrad ME70 is a broadband MBE that operates between 70 and 120 kHz, enabling dB differences to be used. However, this system requires permanent installation on a large research vessel, so could not have been used for this research. The Reson 7000 series MBEs are dual frequency (200 and 300 kHz), and are compact enough to be fitted to vessels of opportunity. The dual-frequency and improved sampling resolution of newer MBE systems may allow the identification of mackerel icefish (*Champsocephalus gunnari*) that recent research suggests are found on the edges of krill swarms at South Georgia (Fielding et al., 2007).

It should be remembered that MBEs deployed during line transect surveys still only provide a snap shot image of aggregations. This is analogous to observing a flock of birds using sterophotography, where each flock of birds is photographed once. Little would be learnt about the behaviour of an individual flock, only its dimensions. With sufficient bird flock observations it would be possible to determine the distributions of flock dimensions. However, the formation and splitting of bird flocks would remain unobserved. Moored acoustic instruments may partially overcome this limitation for krill (see Brierley et al. 2006). An acoustic lander, equipped with an upward looking SM20 MBE would allow the behaviour of individual krill swarms to be observed, and Livingston Island would make an ideal site for such an experiment.

To overcome the limited acoustic sampling volume of most ship-based acoustic instruments Makris et al. (2006) acoustically sampled fish populations on entire continental shelf environments (grey area, Figure 8.1, which could be extended in time depending upon the mooring deployment duration). At South Georgia this instrument offers the capability to obtain instantaneous measurements of acoustic back scatter of in each of the core box study sites. The instrument could be mounted on moorings (see Brierley et al. 2006) for long-term deployment and has the potential to reveal total areal prey field available to South Georgia predators, combining both high temporal and spatial resolution.

However, there are several limitations to overcome prior to deploying the instrument: (1) the instrument frequency may not be appropriate for sampling krill; (2) despite research being carried out (Hewitt and Demer, 1996) there are no parameterised lateral target strength models available for krill; and (3) this instrument collapses the depth dimension to estimate areal density, which means the accessibility of krill to non-diving predators cannot be determined.

8.4 Conclusions

Krill predator-prey interactions at both South Georgia and Livingston Island are highly scale dependent, both spatially and temporally. This variation makes the at-sea collection and interpretation of krill and krill predator interactions difficult. Consequently, careful consideration must be given to the observation methods and the spatial and temporal scale at which surveys should be conducted. Links between small-scale (<10 km) predator foraging activity and krill distribution must be understood before krill swarm characteristics can be used in ecosystem management models. The link established between $n_s \sim \hat{\rho}$ is important, as it is the first step in quantifying how the availability of krill swarms influences predators, and how the catchability of krill might vary with $\hat{\rho}$.

Using a MBE enabled krill swarms to be observed in 3D. However, absolute krill density cannot yet be estimated using MBE, because of calibration difficulties and inadequate lateral target strength models (see Cutter and Demer 2007). Many sources of uncertainty remain in krill density estimates derived from conventional acoustic observations (Demer, 2004). Formally combining moored instruments, with high-temporal resolution and line-transect acoustic data, with high spatial resolution, is important for ecosystem monitoring.

For observing krill predator-prey interactions a remote sensing technique that samples the top 10 m of the water column would markedly improve investigations, particularly as most flying bird krill predators are only able to forage to a 2 m maximum depth.

Finally, even in a data replete situation, interpretation is still important, since it is likely that analysis techniques will lag data collection. Additional inter-disciplinary collaboration may reduce this data-analysis gap. Nevertheless, as in most subject areas, scope for reinterpretation of data will remain (*cf* recent analysis on data from the Discovery era, 100 years ago, Atkinson et al. 2004).

8.5 Further directions

Formalising 3D krill target strength models is an important step towards obtaining absolute krill density estimates from MBE observations, as would a standard procedure

for calibrating MBEs. Utilising dual- or multi-frequency MBEs would allow the acoustic identification of krill and when analysed in the 2D distance sampling framework would allow MBEs to be routinely used in surveys to estimate krill biomass and variance.

During the small-scale data investigation and analysis, it became apparent that it is vital that consideration be given to data collection methods for observing krill predator-prey interactions. Given a research vessel equipped with a conventional hull-mounted, vertically-downward looking echosounder for studying predator-prey interactions it is recommended that: (1) conventional distance sampling techniques (Buckland et al., 2001) are used to record Macaroni penguin and Antarctic fur seal encounters; and (2) snap shot observations of flying bird distributions are made at fixed time or space intervals. Distance sampling may not require additional personnel, since techniques are available to take in account observation saturation (where more targets are detected than the observer can record, Buckland et al. 2001). The collecting of distance data would enable predator abundance and variance to be estimated, and may improve perception of spatial association between krill and predators. It would also account for differences in predator detectability between surveys caused by sea state (Reid et al., 2000b) or reduced visibility.

A combination of an adaptive line-transect survey design, individual satellite tagged predators and distance sampling would improve understanding of predator search strategies. These observations would in turn allow predator-prey interactions to be described using a combined multiple scale approach, such as analyses conducted using the Lévy distribution (Sims et al., 2008).

An autonomous underwater vehicle (*e.g.* Brierley et al. 2002) equipped with upward and downward looking echosounders (*e.g.* Fernandes et al. 2000) would enable acoustic sampling of the near-surface zone that is currently inaccessible to conventional vertically downward looking echosounders, and would allow examination of krill predator-prey interactions in the surface zone.

Bibliography

Agnew, D. J. (1997). Review- The CCAMLR Ecosystem Monitoring Programme. *Antarctic Science*, 9:235–242.

Ainley, D. G., Ribic, C. A., and Fraser, W. R. (1993a). Does prey preference affect habitat choice in Antarctic seabirds? *Marine Ecology Progress Series*, 90:207–221.

Ainley, D. G., Ribic, C. A., and Speark, L. B. (1993b). Species-habitat relationships among Antarctic seabirds: functional or physical biological factors. *The Condor*, 95:806–816.

Akaike, H. (1974). A new look at the statistical model identification. *IEEE Transactions on Automatic Control*, 6:716–723.

Allen, T. F. H. and Hoekstra, T. W. (1982). *Hierarchy*. University of Chicago Press, Chicago.

Anonymous (2002). Introducing nature in fisheries research: the use of underwater acoustics for an ecosystem approach of fish population. *Aquatic Living Resources*, 16:107–112.

Armstrong, A. J. and Siegfried, W. R. (1991). Consumption of Antarctic krill by Minke whales. *Antarctic Science*, 3(1):13–18.

Arnould, J. P. Y. and Whitehead, M. D. (1991). The diet of Antarctic petrels, cape petrels and southern fulmars rearing chicks in Prydz Bay. *Antarctic Science*, 3:19–27.

Atkinson, A., Siegel, V., Pakhomov, E., and Rothery, P. (2004). Long-term decline in krill stock and increase in salps within the Southern Ocean. *Nature*, 432:100–103.

Atkinson, A., Whitehouse, M. J., Priddle, J., Cripps, G. C., and Brandon, M. A. (2001). South Georgia, Antarctica: a productive, cold water, pelagic ecosystem. *Marine Ecology Progress Series*, 216:279–308.

Axelsen, B. E., Anker-Nilssen, T., Fossum, P., and L., N. (2001). Pretty patterns but a simple strategy: predator-prey interactions between juvenile herring and Atlantic puffins observed with multibeam sonar. *Canadian Journal of Zoology*, 79:1586–1596.

Barange, M. (1994). Acoustic identification, classification and structure of biological patchiness on the edge of the Agulhas bank and its relation to frountal features. *South African Journal of Marine Science*, 14:333–347.

Barange, M., Miller, D. G. M., Hampton, I., and Dunne, T. T. (1993). Internal structure of Antarctic krill *Euphausia superba* swarms based on acoustic observations. *Marine Ecology Progress Series*, 99:205–213.

Barange, M. and Piller, S. C. (1992). Cross-shelf circulation, zonation and maintenance mechanims of *Nyctiphanes capensis* and *Euphausia hanseni* (euphausiacea). *Continental Shelf Research*, 12(9):1027–1042.

Barlow, K. E., Boyd, I. L., Croxall, J. P., Reid, K., Staniland, I. J., and Brierley, A. S. (2002). Are penguins and seals in competition for Antarctic krill at South Georgia? *Marine Biology*, 140:205–213.

Barlow, K. E. and Croxall, J. P. (2002). Seasonal and interannual variation in foraging range and habitat of macaroni penguins *Eudyptes chrysolophus* at South Georgia. *Marine Ecology Progress Series*, 232(291-304).

Beare, D. J., Reid, D. G., and Petitgas, P. (2002). Spatio-temporal patterns in herring (*Clupea harengus* L.) school abundance and size in the northwest North Sea: modelling space-time dependencies to allow examination in the impact of local school abundance on school size. *ICES Journal of Marine Science*, 59:469–479.

Beck, J. R. and Brown (1972). The biology of Wilson's Storm Petrel *Oceanites oceanicus* (Kuhl), at Signy Island. Scientific Report 69, British Antarctic Survey. 1-54.

Beever, E. A., Swihart, R. K., and Bestelmeyer, B. T. (2006). Linking the concept of scale to studies of biological diversity: evolving approaches and tools. *Diversity and Distributions*, 12:229–235.

Blaine, T. W. and DeAngelis, D. L. (1997). The interaction of spatial scale and predator-prey functional response. *Ecological Modelling*, 95(2):319–328.

Box, G. and Jenkins, G. (1976). *Time series analysis: forecasting and control*. Holden-Day, San Francisco.

Boyd, I. L. (1993). Pup production and distribution of breeding Antarctic fur seals (*Arctocephalus gazella*) at South Georgia. *Antarctic Science*, 5(17-24).

Boyd, I. L. (1996). Temporal scales of foraging in a marine predator. *Ecology*, 77(2):426–434.

Boyd, I. L. (2002). Estimating food consumption of marine predators: Antarctic fur seals and macaroni penguins. *Journal of Applied Ecology*, 39:103–119.

Boyd, I. L., Arnould, J. P. Y., Barton, T., and Croxall, J. P. (1994). Foraging behaviour of Antarctic fur seals during periods of contrasting prey abundance. *Journal of Animal Ecology*, 63:703–713.

Boyd, I. L. and Croxall, J. P. (1992). Diving behaviour of lactating Antarctic fur seals. *Canadian Journal of Zoology*, 70:919–928.

Boyd, I. L. and Croxall, J. P. (1996). Preliminary estimates of krill consumption by Antarctic fur seals and macaroni penguins at South Georgia. Technical Report WG-EMM-96/96, CCAMLR, Hobart.

Boyd, I. L., McCafferty, D., and T., W. (1997). Variation in foraging effort by lactating Antarctic fur seals: response to simulated increased foraging costs. *Behavioural Ecological Sociobiology*, 40:135–144.

Boyd, I. L., McCafferty, D. J., Reid, K., Taylor, R., and Walker, T. R. (1998). Dispersion of male and female Antarctic fur seals *Arctocephalus gazella*. *Canadian Journal of Fisheries Aquatic Science*, 55:845–852.

Boyd, I. L. and Murphy, A. W. A. (2001). Monitoring a marine ecosystem using responses of upper tropic level predators. *Journal of Animal Ecology*, 70(5):747–760.

Boyd, I. L., Staniland, I. J., and Martin, A. R. (2002). Distribution of foraging by female Antarctic fur seals. *Marine Ecology Progress Series*, 242:285–294.

Brandon, M. A., Murphy, E. J., Whitehouse, M. J., Trathan, P. N., Murray, A. W. A., Bone, D. G., and Priddle, J. (1999). The shelf break front to the east of the sub-Antarctic island of South Georgia. *Continental Shelf Research*, 19:799–819.

Brierley, A. S., Demer, D. A., Watkins, J. L., and Hewitt, R. P. (1999a). Concordance of interannual fluctuations in acoustically estimated densities of Antarctic krill around South Georgia and Elephant Island: biological evidence of same-year teleconnections across the Scotia Sea. *Marine Biology*, 134:675–681.

Brierley, A. S., Fernades, P. G., Brandon, M. A., Armstrong, E., Millard, N. W., McPhail, S. D., Stevenson, P., Pebody, M., Perrett, J., Squires, M., Bone, D. G., and Griffiths, G. (2002). Antarctic krill under sea ice: Elevated abundance in a narrow band just South of ice edge. *Science*, 295:1890–1892.

Brierley, A. S., Fernandes, P. G., Brandon, M. A., Armstrong, F., Millard, N. W., McPhail, S. D., Stevenson, P., Pebody, M., Perrett, J., Squires, M., Bone, D. G., and Griffiths, G. (2003a). An investigation of avoidance by Antarctic krill of RRS *James Clark Ross* using the *Autosub*-2 autonomous underwater vehicle. *Fisheries Research*, 60:569–576.

Brierley, A. S., Gull, S. F., and Wafy, M. H. (2003b). A Bayesian maximum entropy reconstruction of stock distribution and inference of stock density from line-transect acoustic-survey data. *ICES Journal of Marine Science*, 60:446–452.

Brierley, A. S., Saunders, R. S., Bone, D. G., Murphy, E. J., Enderlein, P., Demer, D. A., and Conti, S. G. (2006). Use of moored instruments to measure short-term variability in abundance of Antarctic krill. *Limnology and Oceanography: Methods*, 4:18–29.

Brierley, A. S., Ward, P., Watkins, J. L., and Goss, C. (1998). Acoustic discrimination of Southern Ocean zooplankton. *Deep Sea Research II*, 45:1155–1173.

Brierley, A. S. and Watkins, J. L. (1996). Acoustic targets at South Georgia and the South Orkney Islands during a season of krill scarcity. *Marine Ecology Progress Series*, 138:51–61.

Brierley, A. S., Watkins, J. L., and Goss, C. (1997a). Krill biomass estimates for South Georgia, December and January 1996/97. Technical Report WG-EMM-97/48, CCAMLR, Hobart, Asutralia.

Brierley, A. S., Watkins, J. L., Goss, C., Wilkinson, M. T., and Everson, I. (1999b). Acoustic estimates of krill density at South Georgia, 1981 to 1998. *CCAMLR Science*, 6:47–57.

Brierley, A. S., Watkins, J. L., and Murray, A. W. A. (1997b). Interannual variability in krill abundance at South Georgia. *Marine Ecology Progress Series*, 150:87–98.

Brown, D. J., Boyd, I. L., Cripps, G. C., and Butler, P. J. (1999). Fatty acid signature analysis from the milk of Antarctic fur seals and Southern elephant seals from South Georgia: implications for diet determination. *Marine Ecology Progress Series*, 187:251–263.

Buckland, S. T., Anderson, D. R., Burnham, K. P., Laake, J. L., Borchers, D. L., and Thomas, L. (2001). *Introduction to Distance Sampling*. Oxford University Press.

Calder, W. A. (1983). Ecological scaling: Mammals and birds. *Annual Review of Ecology and Systematics*, 14:213–230.

Casaux, R. J. and Barrera-Oro, E. R. (1993). The diet of the blue-eyed shag, *Phalacrocorax atriceps bransfieldensis* feeding in the Bransfield Strait. *Antarctic Science*, 5:335–338.

CCAMLR (2000). Statistical Bulletin. Technical report, CCAMLR, Hobart, Australia.

Chastel, O. and Bried, J. (1996). Diving ability of blue petrels and thin-billed prions. *The Condor*, 98:627–629.

Clarke, A., Murphy, E. J., Meredith, M. P., King, J. C., Peck, L. S., Barnes, D. K. A., and Smith, R. C. (2007). Climate change and the marine ecosystem of the western Antarctic Peninsula. *Philosophical Transactions of the Royal Society, Series, B.*, 362:149–166.

Clarke, E. D., Speirs, D. C., Heath, M. R., Wood, S. N., Gurney, W. S. C., and Holmes, S. J. (2006). Calibrating remotely sensed chlorophyll-a data by using penalized regression splines. *Applied Statistics*, 55(3):331–353.

Cochrane, N. A., Li, Y., and Melvin, G. D. (2003). Quantification of a multibeam sonar for fisheries assessment applications. *Journal of the Acoustical Society of America*, 114(2):745–758.

Coetzee, J. (2000). Use of a shoal analysis and patch estimation system (SHAPES) to characterise sardine schools. *Aquatic Living Resources*, 13(1):1–10.

Constable, A. J., de la Mare, W. K., Agnew, D. J., Everson, I., and Miller, D. (2000). Managing fisheries to conserve the Antarctic marine ecosystem practical implementation of the Convention on the Conservation of Antarctic Marine Living Resources (CCAMLR). *ICES Journal of Marine Science*, 57:778–791.

Conti, S. G. and Demer, D. (2006). Improved parameterization of the SDWBA for estimating krill target strength. *ICES Journal of Marine Science*, 63(5):928–935.

Cresswell, K., Tarling, G., and Burrows, M. (2007). Behaviour affects local-scale distributions of Antarctic krill around South Georgia. *Marine Ecology Progress Series*, 343:193–206.

Croll, D. A., Demer, D. A., Hewitt, R. P., Jansen, J. K., Goebel, M. E., and Tershy, B. R. (August 2006). Effects of variability in prey abundance on reproduction and foraging in chinstrap penguins (*Pygoscelis antarctica). Journal of Zoology*, 269:506–513.

Croll, D. A., Tershy, B. R., Hewitt, R. P., Demer, D. A., Fiedler, P. C., Smith, S. E., Armstrong, W., Popp, J. M., Kiekhefer, T., Lopez, V. R., Urban, J., and Gendron, D. (1998). An integrated approach to the foraging ecology of marine birds and mammals. *Deep-Sea Research II*, 45(7):1357–1371.

Croxall, J. P. and Furse, J. R. (1980). Food of Chinstrap Penguins *Pygoscleis antarctica* and Macaroni Penguins *Eudyptes chrysolophus* at Elephant Island group, South Shetland Islands. *Ibis*, 122:237–245.

Croxall, J. P., Hill, H. J., Lidstone-Scott, R., O'Connell, M. J., and Prince, P. A. (1988a). Food and feeding ecology of Wilson's storm petrel *Oceanites oceanicus* at South Georgia. *Journal of Zoology*, 216(1):83–102.

Croxall, J. P., McCann, T. S., Prince, P. A., and Rothery, P. (1988b). *Antarctic Ocean and Resources Variability*, chapter Reproductive performance of seabirds and seals at South Georgia and Signy Island, South Orkney Islands, 1976-1897: implications for Southern Ocean monitoring studies., pages 261–285. Springer, Berlin.

Croxall, J. P. and Prince, P. A. Reid, K. (1997). Dietary segregation of krill-eating South Georgia seabirds. *Journal of Zoology*, 242:531–556.

Croxall, J. P. and Prince, P. A. (1980a). Food, feeding ecology and ecological segregation of seabirds at South Georgia. *Biological Journal of the Linnean Society*, 14:103–131.

Croxall, J. P. and Prince, P. A. (1980b). The food of Gentoo Penguins *Pygosleis papua* and Macaroni Penguins *Eudyptes cchrysolophus* at South Georgia. *Ibis*, 122:245–253.

Croxall, J. P. and Prince, P. A. (1996). Cephalopods as Prey. I. Seabirds. *Philosophical Transactions: Biological Sciences*, 351(1343):1023–1043.

Croxall, J. P., Reid, K., and Prince, P. A. (1999). Diet, provisioning and productivity responses of marine predators to differences in availability of Antarctic krill. *Marine Ecology Progress Series*, 177:115–131.

Cutter, G. R. and Demer, D. A. (2007). Accounting for scattering directivity and fish behaviour in multibeam-echosounder surveys. *ICES Journal of Marine Science*, 64(9):1664–1674.

Demer, D. A. (2004). An estimate of error for the CCAMLR 2000 survey of krill biomass. *Deep-Sea Research Part II*, 51:1237–1251.

Demer, D. A. and Conti, S. G. (2003). Validation of the stochastic distorted-wave Born approximation model with broad bandwidth total target strength measurements of Antarctic krill. *ICES Journal of Marine Science*, 60:625–635.

Demer, D. A. and Conti, S. G. (2005). New target-strength model indicates more krill in the Southern Ocean. *ICES Journal of Marine Science*, 62:25–32.

Demer, D. A. and Hewitt, R. P. (1995). Bias in acoustic biomass estimates of *Euphausia superba* due to diel vertical migration. *Deep-Sea Research Part I*, 42:455–475.

Diner, N. (2001). Correction on school geometry and density: approach based on acoustic image simulation. *Aquatic Living Resources*, 14:211–222.

Everson, I. and Bone, D. G. (1986). Detection of krill (*Euphausia superba*) near the sea surface: preliminary results using a towed upward-looking echosounder. *British Antarctic Survey Bulletin*, 72:61–70.

Everson, I., Parkes, G., Kock, H., and Boyd, I. L. (1999). Variation in standing stock of the mackerel icefish *Champsocephalus gunnari* at South Georgia. *Journal of Applied Ecology*, 36(4):591–603.

Fauchald (1999). Foraging in a hierarchical patch system. *The American Nauralist*, 153(6):603–613.

Fauchald, P. and Erikstad, K. E. (2002). Scale-dependent predator-prey interactions: the aggregative response of seabirds to prey under variable prey abundance and patchiness. *Marine Ecology Progress Series*, 231:279–291.

Fauchald, P., Erikstad, K. E., and Skarsfjord, H. (2000). Scale-dependent predator-prey interactions: The hierarchical spatial distribution of seabirds and prey. *Ecology*, 81(3):773–783.

Fernandes, P. G., Brierley, A. S., Simmonds, E. J., Millard, N. W., McPhail, S. D., Armstrong, F., Stevenson, P., and Squires, M. (2000). Fish do not avoid survey vessels. *Nature*, 404:35–36.

Fielding, S., Collins, M., Everson, I., and Reid, A. (2007). Improving target identification of mackerel icefish using commercial and scientific acoustic observations. ICES Working Group on Fisheries Acoustics, Science and Technology (WGFAST).

Foote, K. G., Knudsen, H. P., Vestnes, G., MacLennan, D. N., and Simmonds, E. J. (1987). Calibration of acoustic instruments for fish density estimation: a practical guide. *ICES Cooperative Research Report*, 144:57.

Fraser, W. R. and Hoffman, E. E. (2003). A predator's perspective on casual links between climate change, physical forcing and ecosystem response. *Marine Ecology Progress Series*, 265:1–15.

Fréon, P. and Misund, O. A. (1999). *Dynamics of Pelagic Fish Distribution and Behaviour*. Wiley-Blackwell, Oxford.

Garcia, S. M. and Cochranem, K. L. (2005). Ecosystem approach to fisheries: a review of implementation guidelines. *ICES Journal of Marine Science*, 62:311–318.

Garlaschelli, D., Caldarelli, G., and Pietronero, L. (2003). Universal scaling relations in food webs. *Nature*, 423:165–168.

Genin, A. (2004). Bio-physical coupling of the formation of zooplankton and fish aggregations over abrupt topographies. *Journal of Marine Systems*, 50:3–20.

Gerlotto, F., Bertrand, S., Bez, N., and Gutierrez, M. (2006). Waves of agitation inside anchovy schools observed with multibeam sonar: a way to transmit information in response to predation. *ICES Journal of Marine Science*, 63:1405–1417.

Gerlotto, F., Castillo, J., Saavedra, A., Barbieri, M. A., Espejo, M., and Cotel, P. (2004). Three-simensional structure and avoidance behaviour or anchovy and common sardine schools in central Chile. *ICES Journal of Marine Science*, 61:1120–1126.

Gerlotto, F. and Paramo, J. (2003). The three-dimensional morphology and internal structure of clupeid schools as observed using vertical scanning multibeam sonar. *Aquatic Living Resources*, 16:113–122.

Gerlotto, F., Soria, M., and Freon, P. (1999). From two dimensions to three: the use of multibeam sonar for a new approach in fisheries acoustics. *Canadian Journal of Fisheries and Aquatic Science*, 56:6–12.

Gonzalez, C., Bruno, I., and Paz, X. (2000). Food and feeding of deep-sea redfish (*Sebastes mentella* Travin) in the North Atlantic. *NAFO Scientific Council Studies*, 33:89–101.

Granadeiro, J. P., Andrade, J., and Palmeirim, J. M. (2004). Modelling the distribution of shorebirds in estuarine areas using generalised additive models. *Journal of Sea Research*, 53(3):227–240.

Greene, C. H., Stanton, T. K., Wiebe, P. H., and McClatchie, S. (1991). Acoustic estimates of Antarctic krill. *Nature*, 349:110.

Grënbaum, D. and Veit, R. R. (2003). Black-Browed Albatrosses foraging on Antarctic krill: Density-dependence through local enhancement? *Ecology*, 84(12):3265–3275.

Guisan, A. and Zimmermann, N. E. (2000). Predictive habitat distribution models in ecology. *Ecological Modelling*, 135:147–186.

Hahn, S. (1998). The food and chick feeding of black-bellied storm petrel (*Fregetta tropica*) at King George Island, South Shetlands. *Polar Biology*, 19(5):354–357.

Hamer, W. M. (1984). Aspects of schooling of *Euphausia superba*. *Journal of Crustacean Biology*, 4:67–74.

Hamilton, W. (1971). Geometry for the selfish herd. *Journal of Theoretical Biology*, 31:295–311.

Hamner, W. M. and Hamner, P. P. (2000). Behavior of Antarctic krill (*Euphausia superba*): schooling, foraging, and antipredatory behavior. *Canadian Journal of Fisheries and Aquatic Sciences*, 57:192–202.

Hamner, W. M., Hamner, P. P., Strand, S. W., and Gilmer, R. W. (1983). Behaviour of Antarctic krill, *Euphausia superba*: chemoreceptor, feeding, schooling and moulting. *Science*, 220:433–435.

Hamner, W. M., Stone, G. S., and Obst, B. S. (1988). Behaviour of southern right whales *Eubalaena australis*, feeding on Antractic krill, *Euphausia superba*. *Fisheries Bulletin*, 86:143–150.

Hardy, A. C. and Gunther, E. R. (1935). The plankton of the South Georgia whaling grounds and adjacent waters, 1926-1927. *Discovery Reports*, 11:1–456.

Harrison, N. M., Whitehouse, M. J., Heinemann, D., Prince, P. A., Hunt, G. L., and Veit, R. R. (1991). Observations of multispecies seabird flocks around South Georgia. *Auk*, 108:801–810.

Hassell, M. P., Comins, H. N., and May, R. M. (1994). Species coexistence and self-organizing spatial dynamics. *Nature*, 370:290–292.

Haury, L. R., McGowan, J. A., and Wiebe, P. H. (1985). *Spatial Pattern in Plankton Communities*, chapter Patterns and processes in the time-space scales of plankton distributions, pages 239–327. Plenum Press, London.

Hewitt, R. P. and Demer, D. A. (1991). Krill abundance. *Nature*, 353:310.

Hewitt, R. P. and Demer, D. A. (1993). Dispersion and abundance of Antarctic krill in the vicinity of elephant island in the 1992 austral summer. *Marine Ecology Progress Series*, 99:29–39.

Hewitt, R. P. and Demer, D. A. (1994). Acoustic estimates of krill biomass in the Elephant Island area: 1981-1993. *CCAMLR Science*, 1:1–6.

Hewitt, R. P. and Demer, D. A. (1996). Lateral target strength of Antarctic krill. *ICES Journal of Marine Science*, 53:297–302.

Hewitt, R. P. and Demer, D. A. (2000). The use of acoustic sampling to estimate the dispersion and abundance of euphausiids, with an emphasis on Antarctic krill, *Euphausia superba*. *Fisheries Research*, 47:215–229.

Hewitt, R. P. and Demer, D. A. (2003). An 8-year cycle in krill biomass density inferred from acoustic surveys conducted in the vicinity of the South Shetland Islands during the austral summers of 1991-1992 through 2001-2002. *Aquatic Living Resources*, 16:205–213.

Hewitt, R. P., Watkins, J. L., Naganobu, M., Sushin, V., Brierley, A. S., Demer, D. A., Kasatkina, S., Takao, Y., Goss, C., Malyshko, A., Brandon, M., Kawaguchi, S., Siegel, V., Trathan, P., Emery, J., Everson, I., and Miller, D. (2004). Biomass of Antarctic krill in the Scotia sea in January/February 2000 and its use in revising an estimate of precautionary yield. *Deep Sea Research Part II*, 51(12-13):1215–1236.

Hofmann, E. E., Haskell, A. G. E., Klinck, J. M., and M., L. C. (2004). Lagrangian modelling studies of Antarctic krill *Euphausia superba* swarm formation. *ICES Journal of Marine Science*, 61:617–631.

Horne, J. K. and Schneider, D. C. (1994). Lack of spatial coherence of predators with prey: a bioenergetic explanation for Atlantic cod feeding on capelin. *Journal of Fish Biology*, 45:191–207.

Horne, J. K. and Schneider, D. C. (1995). Spatial variance in ecology. *OIKOS*, 74:18–26.

Huin, N. (1994). Diving depths of white-chinned petrels. *The Condor*, 96:1111–1113.

Hunt, G. L. (1991). Marine ecology of seabirds in polar regions. *American Zoologist*, 31:131–142.

Hunt, G. L., Heinemann, D., and Everson, I. (1992a). Distributions and predator-prey interactions of Macaroni penguins, Antarctic fur seals, and Antarctic krill near Bird Island, South Georgia. *Marine Ecology Progress Series*, 86:15–30.

Hunt, G. L., Priddle, J., Whitehouse, M. J., Veit, R. R., and Heywood, R. B. (1992b). Changes in seabird species abundance near South Georgia during a period of rapid change in sea surface temperature. *Antarctic Science*, 4(1):15–22.

Imber, M. J. (1999). Diet and feeding ecology of the Royal Albatross *Diomedea epomophora* - King of the shelf break and inner slope. *Emu*, 99(2):200–211.

Jackson, S. (1988). Diets of the white-chinned petrel and sooty shearwater in the Southern Benguela region, Soouth Africa. *The Condor*, 90:20–28.

Jazdzewski, K. and A., K. (1999). *Necrophagous lysianassoid amphipoda* in the diet of Antarctic tern at King George Island, Antarctica. *Antarctic Science*, 11:316–321.

Johnson, D. (1998). *Applied multivariate methods for data analysis*. Duxbury Press, California.

Jolliffe, I. (2002). *Principal Component Analysis*. Springer-Verlag, 2 edition.

Jolly, G. M. and Hampton, I. (1990). A stratified transect design for acoustic surveys of fish stocks. *Canadian Journal of Fisheries and Aquatic Science*, 47:1282–1291.

Kaiser, M. J., Attrill, M. J., Jennings, S., Thomas, D. N., Barnes, D. K. A., Brierley, A. S., Polunin, N. V. C., Raffaelli, D. G., and Williams, P. J. l. B. (2005). *Marine Ecology: Processes, Systems and Impacts*. Oxford University Press.

Kneitel, J. M. and Chase, J. M. (2004). Trade-offs in community ecology: linking spatial scales and species coexistence. *Ecology Letters*, 7(1):69–80.

Knowlton, N. (1992). Thresholds and Multiple Stable States in Coral Reef Community Dynamics. *American Zoologist*, 32:674–682.

Kock, K. H. (2000). Understanding CCAMLRs Approach to Management. Technical report, CCAMLR, Hobart, Australia.

Kock, K. H., Wilhelms, S., Everson, I., and Grëger, J. (1994). Variations in the diet composition and feeding intensity of mackerel icefish *Champsocephalus gunnari* at South Goergia (Antractic). *Marine Ecology Progress Series*, 108:43–57.

Krakauer, D. C. (1995). Groups confuse predators by exploiting perceptutal bottlenecks: a connectionist model of the confusion effect. *Behavioural Ecology and Sociobiology*, 36:421–429.

Krause, J. and Ruxton, G. D. (2002). *Living in Groups*. Oxford University Press.

Landeau, L. and Terborgh, J. (1986). Oddity and the 'confusion effect' in predation. *Functional Ecology*, 3:21–27.

Lascara, C. M., Hoffmann, E. E., Ross, R. M., and Quetin, L. B. (1999). Seasonal variability in the distribution of Antarctic krill, *Euphausia superba*, west of the Antarctic Peninsula. *Deep-Sea Research Part I*, 46:951–984.

Lavoie, D., Simard, Y., and saucier, F. J. (2000). Aggreation and dispersion of krill at channel heads and shelf edges: the synamics in the Saguenay - St. Lawrence Marine Park. *Canadian Journal of Fisheries and Aquatic Sciences*, 57:1853–1869.

Lawson, G. L., Barange, M., and Freéon (2001). Species identification of pelagic fish schools on the South Afrcan continental shelf using acoustic descriptors and ancillary information. *ICES Journal of Marine Science*, 58:275–287.

Legendre, P. and Legendre, L. (1998). *Numerical Ecology*. Number 20 in Developments in Environmental Modelling. Elsevier, Oxford, 2nd edition.

Levin, S. A. (1992). The problem of pattern and scale in ecology. *Ecology*, 73(6):1943–1967.

Lima, S. L. and Zollner, P. A. (1996). Towards a behavioral ecology of ecological landscapes. *Trends in Ecology and Evolution*, 11:131–135.

Logerwell, E. A., Hewitt, R. P., and A., D. D. (1998). Scale-dependent spatial variance patterns and correlations of seabirds and prey in the southeastern Bering Sea as revealed by spectral analysis. *Ecography*, 21(2):212–223.

MacCall, A. (1990). *Dynamic geography of marine fish populations*. University of Washington Press, Seattle.

Mackas, D. L., Denman, K. L., and Abbott, M. R. (1985). Plankton patchiness: Biology in the physical vernacular. *Bulletin of Marine Science*, 37:652–674.

MacLennan, D. N. and Simmonds, J. E. (1992). *Fisheries Acoustics*. Chapman and Hall, London.

MacNally, R. and Quinn, G. P. (1998). Symposium introduction: The importance of scale in ecology. *Austral Ecology*, 23(1):1–7.

Madureira, L. S. P., Everson, I., and Murphy, E. J. (1993). Interpretation of acoustic data at two frequencies to discriminate between Antarctic krill (*Euphausia superba*, Dana) and other scatterers. *Journal of Plankton Research*, 15:787–802.

Makris, N. C., Ratilal, P., Symonds, D. T., Jajannathan, S., Lee, S., and Nero, R. W. (2006). Fish population and behavour revealed by instanteous continental shelf-scale imaging. *Science*, 311:660–662.

Mangel, M. and Nicol, S. (2000). Krill and the unity of biology. *Canadian Journal of Fisheries and Aquatic Sciences*, 57:1–5.

Maniscalco, J. M., Oxtrand, W. D., Suryan, R. M., and Irons, D. B. (2001). Passive interference competition by Glaucous-winged Gulls on Black-legged Kittiwakes: a cost of feeding in flocks. *Condor*, 103:616–619.

Maravelias, C. D., Reid, D. G., and Swartzman, G. (2000). Modelling spatio-temporal effects of environment on Atlantic herring, *Clupea harengus*. *Environmental Biology of Fishes*, 58:157–172.

Marin, V. M. and Delgado, L. E. (2001). A spatially explicit model of the Antarctic krill fishery off the South Shetland islands. *Ecological Applications*, 11(4):1235–1248.

Marques, T. (2007). *Incorporating measurement error and density gradients in distance sampling surveys*. Unpublished PhD thesis, Univerity of St. Andrews.

Marques, T. A., Buckland, S. T., Borchers, D. L., Tosh, D., and McDonald, R. A. (2007). Point transect sampling along non-random routes. *Biometrics*.

Marr, J. W. S. (1962). The natural history and geography of Antarctic krill (*Euphausia superba* Dana). *Discovery reports*, 32:33–464.

Martin, A. P. (2003). Phytoplankton patchiness: the role of lateral stirring and mixing. *Progress in Oceanography*, 57:125–174.

Mauchline, J. (1980). Studies on patches of krill, (*Euphausia superba* dana). Technical report, BIOMASS Handbook No. 6.

Mayer, L., Yanchao, L., and Melvin, G. (2002). 3D visualization for pelagic fisheries research and assessment. *ICES Journal of Marine Science*, 59:216–225.

McCann, K. S. (2000). The diveristy-stability debate. *Nature*, 405:228–233.

McClatchie, S., Greene, C. H., Macaulay, M. C., and Sturley, D. R. M. (1994). Spatial and temporal variability of Antarctic krill: implications for stock assessment. *ICES Journal of Marine Science*, 51(1):11–18.

Melvin, G. D., Cochrane, N. A., and Yanchao, L. (2003). Extraction and comparison of acoustic backscatter from a calibrated multi- and single-beam sonar. *ICES Journal of Marine Science*, 60:669–677.

Melvin, G. D., Li, Y., Mayer, L. A., and Clay, A. (2002). Commercial fishing vessels, automatic acoustic logging systems and 3-D data visualization. *ICES Journal of Marine Science*, 59:179190.

Meredith, M. P., Murphy, E. J., Hawker, E. J., King, J. C., and Wallace, M. I. (2007). On the interannual variability of ocean temperatures around South Georgia, Southern Ocean: forcing by El Niño Southern Oscillation and the Southern Annular Mode. *Deep Sea Research Part II*.

Meredith, M. P., Randon, M. A., Murphy, E. J., Trathan, P. N., Thorpe, S. E., Bone, D. G., Chernyshkov, P. P., and Sushin, V. A. (2005). Variability in hydrographic conditions to the east and northwest of South Georgia, 1996-2001. *Journal of Marine Systems*, 53:143–167.

Miller, D. G. M. and Hampton, I. (1989). *Biology and ecology of the Antarctic krill (Euphausia superba Dana.)*, volume 9 of *BIOMASS*. BIOMASS Science Series, Cambridge.

Mori, Y. and Boyd, I. L. (2004). The behavioural basis form non-linear functional responses and optimal foraging in Antarctic fur seals. *Ecology*, 85(2):398–410.

Morris, D. J., Watkins, J. L., Ricketts, C., Buchholz, F., and Priddle, J. (1988). An assessment of the merits of length and weight measurements of Antarctic krill *Euphausia superba*. *British Antarctic Survey Bulletin*, 79:27–50.

Murphy, E., Watkins, J. L., Reid, K., Trathan, P. N., Everson, I., Croxall, J. P., Priddle, J., Brandon, M. A., Brierley, A. S., and Hofman, E. (1998). Inter anuual variability of the South Georgia marine ecosystem: biological and physical scorces of variation in the abundance of krill. *Fisheries Oceanography*, 7:381–390.

Murphy, E. J. (1995). Spatial structure of the Southern Ocean ecosystem: predator-prey linkages in Southern Ocean food webs. *Journal of Animal Ecology*, 64:333–347.

Murphy, E. J., Everson, I., and Murray, A. W. A. (1991). *Analysis of acoustic line transect data around South Georgia: esitmation of krill (Euphausia superba) biomass*, chapter CCAMLR Selected Scientific Papers, pages 225–243. SC-CCAMLR-SSP/8.

Murphy, E. J., Morris, D. J., Watkins, J. L., and Priddle, J. (1988). *Antarctic ocean and resources variability*, chapter Scales of interactions between Antarctic krill and the environment, pages 120–130. Springer-Verlag, Berlin, Germany.

Murphy, E. J., Trathan, P. N., Everson, I., Parkes, G., and Daunt, F. (1997). Krill fishing in the Scotia Sea in relation to bathymetry, including detailed distribution around South Georgia. *CCAMLR Science*, 4:1–17.

Murphy, E. J., Watkins, J. L., Meredith, M. P., Ward, P., Trathan, P. N., and Thorpe, S. E. (2004). Southern Antarctic Circumpolar Current Front to the northeast of South Georgia: Horizontal advection of krill and its role in the ecosystem. *Journal of Geophysical Research (Oceans)*, 109:1029–+.

Murphy, E. J., Watkins, J. L., Trathan, P. N., Reid, K., Meredith, M. P., Thrope, S. E., Johnston, N. M., Clarke, A., Tarling, G. A., Collins, M., Forcada, J., Shreeve, R. S., Atkinson, A., Korb, R., Whitehouse, M., Ward, P., Rodhouse, P. G., Enderline, P., Hirst, A., Martin, A., Hill, S., Staniland, I. J., Pond, D. W., Briggs, D. R., Cunningham, N. J., and Fleming, A. H. (2007). Spatial and temporal operation of the Scotia Sea ecosystem: a review of large-scale links in a krill centred food web. *Philosophical transactions of the Royal Society Series B*, 362:113–148.

Nee, S., Read, A.F. amd Greenwood, J. J. D., and Harvey, P. H. (1991). The relationship between abundance and body size in British birds. *Nature*, 351:312 – 313.

Nero, R. W. and Magnuson, J. J. (1989). Characterization of patches along transects using high-resolution 70-khz integrated acoustic data. *Canadian Journal of Fisheries and Aquatic Sciences*, 46:2056–2064.

Nevitt, G., Reid, K., and Trathan, P. (2004). Testing olfactory foraging strategies in an Antarctic seabird assemblage. *Journal of Experimental Biology*, 207:3537 –3544.

Nevitt, G. A., Veit, R. R., and Kaeiva, P. M. (1995). Dimethyl sulfide as a foraging cue for Antarctic procellariiform seabirds. *Nature*, 376:680–682.

Nicol, S. and Foster, J. (2003). Recent trends in the fishery for Antarctic krill. *Aquatic Living Resources*, 4:42–45.

O'Brien, D. P. (1987). Description of escape responses of krill (crustacea: *Eupausiacea*), with particular reference to swarming behaviour and the size and proximity of the predator. *Journal of Crustacean Biology*, 7(3):449–457.

O'Brien, D. P. (1989). Analysis of the internal arrangement of individuals within crustacean aggregations (*Eupausiacea, Mysidacea*). *Journal of Experimental Marine Biology and Ecology*, 128:1–30.

Okubo, A. (1986). Dynamical aspects of animal grouping: swarms, schools, flocks, and herds. *Advances in Biophysics*, 22:1–94.

Olsson, O. and W., N. A. (1997). Diet of the King Penguin *Aptenodytes patagonicus* during three summers at South Georgia. *Ibis*, 139:504–512.

Paramo, J., Quiñones, R. A., Ramirez, A., and Wiff, R. (2003). Relationship between abundance of small pelagic fishes and environmental factors in the Colombian Caribbean Sea: an analysis based on hydroacoustic information. *Aquatic Living Resources*, 16:239–245.

Paramoa, J., Bertrand, S., Villalobos, H., and Gerlotto, F. (2007). A three-dimensional approach to school typology using vertical scanning multibeam sonar. *Fisheries Research*, 84(2):171–179.

Parkinson, C. I. (2002). Trends in the length of the Southern Ocean sea-ice season, 1979-99. *Annals of Glaciology*, 34:435–440.

Petitgas, P., Reid, D., Carrera, P., Iglesias, M., Georgakarakos, S., Liorzou, B., and Massé, J. (2001). On the relation between schools, clusters of schools, and abundance in pelagic fish stocks. *ICES Journal of Marine Science*, 58:1150–1160.

Phillips, R. A., Silk, J. R. D., and Croxall, J. P. (2005). Foraging and provisioning strategies of the light-mantled sooty albatross at South Georgia: competition and co-existence with sympatric pelagic predators. *Marine Ecology Progress Series*, 285:259–270.

Pinaud, D. and Weimerskirch, H. (2007). At-sea distribution and scale-dependent foraging behaviour of petrels and albatrosses: a comparative study. *Journal of Animal Ecology*, 76:9–19.

Powell, T. M. (1989). *Perspectives in Ecological Theory*, chapter Physical and biological scales of variability in lakes, estuaries, and the coastal ocean, pages 157–176. Princeton, NJ.

Prince, P. A. (1980). The food and feeding ecology of Blue petrel *Halobaena caerulea* and Dove prion *Pachyptila desolata*. *Journal of Zoology*, 190:59–76.

Prince, P. A. and Croxall, J. P. (1983). Birds of South Georgia: new records and re-evaluation of status. *British Antarctic Survey Bulletin*, (59):15–27.

Prince, P. A., Huin, N., and Weimerskirch, H. (1994). Short note: Diving depths of albatrosses. *Antarctic Science*, 6(3):353–354.

Prince, P. A. and Jones, M. (1992). Maximum dive depths attained by South Georgia diving petrel *Pelecanoides georgicus* at Bird Island, South Georgia. *Antarctic Science*, 4:433–434.

Rainbow, P. S. (1989). Copper, cadmium and zinc concentrations in oceanic amphipod and euphausiid crustaceans, as a source of heavy metals to pelagic seabirds. *Marine Biology*, 103(4):513–518.

Reid, D. G., Scalabrin, C., P., P., Masse, J., Aukland, R., Carrera, P., and Georgakarakos, S. (2000a). Standard protocols for the analysis of school based data from echosounder surveys. *Fisheries Research*, 47:125–136.

Reid, D. G. and Simmonds, E. J. (1993). Image analysis techniques for the study of fish school structure from acoustic survey data. *Canadian Journal of Fisheries and Aquatic Science*, 50(886-893).

Reid, K. and Arnould, J. P. Y. (1996). The diet of Antarctic fur seals *Arctocephalus gazella* during the breeding season at South Georgia. *Polar Biology*, 16:105–114.

Reid, K., Barlow, K. E., Croxall, J. P., and Taylor, R. I. (1999a). Predicting changes in the Antarctic krill, *Euphausia superba*, population at South Georgia. *Marine Biology*, 135:647–652.

Reid, K., Croxall, J. P., and Edwards, T. M. (1997a). Interannual variation in the diet of the Antarctic prion *Pachyptila desolata* at South Georgia. *Emu*, 97:126–132.

Reid, K., Croxall, J. P., Edwards, T. M., Hill, H. J., and Prince, P. A. (1997b). Diet and feeding ecology of diving petrels *Pelecanoides georgicus* and *P. urinatrix* at South Georgia. *Polar Biology*, 17:17–24.

Reid, K., P., C. J., Briggs, D. R., and Murphy, E. J. (2005). Antarctic ecosystem monitoring: quantifying the response of ecosystem indicators to variability in Antarctic krill. *ICES Journal of Marine Science*, 62:366–373.

Reid, K., Sims, M., White, R. W., and Gillon, K. W. (2004). Spatial distribution of predator/prey interactions in the Scotia Sea: implications for measuring predator/fishers overlap. *Deep Sea Research Part II*, 51:1383–1396.

Reid, K. R., Brierley, A. S., and Nevitt, G. A. (2000b). An initial examination of relationships between the distribution of whales and Antarctic krill (*Euphausia superba*) at South Georgia. *Journal of Cetacean Research and Management*, 2(2):143–149.

Reid, K. R. and Croxall, J. P. (2001). Environmental response of upper trophic level predators reveals a system change in an Antarctic marine ecosystem. *Proceedings of the Royal Society London Series B*, 268:377–384.

Reid, K. R., Watkings, J. L., Croxall, J. P., and Murphy, E. J. (1999b). Krill population dynamics at South Georgia. *Marine Ecology Progress Series*, 177:103–114.

Reiss, C. S., Cossio, A. M., Loeb, V., and Demer, D. A. (2008). Variations in the biomass of Antarctic krill (*Euphausia superba*) around the South Shetland Islands, 1996-2006. *ICES Journal of Marine Science*, 65.

Ricketts, C., Watkins, J. L., Proddle, J., Morris, D. J., and Buchholz, F. (1992). As assessment of the biological and acoustic characteristics of swarms of Antarctic krill. *Deep Sea Research*, 39(2):359–371.

Ridoux, V. (1994). The diets and dietary seggregation of seabirds at the Sub-Antarctic Crozet Islands. *Marine Ornithology*, 22:1–192.

Ridoux, V. and Offredo, C. (1988). The diets of five summer breeding seabirds in Adèlie Land, Antarctica. *Polar Biology*, 9(3):137–145.

Ritz, D. A. (1994). Social aggregation in pelagic invertebrates. *Advances in Marine Biology*, 30:155–216.

Ritz, D. A. (2000). Is social aggregation in aquatic crustaceans a strategy to conserve energy? *Canadian Journal of Fisheries and Aquatic Sciences*, 57(S3):56–67.

Roe, H. S. J. and Shale, D. M. (1979). A new multiple rectangular midwater trawl (RMT1+8 M) and some modification to the Institute of Oceanographic Sciences (RMT1+8). *Marine Biology*, 50:283–288.

Romey, W. L. (1995). Individual differences make a difference in the trajectories of simulated schools of fish. *Ecological Modelling*, 92:65–77.

Rose, G. A. and Leggett, W. C. (1990). The importance of scale to predator-prey spatial correlations: An example of Atlantic fisheries. *Ecology*, 71(1):33–43.

Russell, R. W., Hunt, G. L., Coyle, K. O., and Cooney, R. T. (1992). Foraging in a fractal environment: spatial patterns in a marine predator-prey system. *Landscape ecology*, 7:195–209.

Saunders, R. A., Brierley, A. S., Watkins, J. L., Reid, K., Murphy, E. J., Enderline, P., and Bone, D. G. (2007). Intra-annual variability in the density of Antarctic krill (*Euphausia superba*) at South Georgia, 2002-2005: within-year variation provides a new framework for interpreting previous 'annual' estimates of krill density. *CCAMLR Science*, 14:27–41.

Scalabrin, C. and Mass, J. (1993). Acoustic detection of the spatial and temporal distribution of fish shoals in the Bay of Biscay. *Aquatic Living Resources*, 6:269–283.

Scheider, D. C. and Piatt, J. F. (1986). Scale-dependent correlation of seabirds with schooling fish in a coastal ecosystem. *Marine Ecology Progress Series*, 32:237–246.

Schmid, P. E., Tokeshi, M., and M., S.-A. J. (2000). Relation Between Population Density and Body Size in Stream Communities. *Science*, 289(5484):1557 – 1560.

Schneider, D. (2001). The Rise of the Concept of Scale in Ecology. *BioScience*, 51(7):545–553.

Schneider, D. C. (1989). Identifying the spatial scale of density-dependent interaction of predators with schooling fish in the southern Labrador Current. *Journal of Fish Biology*, 35:109–115.

Schreiber, S. J. and Vejdani, M. (2006). Handling time promotes the coevolution of aggregation in predator-prey systems. *Proceedings of the Royal Society Series B*, 273:185–191.

Siegel, V. (1988). *Antarctic Ocean and Resources Variability*, chapter A concept of seasonal variation of krill (*Euphausia superba* distribution and abundance west of the Antarctic Peninsula), pages 219–230. Springer, Berlin.

Siegel, V. (2000). Krill (*euphausiacea*) demography and variability in abundance and distribution. *Canadian Journal of Fisheries and Aquatic Science*, 57(3):151–167.

Siegel, V. (2005). Distribution and population dynamics of *Euphausiacea*: summary and recent findings. *Polar Biology*, 29:1–22.

Silverman, E. D. and Veit, R. R. (2001). Associations among Antarctic seabirds in mixed-species feeding flocks. *Ibis*, 143(1):51–62.

Simmonds, J. and MacLennan, D. N. (2005). *Fisheries Acoustics*. Blackwell, 2nd edition.

Sims, D. W. and Quayle, V. A. (1998). Selective foraging behaviour of basking sharks on zooplankton in a small-scale front. *Nature*, 393:460–464.

Sims, D. W., Southall, E. J., Humphries, N. E., Hays, G. C., Bradshaw, C. J., Pitchford, J. W., James, A., Ahmed, M. Z., Brierley, A. S., Hindell, M. A., Morritt, D., Musyl, M. K., Righton, D., Shepard, E. L., Wearmouth, V. J., Wilson, R. P., Witt, M. J., and Metcalfe, J. (2008). Scaling laws of marine predator search behaviour. *Nature*, 451(7182):1098–1102.

Sims, D. W., Witt, M. J., Richardson, A. J., Southall, E. J., and Metcalfe, J. D. (2006). Encounter success of free-ranging marine predator movements across a dynamic prey landscape. *Proceedings of Royal Society Series B*, 273:1195–1201.

Sole, R. V. and Manrubia, S. C. (1995). Are rainforests self-organized in a critical state? *Journal of Theoretical Biology*, 173:31–40.

Soria, M., Bahri, T., and Gerlotto, F. (2003). Effect of external factors (environment and survey vessel) on fish school characteristics observed by echosounder and multibeam sonar in the Mediterranean Sea. *Aquatic Living Resources*, 16:145–157.

Soria, M., Fréon, P., and Gerlotto, F. (1996). Analysis of vessel influence on spatial behaviour of fish schools using a multi-beam sonar and consequences for biomass estimates by echo-sounder. *ICES Journal of Marine Science*, 53:453–458.

Southwell, C., Paxton, C. G. M., D., B., Boveng, P., and de la Mare, W. (2007). Taking account of dependent species in management of the Southern Ocean krill fishery: estimating crabeater seal abundance off east Antarctica. *Journal of Applied Ecology*.

Speirs, D. C., Gurney, W. S. C., Heath, M. R., Horbelt, W., Wood, S. N., and de Cuevas B. A. (2006). Ocean-scale modelling of the distribution, abundance, and seasonal dynamics of the copepod *Calanus finmarchicus*. *Marine Ecology Progress Series*, 313(173-192).

Staniland, I. J., Reid, K., and Boyd, I. L. (2004). Comparing individual and spatial influences on foraging behaviour in Antarctic fur seals *Arctocephalus gazella*. *Marine Ecology Progress Series*, 275:263–274.

Stephens, D. W. and Krebs, J. R. (1986). *Foraging theory*. Princeton Univesrity Press, Princeton, New Jersey, USA.

Taki, K., Hayashi, T., and Naganobu, M. (2005). Characteristics of seasonal variation in diurnal vertical migration and aggregation of Antarctic krill (*Euphausia superba*) in the Scotia Sea, using Japanese fishery data. *CCAMLR Science*, 12:163–172.

Tarling, G. A., Matthews, J. B. L., Saborowski, R., and Buchholz, F. (1998). Vertical migratory of the euphausiid, *Meganyctiphanes norvegica*, and its dispersion in the Kattegat channel. *Hydrobiologia*, 376:331–341.

Tarling, G. A., Roudy-Cuzin, J., Thorpe, S. E., Shreeve, R. S., Ward, P., and Murphy, E. J. (2007). Recruitment of Antarctic krill *Euphausia superba* in the South Georgia region: adult fecundity and the fate of larvae. *Marine Ecology Progress Series*, 331:161–179.

Tasker, M. L., Jones, P. J., Dixon, T., and Blake, B. F. (1984). Counting seabirds at sea from seas: a review of methods employed and a suggestion for a standardized approach. *Auk*, 101:567–577.

Thomas, G. (1982). The food and feeding ecology of the light-mantled sooty albatross at South Georgia. *Emu*, 82:92–100.

Thorpe, S. E., Heywood, K. J., Brandon, M. A., and Stevens, D. P. (2002). Variability of the Southern Antarctic Circumpolar Current Front north of South Georgia. *Journal of Marine Systems*, 37:85–105.

Trathan, P. N., Brierley, A. S., Brandon, M. A., Bone, D. G., Goss, C., Grant, S. A., Murphy, E. J., and Watkins, J. L. (2003). Oceanographic variability and changes in Antarctic krill (*Euphausia superba*) abundance at South Georgia. *Fisheries Oceanography*, 12(6):569–583.

Trathan, P. N. and Croxall, J. P. (2004). Marine predators at South Georgia: an overview of recent bio-logging studies. *Mem. National Institute of Polar Research*, 58:118–132.

Trathan, P. N., Green, C., Tanton, J., Peat, H., Poncet, J., and Morton, A. (2006). Foraging dynamics of macaroni penguins, *Eudyptes chrysolophus* at South Georgia during brood-guard. *Marine Ecology Progress Series*, 323:239–251.

Trathan, P. N. and Murphy, E. J. (2003). Sea surface temperature anomalies near South Georgia: relationships with the El Niño regions. *Journal of Geophysical Research*, 108(C4).

Trathan, P. N., Murphy, E. J., Croxall, J. P., and Everson, I. (1998). Use of at-sea distribution to derive potential foraging ranges of Macaroni penguins during the breeding season. *Marine Ecology Progress Series*, 169:263–275.

Trathan, P. N., Watkins, J. L., Murray, A. W. A., Brierley, A. S., Everson, I., Goss, C., Priddle, J., Reid, K. R., Ward, P., Hewitt, R. P., Demer, D. A., Naganobu, S., and Kawaguchi, S. (2001). The CCAMLR-2000 krill synoptic survey: a description of the rationale and design. *CCAMLR Science*, 8:1–23.

Van de Koppel, J., Bardgett, R. D., Bengtsson, J., Rodriguez-Barrueco, C., Rietkerk, M., Wassen, M. J., and Wolters, V. (2005). The effects of spatial scale on trophic interactions. *Ecosystems*, 8:801–807.

Veit, R. R., Silverman, E. D., and Everson, I. (1993). Aggregation patterns of pelagic predators and their principal prey, Antarctic krill, near South Georgia. *Journal of Animal Ecology*, 62(3):551–564.

Watkins, J. L. (2000). *Krill biology, ecology and fisheries*, chapter Aggregation and vertical migration, pages 80–102. Fish and aquatic resources series. Blackwell Scinec, Oxford.

Watkins, J. L. and Brierley, A. S. (1996). A post-processing technique to remove background noise from echo-integration data. *ICES Journal of Marine Science*, 53:339–344.

Watkins, J. L. and Brierley, A. S. (2002). Verification of the acoustic techniques used to identify Antarctic krill. *ICES Journal of Marine Science*, 59:1326–1336.

Watkins, J. L., Buchholz, F., Priddle, J., Morris, D. J., and Ricketts, C. (1992). Verification in reproductive status of Antarctic krill swarms; evidence of size-related sorting mechanism? *Marine Ecology Progress Series*, 82:163–174.

Watkins, J. L., Morris, D. J., Ricketts, C., and Priddle, J. (1986). Difference between swarms of Antarctic krill and some implications for sampling krill populations. *Marine Biology*, 93:137–146.

Watkins, J. L. and Murray, A. W. A. (1998). Layers of Antarctic krill, *Euphausia superba*: are they just long krill swarms? *Marine Biology*, 131:237–247.

Weill, A., Scalabrin, C., and Diner, N. (1993). MOVIES-B: an acoustic detection description software. application to shoal species' classification. *Aquatic Living Resources*, 6:255–267.

Weimerskirch, H., A., G., and Cherel, Y. (2005). Prey distribution and patchiness: factors in foraging success and efficiency of wandering albatrosses. *Ecology*, 86(10):2611–2622.

Weissburg, M. J. and Browman, H. I. (2005). Sensory biology: linking the internal and external ecologies of marine organisms. *Marine Ecology Progress Series*, 287:263307.

Williams, T. D. and Croxall, J. P. (1991). Annual variation in breeding biology of macaroni penguins *Eudyptes chrysolophus* at Bird Island, South Georgia. *Journal of Zoology*, 223:189–202.

Wintle, B. A., Elith, J., and Potts, J. M. (2005). Fauna habitat modelling and mapping: A review and case study in the Lower Hunter Central Coast region of NSW. *Austral Ecology*, 30:719–738.

Wood, S. N. (2006). *Generalized Additive Models An Introduction with R*. Chapman and Hall, London.

Woodd-Walker, R. S., Watkins, J., and Brierley, A. S. (2003). Identification of Southern Ocean acoustic targets using aggregation backscatter and shape characteristics. *ICES Journal of Marine Science*, 60:641–649.

Wu, J. and Louckes, O. L. (1995). From balance of nature to hierarchical dynamics: paradigm shift in ecology. *The Quarterly Review of Biology*, 70(4):439–466.

Zaniewski, A. E., Lehmann, A., and McC Overton, J. (2002). Predicting species spatial distributions using presence-only data: a case study of native New Zealand ferns. *Ecological Modelling*, 157:261–280.